1992

The Geochemistry And Structural Controls Of Auriferous Shear Zones At Yellowknife, Mackenzie District, Northwest Territories, Canada

David R. Webb

Follow this and additional works at: https://ir.lib.uwo.ca/digitizedtheses

The Geochemistry and Structural Controls of
Auriferous Shear Zones at Yellowknife,
Mackenzie District, Northwest Territories, Canada.

by

David R. Webb

Department of Geology

Submitted in partial fulfilment
of the requirements for the degree of
Doctor of Philosophy

Faculty of Graduate Studies
The University of Western Ontario
London, Ontario
March, 1992

Canada

ABSTRACT

Mines in the Yellowknife Greenstone Belt have produced more than 435 tonnes of gold, largely from auriferous quartz veins hosted within shear zones that transect tholeiitic mafic volcanic rocks of the Kam Group. The existing stratigraphic and structural subdivisions are refined, and temporal constraints indicate two prograde metamorphic events at Yellowknife. Four generations of structures are identified: (1) brittle syn-volcanic, (2) brittle-ductile, late first metamorphism, (3) brittle, post-first metamorphism, pre second metamorphism, and (4) brittle, post second metamorphism, Proterozoic faults. Type 1 structures may be reactivated as type 3 structures, offsetting type 2. The largest concentrations of gold mineralization are hosted within type 2 structures that post-date the first metamorphic event (ca. 2,620 Ma), and are constrained to greenschist to amphibolite facies volcanic rocks by structural considerations. Mineralization is post first metamorphism and pre second metamorphism (ca. 2,585 to 2,525 Ma), constrained by existing structural anisotropies, and enhanced near type 3 faults. Gold mineralization occurs in P-shears which became dilatant during seismic-aseismic events after a passive ductile state had been achieved, and is reflected at all scales, from hand sample, stope, orebody, ore zone, to mining camp-scales.

Structural studies at Yellowknife, and geochemical analyses of the igneous rocks are consistent with greenstone belt development in a back-arc basin that accreted obliquely onto an older crustal terrain, with emplacement of shoshonitic lamprophyres duri.ig late convergence, post-granite. Geochronological work places this framework into: (1) synvolcanic, at 2,683 Ma, (2) syn-I-type batholith, syn first metamorphism at 2,620 Ma, (3) mineralization between 2,620 - 2,585 Ma, (4) second metamorphism at 2,585 Ma, and (5) Proterozoic dykes.

Ore-related metasomatic alteration is imparted upon structurally and chemically modified mafic volcanic rocks of :he Yellowknife Bay Formation. The chemical composition of these rocks, now chlorite schists reveals a fluid history consistent with metasomatic alteration by large volumes of weakly saline, near neutral, CO_2/CH_4-rich fluids at temperatures near 390° ±15°C, and log f_{O2} near the pyrite-pyrrhotite transition. Gold mineralization was enhanced by fluid-gas unmixing induced by pressure fluctuations, causing periodic excursions in the Eh of the remaining aqueous fluids, resulting in destabilization of soluble gold complexes, changes in mineral phase relationships and chemistries, and shifts in the $\delta^{13}C$ of related carbonates. Pressure fluctuations were promoted by structural discontinuities generated by the intersection of type 1 and 2 structures; the

former was reactivated during type 3, to generate the present distribution of mineralization. Related metasomatic effects can be detected up to 100 m from ore zones, within macroscopically unaltered chlorite schists. Later, surface-related fluids locally modified the $\delta^{18}O$ of less robust minerals.

ACKNOWLEDGEMENTS

TABLE OF CONTENTS

LIST OF FIGURES

LIST OF TABLES

LIST OF PLATES

CHAPTER 1

INTRODUCTION AND STATEMENT OF OBJECTIVES

1.0 Introduction

More than 14 million ounces (435 tonnes) of gold have been produced from the Yellowknife Greenstone Belt since development at the Con Mine (now NERCO-Con Mine) commenced in 1938 (McDougall and Goad, 1990; Padgham, 1991). The majority of the gold has been extracted from auriferous quartz veins and silicified zones hosted within shear zones which transect tholeiitic meta-basalts and meta-volcanic rocks of the Yellowknife Supergroup (Boyle 1961, 1979; Padgham, 1987). In previous studies, the Yellowknife Supergroup at Yellowknife has been subdivided into three groups, with work focused on the lowest two groups where much of the mineralization occurs.

Despite intermittent research over the past 50 years on the geology, structure, paragenesis, metallurgical properties and geochemistry of the Yellowknife gold deposits, many problems remain. These include: (1) the stratigraphy of the greenstone belt, specifically defining the top of, and the rocks underlying, the Kam Group, and the relationship of the Burwash Formation to the Kam Group; (2) the temporal development of various structural elements within the greenstone belt; (3) the subdivision and genetic implications of the various intrusions within the greenstone belt; (4) the relationship of

metamorphism to the development of the greenstone belt and the shear zone-hosted gold deposits; and (5) the source, nature, and timing of the mineralizing events.

Previous work in the Yellowknife Greenstone Belt has addressed the stratigraphy (Jolliffe, 1938, 1942, 1946; Boyle, 1961; Henderson and Brown, 1966; Henderson, 1970, 1975, 1978, 1985; Helmstaedt et al., 1979, 1980; Bullis et al., 1987; Brophy, 1987; Helmstaedt and Bailey, 1987a, 1987b; Bailey, 1987; Relf, 1987; Falck, 1988), structure (Helmstaedt et al., 1979, 1980, 1986; Bullis, 1983; Helmstaedt and Padg.am, 1986a, 1986b; Padgham, 1979, 1980, 1985, 1986, 1987a, 1987b, 1987c, 1990), geochemistry (Baragar, 1966; Jenner et al., 1981; Cunningham, 1984; Goodwin, 1988; Atkinson, 1989; Cunningham and Lambert, 1989; Atkinson and Fyfe, 1991), geochronology (Green and Baadsgaard, 1971; Isachsen and Bowering, 1989; Isachsen et al., 1990, 1991a, 1991b; Atkinson and van Breeman, 1990), and mineral deposits (Sproule, 1953; Boyle, 1961; Osantenko, 1971; Jardine, 1974; Breakey, 1975; Myers, 1976; Webb, 1983; Kerrich and Fyfe, 1988; Duke et al., 1990). These papers collectively embody the current understanding of the Yellowknife Greenstone Belt and is synthesised in this thesis. Specific problems and ambiguities are identified and discussed in light of mapping and structural studies completed by the writer over the past 9 years. Possible solutions are suggested.

The structural evolution of the greenstone belt has been addressed to some extent by all of the above authors, with particular contributions by Campbell (1947), Henderson (1970), Tuborg (1975), Kerrich and Allison (1978), Allison and Kerrich (1979), Webb (1984, 1988), Helmstaedt and Bailey (1988) Brown (1989), and Duke et al. (1990). This work is also synthesized, and new observations are incorporated to provide a revised and more precise subdivision of the structural elements within the Yellowknife Greenstone Belt.

The geochemistry of the principal lithologies in the greenstone belt has been studied by several authors who have attempted to characterize the host rocks, identify distinct lithological units or magmatic events, and address the geodynamic environment of the belt (Boyle, 1961; Baragar, 1966; Jenner et al., 1981; Webb, 1983; Cunningham, 1984; Goodwin, 1986; Cunningham and Lambert, 1989). In this thesis, these data are interpreted in light of, and consistent with the existing understanding of the stratigraphy. Additional geochemical data on a newly recognized magmatic event, defined and characterized as a lamprophyre dyke (Webb, 1983; Webb and Kerrich, 1986) is presented in this thesis.

The geochemistry of metasomatism associated with gold-bearing shear zones has been addressed in the published literature by

several authors (Boyle, 1961, 1979; Myers, 1979; Kerrich and Fyfe, 1981; Webb, 1984). This thesis draws upon the above, and unpublished reports (Gill, 1964; Osatenko, 1971; Jardine, 1974, 1975; Myers, 1978, 1979; Gates, 1979; Webb, 1985; Head, 1985; McCartney and Webb, 1986), and extensive new work by the author to characterize the geochemical trends of the metasomatism.

This study examines gold mineralization within the NERCO-Con Mine (Campbell, Con, Negus, and Rycon shear zones) and surrounding area, and addresses the mineralogical, metallurgical, and geochemical zoning patterns that are recognized. These distributions are quantified in terms of primary, and secondary factors, including early synvolcanic, metamorphic and metasomatic, post metamorphic, and late metasomatic alteration. Based on these results the nature and source of fluids, fluid and solute transport, and precipitation mechanisms are discussed and interpreted.

Geochemical studies of the host-rocks and ore samples include whole-rock, trace element, and isotopic analyses. These data are supplemented with petrographic studies of the host-rocks and mineralized samples, and structural measurements collected and compiled over the past 9 years. The data have been processed and analyzed using standard statistical tests and plots. Tests for inter-element correlations, and sample

correlations, enable identification of groups of data that are associated with specific events. The physical and chemical characteristics of the various fluids that are implicated in these events are evaluated on this basis, and probable sources for the fluids are examined. The principal processes involved in the formation of the auriferous quartz veins in Yellowknife are summarized, various genetic models are discussed, and a viable exploration model is proposed.

Recent studies have identified six different varieties of quartz veining at the NERCO-Con Mine, and at least two distinct types of gold ore within the Campbell shear zone. The distribution of both the quartz vein varieties, and the different types of gold ore are domainal, with a systematic or generally predictable spatial distribution within the Campbell shear zone. An ore mineral zoning, from refractory gold ores near surface to free-milling gold ores at depth, has been recognized at the NERCO-Con Mine, and a similar zoning in a somewhat horizontal orientation has previously been documented at the Giant Yellowknife Mine (Breakey, 1975; Myers, 1978; Nikic, pers com., 1982; Webb, 1985, Appendix 2).

A zonal distribution of alteration assemblages has also been described, and several workers speculated on the origin of the zonation (Osatenko, 1971; Jardine, 1974; Breakey, 1975; Myers, 1976, 1978); however, no systematic research had been

completed to document or describe these spatial alteration trends. These trends are presented and discussed, and incorporated into the models presented above.

Chapter 2 of this thesis scribes the general geological relationships of the Yellowknife Greenstone Belt, and Chapter 3 addresses the structural architecture of the belt and detailed structural controls on the mineralization. New geochemical data for a major lamprophyre dyke are reported in Chapter 4, and implications for geodynamic settings and mineralization are discussed. Chapter 5 deals with the geochemistry of chlorite schists as it relates to primary volcanic compositions and secondary alteration, and discusses the spatial distribution of alteration patterns and ore zonation. Stable isotope characteristics of the ore-bearing shear zones are presented in Chapter 6, and a reconnaissance Ar-Ar age study of the mineralizing event(s) is reported in Chapter 7. The results are drawn together to formulate an integrated model for the development of the greenstone belt in the final chapter.

1.1 Location, Access, and Physiography

The city of Yellowknife, located on the west-side of Yellowknife Bay on Great Slave Lake has a population of ≈15,000, serving as the supply, distribution, and administrative centre for much of the western Northwest

Territories.   Yellowknife can be reached by scheduled air service via Edmonton, Winnipeg, or Ottawa, or by an all-weather road from Edmonton, Alberta.

The Slave Structural Province is an Archean terrane encompassing 225,000 km^2 in the northern portion of the Canadian Shield.   The Province is bounded on the west and north by the Proterozoic Bear Province, on the south and east by the Proterozoic Churchill Province, and is covered to the southwest by Paleozoic rocks of the Interior Platform.   The Yellowknife Greenstone Belt lies at the southern edge of the Archean Slave Structural Province (Figure 1).   The greenstone belt extends for approximately 110 km from the north shore of Great Slave Lake up to and including the rocks around Discovery Mine and Nicholas Lake (Figure 2).   It is bounded to the west by granitic terrane, and to the east by sediments of the Yellowknife Supergroup.

The southern third of the greenstone belt is dominated by volcanic rocks, and has been referred to as the Yellowknife volcanic belt (Henderson, 1985).   It is easily accessed by road or boat from Yellowknife, whereas the northern two thirds of the greenstone belt is dominated by sedimentary rocks, and is more readily visited by float- or ski-equipped aircraft. Two winter roads, one up the Yellowknife River system, and another, located to the east, across Gordon Lake and
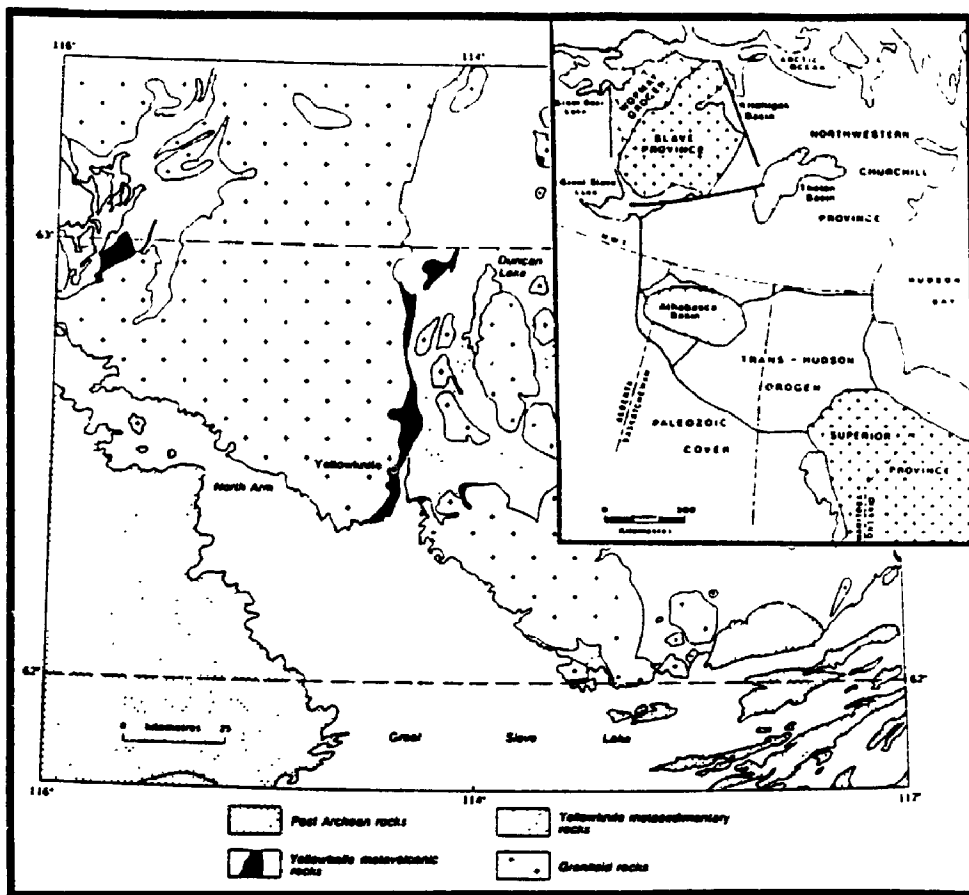
Figure 1. Location of the Yellowknife Greenstone Belt, after Henderson (1985) and Aspler (1988).
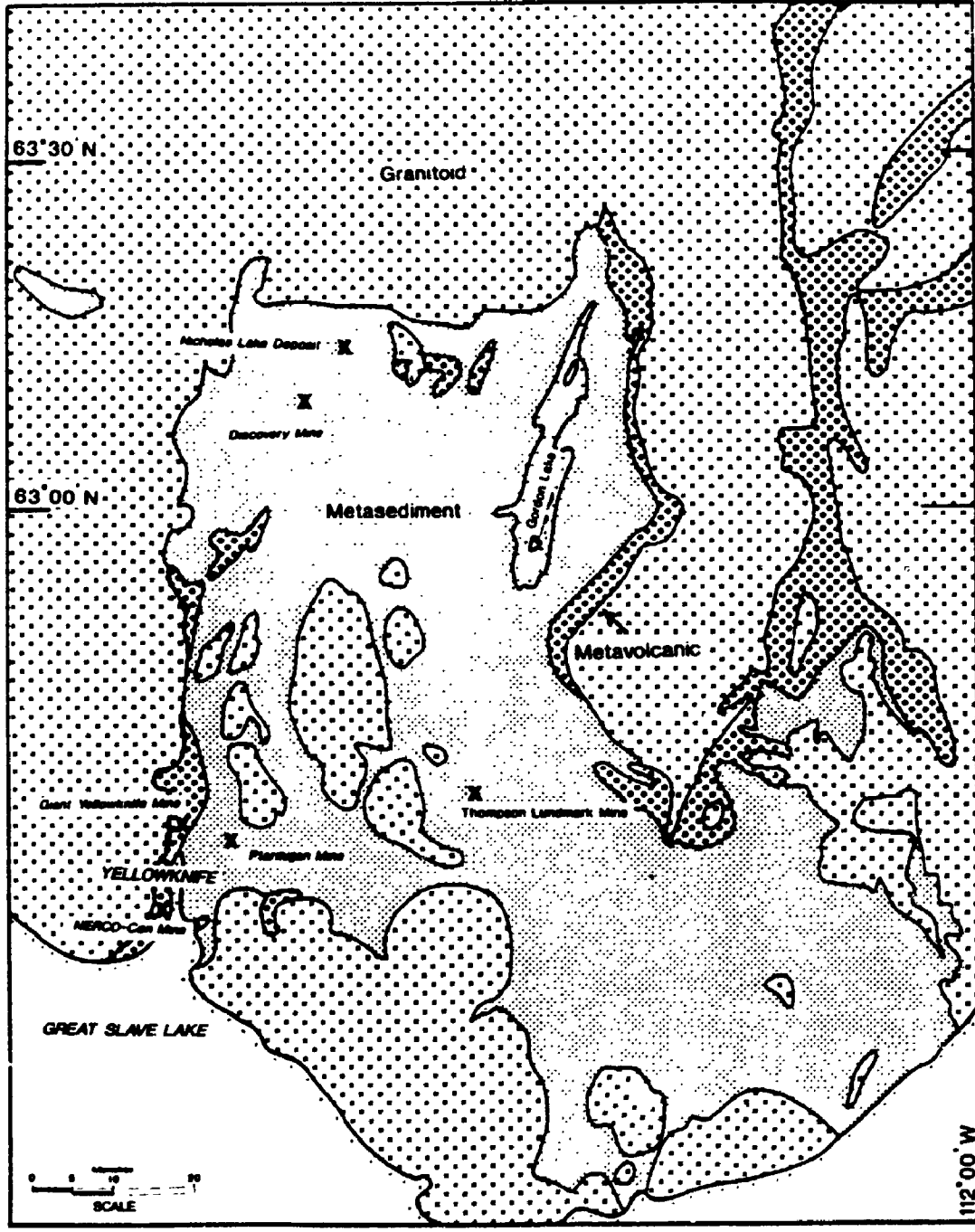
Figure 2. Extent of the Yellowknife Greenstone Belt, on the west-side of the Yellowknife Basin, after Padgham (1987).

Thistlewaite Lake, ⌣vide access to the Discovery Mine site near the north-end of the greenstone belt.

The physiography of the Yellowknife Greenstone Belt includes low rounded hills of outcrop interspersed with shallow lakes and marshes. The lakes are for the most part bordered by swampy terrain with significant areas of outcrop exposed on some lake shores. Vegetation consists of bushes and black spruce in the swampier areas, widely spaced pines trees in the sandy areas, and spruce, aspen, and birch on the outcrops, hills, and flatter-lying areas. The trees are generally stunted compared to their southern counterparts, but larger trees, up to 30 or 40 cm in diameter exist in more protected areas. Outcrop is generally covered by diverse species of moss and lichen, except in an area within 5 to 10 km around the Giant Yellowknife and NERCO-Con mines, where mining and milling activity, including the past and present operation of roasters has eliminated much of the moss and lichen cover.

CHAPTER 2

GENERAL GEOLOGY

2.0 Introduction

The Yellowknife Greenstone Belt has been defined by various workers to include rocks of Division A, B, and C (Jolliffe, 1938, 1946; Hendeson and Brown, 1966), later referred to as part of the Yellowknife Supergroup (Henderson, 1970; Helmstaedt and Padgham, 1986). The belt has not been geographically restricted, although historically studies on the greenstone belt have been restricted to the area west of Yellowknife Bay, and up to 25 km north, immediately west of the Yellowknife River (Boyle, 1961; Henderson and Brown, 1966). Others have considered the Yellowknife Greenstone Belt to extend further north, to latitude 63° north (Hurdle, 1984; Helmstaedt and Padgham, 1986b; Padgham, 1990). In this thesis, the Yellowknife Greenstone Belt will refer to a belt of contiguous or near contiguous volcanic and subvolcanic rocks, and associated sedimentary rocks extending from Great Slave Lake up to and including the rocks around the Discovery Mine, 100 km north of Yellowknife. The southern portion of the greenstone belt encompasses all of the volcanic and associated sedimentary rocks, including the Kam, and Banting Groups, the Jackson Lake Formation, and portions of the Burwash Formation (see Section 2.1), whereas the northern portion is less well studied and is dominated by rocks asigned to the Burwash Formation.

11

The Yellowknife Greenstone Belt is located near the southern margin of the Archean Slave Structural Province (Stockwell, 1962). It extends from under the waters of Great Slave Lake northward to the Discovery Mine area, in a 30 km wide belt of volcanic and sedimentary rocks, with mafic intrusions, and granitoids of stock to batholithic dimensions. The Yellowknife Greenstone Belt is in the western portion of the Yellowknife sedimentary basin, a depositional area bounded by volcanic rocks in the east and west, which in turn are thought to be bounded by older basement terranes (Henderson, 1985). The northern part of the greenstone belt is dominated by sediments, a feature characteristic of many greenstone belts in the Slave Structural Province (Padgham, 1985, 1986). The term greenstone belt is used here in this context; it is recognized that the northern portion of the Yellowknife Greenstone Belt is dominated by sediments, and is defined by The geology of the southern portion of the belt has been more intensively studied, and is summarized below from Henderson (1985) and Helmstaedt and Padgham (1986a).

The Yellowknife Greenstone Belt has been mapped by several workers (Jolliffe, 1938, 1946; Boyle, 1961; Henderson and Brown, 1966), with local contributions on the north-end of the greenstone belt (Yardley, 1949; Tremblay, 1952; Moore et al., 1953; Hauer, 1979; Helmstaedt et al., 1985), the Banting Group (Easton et al., 1980; Pelletier and Wahlroth, 1985; Relf and

Nicholson, 1985; Bailey, 1987), the Chan Formation (Brophy, 1985), Yellowknife Bay Formation (Padgham, 1981; Falck, 1988), and local mine geology (Webb, 1983; Bullis et al., 1987; Lewis, 1987; Duke et al., 1990; Gaucher, 1990) Overviews of the Yellowknife Greenstone Belt are given by Bullis et al. (1987), Helmstaedt and Padgham (1986a, 1986b), and Padgham (1987).

More specific problems have been addressed, including geochronology (Leech, 1966; Green and Baadsgaard, 1971; Nikic et al., 1975, 1980; Gibb and Thomas, 1980; Easton, 1984; Isachsen et al., 1990a, 1990b), structure (Campbell, 1947; Sproule, 1952; Tuborg, 1976; Kerrich and Allison, 1978; Allison and Kerrich, 1979; Webb, 1983), diatremes and lamprophyre dykes (Nikic et al., 1975, 1980; Webb, 1983; Webb and Kerrich, 1987), geochemistry (Osatenko, 1971; Jardine, 1974, 1975; Myers, 1979; Gates, 1981; Jenner et al., 1981; Cunningham, 1984; Goodwin, 1988), and stable isotopes (Chary, 1977; Allison and Kerrich, 1979; Kerrich, 1981; Webb, 1986).

All Archean rocks have been metamorphosed to some degree; the prefix "meta" is omitted for simplicity, but is implicit below for all lithified units.

2.1 Stratigraphy

Stratigraphic nomenclature or subdivisions of the Yellowknife

Greenstone Belt, according to Helmstaedt and Padgham (1986) are given in Figure 3. The greenstone belt is transected by a number of faults, and numerous reconstructions have been proposed to align stratigraphy (Bailey, 1986), major sills (Helmstaedt, 1986b), or structures (Campbell, 1947; Webb, 1983; Bailey and Helmstaedt, 1987). Correlation across these fault blocks affects stratigraphic interpretations, and alternative correlations and stratigraphic reconstructions will be discussed below in Section 2.5.

2.1.1 Basement rocks

The Yellowknife Greenstone Belt is deposited on, or thrust over, a pre-Yellowknife Supergroup basement of sialic rocks. The relevant geochronological data is presented in Table 1.

Basement rocks mapped and recognized to date include gneisses and sediments of the Dwyer Formation, and volcanic and sedimentary rocks of the Octopus Formation. Radiometric ages from detrital zircons from the basement rocks range from 2.9 to >3.7 Ga (U-Pb zircon) from the Dwyer Formation in situ (Isachsen et al., 1991b), and >3.39 Ga (Sm-Nd whole rock) in xenoliths from a lamprophyre dyke at the NERCO-Con Mine (Bibikova et al., 1986).

The Dwyer Formation is a succession of quartz arenite overlain by rhyolite and banded iron formation, structurally underlying
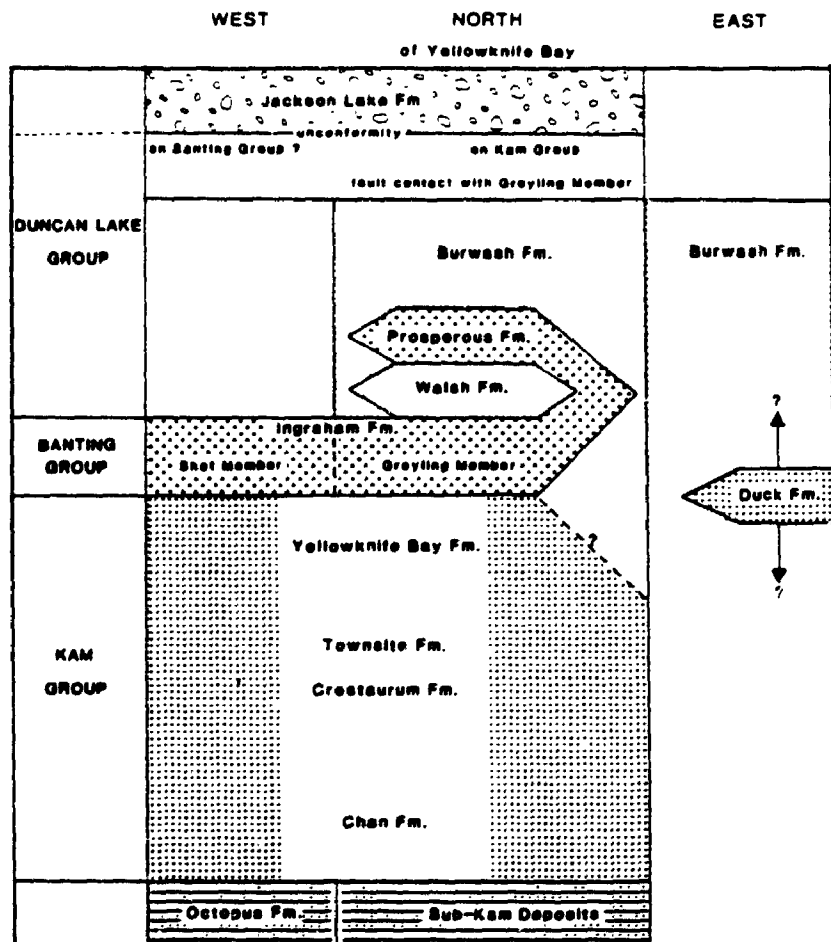
Figure 3. Stratigraphy of the Yellowknife Greenstone Belt
(Helmstaedt and Padgham 1986b).

TABLE 1

DUPLICATE SAMPLES, AND AVERAGE ERROR

Tag	CALCITE $\delta^{18}O$	CALCITE $\delta^{13}C$	Fe-DOLOMITE $\delta^{18}O$	Fe-DOLOMITE $\delta^{13}C$
X1181	7.54	−5.31	8.63	−5.39
X4119	7.88	−4.76	8.99	−5.20
X4120	7.86	−4.03	8.91	−4.54
X1185	8.09	−4.34	8.91	−4.16
X4134	8.36	−5.96	8.63	−6.20
X4121	8.05	−5.68	8.61	−6.42
X4122	8.10	−4.87	8.90	−5.40
X4132	8.30	−4.63	8.93	−5.38
X4126	7.81	−3.39	8.97	−3.78
X4123A	7.95	−3.83	9.33	−3.89
X4123B	8.38	−4.62	9.43	−5.20
X4124	8.49	−5.35	9.50	−5.56
X1190	8.18	−4.21	9.52	−4.09
X1195	8.27	−4.34	9.91	−4.13
X1170			9.59	−4.48
X1196	9.28	−4.21	13.04	−4.18
X144945				
X144913	7.75	−5.43	9.08	
X144910	7.94	−5.15	9.02	−5.42
X144946	8.23	−4.26	8.96	−5.53
X144912	7.93	−4.47	9.03	−4.74
X144947	7.88	−3.88	8.79	−4.89
X144908	8.89	−2.88	9.02	
X144948	8.89	−2.88		
X144909	7.37	−4.36	8.88	−3.95
X144949	7.65	−2.70	8.84	−4.09
AVERAGE ERROR	2.33	12.56	4.33	3.84

$\delta^{18}O$ values in per mil relative to SMOW

$\delta^{13}C$ values in per mil relative to PDB

AVERAGE ERROR is percentage variation

parts of the Kam Group (Isachsen et al., 1991b). Portions of this formation can be traced for over 25 km of strike length, and in one locality is in apparent depositional contact with an older gneissic terrane (Isachsen et al., 1991b). Further north, on the east-side of Nelson Lake, Helmstaedt et al. (1985), McDougall and Goad (1990), and the author, mapped a quartz-rich sedimentary unit, including sporadic chert magnetite iron formation, as conformably overlain by mixed mafic volcanic and turbiditic sediments. Overlying rocks appear to be comparable to portions of the Kam and Duncan Lake Groups.

The Octopus Formation is a sequence of basalts, amphibolites, greywacke, siltstones, conglomerates, and probable felsic pyroclastic rocks within a zone up to 750 m wide (Helmstaedt and Padgham, 1986a; Padgham, pers com., 1992). It is only exposed as xenoliths and septa within the Western Granodiorite, 8 km south-southwest of the NERCO-Con Mine (Helmstaedt et al., 1979; Pelletier and Wahlroth, 1985).

2.1.2 Kam Group

The Kam Group is a sequence of mafic volcanic rocks exposed or projected in a northerly-striking domain encompassing 120 km^2. Sequences of mafic volcanics that cannot directly be correlated with the Kam Group but may be of equivalent age or older have been described 25 km north of Yellowknife, north of

Bluefish Lake, from Quyta Lake, north to Nelson Lake, and northeast to the Discovery Mine (Tremblay, 1952; Helmstaedt et al., 1986; Goad and McDougall, 1986; Gachnauer, 1988).

The Kam Group near Yellowknife contains a tuff horizon that has been dated at 2,704 ±5 Ma (U-Pb zircon; Isachsen et al., 1991a) and is unconformably to conformably overlain by a sequence of calc-alkaline basalts and dacites, epiclastic and pyroclastic rocks, and clastic sediments termed the Banting Group, dated at 2,667 ±4 Ma (U-Pb zircon; Helmstaedt and Padgham, 1986a). A sequence of undifferentiated turbidites (Burwash Formation of the Duncan Lake Group) is coeval with, and conformably overlies the upper portion of the Banting Group, and may in part be coeval with portions of the Kam Group (Padgham 1990).

The Kam Group includes most of the mafic volcanic rocks exposed immediately west of Yellowknife Bay, and the fault-offset equivalents north of the city of Yellowknife. The Kam Group has been subdivided into the Chan, Crestaurum, Townsite, and Yellowknife Bay Formations (Helmstaedt and Padgham, 1986a). The four formations all strike northeasterly, dip steeply to the southeast or northwest, and face consistently to the southeast. All of the formations are dominated by massive, pillowed, or variolitic pillowed mafic flows, and commonly contain thin cherty, tuffaceous or sedimentary

interbeds that can be traced for several kilometres along strike. Many of the correlations between various fault blocks are based upon correlations of these individual flow units and the thin, laterally continuous interbeds. The reconstructed Kam Group has an apparent thickness of 10 to 12 km, and includes many subvolcanic mafic intrusions which appear to form an integral part of the group (Helmstaedt and Padgham, 1986a).

The Chan Formation has an apparent thickness of at least 6 km; however the base of the formation has been intruded and partly assimilated, or is in structural contact with underlying rocks (see 2.1.1 Basement Rocks; Helmstaedt and Padgham, 1986a; Isachsen et al., 1991b). It is exposed 5 km north of the city of Yellowknife near Fred Henne Park (Brophy, 1986) and 12 to 16 km north of the city of Yellowknife. The Chan Formation is composed of pillowed and massive tholeiitic flows; numerous gabbroic dykes, sills, and irregular bodies intrude, and form an integral part of the formation.

Helmstaedt et al. (1986) identified several sheeted dyke complexes within this unit, and Henderson and Brown (1966) recognized numerous gradational relationships between mafic flows and gabbroic intrusions. Much of the Chan Formation has been metamorphosed to amphibolite-grade (Boyle, 1961; Helmstaedt and Padgham, 1986a; Brophy, 1986; Duke et al.,

1990), characterized, but not defined by hornblende, and locally garnet, and the absence of epidote. The rocks are generally black to dark green, and locally have been ductiley deformed.

The Crestaurum Formation conformably overlies the Chan Formation and is characterized by more laterally continuous massive to pillowed mafic tholeiitic volcanic flows, and minor tuffaceous to sedimentary interbeds. It is up to 2 km thick, and is metamorphosed to amphibolite facies in the west to transitional greenschist-amphibolite facies to the east (Boyle, 1961).

The Townsite Formation conformably overlies the Crestaurum Formation. It is up to 550 m thick, and comprises the Townsite flows and related intrusions in the west, and the Brock flows and related intrusions in the east, that can be correlated across the West Bay Fault (Jolliffe, 1938; Boyle, 1961; Henderson and Brown, 1966; Bullis, 1983; Helmstaedt and Padgham, 1986a). The Townsite Formation is composed of calc-alkaline dacite breccias, tuffs, massive and pillowed dacites, and minor andesites (Helmstaedt and Padgham, 1986a; Bullis, 1983). In places the pillowed dacites contain amygdules (Bullis, 1983). Minor variolitic pillowed basalts occur within the more felsic rocks, in thicknesses up to 15 m, however contact relationships are obscured in outcrop (Bullis,

1983). Large gabbro sills, up to 300 m thick, intrude both within and on the contacts of the Townsite Formation (Henderson and Brown, 1966).

Recent geochronological work suggests that the former correlation of this formation across the West Bay Fault may be in error. Data introduced by Isachsen et al. (1991a) indicates that the formation west of the West Bay Fault is 25 Ma younger than its eastern equivalents and an overlying tuff horizon. Alternatively, the zircons that provided the anomalously old ages may be detrital or xenocrystic, as the Townsite Formation includes abundant volcaniclastic rocks (Padgham, pers com., 1992)

The Townsite Formation is conformably overlain by the Yellowknife Bay Formation. According to Helmstaedt and Padgham, (1986a) it consists of 6.5 km of massive, pillowed, and variolitic pillowed tholeiitic basalts, with minor tuffaceous and sedimentary interbeds. The position of the top of the Yellowknife Bay Formation is a subject of controversy. Ac ding to Helmstaedt and Padgham (1986a) the top is 8 km sou... of Yellowknife, near Kam Point, at the Kam Point Sill, and the overlying rocks are part of the Banting Group. Other workers place the rocks immediately overlying the Kam Point Sill with the rest of the Yellowknife Bay Formation as part of the Kam Group (Jenner et al., 1981; Pelletier, 1988; Goodwin,

1988). Helmstaedt and Padgham's (1986a) subdivision is largely based upon gross textural differences between lithological units, whereas Jenner et al. (1981) and Goodwin (1988) formed their subdivision on the basis of geochemical discriminants. This controversy is in part fostered by stratigraphic differences apparent in the two main fault blocks, separated by the West Bay Fault.

2.1.3 Banting Group

The extent of the Banting Group, as currently defined, encompasses an area of approximately 50 km^2. Similar rocks north of Bluefish Lake, 20 km north of Yellowknife, may be correlative with the Banting Group (Helmstaedt et al., 1986; Gochnauer, 1988).

The Banting Group is defined by Henderson (1970) as the rocks between the Yellowknife River and the southern-most bay on Walsh Lake. The Banting Group is discordant in strike to the adjacent Kam Group; however at these localities the Banting and Kam Groups are separated by a postulated fault, and the Jackson Lake Formation (Henderson, 1978; Helmstaedt and Bailey, 1987). The fault may in part be related to the Proterozoic Hay-Duck Fault, dominated by sinistral displacements of unknown magnitude (Helmstaedt and Padgham, 1986a; Bailey, 1987).

The Banting Group is a sequence of bimodal calc-alkaline volcanic flows, tuffs, and subvolcanic sills and dykes, and sediments. It is up to 2 km thick and subdivided into three formations termed the Ingraham, Walsh, and Prosperous Formations in sequence (Helmstaedt and Padgham, 1986a; Padgham, 1986b). The Ingraham Formation consists of two members, the Shot Lake, and Greyling Lake members. The Shot Lake Member is composed of massive rhyolite, mafic flows, crystal tuff, and fragmental flows and breccia with minor conglomerate. A zircon from a quartz-feldspar porphyry that grades from flow to a subvolcanic intrusion in this member yielded an age of 2,667 ±4 Ma (U-Pb zircon; Helmstaedt and Padgham, 1986a). The Greyling Lake Member of the Ingraham Formation is composed of felsic volcaniclastic rocks, overlain by up to 500 m of mafic to intermediate pillowed flows. Rapid facies changes are prevalent, and succeeding intercalated felsic tuffs and mafic flows are conformably overlain by the Walsh Formation.

The Walsh Formation is a sequence of thin-bedded argillites and arenites that overlies the Ingraham Formation volcanic rocks. The Walsh Formation is overlain to the east by the Prosperous Formation, consisting mainly of massive to bedded felsic tuffs, mafic flows and tuffs, and conglomerates. It is conformably overlain, and laterally intercalates with, greywacke-argillite assemblages of the Burwash Formation of

the Duncan Lake Group (Helmstaedt and Padgham, 1986a).

At the north-end of Yellowknife Bay, rocks assigned to the Banting Group by Helmstaedt and Padgham (1986a), are dominantly felsic to intermediate in composition, and are largely conformable to the underlying Kam Group. These rocks are interpreted differently in this thesis, and assigned to the Kam Group, as detailed in the discussion (Section 2.5). They are in a similar stratigraphic position and orientation to the rocks stratigraphically above the Kam Point Sill, and are unconformably overlain by a terrigenous clastic sedimentary unit termed the Jackson Lake Formation.

2.1.4 Duncan Lake Group

The Duncan Lake Group contains the aerially most extensive group of rocks, including all of the rocks overlying the Banting Group, and may in part be laterally equivalent to portions of the Banting and Kam Groups. According to Helmstaedt and Padgham (1986a) the Burwash, Walsh, and Prosperous Formations are part of, or correlative with, the Duncan Lake Group.

The Burwash Formation occupies the largest portion of the Yellowknife Sedimentary Basin by exposure, and is in part included in the Yellowknife Greenstone Belt due to its intercalated relationship with the Banting, and likely Kam

Groups (Helmstaedt and Padgham, 1986a, 1986b; Padgham, 1991)
The Burwash Formation is largely unsubdivided, and consists of
greywacke-argillite assemblages that show most of the
characteristics of Bouma sequences. Accordingly, they are
interpreted as turbidites (Henderson, 1970, 1975, 1986;
Padgham, 1986a, 1986b).

2.1.5 Jackson Lake Formation

A late fluviatile sequence termed the Jackson Lake Formation
postdates all of the above rocks, and has not been assigned to
any group (Helmstaedt and Padgham, 1986a; Padgham, pers com.,
1992). It is considered separately because of the unique
position it holds. It is composed of conglomerates and
sandstones disposed unconformably on the Kam Group, and in
fault contact with the Banting Group. Helmstaedt and Padgham
(1986a) show the Jackson Lake Formation to be in unconformable
contact with the Banting Group at the north-end of Yellowknife
Bay. Interpretation of this exposure is subject to
controversy, as the rocks assigned to the Banting Group may be
disputed (see discussion above). No contact relationships
have been observed with the Burwash Formation, however,
conglomeritic horizons containing granitic cobbles have been
identified within the Burwash Formation along the east shore
of Yellowknife Bay (Henderson, 1985; 1987).

Zircons   extracted   from   clasts   within   Jackson   Lake

conglomerates yield ages as young as 2,605 ±7 Ma (U-Pb), and $^{207}Pb/^{206}Pb$ ages to 2,534 Ma (Green and Baadsgaard, 1971; Easton, 1984; Isachsen et al., 1991a).

2.2 Intrusions

Intrusions in the Yellowknife area have been classified on the basis of composition, geometry and intrusive relationships, and age. This section reviews previous work, largely by Boyle (1961), Henderson and Brown (1966), Leech (1966), and Helmstaedt et al. (1986).

2.2.1 Mafic Dykes and Sills

Numerous .fic dykes and sills of various ages (Leech, 1966) intrude the supracrustal sequence at Yellowknife (Boyle, 1961; Henderson and Brown, 1966). These can generally be subdivided into three groups, as follows: (1) large sills in the lower portion of the Kam Group termed by Henderson and Brown (1966) as unit 7, meta-gabbro sills and irregular intrusions. These were interpreted by Boyle (1961) and Henderson and Brow. (1966) to be pre-shear zone dykes and sills; (2) early synvolcanic intrusions, related to the formation of the Kam Group. These include the sheeted dykes of Helmstaedt et al. (1986), and some of Henderson and Brown's (1966) unit 8, meta-gabbro and meta-diorite; (3) lamprophyre dykes, some with diatreme phases (see chapter 4); and (4) a number of Proterozoic diabase dykes (Leach, 1966). Most of the Archean

dykes are gabbroic with minor dioritic bodies, and show various types of metasomatic effects, some interpreted to be syn-intrusion and others related to post-emplacement events such as gold mineralization (Duke et al., 1990).

The north-northeast orientation of the early dykes was controlled during emplacement by an early extensional setting. Later the dykes were rotated into their present north-northeast to northwest strike during a prograde tectono-metamorphic event (Duke et al., 1990). The majority of the early gabbro dykes in the Crestaurum, Townsite, and Yellowknife Bay formations are subparallel, and represent 10 to 15% of the greenstone belt by volume (Henderson and Brown, 1966; Padgham, pers com., 1992).

Three sets of Proterozoic mafic dykes intrude the Yellowknife Greenstone Belt in the vicinity of Yellowknife (Leech, 1966; Easton, 1985). An east-northeast striking set of diabase dykes, named the Dogrib dykes yield ages of 2,400 ± 200 Ma by the K/Ar whole rock technique (Leech, 1965; McGlynn and Irving, 1975). A second set, the Indin dykes, are diabase dykes generally lacking a magnetic expression, are rare in the Yellowknife area, and strike northeasterly or northwesterly. They have been dated by K/Ar whole rock techniques to yield ages to 2,495 ± 100 Ma (Leech, 1965). A younger, northwest-striking set of diabase dykes with a pronounced magnetic

expression belong to the Mackenzie swarm, are abundant in the Yellowknife area, and have K/Ar whole rock ages of 1,200 ± 100 Ma (Leech, 1965), elsewhere dated at 1,267 ± 2 Ma (LeCheminant and Heaman, 1991).

2.2.2 Felsic Dykes and Plutons

Dykes of intermediate to felsic composition, most abundant north of Giant Yellowknife Mines, intrude all previously described Archean rocks, except the Jackson Lake Formation. Henderson and Brown (1966) refer to these intrusions as unit 9 (porphyritic (quartz-feldspar) leucodacite). A felsic dyke intruded into the Kam Group north of the Giant Yellowknife Mine has been dated at 2,678 ±8.2 Ma (Helmstaedt and Padgham, 1986a). This, and a compositional similarity to the volcanic rocks of the Banting Group suggests a consanguineous relationship (Helmstaedt and Padgham, 1986a).

There is another set of felsic dykes comprised of aplite-pegmatite-quartz veins intrusive into the Yellowknife Greenstone Belt (Atkinson and Fyfe, 1991). This set has been related to a 2,585 to 2,525 Ma event coeval with the development of anatectic granites of the Awry Complex west of Yellowknife and the Prosperous Lake Granite east of Yellowknife. These were emplaced during final closure of the Yellowknife sedimentary basin (Atkinson and van Breeman, 1990; Atkinson and Fyfe, 1991). Within a domain refered to as an

intrusive corridor, felsic dykes with a similar appearance are related to the Stock Lake, and Negus intrusions, considered to be equivalent to the Western Granodiorite of the Western Plutonic Complex (Duke et al., 1990; Duke and McDonald, 1990; Duke et al., 1991).

The Western Plutonic Complex includes part of the Defeat Plutonic Suite, which is comprised of the Western Granodiorite, Southeastern Granodiorite and a number of small related intrusions. The Defeat Plutonic Suite intrudes into the western margin of the Kam Group at Yellowknife and has been referred to as the Western Granodiorite. Southeast of Yellowknife it has been referred to as the Southeastern Granodiorite (Henderson, 1985). The Western Granodiorite, has been dated at 2,620 ±8 Ma (U-Pb zircon; Boyle, 1961; Henderson and Brown, 1966; Helmstaedt and Padgham, 1986a; Henderson et al., 1987). The Southeast Granodiorite intrudes into the greenstone belt from the east and yields a zircon age of 2,618 +7 -20 Ma (U-Pb zircon) (Boyle, 1961; Henderson and Brown, 1966; Henderson et al., 1987).

The Defeat Plutonic Complex consists of a lower and an upper suite of rocks (Atkinson and van Breeman, 1990). The lower suite is composed of a coarse-grained, moderately to strongly deformed tonalite-granodiorite, containing partially

assimilated mafic xenoliths. The upper suite is composed of small intrusive bodies of fine to medium-grained, massive to foliated porphyritic trondhjemite-granodiorite-granite. These rocks are much more homogenous compared to the lower suite, and represent the upper plutonic levels of the Defeat Suite (Atkinson and van Breeman, 1990).

The Awry Complex is composed of massive, heterogeneous medium to coarse-grained leucocratic granitic rocks, and hosts numerous pegmatoid dykes and patches (Henderson, 1985; Atkinson and van Breeman, 1990). Rocks from the Awry Complex are more potassic (5.3% 1.2σ, n=3) compared to those from the Defeat Suite (2.5% 1.1σ, n=11), and hosts patches of bright yellow stains of secondary uranium minerals (Henderson, 1985). This complex has been dated between 2,585 and 2,565 Ma (Atkinson and van Breeman, 1990; Atkinson and Fyfe, 1991).

The Prosperous Lake Granite comprises medium-grained phases of massive biotite-muscovite granites and related pegmatites, intruding Burwash Formation sediments north and east of Yellowknife, and has a Rb-Sr isochron age of 2,520 ±25 Ma (Rb-Sr whole rock; Henderson, 1985). Easton (1984) and Helmstaedt and Padgham (1986a) consider this to be a minimum age, and Atkinson and van Breeman (1990) related the Prosperous Lake Granite to a 2,585 to 2,525 Ma intrusive event, which includes the Awry Complex of the Western Plutonic Complex.

2.3 Structure

Henderson and Brown (1966) and Boyle (1961) subdivided the structures in the Yellowknife Greenstone Belt on the basis of their relationship to Proterozoic diabase dykes. Bullis (1983), Webb (1983), Helmstaedt and Bailey (1986) and others have shown this scheme to oversimplify a complex structural system. This section reviews the current understanding of the structural architecture and development of the Yellowknife Greenstone Belt, and the succeeding section presents the observations and interpretations of this study.

According to Fyson (1982,, Webb (1983), and Henderson (1985), the structure of the Yellowknife Greenstone Belt is distinctly different east and west of the Yellowknife River, coinciding with, and possibly related to, the separation of the volcanic-dominated domain in the west from the sedimentary-dominated domain to the east. It is proposed in this thesis, that the Yellowknife Greenstone Belt be divided into domains possessing generally similar structural features. The southern portion of the Yellowknife Greenstone Belt is therefore subdivided into three structural domains: (1) a volcanic dominated domain west of the West Bay Fault; (2) a domain east of the West Bay Fault, excluding (3) below; and (3) a sedimentary-dominated domain east of the volcanic sequence (Figure 4). The first two structural domains are dominated by brittle and brittle-ductile deformation, whereas the sedimentary-dominated domain

Structural Terrains at Yellowknife
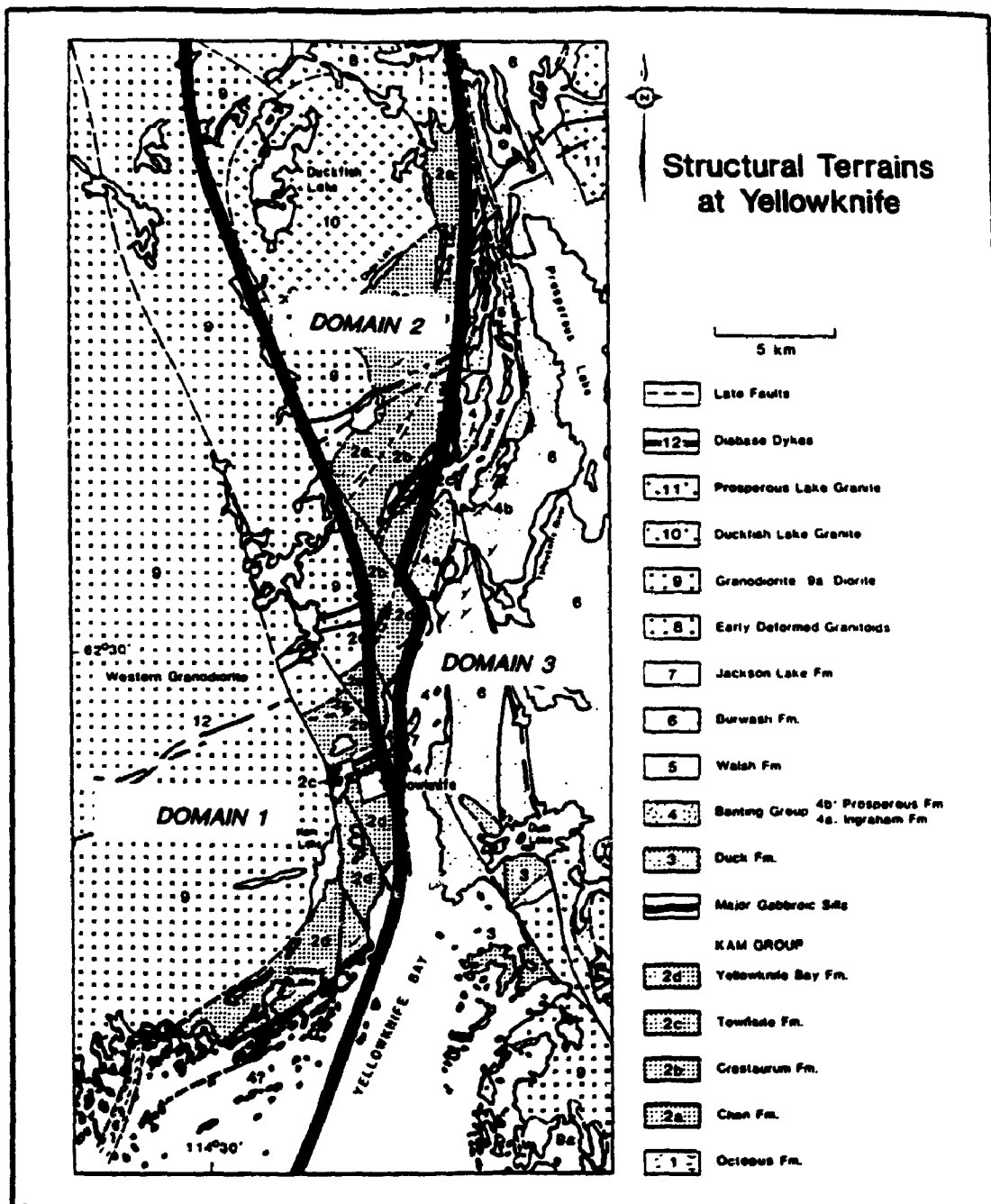
Figure 4. Structural domains in the Yellowknife Greenstone Belt. Base map after Helmstaedt and Padgham (1986b).

is dominated by ductile deformation. This is considered in more detail in Chapter 3.

2.3.1 Early Structures

The Kam and Banting groups are disposed in a north-northeast striking, steeply dipping, southeast facing homocline. Evidence of syndepositional faulting is presented by Bullis (1983) who documented significant stratigraphic thickening across faults in portions of the Yellowknife Bay Formation (see also Padgham, 1980). This stratigraphic thickening is not observed literally within individual fault blocks, nor down dip, nor is it observed at all stratigraphic levels (Bullis, 1983; Webb, 1983). Most of the faults mapped by Bullis (1983) had been reactivated during later tectonic events, and have been presented as Proterozoic faults by Boyle (1961) and Henderson and Brown (1966). Similar faults have been mapped in the Cameron River Greenstone Belt, 200 km east by Fyson (1990).

Boyle (1961) and Henderson and Brown (1966) mapped a series of dominantly north-northeast striking structures in the Kam and Banting groups as early faults. They offset stratigraphy, and all felsic and pre-Proterozoic mafic intrusions. Specific exceptions are documented, and shown on Henderson and Brown's 1966 mapping.

Early faults are generally characterized by the development of chlorite ± sericite ± carbonate schist, and include both short, narrow structures, less than 1 km long, and the large ore-bearing shear zones, in excess of 10 km in length and up to 100 m in width. Most of the early faults are subvertical or dip moderately, and generally possess minor sinistral displacements. They generally dip 50 to 70° W in domain 1, and 30 to 60° E in domain 2. There is evidence of several generations of movement across some of these faults, but rarely extending to post-Proterozoic displacement.

Another type of early structure occurs as a series of regularly distributed close-spaced fractures in the hanging wall rocks of the Campbell Shear Zone (Tuborg, 1975; Webb, 1983, 1987). They have been interpreted to predate mineralization, and are on that basis are considered to be early structures, although they also reveal significant post-mineralization displacements. These fractures are referred to herein as sheeted joints, and although individual offsets are minor, they cumulatively may accommodate over 800 m of dip-slip displacement across zones that may be in excess of 600 m in width (Webb, 1983, 1987).

2.3.2 Late Structures

Several long, northwest striking sinistral faults transect all previously described rock types, and have been termed late

faults (Boyle, 1961; Henderson and Brown, 1966). These regionally extensive structures have been documented throughout the southern Slave Province, and possess displacements up to 4.9 km (Henderson, 1985).

Most prominent in the Yellowknife area are the Kam, Pud, West Bay, Vega, and Madeline faults, with several "crossover" faults, such as the Martin, Townsite, AYE, and Akaitcho faults. These faults are characteristically narrow, vertical zones of fault gouge and breccia. There is evidence that some of these faults, such as the West Bay, Pud and Kam Faults, may be reactivated Archean structures, as recognized by Bullis (1983), Webb (1989). Evidence includes: (1) abrupt stratigraphic changes in thickness and depositional styles across these faults as shown by Henderson and Brown (1966), not otherwise noted down-dip or along strike (Bullis, 1983; Webb, 1989); (2) an apparent spatial control over the localization of mineralization and metasomatic alteration interpreted as Archean in age (Webb, 1989); and (3) cross-cutting relationships with metamorphic isograds related to Archean intrusions (from maps by Boyle, 1961; and Duke et al., 1990).

In summary, there are four principal groups of faults identified in this thesis; type 1 are synvolcanic and account for stratigraphic differences; type 2 are the shear zones, and

are early syntectonic, postdating the metamorphism related to the Western Granodiorite; type 3 are late syntectonic, predating an infered late metamorphic event; and type 4 are Proterozoic, and post date all other structures and metamorphism. This is addressed in more detail in chapter 3.

2.4 Metamorphism

As stated previously, all supracrustal rocks in the Yellowknife Greenstone Belt have been metamorphosed to variable degrees. The distribution of metamorphic facies, from lower greenschist in the east, to upper amphibolite in the west and near the Prosperous Lake Granites reflects the distribution of intrusions within the north-south striking depositional basin. In mafic volcanic rocks the diagnostic mineral assemblages are;

greenschist actinolite, chlorite, albite, leucoxene, quartz, and epidote.

amphibolite hornblende, andesine, sphene, magnetite, ilmenite, quartz and epidote.

Boyle (1961) included the epidote amphibolite facies, defined by actinolite and albite-oligoclase, as intermediate between amphibolite and greensch_st facies. Turner (1981) describes this as the transition between amphibolite and greenschist facies, and it is distinctive only in that it generally possesses both albite and andesine.

In the turbidites the diagnostic mineral of the amphibolite facies is cordierite. All other turbidites with cordierite absent are classified as greenschist facies. In detail however, these rocks are characterized by a range of metamorphic assemblages, in part dependent upon composition, defined by Henderson (1985) as follows;

lower greenschist   quartz, plagioclase, muscovite and chlorite

mid greenschist   the above assemblage plus biotite

upper greenschist   the above assemblage + garnet

lower amphibolite   the above assemblage + cordierite ± garnet ± andalusite

upper amphibolite   the above assemblage ± sillimanite

The presence of chlorite in all assemblages is in part due to its common appearance as a retrograde mineral (Henderson, 1985), and in part due to its stability at different compositions (Dr. N. Duke, pers com., 1992). Staurolite is present in rare instances in amphibolite grade rocks, and its restricted distribution is interpreted to be a function of an iron-rich bulk rock composition as well as metamorphic conditions (Henderson, 1985).

Amphibolite grade rocks are restricted to the margins of the depositional basin or thermal ridges in the central portion of the sedimentary basin (Henderson, 1985). The largest of these thermal ridges occurs 20 km east of Yellowknife and extends

northward for 30 km from the south-end of Prosperous Lake (Henderson, 1985). From mapping and petrography, the author has extended this ridge for an additional 20 km northward. At the north-end of the Yellowknife Greenstone Belt, 100 km north of Yellowknife, sillimanite is abundant in a domain extending for up to 1 km from intrusions within this thermal ridge.

Greenschist facies rocks are distributed throughout the Yellowknife Sedimentary Basin distal from intrusions, with a broad amphibolite-greenschist transition zone identified within the mafic volcanic sequence at Yellowknife. Isograds parallel intrusive contacts, and are thought to be related to the intrusions (Drury, 1977; Henderson, 1985). Overlapping prograde metamorphic facies are apparent in the Yellowknife Sedimentary Basin wherever isograds related to the Defeat Plutonic Suite intersect isograds related to the Prosperous Granite. Intersecting isograds can be observed 50 km east of Yellowknife at Jennejohn and Reid Lakes, and at Buckham Lake, where the amphibolite isograd related to the Defeat Plutonic Complex (2,620 Ma) intersects the amphibolite isograd related to the Prosperous Granite (2,520 Ma) (Henderson, 1985). Intrusions related to these two plutonic events are present in the Western Plutonic Complex west of Yellowknife; therefore it is proposed here, that two metamorphic events may also be present (Atkinson and van Breeman, 1990; Atkinson and Fyfe, 1991). This is considered in more detail below, and in

Chapter 3.

Regional metamorphic assemblages are overprinted by
greenschist facies assemblages related to the ore-bearing
(type 2) shear zones in volcanic rocks at Yellowknife
(Henderson and Brown, 1966; Webb, 1983; Henderson, 1985; Duke
et al., 1990), in sedimentary rocks at Cassidy Point, 15 km
east of Yellowknife, and in some of the late (type 3) faults
in the sedimentary rocks east of Yellowknife such as the
Ptarmigan Fault (Ramsay and Kamineni, 1977; Henderson, 1985).

2.5 Discussion

There is a general consensus regarding the overall
stratigraphic divisions in the Yellowknife Greenstone Belt,
however, significant controversy exists over detail. This
section considers differences of interpretation of the Banting
Group, geochronology, and structural and metamorphic aspects
in light of the author's new mapping and structural
measurements. Figure 5 reveals the location of samples
collected by Goodwin (1986) and Cunningham and Lambert (1989),
and Figure 6 reveals the location of the stratigraphic units
as defined by Helmstaedt and Padgham (1986).

2.5.1 Banting Group

Two major cycles of tholeiitic volcanism are recognized in the
Kam Group, the first culminating in the intermediate to felsic

Townsite Formation, and the second in the intermediate to felsic rocks stratigraphically above the Kam Point Sill (Baragar, 1966; Jenner et al., 1981; Goodwin, 1986).

The Kam Group volcanic sequence, including the Townsite Formation and the rocks on top of the Kam Point Sill, are geochemically similar, characterized by chondrite normalized Yb/La ratios (Yb/La_n) less than or equal to 10, Sm/Yb_n <3, and Zr/Y <8 (Jenner et al., 1981; Goodwin, 1988). The type section of the Banting Group, on the other hand, is characterized by calc-alkaline rocks, with Yb/La_n >30, Sm/Yb_n >8, and Zr/Y >12 (Cunningham, 1984; Goodwin, 1986; Cunningham and Lambert, 1989). This portion of the Banting Group is discordant to the Kam Group.

The Banting Group that underlies the Jackson Lake Formation on the shore at the north-end of Yellowknife Bay (Giant Section), however, is conformable with the Kam Group (Helmstaedt and Padgham, 1986a; Padgham, 1988). Stratigraphically equivalent rocks exposed south of Kam Point are geochemically similar to the Kam Group (Figure 7; Baragar, 1966; Jenner et al., 1981; Cunningham, 1984; Goodwin 1988; Cunningham and Lambert, 1989). Accordingly, it would appear that the rocks stratigraphically beneath the Jackson Lake Formation in the Giant Section, previously assigned to the Banting Group, are part of a more intermediate to felsic cycle of the Kam Group, perhaps
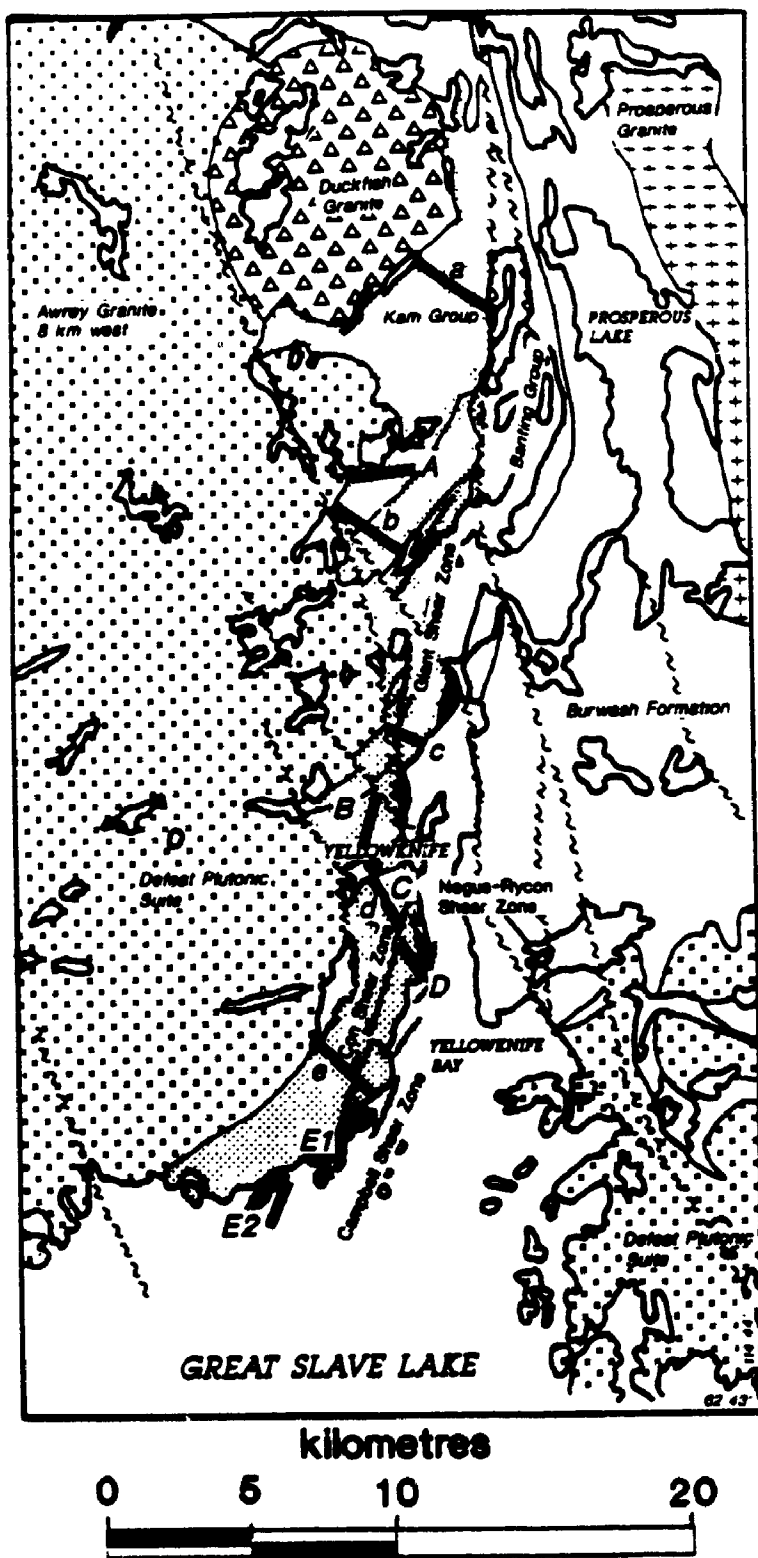
Figure 5. Location of samples collected by Cunningham (1983)
and Cunningham and Lambert (1989) - a to d; and
location of samples collected by Goodwin (1987) -
A to E^2. Base map after Padgham (1990).
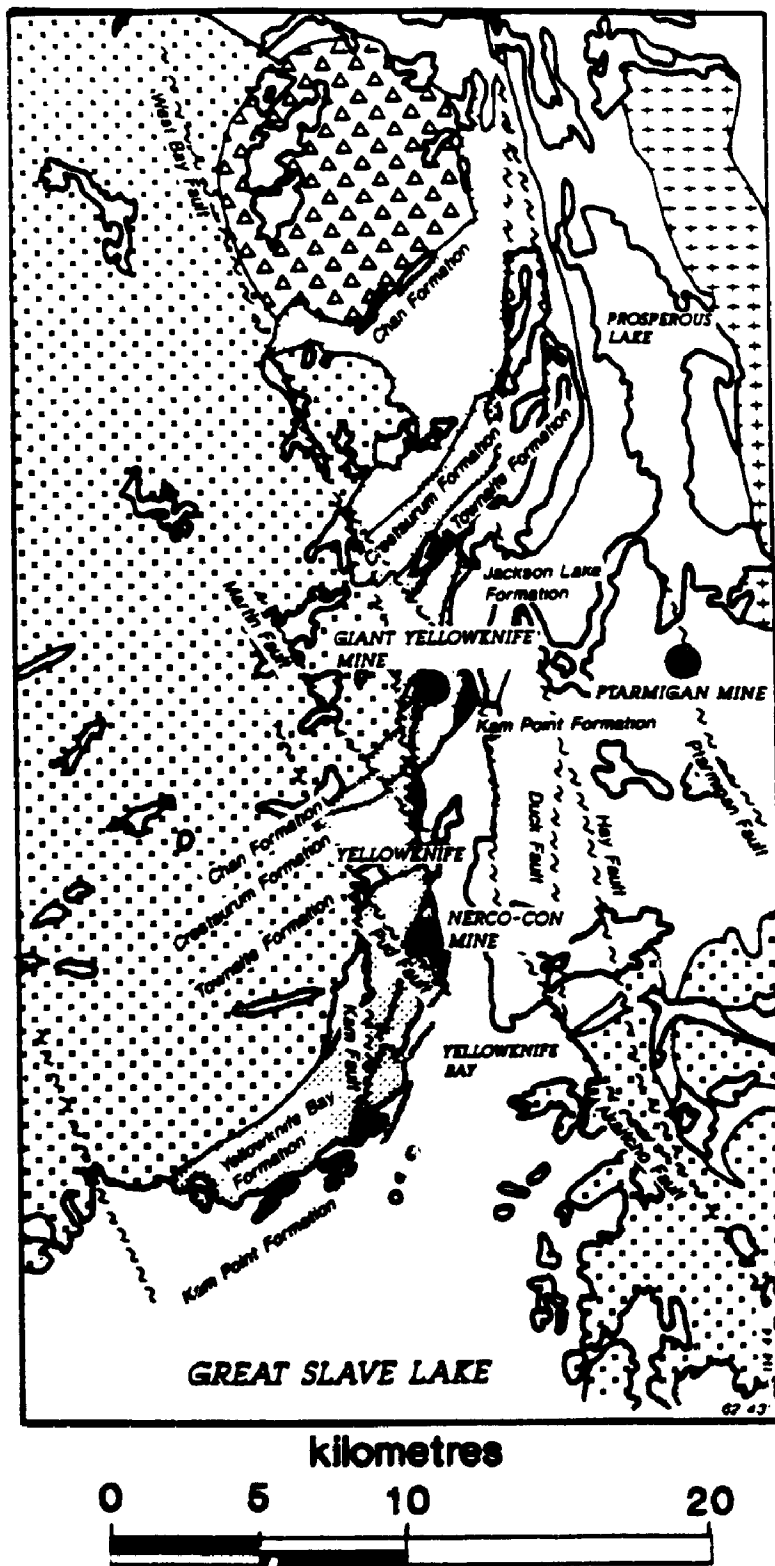
Figure 6. Location of formations within the Kam Group, including the proposed Kam Point Formation, as well as some of the prominant structures within the Yellowknife Greenstone Belt. Base map after Padgham (1990).
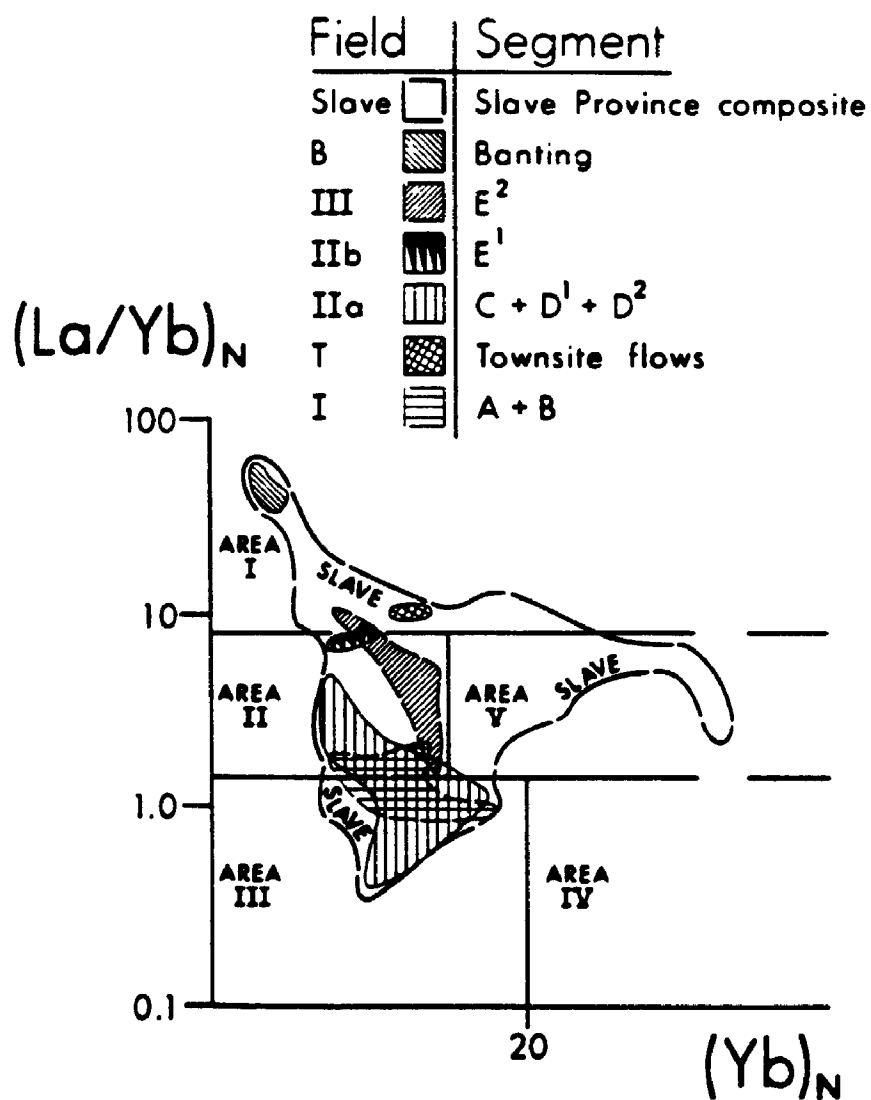
Figure 7. Figure from Goodwin (1987) revealing the rocks from segment E_1 and E_2 to plot within a field similar to rocks from the Kam Group (segments A, B, Townsite Flows, C, D^1 and D^2), distinct from rocks from the Banting Group.

stratigraphically equivalent to rocks south of Kam Point (Helmstaedt and Padgham, 1986a). It is proposed here to rename the rocks south of Kam Point the Kam Point Formation, part of the Kam Group, in reference to its location south of the Kam Point. Rocks mapped on the islands south and southwest of Kam Point may be part of this formation (Pelletier and Wahlroth, 1985; Pelletier, 1988). The intermediate to felsic rocks stratigraphically beneath the Jackson Lake Formation in the Giant Section may be stratigraphic equivalents; the geochemistry of the rocks in the Giant Section may confirm this.

2.5.2 Geochronology

Recent U/Pb ages of 2,704 ± 5 Ma and 2,716 ±9 Ma on zircons extracted from tuffaceous horizons stratigraphically above the Townsite Formation are older than 2,680 to 2,683 ±5 Ma ages for the Townsite Formation (Isachsen et al., 1991a). Samples from the Townsite Formation in a moi ˙ northerly location (Brock Flows) yielded an age of approximately 2,705 Ma (Isachsen et al., 1991a). From this, and other lines of evidence, Isachsen et al. (1991a) suggested that the southern fault segment (Townsite Flows) of the Townsite Formation is a structurally emplaced unit correlative with the Banting Group (2,667 ± 4 Ma; Helmstaedt and Padgham, 1986a). This interpretation ignores stratigraphic correlations based upon detailed lithological and geochemical mapping by numerous workers (Jolliffe, 1938, 1946; Boyle, 1961; Henderson and Brown, 1966; Baragar, 1966; Bullis, 1983; Jenner et al., 1981; Cunningham, 1984; Helmstaedt and Padgham, 1986a; Cunningham and Lambert, 1989; and others).

The age discrepancies are more likely related to detrital or xenocrystic zircons in the tuff rather than the true timing of the igneous event. Webb (1983) identified at least two generations of zircons from tuffaceous horizons in the Kam Group, and Henderson (1985) reported two distinct populations of zircons within the Burwash Formation, which appears to have been deposited contemporaneously with parts of the Kam Group (Helmstaedt and Padgham, 1986a). The dominant set of zircons dates are around 2.7 Ga, whereas a less abundant set is about 2.9 Ga (Henderson, 1985).

2.5.3 Structure and Metamorphism

The structural evolution of the Yellowknife Greenstone Belt is poorly constrained. Rheological differences result in different responses to the same stresses in distinct lithological and metamorphic units, thereby complicating interpretation of the structural patterns. Recent age determinations, and more detailed mapping have helped elucidate the structural architecture and development of the greenstone belt, and this is considered in chapter 3 (Structure).

Metamorphism of the Yellowknife Greenstone Belt constrains the evolutionary models for the belt and the mineralization. The 10 to 12 km apparent thickness of the Kam Group, with greenschist facies conditions from near the base of the sequence to the top, suggests that temperatures and pressures remained below 475 °C and 5 kb (upper greenschist facies, Turner, 1981). For average geotherms of 30 °C and 50 °C per km, and assuming no tectonic thickening, this corresponds to depths of 16 and 10 km respectively. The distribution of the prograde amphibolite facies around the basin margin, and along a central thermal ridge, in zones 2 to 10 km wide, indicates a regional rather than contact-type of metamorphism (Ramsay and Kamineni, 1977; Turner, 1981; Henderson, 1985). The paucity of staurolite in iron-rich sediments, lack of kyanite and the presence of andalusite and sillimanite in the sediments, collectively suggest low pressure metamorphic conditions (Turner, 1981; Henderson, 1985).

There is some evidence for a more complex metamorphic history in the rocks west of the West Bay Fault, and this is considered below.

Metamorphism is related to the felsic plutons, and post-dates all of the supracrustal units, except perhaps the Jackson Lake Formation (Drury, 1977; Henderson, 1985). The Jackson Lake

Formation contains only low-grade metamorphic assemblages (Henderson, 1985) This is true even at the north-end of Jackson Lake where it is bounded to the east and west by amphibolite grade rocks. It is probable that the Jackson Lake Formation post-dated the regional metamorphism, as it includes granitic clasts dated at 2,605 ±7 Ma (U/Pb, zircon; Isachsen et al., 1991a) and 2,534 Ma (Pb/Pb, whole rock; Green and Baadsgaard, 1971; Easton, 1984) derived from intrusions with which the metamorphism has been related. This evidence further confirms Helmstaedt and Padgham's (1986a) assertion of the Jackson Lake Formation's relative age as the youngest supracrustal rocks in the greenstone belt.

Metamorphic isograds within the Kam Group are not offset across the Kam, Pud, Martin, AYE, Townsite, or Akaitcho (type 3) faults (Boyle, 1961), or they show minimal offsets (Duke et al., 1990). In contrast, these faults offset the Western Granodiorite-Kam Group contact by hundreds or thousands of metres. The isograds show significant offsets of hundreds of metres, across the West Bay Fault (type 4). This would suggest that the Kam, Pud, Martin, AYE, Townsite, and Akaitcho faults pre-date peak metamorphic conditions, whereas the majority of the displacement across the Proterozoic West Bay Fault is clearly post-metamorphic. Alternatively, these cross-cutting relationships may be affected by variations in the dip of the isograd, dip slip movement across the faults,

or fluid conditions in part controlled by the faults. Also, it is recognized that defining the position of the isograd is a problem, as bulk rock and mineral chemical differences account for some of the variations in the placement of the isograd.

Both sets of faults offset Dogrib diabase dykes. This apparent age discrepancy, and its significance is considered in the following chapter.

CHAPTER 3

STRUCTURE

3.1 Introduction

The Yellowknife Greenstone Belt hosts three producing mines, the NERCO-Con, Giant Yellowknife, and Ptarmigan Mines, one significant past producer, the Discovery Mine, and many prospects, including the Nicholas Lake deposit. Total cumulative production exceeds 435 tonnes of gold, with current reserves from the three producing mines and one significant prospect exceeding 100 tonnes of gold (Padgham, 1990; Kermeen, 1990; Batchelor, 1990).

All of the economic gold mineralization is structurally controlled, predominantly in brittle-ductile faults or shear zones transecting stratigraphy. The majority of economic mineralization occurs as auriferous quartz veins within the following sets of structures: (1) structures transecting tholeiitic volcanic rocks (NERCO-Con Mine, Giant Yellowknife Mine); (2) structures transecting amphibolite-facies turbidite sediments (Ptarmigan Mine); (3) structures transecting granodiorites within amphibolite-facies turbidites (Nicholas Lake deposit); and (4) isoclinally folded amphibolite-facies sediments (Discovery Mine). Numerous small and subeconomic but often spectacularly rich gold occurrences are found within quartz veins in association with gabbroic dykes and sills

within turbidite sediments of the Burwash Formation. All of these ore-bearing structures are type 2 structures, as described in section 2.3.2.

The mechanics of ductile shear zone development in isotropic material has been well studied (Hobbs and Talbot, 1966; Ramsay, 1967; Tchalenko, 1968; Ramsay and Graham, 1970; Mandl et al., 1977). It is recognised that under conditions dominated by simple shear, rheologically isotropic material behaves in a relatively predictable manner. It develops discrete shear zones of high strain anisotropic material with a systematic geometry, with intervening domains of low strain isotropic material. This geometrical pattern has been applied in economic geology in labelling specific shear or fracture systems, but it has rarely been used as a predictive tool.

An aspect of the deformation within individual structural domains in the Yellowknife Greenstone Belt is that geometric patterns recognized at the kilometre scale are repeated at scales of hundreds of metres, metres, and centimetres (Sproule, 1952; McKinstry, 1953; Boyle, 1961; Henderson and Brown, 1966). However, temporal variations complicate structural patterns that could otherwise be used in a predictive manner. As such, the timing of each event is very critical in interpreting the evolving stress and strain fields.

This chapter attempts to constrain the structural architecture and temporal evolution of structures in the Yellowknife Greenstone Belt and examines the structural features present at Yellowknife in more detail. Various structural elements are identified and labelled according to accepted techniques (Tchalenko, 1968; Ramsay and Huber, 1987). In selected areas, specific structures are examined in detail. Structural observations near the gold deposits are compared with features predicted from theoretical models. The distribution of all orebodies are described within this framework.

3.2   Previous work

Shear zones are anastomosing planar domains of ductile deformation with a continuous displacement field, whereas faults are narrow zones of brittle failure with a discontinuous displacement field (Ramsay, 1980). The transition between brittle and ductile rheological behaviour is a function of strain rate, differential stress, fluid pressure, and temperature, and any structure may undergo transitions between brittle and ductile behaviour as one or more of these variables change magnitude (Fyfe et al., 1978; Poulsen et al., 1988; Kerrich and Fyfe, 1988; Kerrich, 1989; Murphy, 1983).

As described in Chapter 2.3, the southern portion of the Yellowknife Greenstone Belt is subdivided in this thesis, into

three structural domains: (1) a volcanic dominated domain west of the West Bay Fault; (2) a domain east of the West Bay Fault, excluding (3) below; and (3) a sedimentary-dominated domain east of the volcanic sequence (Figure 4; Chapter 2.3). This chapter focuses on the first two domains.

The Kam Group is disposed in a steeply-dipping southward facing homocline west of the West Bay Fault in structural domain 1. The volcanic rocks are intruded by mafic dykes and sills, felsic dykes, and stocks, and an ultramafic lamprophyre dyke. The Western Granodiorite intrudes and bounds the volcanic complex in the west.

Numerous shear zones and faults transect the greenstone belt at Yellowknife. They have been subdivided by Henderson and Brown (1966) into pre-, and post-Proterozoic diabase faults (ca 2,400 Ma). The nature of the pre-diabase deformation appears to be controlled by the metamorphic-grade of the rocks the structures developed in, and thus are syn-, to post-peak metamorphism (Figure 8) (Boyle, 1961; Helmstaedt and Padgham, 1986a; Duke et al., 1990).

Most pre-diabase or early structures are typified by the development of schists, and are broadly speaking ductile structures or shear zones (type 2), whereas the post-diabase or late structures (type 4) and all type 1 and 3 structures
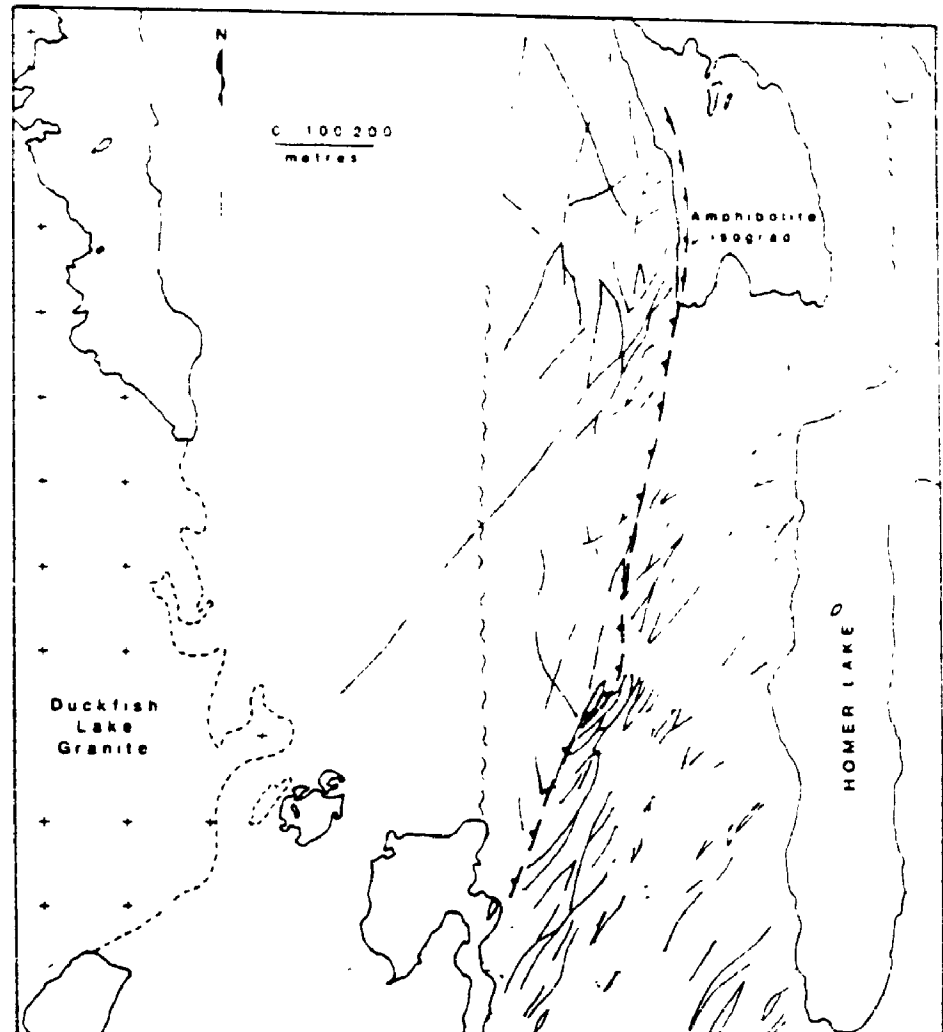
Figure 8. Distribution and geometry of shear zones near the greenschist-amphibolite facies boundary (Helmstaedt and Padgham, 1986b).

are brittle, characterized by cataclasites (as defined by Wise et al., 1984) and have been referred to as faults. All of the auriferous shear zones in Yellowknife belong to the early structural system of ductile shear zones (Boyle, 1961; Henderson and Brown, 1966), although the mineralization is specifically associated with brittle-ductile transitions in the shear zones likely stemming from fluctuations in fluid pressure (Kerrich and Allison, 1977; Allison and Kerrich, 1978; Kerrich and Fyfe, 1987; Brown, 1989; Duke et al., 1990; Goucher, 1990).

3.3 Observations

The structural observations within the Yellowknife Greenstone Belt cannot be accommodated within the existing two-fold (Henderson and Brown, 1966) or three-fold hierarchy (Boyle, 1961). It is proposed here that the general hierarchy by Boyle (1961) be modified to accept the more recent observations of this thesis. Figure 6 reveals the names of some of the structures referred to herein. The often contradictory interpretations with respect to the timing of metamorphism within the Yellowknife Greenstone Belt (see chapter 2) require caution in the application of any structural classification using rigid temporal relationships. In this context, the assumption of general age relationships may be used, and the following system is proposed.

Type 1   Early, brittle structure, may in part be

syndepositional (extensional growth-faults?).
Most of these faults have been reactivated in
subsequent tectonic events (eg. Kam, Pud, West
Bay Faults).

Type 2   Early, ductile structure; commonly post- early
metamorphic, but not syndepositional. These
are pre- mineralization structures, and
include the Con, Campbell, and Giant shear
zones.

Type 3   Late Archean to early Proterozoic, brittle,
pre-, to syn- late metamorphic, syn- to post-
mineralization structures. Commonly
reactivated post-mineralization. Incl des the
Kam, Pud, Martin, Akaitcho faults.

Type 4   Generally late, brittle Proterozoic structure,
includes the West Bay Fault.

All pre-existing structures may be reactivated in subsequent
events, resulting in apparently conflicting age relationships,
such as Bullis's (1981) observation that some late Archean to
Proterozoic (type 3) faults appear to have originally been
syndepositional growth faults. All pre-mineralization
structures may become mineralized or influence mineralization
under favourable structural and chemical conditions

The ore-bearing shear zones are a family of type 2 structures
that have a retrograde mineral assemblage, suggesting a syn-

to post- early metamorphic age. They occupied a favourable structural orientation and provided a chemical environment conducive to the deposition of auriferous quartz veins during an ore-forming event.

Early Faults

Type 1 structures are generally brittle in character, devoid of ductile schist development, S/C structures and stretching lineations (Boyle, 1961), and have been considered synvolcanic (Bullis, 1981). No significant mineralization has been identified in this type of structure.

Type 2 (early ductile shear zones; cf. Boyle, 1961) generally have minor lateral offsets and are dominated by vertical displacements, manifested as a subvertical stretching lineation in the S-C internal fabrics of the shear zones (Campbell, 1947). There is evidence for multiple displacements across some of the Type 2 shear zones (Ransom, 1974; Webb, 1983, 1987; Duke et al., 1990), with several structures exhibiting a late or post-Proterozoic diabase dyke component of displacement (Webb, 1989).

Type 2 structures that generally parallel stratigraphy in strike, also commonly parallel stratigraphy in dip; and those that parallel the early mafic dykes in strike typically parallel the dykes in dip (Number 8 dykes of Henderson and

Brown, 1966). This correlation between the geometry of the early mafic intrusions that cross-cut stratigraphy and the type 2 structures was first recognized by Dr. C.J. Hodgson, (pers. com., 1983).

In domain 2, the dykes and type 2 shear zones generally strike northeasterly and dip moderately to the southeast. In domain 1, west of the West Bay Fault the dykes and type 2 shear zones also strike northeast, but dip 40° to 70° to the northwest. North of the city of Yellowknife in domain 1, however, the dykes and type 2 shear zones (eg. Fox Lake Shear Zone, Brophy, 1987) strike northwesterly and dip steeply to the southwest (Henderson and Brown, 1966).

Ore-bearing shear zones

Many of the ore-bearing shear zones (type 2 structures) have splays and sectors that have received different names. In this chapter these shears will be considered under the most common name. For example, the Con shear zone includes the C4, C31, and C34 shear zones; similarly, shear zones on the Negus property, or Negus shear zones, were renamed Rycon shear zones on the adjacent Rycon property. More recently, individual segments of shear zones have been refered to as shear strands (Duke et al., 1990). Some shear zones were termed veins, eg. the McQueen Vein, in reference to the mineralized portion of

the structure, but they are none the less hosted by ductile shear zones.

Formerly, most of the ore-bearing structures in the Yellowknife area have been called shear zones, or shears, without regard to the structural, temporal, or genetic implications. In structural domain 1, west of the West Bay Fault, these include the Con, Campbell, and Negus-Rycon shear zones. Some well mineralized shear zones that have not produced any ore include the Fox Lake shear zone, and the New and McQueen Veins. These are all type 2 shear zones, and host retrograde mineral assemblages.

In domain 2, east of the West Bay Fault, this class of shear zone is called the Giant Shear Zone, but separately have been referred to as the ASD, GB, HG, Creek, South, East, West, JDB, WJT, North, Muir, Akaitcho, Gold Lake, or Crestaurum zones by Giant Yellowknife Mine's geologists (cf. Lewis, 1987; Goucher, 1990); they are also all type 2 shear zones. Correlation of these shear zones across the West Bay Fault is equivocal, on the basis of geometry, displacement (both magnitude and sense), mineralogy, and geochemistry (Campbell, 1947; Bullis, 1981).

Con Shear Zone

The Con shear zone has been traced for over 4,500 m along strike and to a depth of around 1,500 m. It has not been traced into the West Bay Fault. For the most part, the shear zone strikes 030° dipping 60 to 65° to the west, with an apparent flattening in dip at depth to 45°. It cross-cuts the Yellowknife Bay Formation (Chapter 1). The schistosity within the shear zone strikes 006° and dips 64° west. Structural relationships are summarized in Table 2. There is an apparent horizontal, left-lateral offset of stratigraphy across the Con shear zone, totalling approximately 500 m (Bullis et al., 1987).

The shear zone contains gold lodes distributed sporadically along its length. All of the ore bodies identified to date are located northeast of the Pud Fault and southwest of the northeast end of Rat Lake, a distance of 1,500 m. This productive portion of the shear zone averages 15 m in width, 010° in strike and dips 50° west (Ransom, 1974).

Orebodies occur as prolate ellipsoidal domains of quartz-carbonate veining and silicified sericite-carbonate-sulphide schists, 1 to 12 m wide, 15 to 100 m long, extending down-dip for up to 600 m (Bullis et al., 1987). The orebodies strike on average 007° and dip 54° to the west (Ransom, 1974). Sproule (1952), and Boyle (1961) recognized flexures in the strike of the shear zone, intersections of anastomosing shear

zones, and apices of intervening blocks of unsheared host rock material within the structure as controlling localization of mineralization (Figure 9). The orebodies, and the schistosity strike more northerly and dip steeper than the shear zone as a whole, signifying dextral, west-side up or reverse displacement (Boyle, 1961; Sproule, 1952; Ransom, 1974). This apparent contradiction in displacement with the interpretation of Bullis et al. (1987) may be accounted for by dip-slip movement.

Campbell Shear Zone

The Campbell shear zone has been traced for at least 15 km along strike, and to a depth in excess of 2 km at the NERCO-Con Mine. It strikes variably from 000° to 040°, averaging approximately 030°, dipping 50° west. A horizontal right-lateral offset of stratigraphy is observed across the zone, totalling 740 m (Webb, 1983), and internal shear zone geometry indicates reverse, right-lateral displacement (Ransom, 1974).

The hanging wall of the shear zone is generally well defined, grading from an essentially undeformed basalt to a chlorite-albite schist over approximately 10 cm. Splays of the contact are minor and sparse. The footwall contact of the shear zone is gradational, with abundant and extensive splaying of the structure. To the south, in the upper levels of the productive portion of the Campbell shear zone (upper 100

zone), the footwall contact of the shear zone becomes indistinct, grading over several tens or hundreds of metres into less deformed volcanic units.

The Campbell shear zone is sporadically mineralized throughout its 15 km strike length; however, economically exploitable mineralization is restricted to that portion of the shear zone striking close to 007 degrees.

Recent work in the vicinity of the NERCO-Con Mine, reveals the productive portion of the Campbell Shear Zone to strike 007°, and dip to the west between 50° and 75°, averaging 55°. The schistosity strikes 006°, and dips 60° to 65°, signifying dextral, west-side up displacement (Ransom, 1974) (see Table 2). That part of the shear zone is not continuously mineralized; rather, five discrete ore zones, the 100, 101, 102, 103 and Negus zones are recognized. Other potential ore zones may exist in the Campbell shear zone south of Negus Point, and near Kam Point. Ore zones range from 300 to 800 m in strike length, up to 50 m in width, and extend up to 1,000 m down-dip. They are oriented slightly steeper, and strike more northerly than the shear zone boundary, as is the case for the Con Shear Zone (Figure 10). Orebodies within these zones also reflect this geometry. Each ore zone contains discrete orebodies which in turn are composed of one or more

auriferous quartz veins or domains of silicified schist, somewhat intermediate in strike and dip to the shear zone and schistosity geometries (Figure 11).

Individual quartz veins are typically complexly folded, roudinaged and/or brecciated, and reveal multiple deformation histories (Boyle, 1961; Kerrich and Allison, 1977; Allison and Kerrich, 1978; Webb, 1984; Bullis et al., 1987; Duke et al. 1990). Evidence of this complex localized deformation is largely not expressed in the unsheared Kam Group basalts that are relatively isotropic, but is observed in the sediments, manifest as isoclinal folds in domain 3 (Fyson, 1982, 1990).

An important minor structure identified within the Campbell shear zone is the "footwall roll". This feature is characterized by an asymmetric fold (clockwise, facing north) with a sub-horizontal fold axis (Figure 12). Displacements average 2 to 5 m, and gold contents in this folded portion of the vein are typically enriched by factors of three or more compared to the average for that vein.

Negus-Rycon Shear Zones

The Negus and Rycon shear zones are a group of four or more narrow ductile strictures that lie between the Con and Campbell shear zones. They strike between 165° and 180° and dip 45° to 75° to the west. The shear zones are up to 8 m in

width, but average 1.5 m (Bullis et al., 1987).

Orebodies within these shear zones consist of auriferous quartz and quartz-carbonate veins up to 4 m wide, averaging 0.75 m, up to 120 m in strike length and extend up to 300 m down dip. The shear zones are subparallel to the strike and dip of a swarm of early mafic dykes, and are generally mineralized in places where the shear zones parallel and are bounded, either on the footwall or hanging wall, by one or more of these dykes (Number 8 dykes of Henderson and Brown, 1966).

Other Ore-Bearing Shear Zones

The Fox Lake shear zone is a northwest striking ductile structure, up to 20 m wide, located 5 km northwest of Yellowknife near Fred Henne Park (Brophy, 1987). The shear zone dips to the south-southwest at 50° to 60°, and contains a mineralized zone averaging 2.5 m in width, open along strike and to depth. The shear zone transects amphibolite-grade Chan Formation basalts and sub-parallels the early mafic dykes that transect much of the Yellowknife greenstone belt.

The New and McQueen Veins are mineralized portions of shear zones (Type 2) located immediately north of the Kam Point Sill (Henderson and Brown, 1966). The shear zones parallel stratigraphy in strike and dip, can be traced for 300 and 400

m respectively, and are open in strike. Mineralization consists of auriferous quartz veins approximately 2 m in width, but poorly defined in the strike and down-dip dimensions.

Non-Ore-Bearing Shear Zones

Numerous other type 2 shear zones exist, many of them containing geochemically enriched gold values, sporadically exceeding 5 ppm. For the most part they are less than 300 m long, less than 2 m in width, and either parallel stratigraphy or the early mafic dykes (Number 8 dykes of Henderson and Brown, 1966). When no relative age relationships can be determined, they are normally classified as type 2 by the presence of chlorite or sericite schist (Henderson and Brown, 1966). This includes type 2 and most reactivated type 1 structures.

Some type 2 structures cross-cut the Western Granodiorite in a more brittle manner, and have in the past been grouped with the earliest structures (Henderson and Brown, 1966). These must post-date the intrusion, and some of these structures are mineralized (eg. Rod Claims on the south shore or Martin Lake; see Figure 14), and therefore are classified here as type 2 structures.

Late Faults

Type 3 structures are late syntectonic to post tectonic, pre-late metamorphic faults, and type 4 structures are post tectonic, post-late metamorphic faults. Both types of structures are for the most part vertically oriented, and dominated by strike-slip displacement (Boyle, 1961; Henderson and Brown, 1966). All have been reactivated, and reveal post-Dogrib diabase dyke displacements. Some of the longer structures, such as the West Bay Fault, have strike slip displacements exceeding 4,500 m. The longest late faults strike northwesterly, and are recognized as a distinctive group throughout the southwestern Slave Structural Province (Henderson, 1985; Figure 13). A characteristic feature of these faults is that despite their strike lengths, commonly measured in tens of kilometres, and displacements measured in kilometres, the faults are generally narrow zones of gouge and cataclasite, typically only several centimetres wide.

Boyle (1961) recognized seven major late faults (types 3 and 4) in the Yellowknife area, the Kam-Pud, West Bay, Hay-Duck, Walsh, Ptarmigan, Vega, and Madeline faults, with hundreds of crossover faults, the principal ones being the Martin, Townsite, Negus, Akaitcho, and Duck faults (Figure 14).

Late faults offset all stratigraphic units and all intrusions in the Yellowknife greenstone belt, and are considered to have had final displacement ages between 2.15 and 1.87 Ga (Henderson, 1985). However, with the exception of the West Bay Fault, none of these late faults appear to offset the metamorphic isograds (Figure 15), as mapped by Boyle (1961). Duke et al., (1990) mapped some displacement of the metamorphic facies across these faults, but they show displacements significantly less than the corresponding offset of the Western Granodiorite/Kam Group contact along strike across the same faults. These are type 3 structures. It is recognized that some of the cross-cutting relationships observed between the faults and metamorphic isograds may due to problems in defining the isograd (see Chapter 2) and may not accurately represent true temporal relationships, however, the relationships presented by Boyle (1961) and Duke et al. (1990) are considered to be accurate.

In domain 3, type 3 structures in the Burwash Formation are shown to offset metamorphic isograds related to the Defeat Plutonic Suite, but reveal limited or variable offsets accross isograds related to the Prosperous Granite (Henderson, 1985). Sediments at Jennejohn and Reid Lakes, and at Buckham Lake (domain 3) host two prograde metamorphic assemblages, one related to each of the two intrusive suites in the area (2,620 and 2,525 Ma; Henderson, 1985).

TABLE 2

Summary of structural features within the Con, Campbell, and Negus-Rycon shear zones (Webb, 1984).

SHEAR ZONE	CON	CAMPBELL	NEGUS-RYCON
Strike (ave) Dip (ave) Strike (prod) Dip (prod)	030 60-65W 010 50W	030 60W 007 50W	165-180 45-75W
SCHISTOSITY Strike (prod) Dip (prod)	006 64W	006 60-65W	

ave -average strike for the structure
prod-average strike for the productive portion of
    the structure
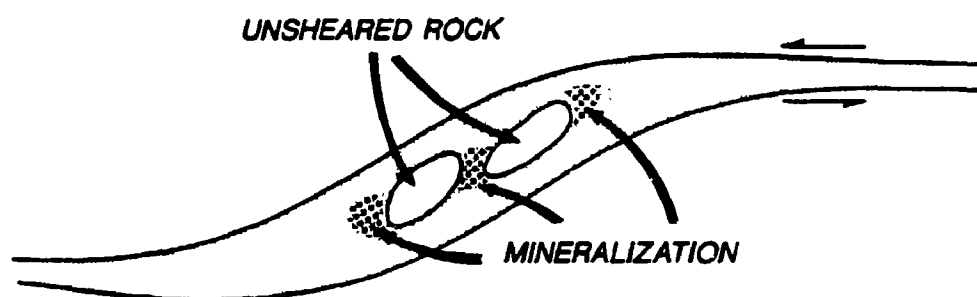
Figure 9. Location of mineralization in relation to unsheared blocks of rock, after Sproule (1953).
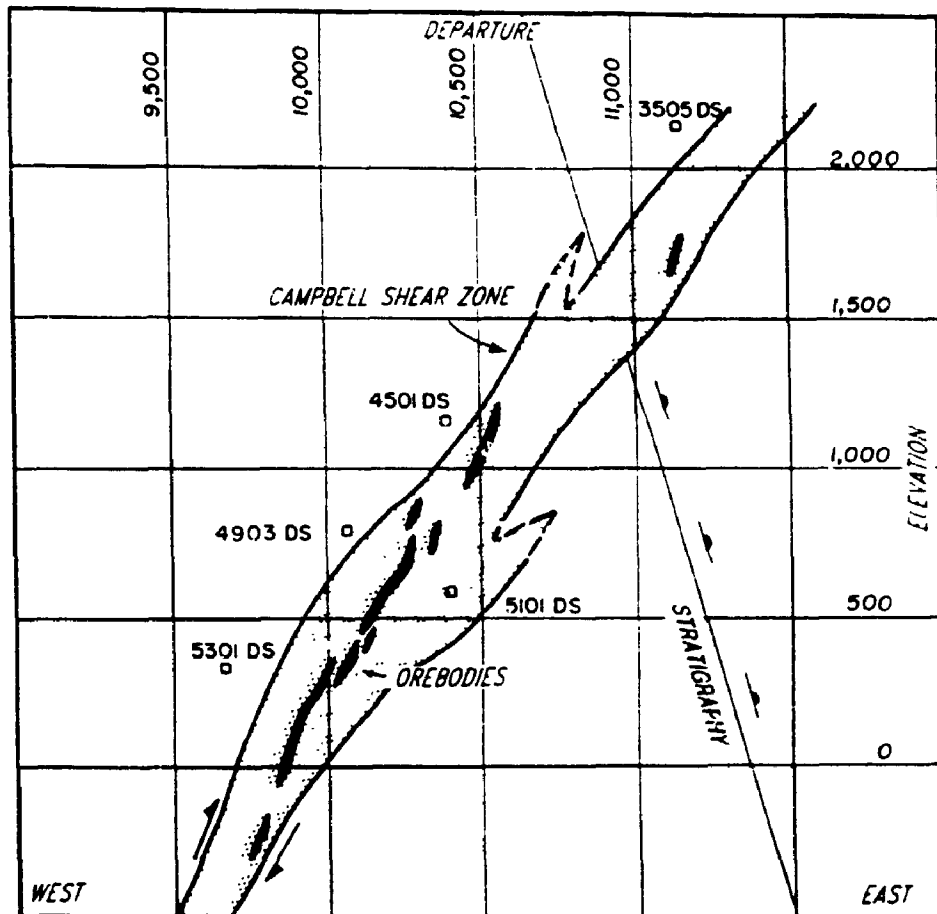
Figure 10. Geometry of gold ore zones within the Campbell
Shear Zone generally transect the shear zone from
footwall to hanging wall with increasing
elevation.
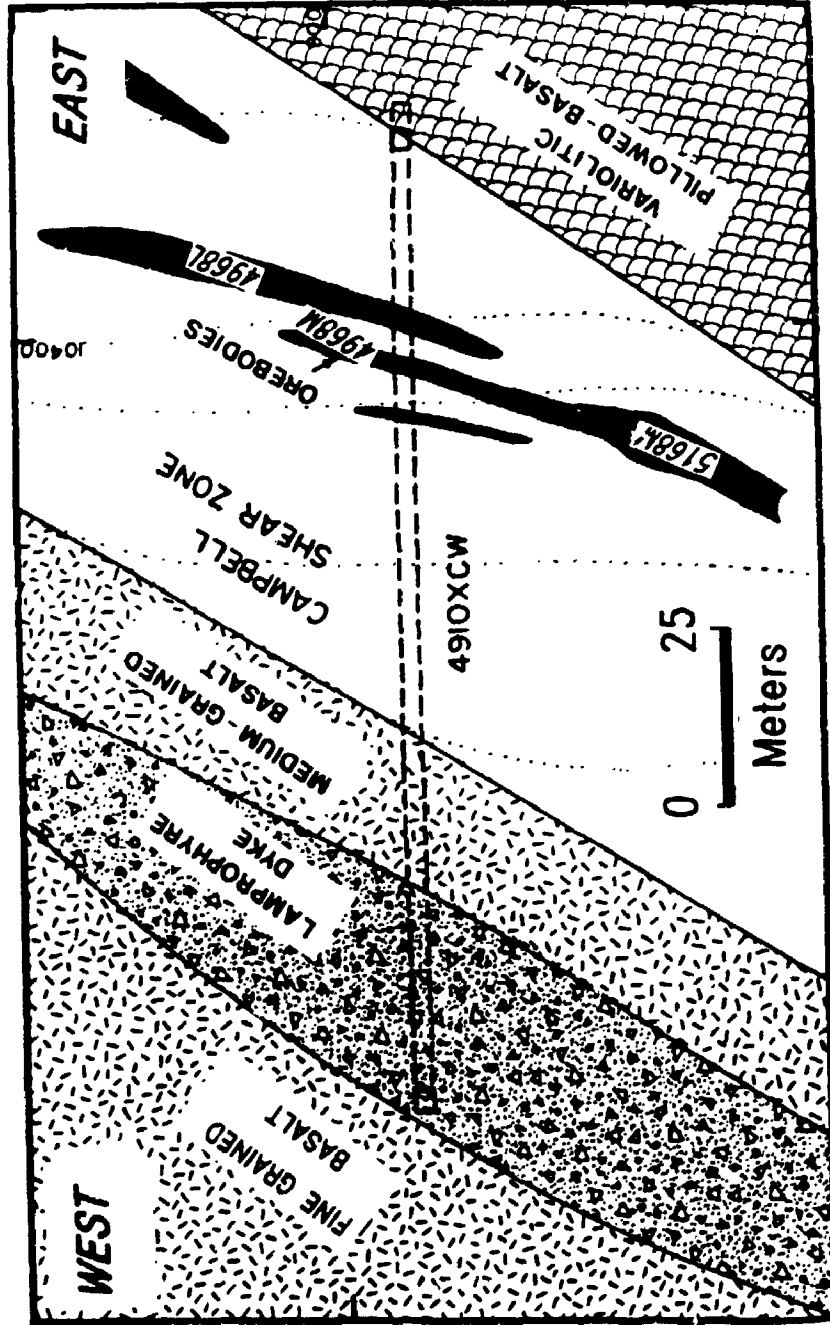
Figure 11. Geometry of gold orebodies within a portion of the 101 ore zone in the Campbell Shear Zone, NERCO-Con Mine. The trace of the schistosity is represented by dotted lines.

June 29, 1983

4785L Slope, Campbell Shear Zone

Chlorite/sericite schist

Auriferous quartz vein

West

East

Broken ore

Scale

0   1

Metres
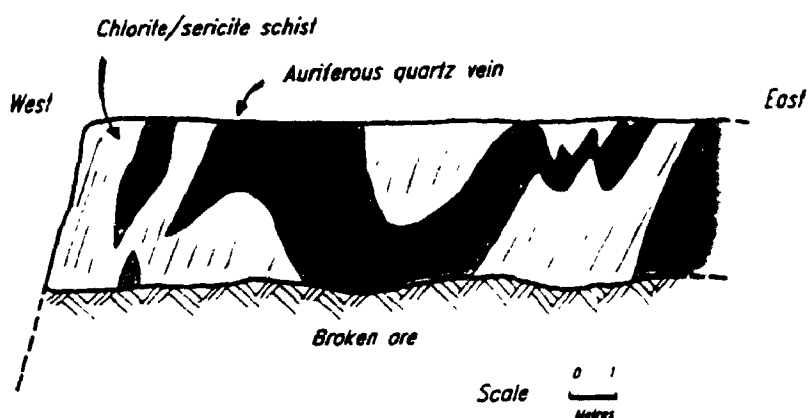
Figure 12. Sketch of a deformed quartz vein, illustrating a
            "footwall roll" geometry from 4785L stope, within
            the Campbell Shear Zone, NERCO-Con Mine.   The
            western limb extends to depth, whereas the
            eastern   limb   extends   upwards.   Gold
            concentrations are commonly enhanced by a factor
            of 2 or 3 across the flatter-lying portion of the
            vein.
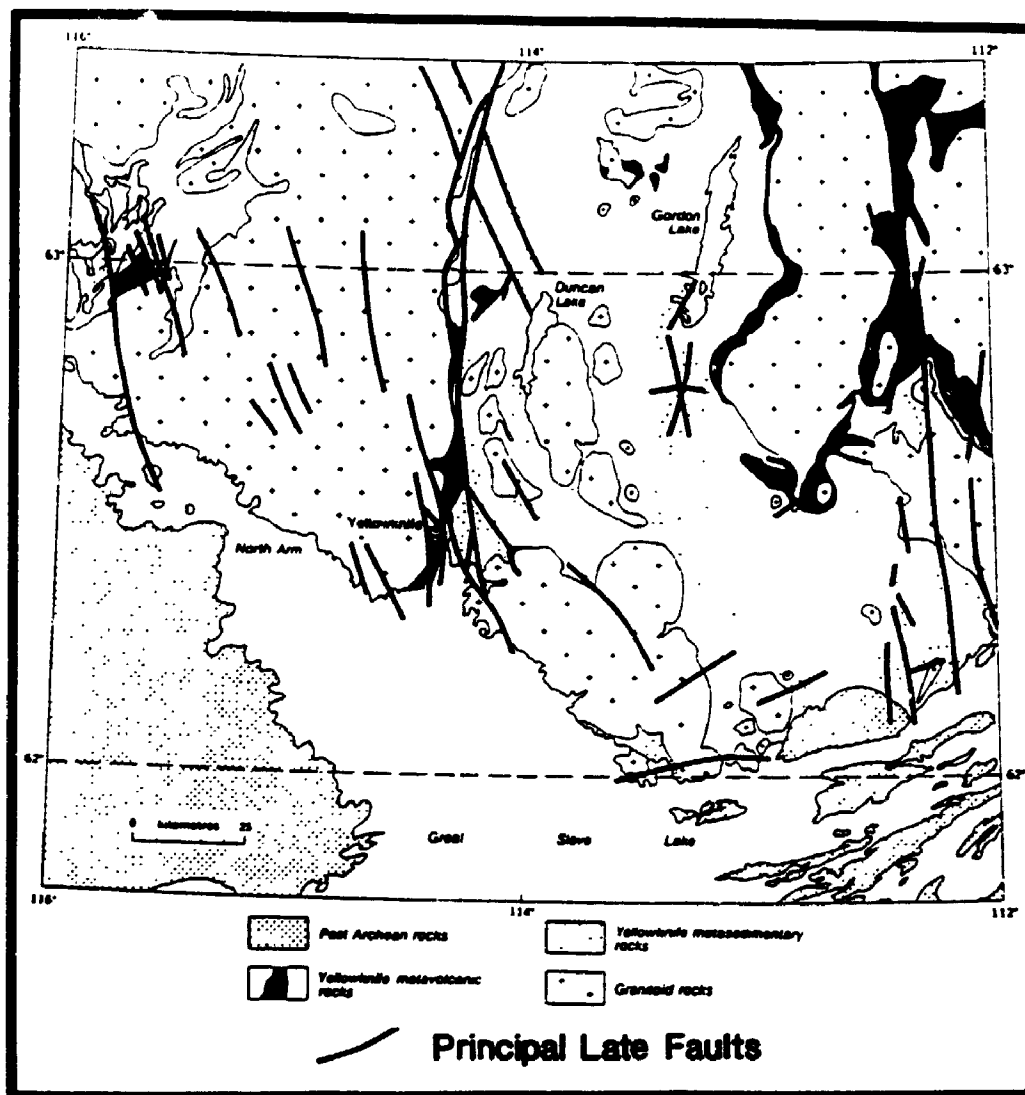
Figure 13. General distribution and orientation of the type
3 and 4 structures, generally possessing
sinistral displacements, in the southern portion
of the Yellowknife Greenstone Belt, after
Henderson (1985).
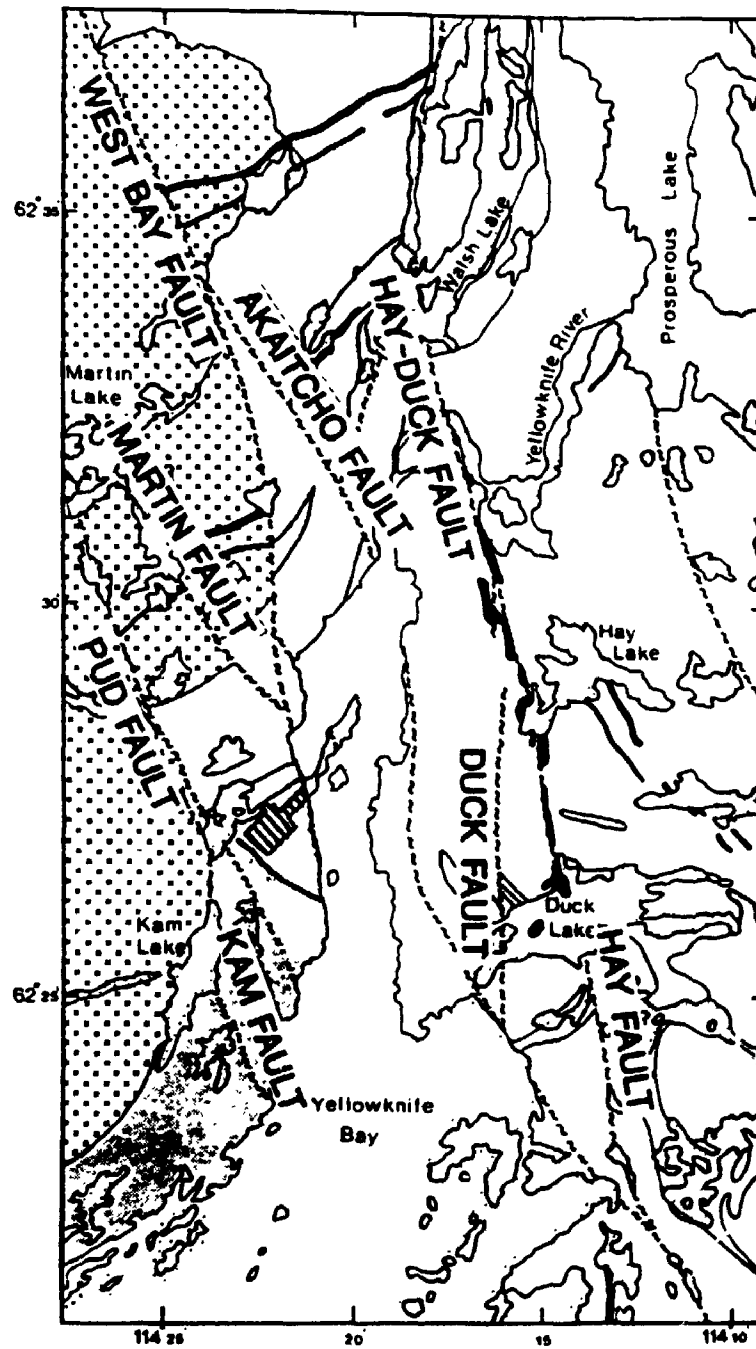
Figure 14. Detailed distribution and orientation, and names of the more prominent type 3 and 4 faults in the southern portion of the Yellowknife Greenstone Belt.
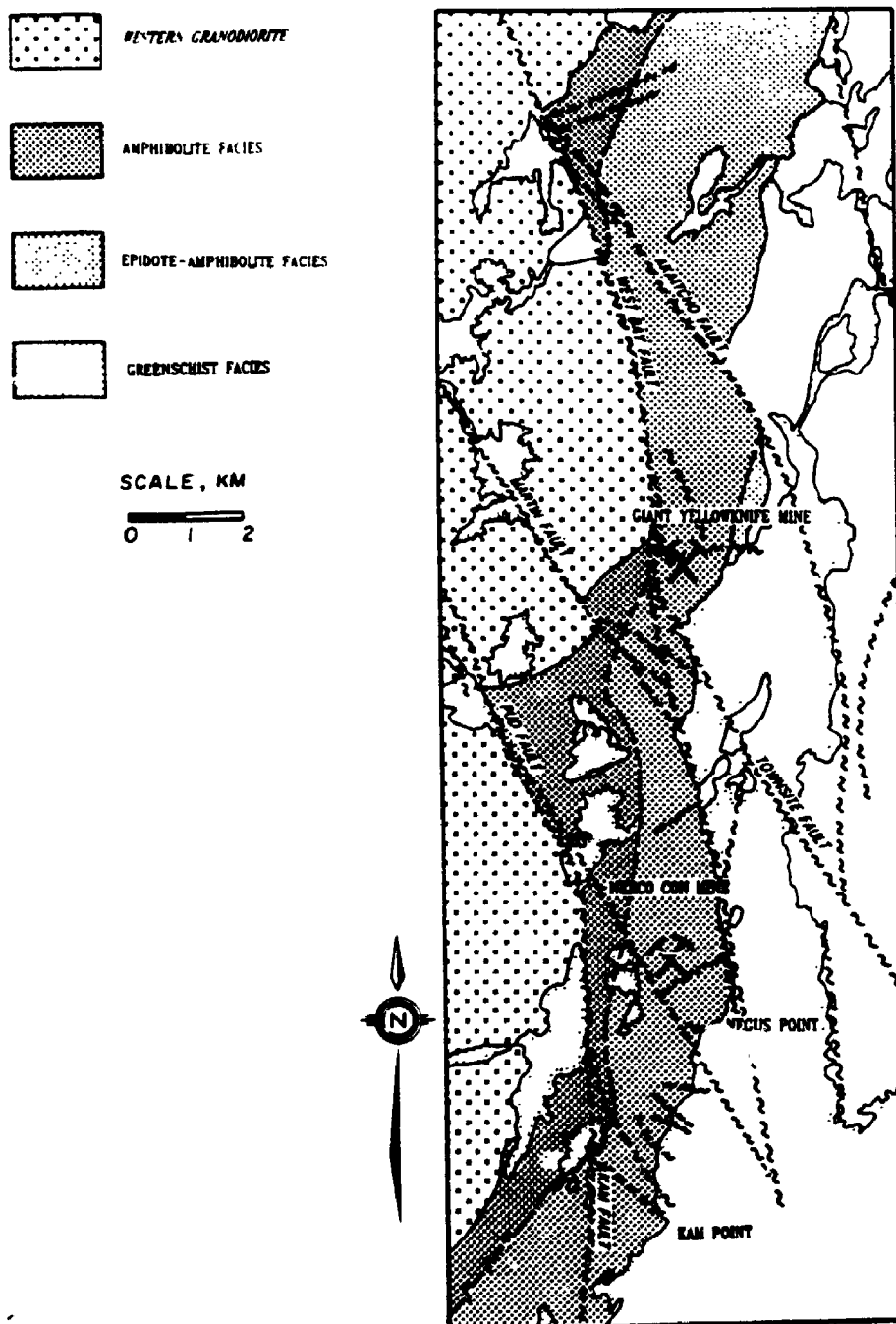
Figure 15. Relationship of type 3 and 4 faults to the
metamorphic isograds mapped by Boyle (1961) and
Duke et al. (1990) at Yellowknife. Note the
minimal offset of the isograd across the Kam, Pud
Martin and Akaitcho Faults, whereas the Western
Granodiorite/Kam Group contact is offset by
hundreds to thousands of metres.

It is suggested that in domains 1 and 2, where a type 3 structure does not offset a metamorphic isograd, that this isograd might be related to a younger intrusion, such as the Awrey Plutonic Suite west of Yellowknife. In this manner, a type 3 structure might not offset a metamorphic isograd in domain 1 or 2, related to a 2,525 to 2,585 Ma intrusion, and yet offset a similar isograd related to a 2,620 Ma intrusion. This is discussed further in the following section.

It is further suggested that there are two, sub parallel metamorphic isograds present at Yellowknife. An early metamorphism related to the Defeat Plutonic Complex predates the type 3 structures and is regional in extent. A late metamorphic event is related to intrusion of the Awery Complex. Some of the isograds may be subparallel to the earlier regional metamorphic isograds. Type 3 structures predate this metamorphic event.

The fault most clearly representing type 4 geometry and temporal relationships is the West Bay Fault, as it offsets all stratigraphy, all other structures, and all metamorphic isograds. It may however be a reactivated segment of an earlier structure.

As mentioned earlier, significant stratigraphic changes have

been mapped across some of the type 1 structures, later reactivated as type 3 and 4 structures. These stratigraphic changes can be observed neither along strike (Boyle, 1961; Baragar, 1966; Henderson and Brown, 1966; Helmstaedt et al., 1979, 1980, 1986; Padgham, 1979, 1980; Bullis, 1983; Cunningham, 1984; Padgham, 1986a, 1986b; Bailey, 1987; Brophy, 1987; Bullis et al., 1987), nor down-dip (Webb, 1984, 1987). These include the progressive thickening of individual flow units (cf. Webb, 1983; Bullis et al., 1987) in successive exposures across type 1 faults, towards the southwest. This was interpreted as evidence of synvolcanic (type 1) structural activity across these faults (Bullis, 1983). All of the faults studied by Bullis (1983) have been reactivated in subsequent events, such that they all possess late Archean to early Proterozoic type 3 and 4 displacements. Based upon this evidence, it is suggested here that some of these faults are type 1 synvolcanic faults that have been reactivated during subsequent events.

There is a distinctive distribution of type 3 and 4 faults within an area bounded by the Kam Fault in the west, and the Vega or Madeline fault to the east that transgresses all of the structural domains. The concentration of type 3 and 4 faults outside of this domain is less than 10% of that within the domain. Essentially 100% of the economic gold mineralization in the Yellowknife Camp is found within this

zone of late faulting. There is a close spatial relationship between the type 3 and 4 faults and all of the gold occurrences within the Yellowknife greenstone belt, although late faults have never been found to contain significant gold mineralization. This apparent age contradiction, of gold mineralization, hosted within pre-mineralization type 2 structures yet spatially related to the type 3 structures that possess post-mineralization displacements is discussed below.

In detail, the Campbell shear zone is most intensely mineralized in portions where the hanging wall rocks are densely cross-cut by late structures, such as at Negus Point, near the Pud Fault, at the Meg Fault, and Kam Fault at Kam Point. These geometric relations define all of the satellite ore zones in the Campbell shear zone outside of the NERCO-Con Mine operations, and the surface projection of the Negus-Campbell ore zone. As well, sheeted joints in the hanging wall of the Campbell shear zone greatly influence the distribution of ore in that part of the Campbell shear zone (Webb, 1983), with perhaps a similar relationship observed in the Con Shear Zone (Armstrong and Duke, 1990; Armstrong, 1991).

An analogous situation exists in the Abitibi Greenstone Belt where Hodgson and Troop (1988) recognized that major gold camps exist where northwest striking Proterozoic faults

intersect the east-west striking ductile Archean shear zones. Kerrich (1989) suggested that the former structures may have been synvolcanic transform faults reactivated in the late Archean and Proterozoic.

3.4 Age-Relationships

The age of each of the sets of structures, their relative geometries, and the timing of the introduction of gold into the system are critical, as shear zones pre-dating or synchronous with mineralization may host significant gold mineralization, whereas those post-dating the mineralization can be expected to be barren, excepting minor post-mineralization redistribution of gold.

The earliest recognized structures are type 1, synvolcanic (2,705 ±4 Ma) growth faults affecting, and in part controlling, the depositional environment of the Kam Group (Bullis, 1983; Fyson and Helmstaedt, 1988; Fyson, 1990). Early ductile type 2 structures cross-cut all lithotypes except the Jackson Lake Formation and the Proterozoic dykes. Mineralized type 2 structures are both affected by, and impose a retrograde mineral assemblage upon the existing metamorphic facies.   These are therefore considered to be post- first metamorphic (<2,620 ±8 Ma), but pre- second metamorphic (ca 2,585 Ma).   The Con and Campbell shear zones, both type 2

shear zones, are cross-cut by Early Proterozoic diabase dykes of the Dogrib and Indin sets with ages of 2.4 ± 0.2 Ga and 2.495 ± 0.1 Ga respectively (see Chapter 2).

The Giant shear zone (type 2 structure) appears to be truncated by the Jackson Lake Formation (which has a maximum age of 2,605 ±7 Ma, or younger at 2534 Ma ($^{207}U/^{206}U$)), although this interpretation is controversial (Helmstaedt and Padgham, 1986a). The shear zones are affected by the metamorphic facies they transect, being best developed within transitional greenschist to amphibolite facies rocks (epidote-amphibolite facies of Boyle, 1961), and generally narrowing rapidly as they transect amphibolite facies rocks (Helmstaedt and Padgham, 1986a; see Figure 8, Section 3.2). They are retrogressive events superimposed upon the metamorphic facies. This indicates that the structures formed post-peak ambient first metamorphism (Allison and Kerrich, 1978; Duke et al., 1990; Armstrong, 1991; Duke and McDonald, 1991), and predate the main gold mineralizing event. If the Giant Shear Zone is truncated by the Jackson Lake Formation which in turn contains cobbles of young (2,605 ±7 Ma to 2,534 Ma) granite, post-dates early metamorphic isograds and is cross-cut by type 3 structures, then the Giant Shear Zone and the mineralizing event are constrained between 2,620 ±8 Ma and 2,534 Ma.

The main mineralizing event at Yellowknife is considered to be

temporally related to the youngest major felsic intrusions in the Western Plutonic Complex, at 2,585 to 2,525 Ma based upon the proximity of the mineralization to these intrusions (Atkinson and van Breeman, 1990). They observed a close spatial relationship between a late felsic intrusive event at 2,525 to 2,585 Ma manifested as mineralogically and chemically similar granitic lenses and discordant dykes within the 2,620 Ma Western Granodiorite, and the Kam Group, cross-cutting hornfelsed metamorphic aureoles. These dykes show phase separations with quartz sulphide-rich veins occurring at higher structural levels, with anomalous As, Au, Cu, Mo, Pb, Sb, and Zn contents. These dykes are spatially associated with all of the gold showings and deposits in the Yellowknife Greenstone Belt (Atkinson and van Breeman, 1990), although this relationship is controversial (Duke, per com., 1992). Atkinson and van Breeman (1990) also note a relationship between a similar felsic intrusive event at 2,520 $\pm$25 Ma represented by the Prosperous Lake Granite, and all of the gold mineralization hosted within the sediments (domain 3). Henderson (1985) reveals that the Awrey Plutonic Suite and the Prosperous Granite are geochemically similar, being the only significant intrusions with 4 to 6 wt% K, <0.3 TiO_2 and common U staining.

From these results, some of the best studied type 2 structures, the ore-bearing shear zones, can be constrained

between 2,620 and 2,585 to 2,525 Ma, the lower age defined independent of the earlier estimate limited by the Jackson Lake Formation (above).

Type 3 and 4 faults transect all rock types, including the Dogrib (2.4 ±0.2 Ga) and Indin (2,495 ±100 Ma) dyke sets, mineralization, but not the late-metamorphic isograds (related to 2,585 to 2,525 Ma intrusions). The constraints on the ages of the dykes is very poor, as indicated by the large errors, but cross-cutting relationships indicate that the Dogrib dykes post-date the late granites. Therefore, the movement across the type 3 structures must have occured very soon after emplacement of the late granite and Dogrib diabase.

As mentioned in Chapter 2, there is evidence to suggest that some of the type 3 structures, such as the Kam, Pud, and Martin, may have also been active during Kam Group deposition (2,705 ±4 M⁻¹. Type 3 faults generally strike northwest, offset rocks and isograds related to the 2,620 Ma Defeat Plutonic Suite but not the late ≈2,525 Ma metamorphic isograds in Domains 1, 2, and 3. There is a distinct spatial relationship on a regional scale between the type 3 structures and mineralization.

Type 4 structures clearly cross-cut all metamorphic isograds and generally strike north-northwest.

An incremental $^{40}Ar/^{39}Ar$ age on a hydrothermal muscovite extracted from an auriferous quartz vein in the Campbell shear zone yielded a disturbed pattern with an upper plateau age of 2,400 Ma, and a secondary plateau corresponding to 2,000 Ma. These ages impact upon the interpretation of the genetic history of the greenstone belt, and are considered in detail in Chapter 7.

3.5 Interpretation

Shear zones and gold mineralization

Ramsay (1980) defined four types of shear zones, ranging from brittle to ductile, defining the brittle class as a special variety where a clear discontinuity exists between the two sides of the zone. The two types of brittle-ductile, and ductile shear zones are of particular interest in this section. Poulsen and Robert (1989, pg 244) defined shear zones as "... narrow, curvilinear displacive zones containing intensely foliated (and lineated) rocks." There are many mechanisms that form shear zones, including extensional and compressional environments (Murphy, 1989).

There is an empirical spatial association of gold deposits to large shear zones, also termed deformation zones, such as the Destor-Porcupine and Kirkland Lake-Larder Lake fault in t ɔ Abitibi Greenstone Belt (Hubert and Marquis, 1989), or second or higher order splays (Kerrich, 1988; Poulsen and Robert,

1989). In addition, there is a propensity for inter-subprovince structures or domain boundaries to be preferentially mineralized in relation to intra-subprovince structures (Kerrich, 1988; Kerrich and Wyman, 1988; Osmani et al., 1989). Inter-subprovince shear zones may be deep-seated, translithospheric structures (Kerrich, 1986, 1988; McNeil and Kerrich, 1986; Wyman and Kerrich, 1988; Hubert and Marquis, 1989). Some feature strike-slip wrench fault displacements or more complex displacement histories (Mueller and Harris, 1987). This geodynamic framework of extensive fault systems dominated by vertical and/or horizontal displacements and related to deep crustal breaks at terrane boundaries may provide an adequate model for some aspects of mesothermal gold deposits (Harris, 1987; Eisenlohr, 1987; Mueller and Harris, 1987; Sibson, 1989; Sibson et al., 1989).

Structures hosting mesothermal gold deposits of all ages have been reinterpreted as terrane boundary faults, or splays of terrane boundaries (Kerrich, 1989; Wyman and Kerrich, 1990).

Gold mineralization in shear zones is most closely related to the presence of quartz veins and silicification. In all cases, this requires a volume increase at the site of deposition, necessitating dilatancy during mineralization. Sibson (1987, 1989) and Sibson et al. (1989) recognized inconsistencies in the interpreted stress fields during shear

zone formation and the dilatancy required during mineralization and reactivation of reverse faults. They proposed a "fault valve" mechanism to accommodate this apparent discrepancy. Shear zones can become dilatant under specific conditions, including;

a)   transtensional or transpressional regimes at jogs or bends in a curviplanar system (Sibson, 1988, 1989), possibly including shear lozenges, and blocks or "horses" of unsheared rock within a shear zone (Sproule, 1952; Boyle, 1961; Hubert and Marquis, 1989).

b)   shear fractures, dilatant C, R, or P shears (Roberts, 1987; Hodgson, 1989).

c)   hydraulic fractures (Kerrich and Allison, 1977; Allison and Kerrich, 1978; Sibson et al., 1989), including extension fractures (Hodgson, 1989).

Shear zone structures and notation

The orientation and sense of displacement that define any structure within a shear zone are not absolute measurements, but are relative measurements (Ramsay and Graham, 1970). Internal fabrics within a shear zone are identified based on

their nature and orientation relative to the bounding margins of the shear zone. Kinematic indicators, such as S-C fabrics, asymmetric augen, boudins etc., by definition, vary within and between shear zones in response to progressive deformation. Measurements of these features have always been considered relative to a rotated Cartesian coordinate system, such that the principal axes are parallel to the shear zone boundary (x), perpendicular to the shear zone boundary (y), and a third axis (z), perpendicular to the first two (Ramsay and Graham, 1970).

Conjugate shear zones develop in different orientations, such that fabrics in one shear zone may not be oriented parllel to fabrics in related shear zones (Beach, 1975, 1977; Hodgson, 1989). To maintain consistency in classifying fabrics, veins, and other structures in different shear zones, a hierarchal notation should be used. For example, a PR-shear should be interpreted as a second-order P-shear relative to a first-order R-shear, and a P'RR' as a third-order P'-shear related to a second-order R-shear, which in turn is related to a first-order R'-shear. For practical purposes, it is unlikely that structures can be sub-divided beyond a third-order, or for that matter, even exist, unless individual shear blocks can be effectively isolated from the regional stress-field.

At Yellowknife, it has been observed that minor structures

within the Campbell Shear Zone appear in a similar orientation
and with the same sense of displacement at different scales
(Figure 16).   This relationship of small scale structures
mirroring larger-scale structures is referred to as fractal
behaviour (Poulsen pers com., 1990).   The diachronous nature
of the shear zones at Yellowknife, with polyphase deformation
of many of the structures, complicates the interpretation of
individual structures.   A single structure may have acted in
several ways.   For example, a PR-shear has a similar geometry
and sense of displacement as a first-order C-shear (Figure
17).   Geometrically there may be little difference between the
two shears, however, it is critical when considering the
overall fluid-dynamics of the system.   R-shears are commonly
dilational features in shear zones (Harris, 1987), whereas C-
shears typically become dilatant at fault-jogs depending on
fluid pressures (Poulsen, 1986; Sibson, 1989).

Shear zone modelling (Tchalenko, 1968; Mandl et al., 1977;
Arch and Maltman, 1988) and fold and geometrical studies
(McKinstry, 1953; Ramsay and Graham, 1970; Beach, 1975, 1977;
Kerrich and Allison, 1977; Allison and Kerrich, 1978; Ramsay,
1979) together with more recent work (Harris, 1987; Eisenlohr,
1987; Skwarnecki, 1987; Bursnall, 1989; Murphy, 1989; Hodgson,
1989; Kerrich, 1989a; Hubert and Marquis, 1989; Osmani et al.,
1989; and Poulsen and Robert, 1989) provide a consistent and
practical guide for the recognition and labelling of shear

zones and associated structures.

Several limiting factors are critical during the progressive development of shear zones, including strain and recovery rates and the effects of temperature, confining pressure, and differential stresses (Kerrich, 1989a; Bursnall, 1989), the interaction of fluids (Sibson, 1987, 1989; Bursnall, 1989), and the rheological properties of the host rocks, including initial and developed anisotropies (Donath, 1961; Kerrich and Allison, 1978; Poulsen and Robert, 1989).

Shear zones at Yellowknife

The structural architecture of the Yellowknife greenstone belt can be considered in relationship to the northwesterly-striking faults as shown in Figure 18. These near vertical faults form left-lateral shear couples, resulting in the interpretation of the other structures.

The majority of the faults and shear zones within the Yellowknife greenstone belt may readily be classified based on these relationships. However, existing anisotropies within the belt, such as stratigraphy at 050° in terrane 1, west of the West Bay Fault, somewhat constrains the development of these faults and shear zones. Examples of anisotropies are the development of the Con and Campbell shear zones, and the lamprophyre dyke at the NERCO-Con Mine, parallel to the early

mafic dyke boundaries. All of the ore-bearing shear zones, which strike within 10° of due north and possess a left-lateral, or reverse sense of displacement are considered to be first-order P-shears. The Negus-Rycon shear zone system may be considered a second-order P-shear, related to a first-order R-shear (Pud Fault). The Fox Lake shear zone is a first-order R-shear, and the New and McQueen veins (shear zones) are stratigraphy parallel right-lateral structures, representing first-order R'-shears.

The distribution of the orebodies in a cross-section of the Campbell shear zone in the NERCO-Con Mine at latitude 16,750, through the 100 Ore Zone reveals a distinct P-shear orientation to the mineralized quartz-carbonate veins and mineralized lenses over a vertical distance of 450 m (see Figure 11). In more detail, the footwall roll feature recognized in individual quartz veins is interpreted to be a dilational jog, more of a primary structure than a deformation feature (Figure 19; cf. Sibson, 1987; Bursnall, 1989; Murphy, 1989).

The S-structure referred to in the inset diagram in Figure 18 is the fold axis predicted in more ductile rocks in the same stress orientation. This may be located east of Yellowknife in structural domain 3, and represented by the Yellowknife syncline, possessing a northeasterly-striking axial plane

Figure 16. Apparent fractal behaviour of mineralized
structures in the Campbell Shear Zone, from
fractions of a metre to hundreds of metres.

WEST   **EAST**
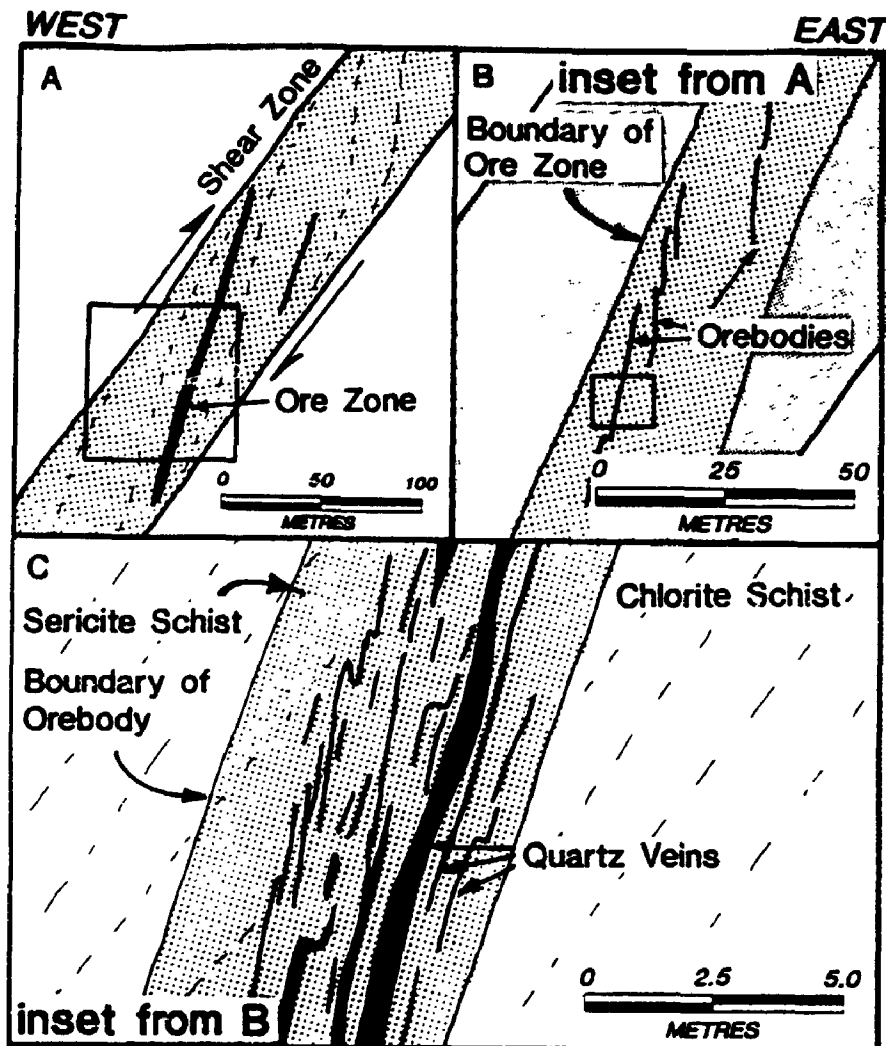
*A. Diagramatic cross-section through the Campbell Shear
Zone illustrating P-shear geometry of ore zone. Trace of
schistosity is shown by dashed lines.*

*B. Distribution of orebodies within an ore zone is shown
to dip at a higher angle than the ore zone in general.*

*C. Quartz veins within a sericite schist envelope cross-
cut schistosity (dashed lines), and generally dip steeper
than the orebody, as hanging wall quartz veins terminate
up-dip, and are replaced by quartz veins on the footwall.*
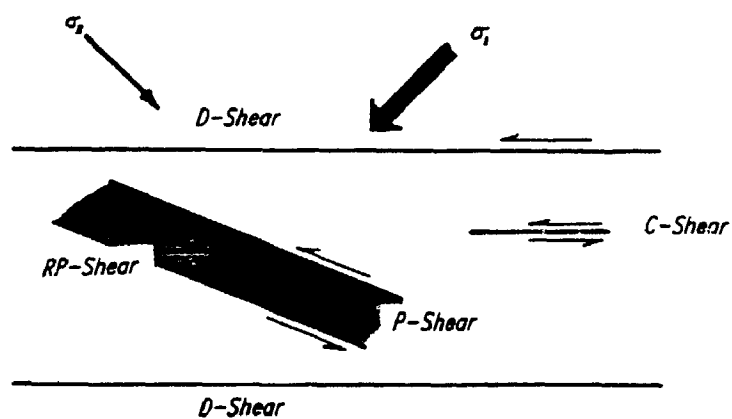
Figure 17. Comparison of two types of structures that may be developed in a shear zone, both revealing sinistral displacements and in a parallel orientation. The maximum compressive stress is illustrated by the dark arrow labelled σ_1.
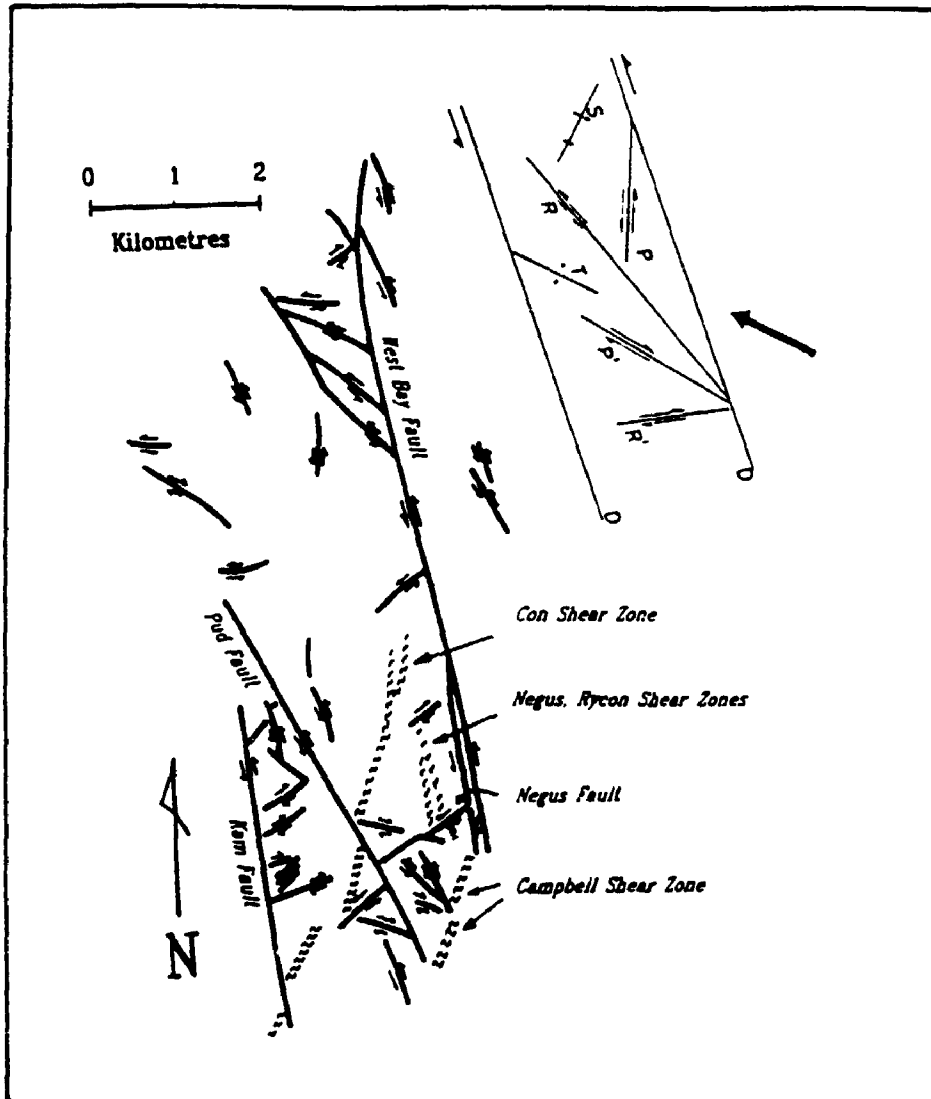
Figure 18. Distribution of the more significant type 3 and 4 shear zones in domain 1 near Yellowknife, with an inset illustrating the nomenclature of the component shear structures (after McKinstry, 1953; Harris, 1987). The maximum compressive stress is interpreted to be from the east-southeast.
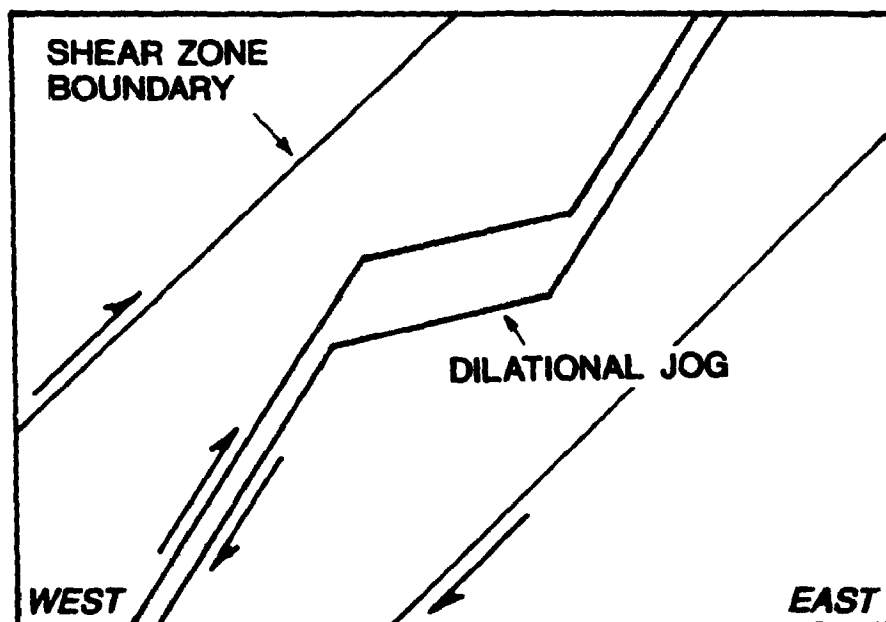
Figure 19. Mineralization in a dilational jog may appear in
a "footwall roll" geometry. Gold concentration
may be intensified in these structures due to
increased pressure fluctuations at these
flexures.

(Henderson, 1970; Fyson, 1982, 1990; Helmstaedt and Padgham, 1986a).

3.6 Discussion

Shear zones and gold mineralization

Most, if not all Archean and younger mesothermal gold deposits have characteristics summarized by Kerrich and Fyfe (1989a, 1989b) which include;

a) Concentration of gold in major transcrustal fracture systems, independent of lithology or stratigraphic position, and,

b) Hydraulic pressure greater than or equal to lithostatic pressure in veins.

Many of the gold deposits in the Abitibi Greenstone Belt in Ontario and Quebec, and the Kalgoorlie-Kambalda area of Western Australia are localized near second-order structures, spatially related to crustal-scale shear zones (Eisenlohr et al., 1989). The large, transcrustal first-order structures are recognized geologically as terrane boundaries, and are expressed by regional topographic or aeromagnetic lineaments (Harris, 1987; Kerrich, 1989; Wyman and Kerrich, 1990). Examples include some of the extensive lineaments within the Pilgangoora area of the Pilbara Block and along the

southwestern margin of the Yilgarn Block of Western Australia (Harris, 1987). Structures exceed 200 km in strike-length, and often transect greenstone belts, although they may, in part, parallel stratigraphic trends.

First-order structures may in part be reactivated synvolcanic structures, and appear to control the distribution of deep crustal felsic magmas, and mantle-derived lamprophyre dykes (McNeil and Kerrich, 1986; Webb and Kerrich, 1988; Eisenlohr et al., 1989). The final major displacement of these first-order structures occurs late in the development of the Yellowknife Greenstone Belt (West Bay, Hay-Duck Faults), and in the Abitibi and Norseman-Wiluna greenstone belts. In all three cases this displacement post-dates the regional metamorphism likely due to thermal rebound following terrane collision (Wyman and Kerrich, 1988; Eisenlohr et al., 1989).

Second-order structures, which host much of the mineralization in these greenstone belts are related to the first-order structures, and may be considered within a regional stress field (Eisenlohr et al., 1989). Eisenlohr et al. (1989) presented several possible controls on the localization of mineralization within second-order structures, such as temperature gradients and various physio-chemical factors including wall rock redox state. Alternately, the localization in second order splays stems from streaming of

fluids from the ductile first order structures into second order splays that experienced fluid pressure fluctuations by seismic-aseismic transitions (Kerrich and Fyfe, 1988; Kerrich, 1989; Duke et al., 1990).

Age of Yellowknife Structures

The age of the early structures in the Yellowknife Greenstone Belt (type 1, and 2) has in the past, been related to a discrete episode related to the intruding granites, either directly (Sproule, 1952) or to metamorphism related to the granites (Allison and Kerrich, 1978). The late faults (type 3 and 4) had been grouped as a single, Proterozoic event. Evidence cited here, and by Fyson (1990) reveals that many of the type 1, 2, 3 or 4 structures possess protracted historys of movement, such that "late" faults can be demonstrated to be reactivated Archean structures, and "early" structures can generally be shown to have been reactivated at a later time, and that it is likely that there has been two prograde metamorphic events related to two different suites of granites.

Most apparent at Yellowknife is the negligible offset of the regional metamorphic facies, which are related to an Archean intrusive event across type 3 faults that induced significant offsets of Archean lithological boundaries. Also recognized is evidence of Archean precursors of some of these type 3 and

4 faults (bullis, 1983), and the close spatial association of mineralization to the intersection of these type 3 structures and type 2 Archean shear zones. It would appear that many of these structures have an overlapping history, and that some of this overlapping history is only apparent, related to multiple plutonic and metamorphic events, where formerly a single metamorphic event had been assumed.

Structural controls on gold mineralization at Yellowknife

The northwest-striking left-lateral type 3 and 4 fault system, including the West Bay, Martin, Pud, Akaitcho, and Hay-Duck faults, is the most prominent fracture system in the southern part of the Slave Structural Province (Henderson, 1985). In this thesis, these structures are interpreted to be related to a major transcrustal fracture system to which first, the extensional Yellowknife depositional basin and second, the compressional shear zone-hosted gold deposits are related (Fyson and Helmstaedt, 1988; Fyson, 1990).

Type 3 structures have the following characteristics: they, (1) exist in an orientation compatible with a simple shear model based on the northwest-striking left-lateral fault systems; (2) are in part contemporaneous with a metamorphic event which is temporally and spatially related to mineralization in type 2 structures; and (3) are spatially related to all of the significant gold deposits within the

Yellowknife Greenstone Belt. From the results of this study, type 3 structures were present and influenceu the localization of mineralization in type 2 structures, but possessed a structural orientation not amenable to host mineralization. Mineralization was localized in type 2 shear zones near type 3 faults because of the structural discontinuities induced at the intersection of these two structures. Subsequent reactivation of type 3 structures offset mineralization. The more significant gold deposits in the Yellowknife Greenstone Belt are shown on Table 3.

All of the ore zones in the type 2 Con, Campbell, Negus, Rycon, and Giant ductile shear zones are spatially related to type 3 brittle structures (Figure 20). The bulk of the reserves and past production comes from these type 2 shear zones in a region between the Akaitcho and the AYE (type 3) faults in the case of the Giant shear zones, and Martin and the Pud (type 3) faults in the case of the Con, Campbell, Negus, and Rycon shear zones. There is however, no significant gold mineralization directly in any of the type 3, northwest-striking late structures.

All of the type 2 ore-bearing shear zones at Yellowknife are in an approximate P-shear geometry ($\approx$005°) relative to the type 3 faults (345°). The shear zones are curvilinear, and the portion of the structure that best conforms to the P-shear

orientation, approximately 007° at Yellowknife, hosts all of the known ore zones. These ore zones are distributed in a P-shear geometry within the shear zone, and most of the orebodies are distributed in a P-shear geometry. Individual auriferous veins commonly show evidence of hydraulic fracturing.

The distribution of ore within the GB ore zone in the Giant shear zone at the Giant Yellowknife Mine is found in a structurally more complicated shear zone; however, a P-shear geometry is apparent for much of this mineralization, as shown in Figure 21. Figure 22 from Andrews et al. (1986) reveals the P-shear orientation of the ore-veins in the Campbell-A.W. White ore complex in Red Lake, a feature also clearly illustrated at the Madsen Mine in Red Lake in Figure 23 from Hodgson (1989).

The P-shear is a structure that occurs in brittle-ductile shear zones after a passive ductile state is achieved (Harris, 1987). These fractures will become dilatant under conditions of high fluid pressures, a condition recognized in many Archean-hosted gold deposits, including those at Yellowknife (Kerrich and Fyfe, 1989a; Kerrich and Allison, 1978; Sibson et al., 1988; Poulsen and Robert, 1989; Andrews et al., 1986; Brown, 1989).

TABLE 3

Tonnage and Grade of Some of the Significant Gold Deposits in the Yellowknife Greenstone Belt.

DEPOSIT	TONS	GRADE (OUNCES OF GOLD PER TON)
Nicholas Lake		
Deposit	1,200,000	0.422 (reserves)
Discovery Mine	1,019,326	1.004 (past production)
Giant Yellowknife		
Mine	16,150,000	0.487 (reserves and past production)
NERCO-Con Mine	10,140,000	0.492 (reserves and past production)
Negus-Rycon Mine	375,000	0.77 (past production)
Ptarmigan Mine	328,000	0.310 (reserves and past production)
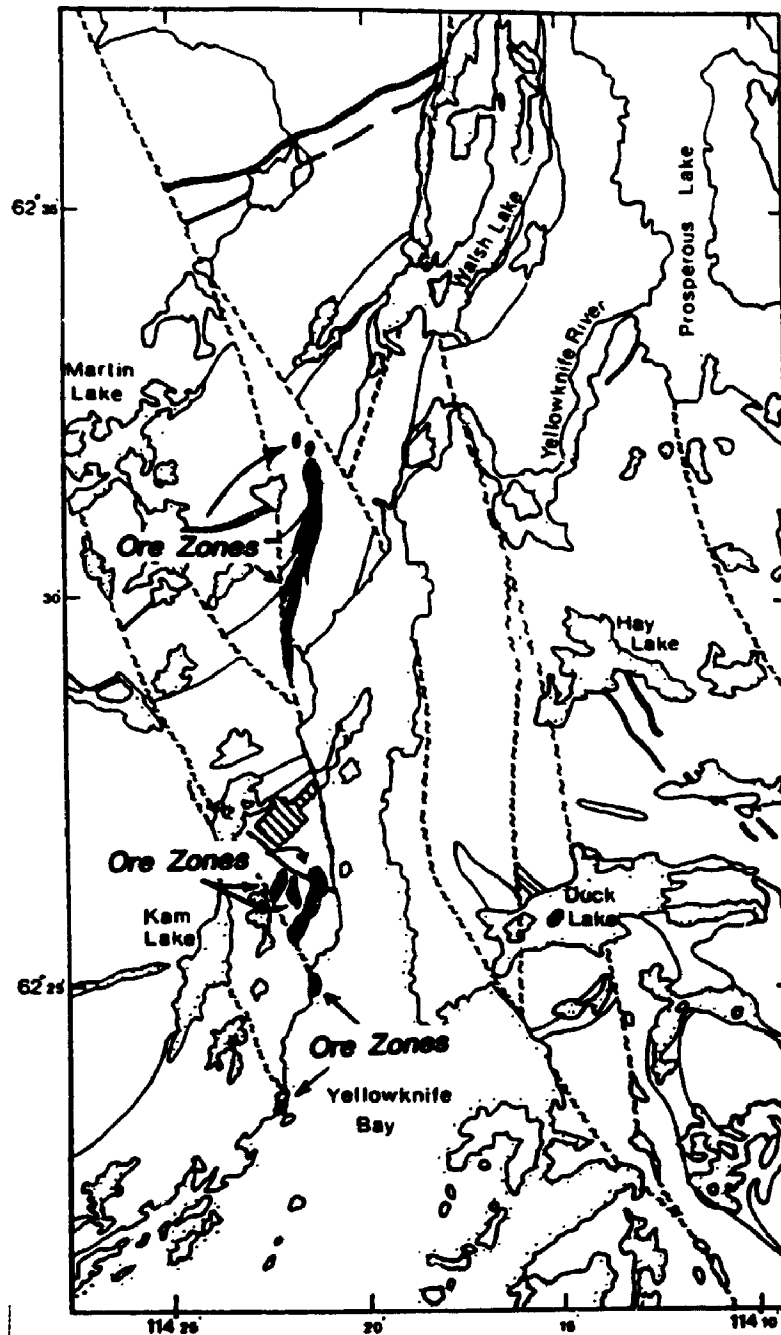
Figure 20. Projection of mineralization hosted within type 2 structures to surface reveals a spatial relationship to type 3 faults.
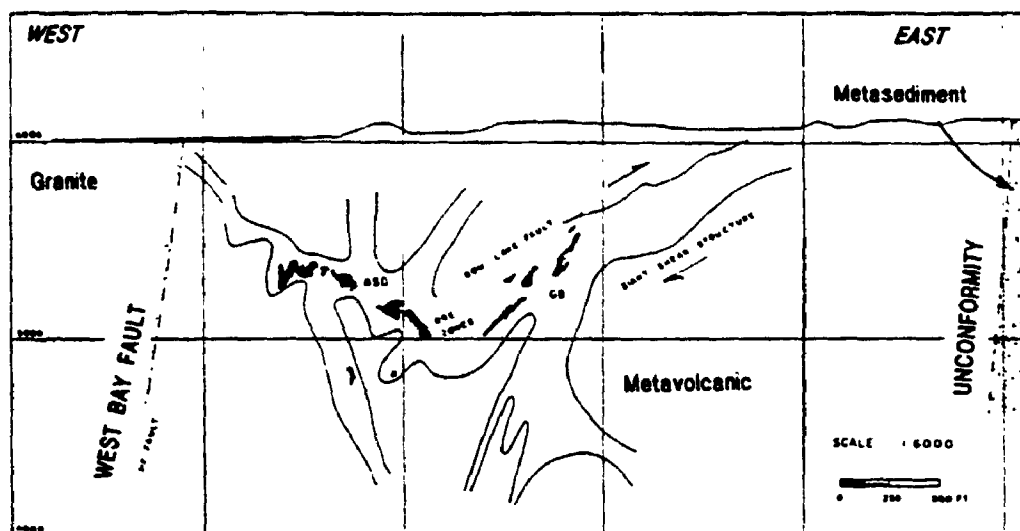
Figure 21. Cross-section of the Giant Shear Zone reveals a complex system of intersecting structures. The GB ore zone within the eastern portion of the shear zone occurs in a P-shear geometry (after Lewis, 1988).
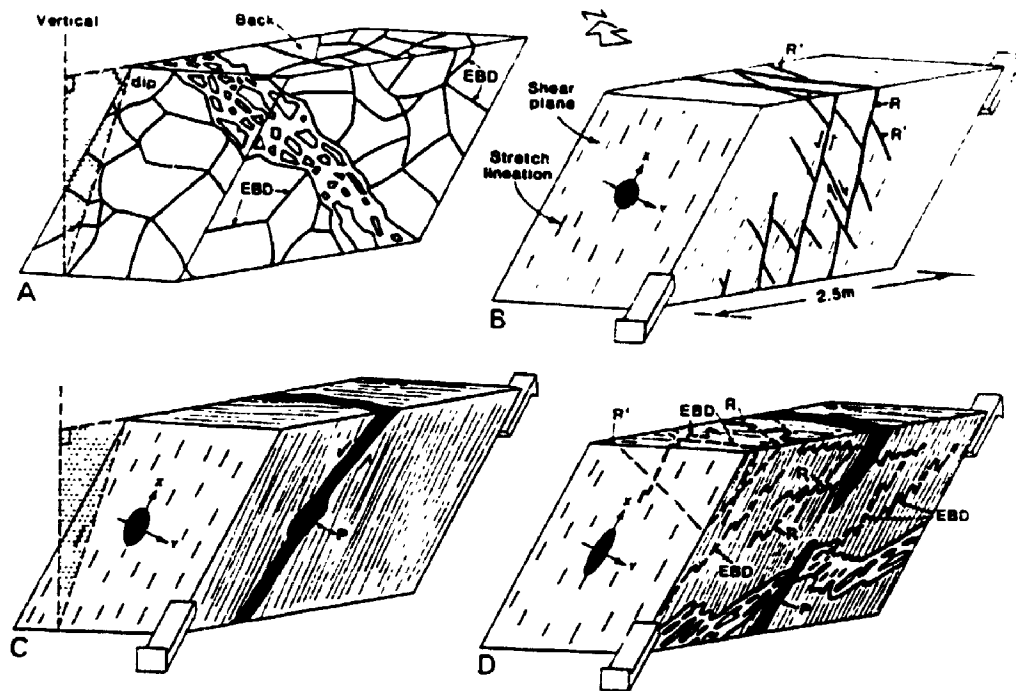
Figure 22. Structural synthesis from Red Lake, Ontario, by
Andrews et al. (1986). Mineralization progresses
with deformation, initiated as an early brittle
ductile stage (EBD; A). A penetrative fabric
develops in (B), and R and R' shears form. The
main mineralizing event occurs with continued
deformation, and auriferous quartz veins form in
P-shears (C). A composite diagram (D)
illustrates the structural features late in the
deformation event.
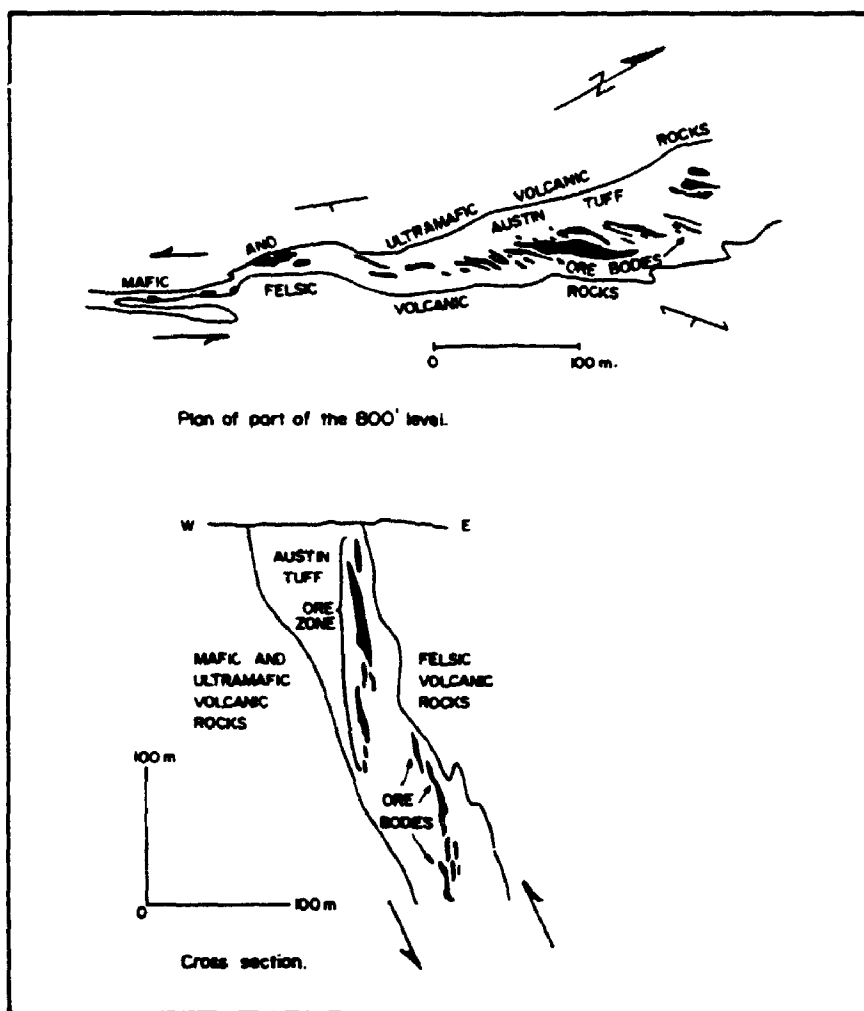
Figure 23. Plan and cross-section showing the distribution
of ore within the Madsen mine, Red Lake, Ontario
after Hodgson (1986), revealing the distribution
of orebodies and ore zones in P-shear
orientations, both in plan and section.

Mineralization not conforming to first- or second-order P-shears generally possesses other unique characteristics. For example, that portion of the Fox Lake shear (R-shear) which hosts significant mineralization occurs entirely within amphibolite-facies rocks. It is the only significant mineralization in the Kam Group within these higher metamorphic-grade rocks. Other significant mineralization within the Yellowknife greenstone belt occurs at the Ptarmigan Mine, where orebodies within the Ptarmigan, Tom, and C veins has been exploited. These veins occur in a T-shear orientation relative to the 345°-striking, left-lateral Ptarmigan Fault, hosted within amphibolite-facies sediments.

Mineralization likely occurs within R and T shears at these locations rather than P-shear geometries due to the different rheological properties of the amphibolite-grade volcanic and sedimentary rocks compared to the transitional greenschist-amphibolite-grade volcanic rocks at the NERCO-Con and Giant Yellowknife mines.

Tectonic models

Padgham (1990) considered four possible tectonic models for the development of the Yellowknife Greenstone Belt, including: (1) intracontinental rift basin, (2) sea-floor spreading, closed by subduction, (3) accreted micro-continental fragment, and (4) prograding arc-trench complexes. Cunningham's (1984)

interpretation of the Kam Group as ocean floor basalts is in general, consistent with Goodwin's (1988) results, and Helmstaedt et al.'s (1986b) back-arc basin model, but this model does not adequately explain the basement complex underlying portions of the Kam Group (Padgham, 1990, pers com., 1992). An ensialic rift setting, while not too different from Helmstaedt et al.'s (1986b) model, may account for the structural, temporal, and petrogenetic evolution of the Yellowknife Greenstone Belt (Cunningham and Lambert, 1989). In this thesis, a stage of late transpressive accretion is added to the back-arc basin model, based on the geodynamic significance of the lamprophyre dyke (Chapter 4).

It is generally agreed that the Kam Group developed subaqueously on or near an older sialic basement complex, and that it has been transected by faults and shear zones ranging in age from synvolcanic to late-Proterozoic. At some point, the Kam Group was tilted into a homocline, and felsic intrusions were emplaced into and within the volcanic sequence at times from 2,620 to 2,525 Ma in discrete events. Significant gold mineralization is constrained to brittle-ductile shear zones (type 2), although economically exploitable mineralization is restricted to type 2 structures with retrograde mineral assemblages, typically concentrated near intersections with type 3 structures. The latter may be reactivated type 1 structures, however, type 3 structures

largely pre-date the final prograde metamorphic event.

The conjunction of structural, temporal and chemical factors are responsible for the distribution of mineralization within the Yellowknife Greenstone Belt (Webb and Kerrich, 1986; Webb, 1987, Armstrong, 1991; Duke et al., 1990). This section has attempted to emphasise the structural considerations constraining shear zone development. The P-shear was clearly dilatant during episodes of high fluid flow. At Yellowknife, conditions within the P-shears were favourable for precipitation of auriferous quartz veins. The localization of the largest orebodies within those portions of these shear zones hosted by transitional amphibolite-greenschist rocks suggests the importance of this metamorphic facies in controlling either the mechanical or chemical factors favourable for gold precipitation. Less significant concentration of gold mineralization occurs in R and T shears in higher-grade rocks. There is some evidence (cross-cutting structures) to suggest that the critical amphibolite-greenschist facies transition is a metamorphic effect related to a late Archean felsic intrusive event.

Other structures in non-P-shear orientations were either not dilatant, did not possess a physio-chemical environment conducive to precipitate gold mineralization, or less likely, did not access the ore-forming fluid reservoirs at that time.

Some of these other structures became mineralized, as mentioned above, albeit to a lesser degree, where hosted in amphibolite-metamorphic grade rocks, and tend to strike more west to northwesterly.

A simple wrench fault shear model, while perhaps not comprehensive enough to predict the actual details of mineralization, adequately explains most of the type 2 and 3 structural relationships observed at Yellowknife. It is not suggested that all of the structures within the Yellowknife Greenstone Belt developed under one structural regime, rather that during a stress field consistent with wrench faulting, existing structural anisotropies deformed in a manner consistent with a simple wrench fault model, and that mineralization occured within this framework. Many of the structural details of gold camps can be interpreted using a wrench fault model.

CHAPTER 4

LAMPROPHYRE DYKE

4.1 Introduction

Nikic et al. (1980) described a diatreme, intersected in the
workings of the Con Mine (now NERCO-Con Mine), characterized
by abundant xenoliths of tonalitic, gneissic, granitic,
volcanic, and vein material. This diatreme is recognized as
part of a larger intrusion which has been identified as a
lamprophyre (Webb, 1983; Webb and Kerrich, 1988). Zircons
from xenoliths in this dyke have yielded U-Pb ages of 3,210
Ma, and Sm-Nd and U-Pb work on the xenoliths give ages up to
3,390 Ma (Nikic et al., 1980; Bibikova et al., 1986). These
results, along with other lines of evidence have been used to
argue for a sialic basement to the Yellowknife supracrustal
sequence. If however, the Yellowknife Greenstone Belt is
allochthonous, the supracrustal sequence definitely
structurally overlay older sialic crust at the time of
lamprophyre intrusion. Basement at the time of mafic
volcanism remains an open question.

Lamprophyres are of special interest inasmuch as they show a
close spatial and temporal association with the regional
structures that host most mesothermal gold camps of all ages
(Rock and Groves, 1988; Wyman and Kerrich, 1988; Rock et al.,
1989; Kerrich and Wyman, 1990). The special interest stems

from the fact that shoshonitic lamprophyres have a highly specific geodynamic setting that may accordingly pertain to the formation of mesothermal gold deposits. Source regions of lamprophyres are at depths of ≈60 to 100 km, which has implications for the depth scale of structures that host both the shoshonites and gold deposits (Wyman and Kerrich, 1988; Kerrich and Wyman, 1990). In addition, the lamprophyre dyke at Yellowknife in particular, is presented in detail because; (1) it occurs in close proximity, and in a geometry parallel, to the Campbell Shear Zone, (2) it reveals temporal relationships that bear directly on the age of mineralization at Yellowknife, and (3) it possesses a chemistry unique to the surrounding rocks which is reflected in the chlorite schists hosting mineralization.

This chapter describes the geometry, petrography, and geochemistry of the lamprophyre. Based on these data, and through comparisons with the tectonic settings of Phanerozoic counterparts, the source regions and tectonic environment of the lamprophyre dyke are discussed. The implications of the lamprophyre dyke for the ore-bearing shear zones at the NERCO-Con Mine, and possible functional relationships between the two are discussed.

4.1.1 Geometry of the Lamprophyre Dyke

Throughout much of its length, the lamprophyre dyke is a single sheet-like intrusion that strikes 007°, and dips to the west at 55°. It has been traced discontinuously by diamond drilling and in mine workings for over 2,800 m along strike and 1,100 m down dip, and is open in all directions. The dyke does not outcrop, probably because upward projection places it beneath the waters of Yellowknife Bay. The dyke averages 4 m in width, but thicknesses of 30 m have been intersected in the NERCO-Con Mine.

The lamprophyre dyke is subparallel to, and with rare exception, lies no more than 20 m from the hanging wall of the Campbell shear zone (Figures 24, 25). Dyke emplacement predates final movement across the Campbell Shear Zone that may be pre-2,534 Ma if the Jackson Lake Formation post-dates the shear zone (see Chapter 3). There is substantial evidence to suggest that the lamprophyre dyke was emplaced prior to ore formation in the Campbell Shear Zone for the following reasons: (1) it is locally cross-cut by the Campbell Shear Zone, (2) portions of it are overprinted by a chlorite-carbonate schist assemblage, and (3) it may in places host gold mineralization (Webb and Kerrich, 1988).

4.2 Petrography of the Lamprophyre Dyke

Macroscopically the lamprophyre dyke is a homogeneous unit, but locally it incorporates variably assimilated xenoliths of exotic and local lithotypes. Xenoliths of tonalite, granite, various gneisses, mafic volcanic rocks, and vein material have been found distributed medially within the dyke. The felsic xenoliths appear to be more resistant to assimilation than mafic counterparts, and constitute the greatest proportion of the exotic lithotypes observed in the dyke. The dyke is for the most part xenolith-free, but xenoliths comprise a major portion of the dyke in some locales, such as on the 3500 level.

The lamprophyre is a medium to coarse-grained panidiomorphic textured rock. Euhedral to subhedral phenocrysts of phlogopite and pargasite predominate, sporadically attaining several centimetres in size. The groundmass is composed of feldspar, quartz and calcite, with abundant accessory minerals. The mineralogy of the lamprophyre dyke, and the distribution of these minerals within five samples representative of the lamprophyre dyke are compiled in Tables 4 and 5 respectively. Rare earth element data for pargasite, apatite, and fluorite separates are presented in Figure 26.

Pargasite, an alkali-rich calcic amphibole occurs ubiquitously

as equant euhedral phenocrysts, typically 2 to 3 mm in size;
phenocrysts up to 30 mm across have been observed. In
plane-polarized light pargasite is pale green, and is of
variable relief (Plate 1). Most phenocrysts show signs of
incipient, or variable degrees of replacement by phlogopite or
chlorite (Plate 2). Microprobe analyses, plotted on Deer et
al.'s (1977) Na+K versus Al^4 diagram for calcic-amphiboles are
illustrated in Figure 27.

Phlogopite, the most abundant mafic mineral, is present in all
samples examined. It occurs in two forms, as corroded primary
phenocrysts and as a secondary alteration product replacing
pargasite (Plates 3 and 4). Primary phenocrysts of phlogopite
appear as euhedral to subhedral grains 2 to 3 mm long by 2 mm
wide. They are typically corroded, showing battlement
terminations. The phlogopite is full of inclusions of rutile,
epidote, and allanite, and these may constitute up to half the
volume of a phlogopite grain. Pleochroic halos are generally
developed around the epidote and allanite inclusions, due to
iron diffusion from the inclusions. The phlogopite is
characteristically bent or deformed (Plate 5).

Secondary phlogopite is pale-brown, strongly pleochroic, and
generally anhedral; it contains few inclusions, dominantly
epidote (Plate 6). Compositionally, the mica plots within the
phlogopite field, midway between the end members phlogopite

and eastonite (Figure 28; Deer et al., 1977). Orthoclase and plagioclase dominate the matrix of the lamprophyre dyke, as optically continuous poikiolitic crystals 6 to 8 mm in diameter (Plate 7). Both feldspars may be twinned and show little if any evidence of alteration (Plate 8). Apatite is abundant in all samples, present as acicular to prismatic crystals averaging 8 to 10 mm long by 2 mm wide. Many of the crystals are bent or fractured, and always contain numerous inclusions, dominantly epidote.

Pyrite, pyrrhotite, and chalcopyrite form net textures with the mafic minerals in the matrix of the rock. Replacement textures are found between sulfides; the most common is pyrrhotite replacing pyrite.

Baddelyite is an accessory ZrO_2 phase, occurring as inclusions within allanite. Commonly a reaction rim has developed between the baddelyite and the allanite. The baddelyite proved to be to fine-grained to be easily separated for age dating purposes. Minor amounts of chlorite occur as an alteration product of pargasite and phlogopite.

The degree of alteration in the dyke is in part due to the nature of lamprophyre dykes (Rock, 1986), and in part due to its proximity to the Campbell shear zone.

4.3 Geochemistry of the Lamprophyre Dyke

The lamprophyre dyke is characterized by relatively low SiO2
(average 41.9 ± 1.8 wt%, 1σ), moderate alkalies (4.7 ± 2.1
wt%, 1σ), and K/Na = 2.2 ± 1.6, 1σ. Elevated light rare earth
elements (LREE) (La= 920 ppm, Ce= 850 ppm) and relatively low
heavy rare earth elements (HREE) (Yb= 8 ppm, Lu= 7 ppm)
generate a highly fractionated chondrite-normalized pattern,
where La/Yb$_n$ occurs in a range ≈ 115 (Figure 29). The
lamprophyre possesses elevated abundances of the large ion
lithophile elements (LILE) (Ba= 1400 ppm, Zr= 330 ppm, Rb= 270
ppm, Th, U and P) and mafic affiliated trace elements (Cr= 360
ppm, V= 220 ppm, Ni= 190 ppm, Co= 19 ppm). Analyses of
representative samples of the lamprophyre dyke are listed in
Table 6.

On an extended normalized diagram, the lamprophyre shows
pronounced troughs at Nb-Ta, and Hf-Ti (Figure 30). The
extreme fractionation of the LIL and compatible elements and
chondrite normalized incompatible element diagrams for the
lamprophyre dyke is similar to other lamprophyres (Rock, 1984;
Cullens and Graff, 1984; Wyman and Kerrich, 1988; Figures 31
and 32). Relatively low abundances of Sr (1274 ppm, n=4) is
a feature noted in the Yellowknife lamprophyre, in all but the
most phlogopite-rich, SiO$_2$-poor sample, where Sr = 6,640 ppm.

4.4 Interpretation

Attempts to classify the lamprophyre dyke attest to the inhomogeneity of the unit, induced in part by the assimilation of sialic xenoliths and in part by later metasomatism. The dyke is a minnette, a vogesite, or a kersantite based upon modal mineralogy, depending on which sample is chosen (Table 5). Chemical discrimination of the lamprophyre is equally inconclusive. It plots as an alkaline igneous rock on total alkalies versus SiO_2 diagrams using Irvine and Baragar's (1971) discriminant (Figure 33) and on Rock's (1986) ternary Al2O3, MgO, and CaO plot (Figure 34) but plots as a subalkaline igneous rock on a Zr/TiO_2 versus Nb/Y diagram (Figure 35; Winchester and Floyd, 1977). A ternary $SiO_2/10$, CaO, and TiO_2 x 4 plot (Rock 1986) reveals the lamprophyre dyke to lie within the fields of both alkaline and ultramafic lamprophyres (Webb and Kerrich, 1988; Figure 36).

Alkaline mafic igneous rocks are notoriously difficult to classify, and this is attested to by the vast number of names assigned to such rocks (Rock, 1977, 1983, 1986; Streckeisen, 1979). Considering Rock's (1986) geochemical classification in conjunction with geodynamic settings of lamprophyres, then his ultramafic lamprophyre class is devoid of Nb-Ta and Ti depletions, and are largely continental rift associated, whereas the alkaline class feature Nb-Ta and Ti depletions,
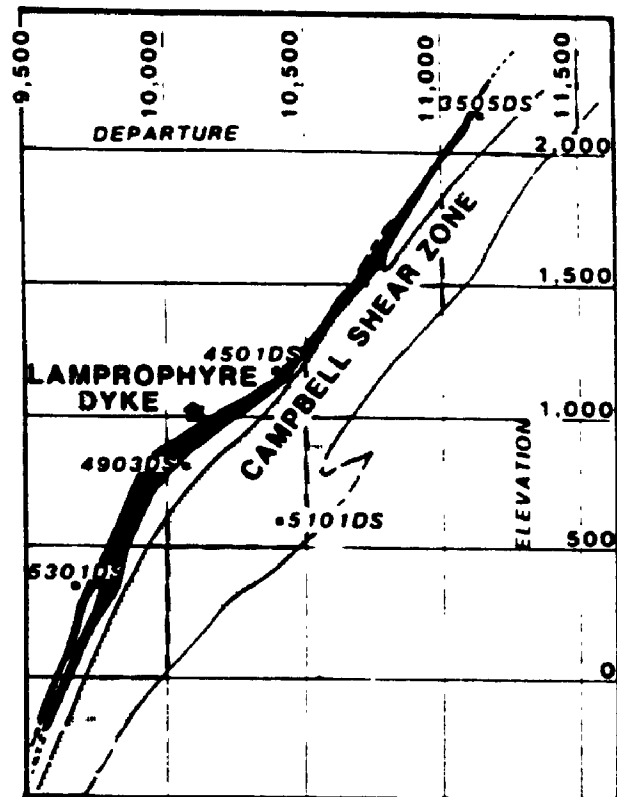
Figure 24. Cross-section of the NERCO-Con Mine at latitude 16,750 showing the location and geometry of the lamprophyre dyke (Webb and Kerrich, 1988).
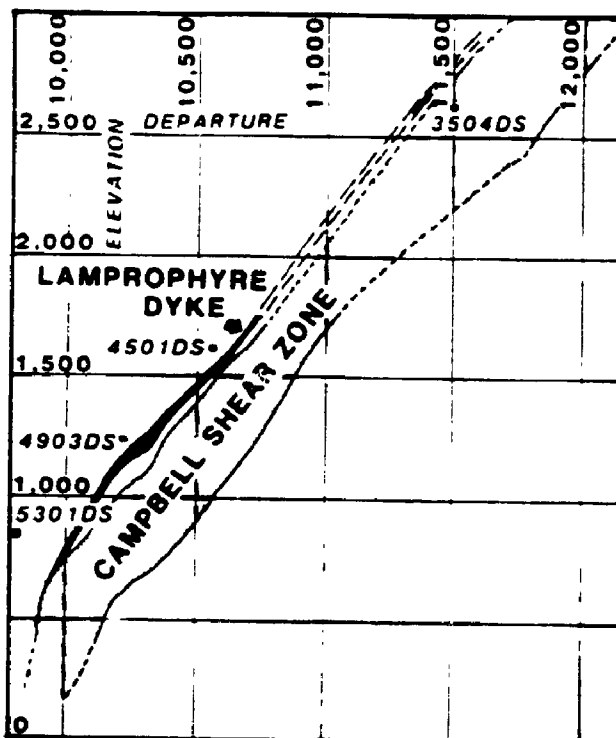
Figure 25. Cross-section of the NERCO-Con Mine at latitude 17,800, 300 m north of Figure 24, revealing the consistency in location and geometry of the lamprophyre dyke (Webb and Kerrich, 1988).

Table 4 *Mineralogical composition of the lamprophyre*

mineral	pheno-cryst	major	acces-sory	second-ary
phlogopite	x			x
pargasite	x			
orthoclase		x		
albite-olig		x		
calcite		x		x
quartz		x	x	x
epidote			x	x
clinozoisite			x	x
allanite			x	x
apatite			x	
prehnite			x	
rutile			x	x
barite			x	
baddelyite			x	x
pyrite			x	x
chalcopyrite			x	x
pyrrhotite			x	x
magnetite			x	
tremolite				x
chlorite				x

Table 5 *Relative modal proportions of specific mineral species in representative samples of the lamprophyre.*

sample	1	2	3	4	5
mineralogy					
phlogopite	22	40	45	40	60
pargasite	44	20	0	8	6
orthoclase	12	9	8	15	8
plagioclase	6	14	1	18	4
calcite	11	8	10	10	8
quartz	tr	3	3	1	9
epidote	2	4	30	4	1
apatite	1	1	2	3	2
other*	2	1	1	1	2

*includes: pyrite, pyrrhotite, chalcopyrite, barite, rutile, magnetite, prehnite, baddelyite, allanite, chlorite, tremolite, clinozoisite.
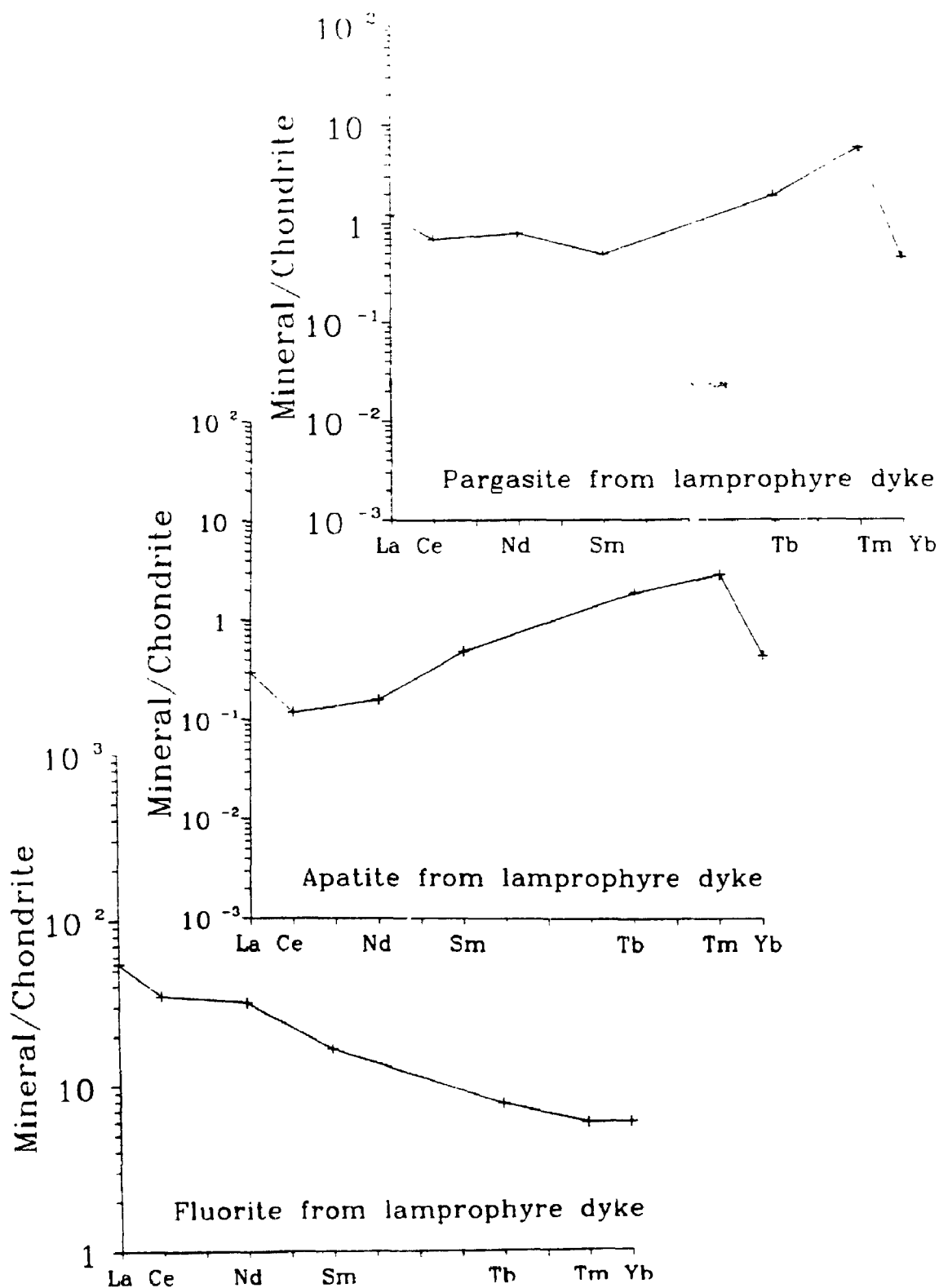
Figure 26. Chondrite-normalized Rare earth element diagram for pargasite, apatite, and fluorite mineral separates from the lamprophyre dyke. The data are presented in Appendix 3.

Plate 1.   Photomicrograph of pargasite from lamprophyre dyke
            in plane polarized light, (field of view ≈ 1 mm).
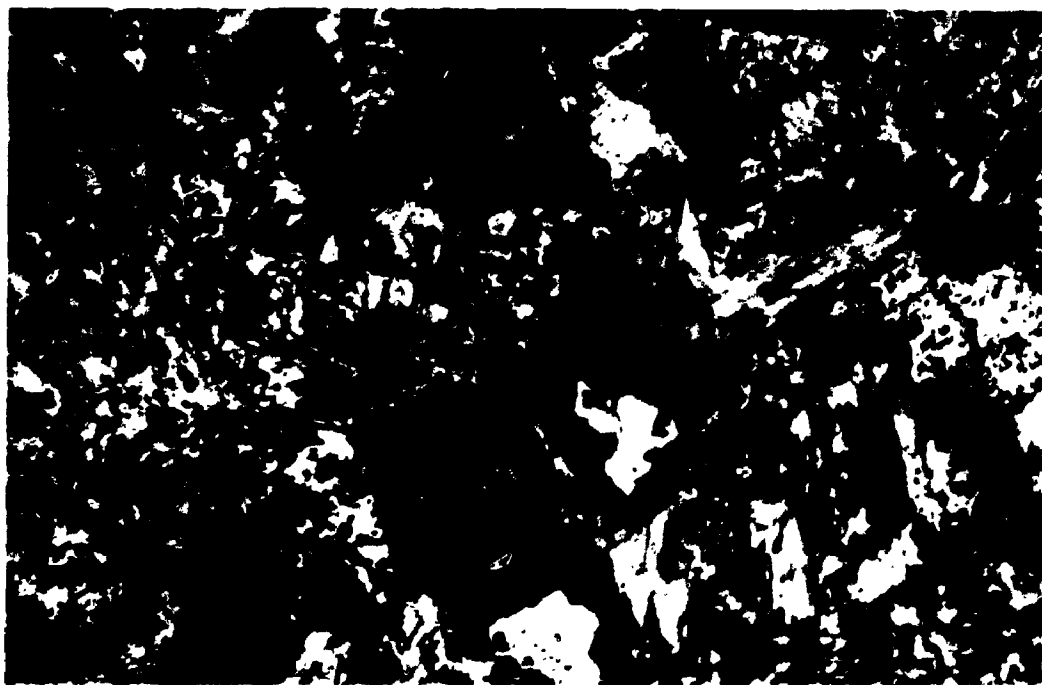
Plate 2.   Photomicrograph of pargasite (P) partly replaced
            by phlogopite (PH) and chlorite (C), plane
            polarized light, (field of view ≈ 3 mm).
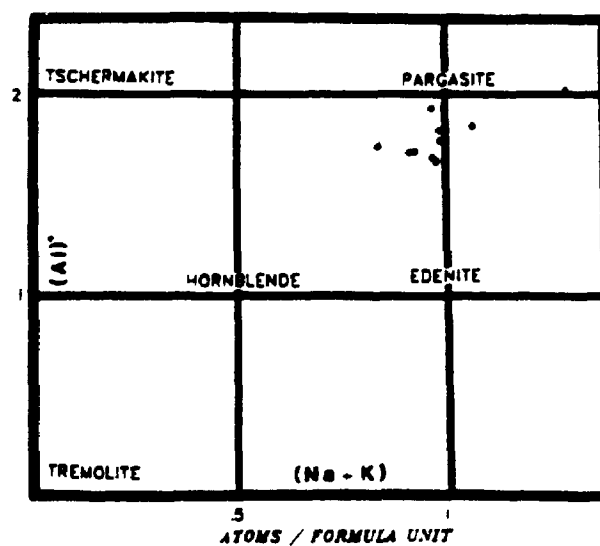
Figure 27. Microprobe analyses of pargasite from the lamprophyre dyke plotted on Deer et al.,'s (1977) Na+K vs Al^{iv} diagram for calcic-amphiboles (Webb and Kerrich, 1988).

Plate 3. Photomicrograph of primary phlogopite, containing abunda⁺ acicular rutile, plane polarized light, (field of view ≈ 1 mm).
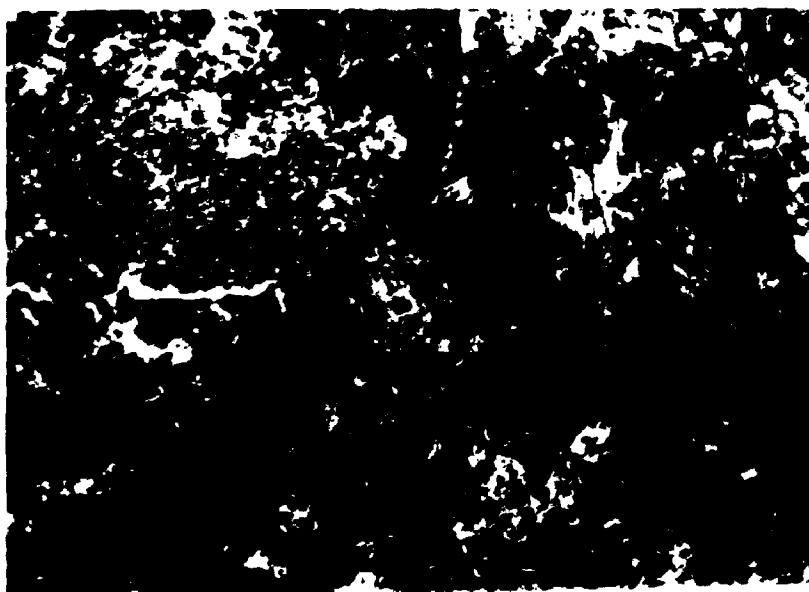
Plate 4. Photomicrograph of secondary phlogopite (PH), characteristically inclusion-free, partly replacing pargasite (P), plane polarized light, (field of view ≈ 3 mm).
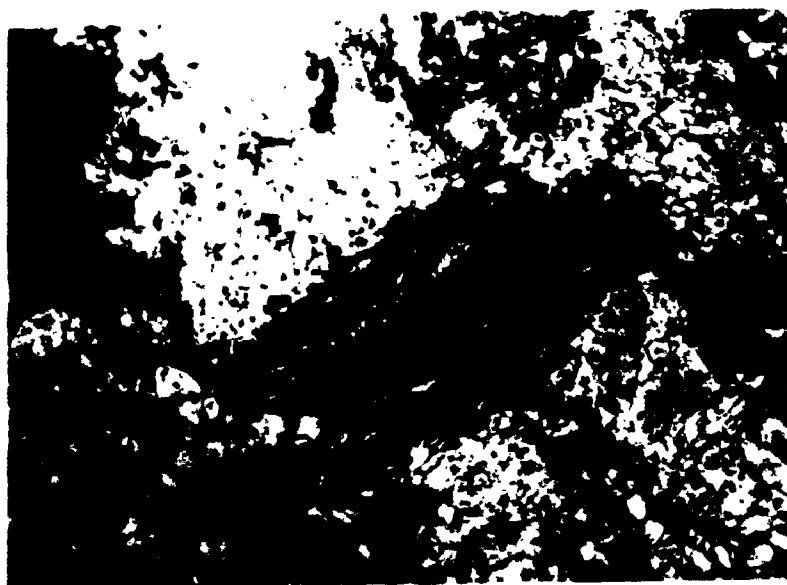
Plate 5. Photomicrograph of deformed, phlogopite (PH), containing inclusions of rutile (R) and apatite (A), plane polarized light (field of view ≈ 3 mm).
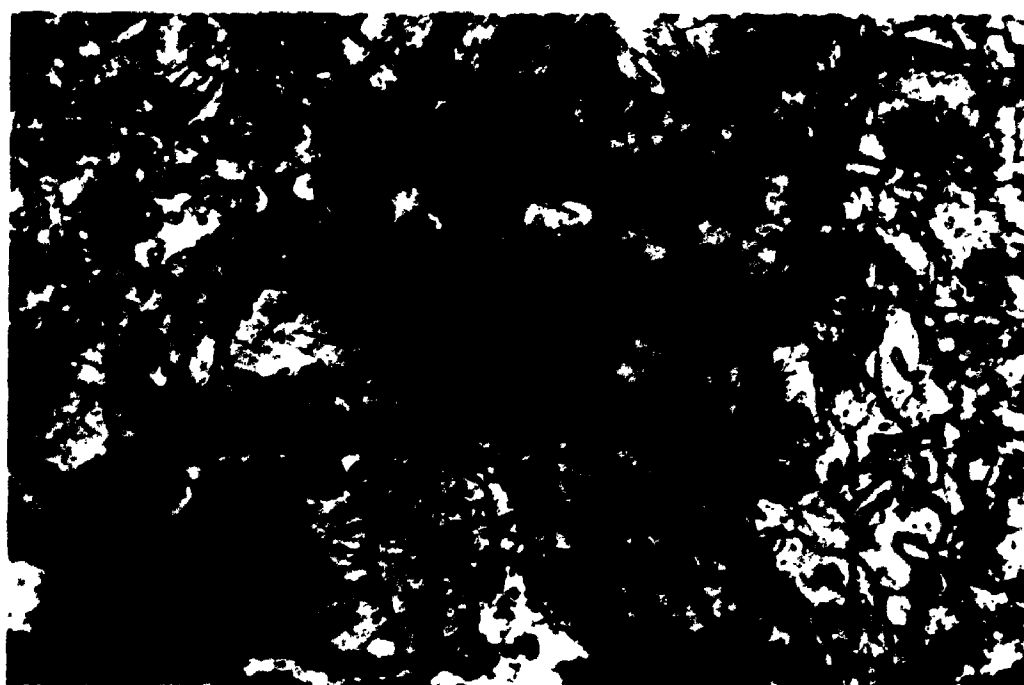
Plate 6. Photomicrograph of abundant epidote inclusions within secondary phlogopite, plane polarized light, (field of view ≈ 1 mm).
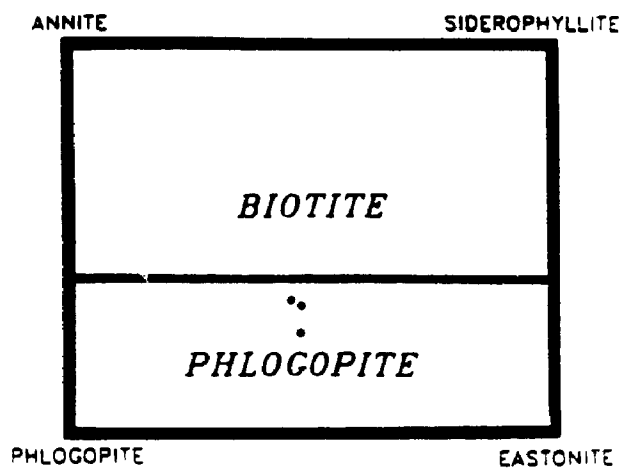
Figure 28. Microprobe analyses of phlogopite from the lamprophyre dyke plotted on Deer et al.,'s (1977) biotite-phlogopite diagram, revealing compositions midway between pure end-member phlogopite and eastonite (Webb and Kerrich, 1988).
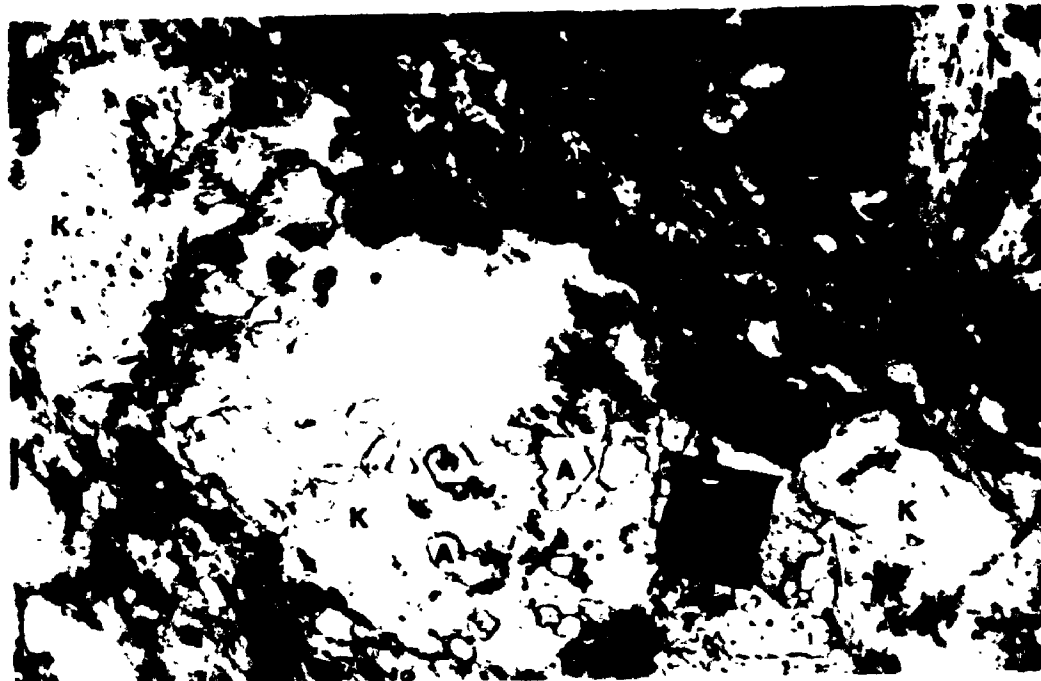
Plate 7.   Photomicrograph of fine-grained apatite (A) within
           unaltered K-feldspar (K), plane polarized light,
           (field of view ≈ 3 mm).
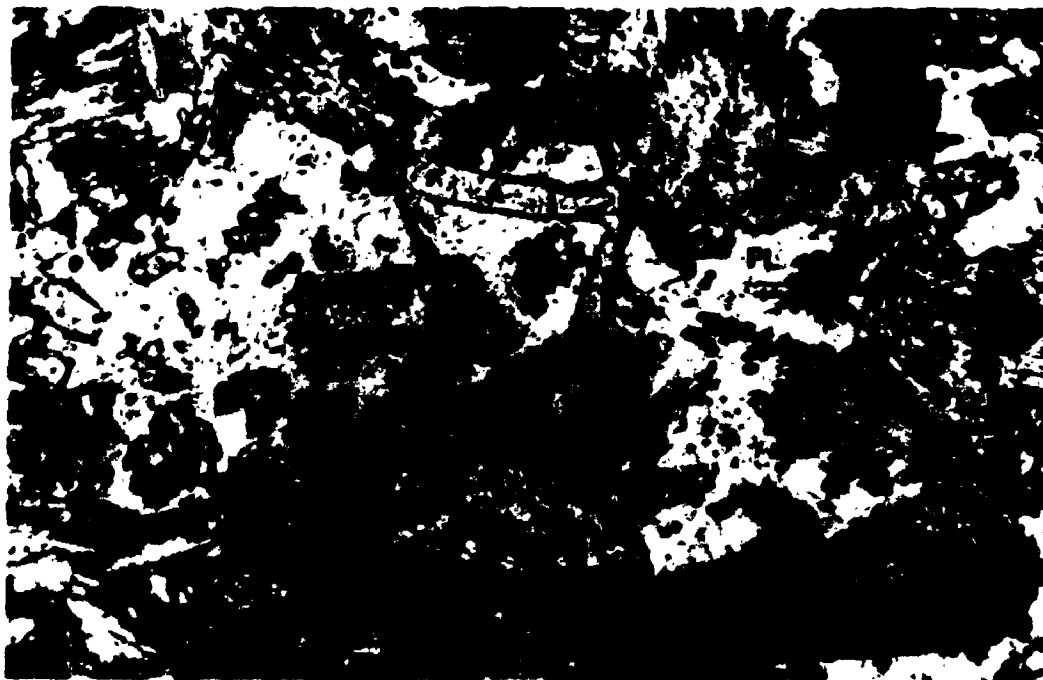
Plate 6.   Photomicrograph of poikiolitic plagioclase (Pl)
           with epidote (E) and apatite (A) inclusions, plane
           polarized light (field of view ≈ 3 mm).

Plate 9   Scanning electron microscope image of baddelyite
as fine-grained fracture filling within allanite,
from lamprophyre dyke intersected in diamond drill
hole B3839 at the NERCO-Con Mine.
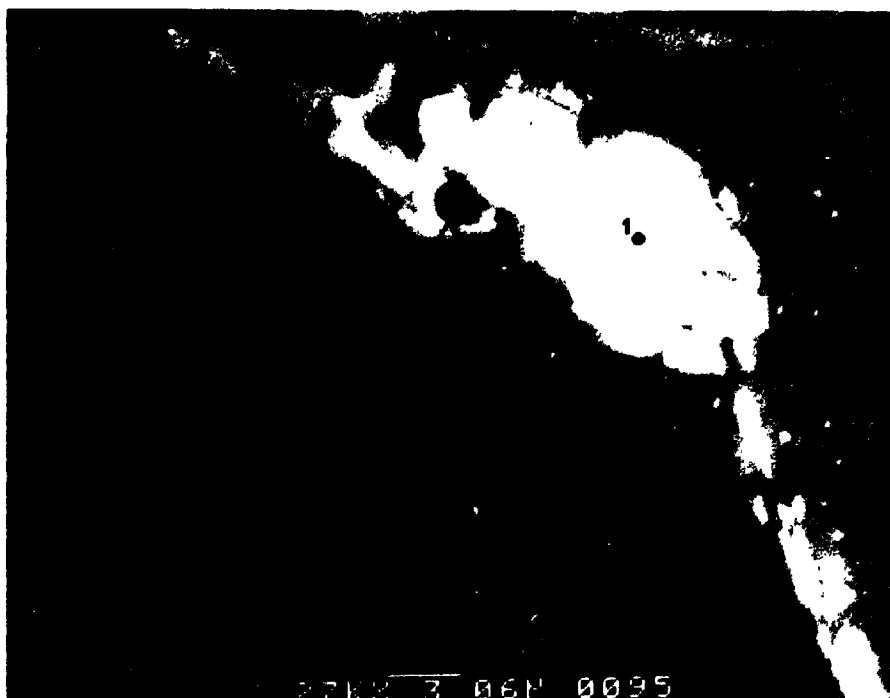
Plate 10   Scanning electron microscope image, close-up of
plate 9 revealing reaction phase between
baddelyite and allanite. Phase 1 is baddelyite,
phase 3 is La and Ce-rich allanite with no Zr, and
phase 2 is intermediate between phase 1 and 3.
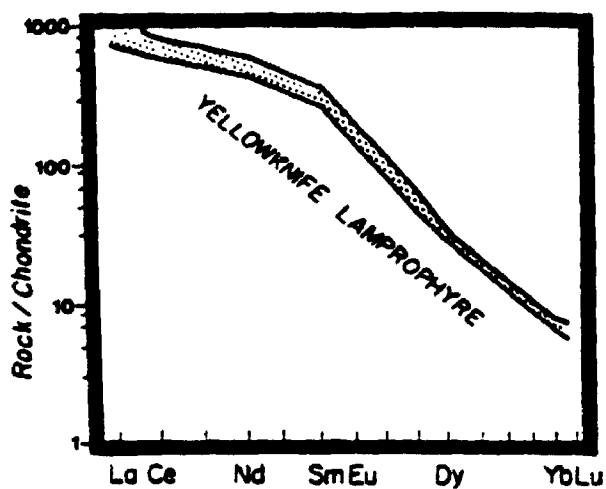
Figure 29. Chondrite-normalized REE plot of the lamprophyre dyke revealing highly fractionated pattern with La/Yb$_n$ >100 (Webb and Kerrich, 1988).
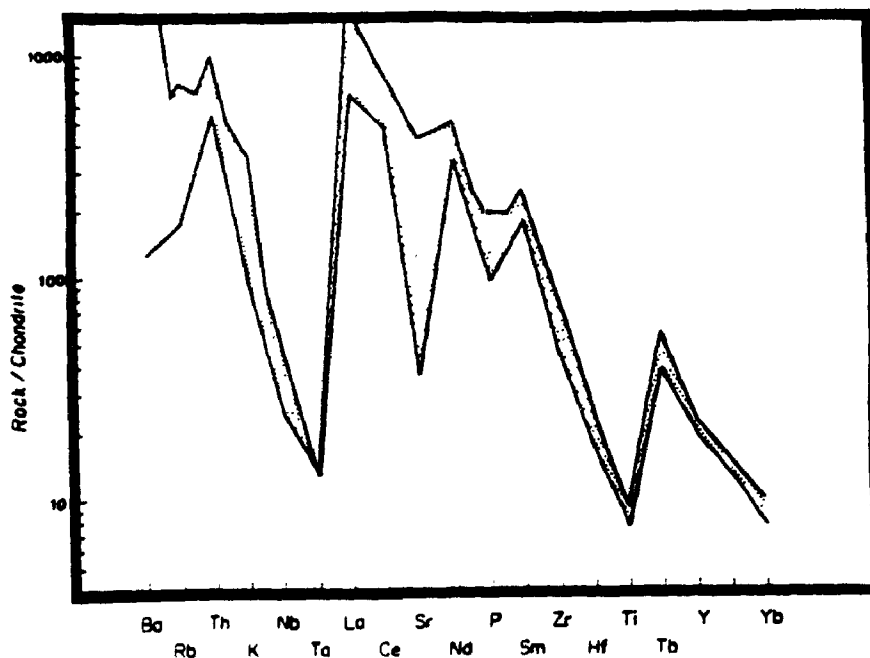
Figure 30. Whole rock analyses of five representative samples of the lamprophyre dyke plotted on an extended chondrite-normalized diagram illustrate extreme relative depletions of Ta-Nb and Ti in a LILE-enriched pattern (Webb and Kerrich, 1988).

Table 6 *Abundances of major element oxides and selected trace elements in representative samples of the lamprophyre dyke.*

	1	2	3	4	5
SiO_2	44 90	44 00	41 70	40 80	39 90
TiO_2	0.66	0 70	0 95	0 86	0 75
Al_2O_3	9 92	10 50	10 40	9 50	12 30
Fe_2O_3	8.33	8.98	8 55	8 50	8 10
MnO	0 12	0.15	0 10	0 14	0 11
MgO	12.50	9.64	10.40	10.60	6 21
CaO	12.50	13 30	10.10	13.80	12 90
K_2O	2 53	2.09	5 15	1 42	2 89
Na_2O	1.72	2 39	1 12	0.32	2 98
P_2O_5	1.01	1 29	1 54	1 19	1 43
L.O I	3.85	4 93	7 00	10 40	6 16
Total	98.40	98.30	97 30	98.40	95.00
S	0.11	0.12	0.19	0.10	0 44
Au	2	3	6	13	9
V	208	208	233	277	174
Cr	606	423	311	356	101
Co	40	41	25	35	3
Ni	276	185	230	190	62
Cu	38	41	58	74	60
Zn	100	115	147	160	111
Pb	18	44	156	327	116
Rb	111	706	304	69	166
Sr	1637	1940	843	679	6640
Y	40	49	40	44	45
Zr	313	377	266	271	425
Nb	10	8	9	9	16
Ba	1216	1100	1044	375	3272
Ga	13	13	12	12	17
Ti/Zr	12.6	11 1	21.4	19.0	10 6
Nb/Y	0.25	0.28	0.23	0.20	0 36
K/Rb	189	25	141	171	145
K/Ba	17.3	15.3	41.0	31.4	7 3
Rb/Sr	0.07	0.36	0.36	0.10	0 03
Ba/Sr	0.74	0.57	1.24	0.55	0 49
Th/U	6.0	6.5	6.9	6.2	7 0

*all major oxides are in weight percent
*all trace elements are in ppm, except Au in ppb.
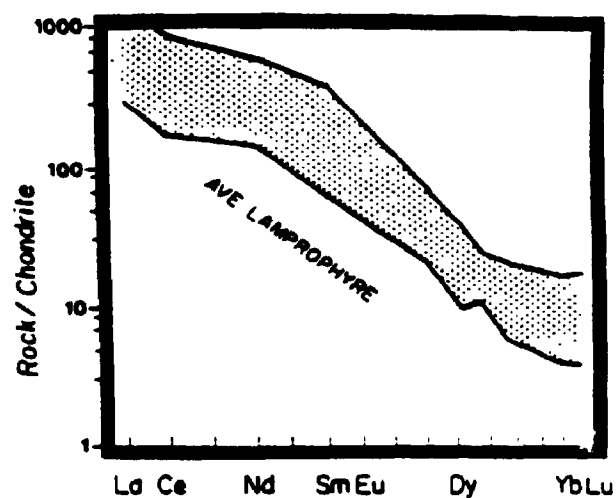
Figure 31. Envelope f - average lamprophyre dyke on chondrite normalized REE diagram revealing consanguinity with the NERCO-Con Mine lamprophyre.
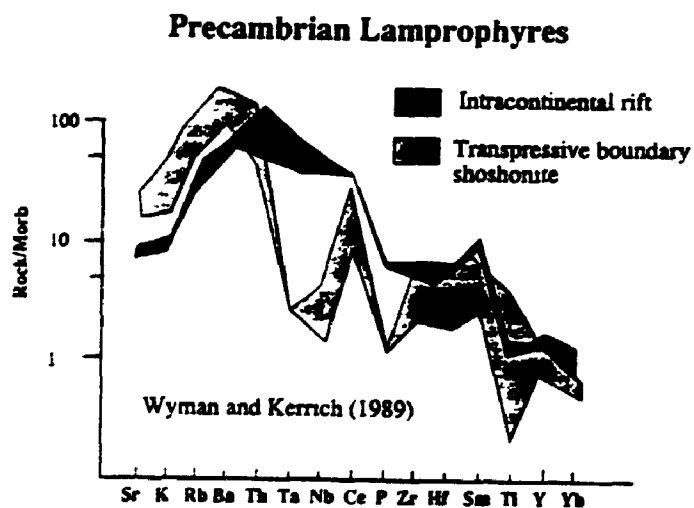
Figure 32. Envelope for average Archean shoshonitic lamprophyre and Proterozoic rift ultramafic lamprophyres plotted on extended chondrite normalized spidergrams.
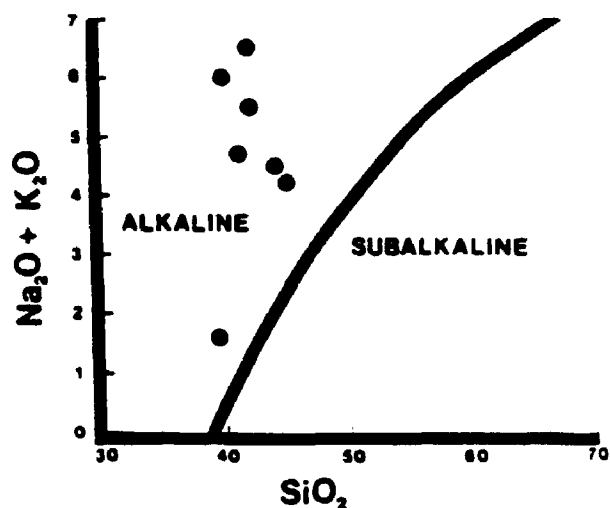
Figure 33. Lamprophyre dyke plotted on total alkalies verses
SiO_2 diagram, using the discriminant line of
Irvine and Baragar (1971) (Webb and Kerrich,
1988).
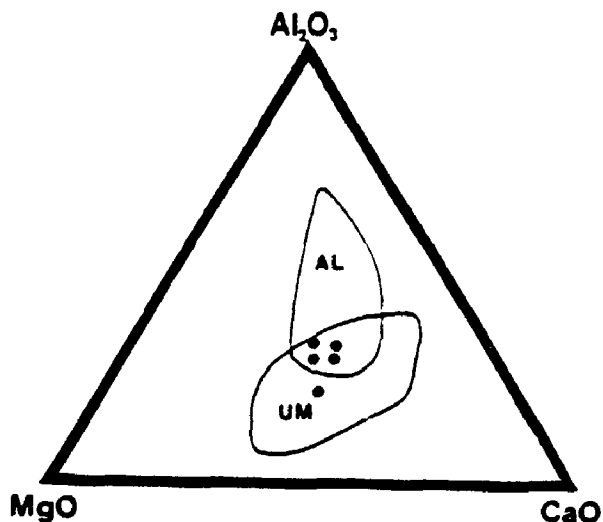
Figure 34. Lamprophyre dyke plotted on ternary Al_2O_3, MgO,
CaO diagram with the fields of ultramafic (UM)
and alkaline (AL) lamprophyres shown for
reference (Rock, 1986; Webb and Kerrich, 1988).
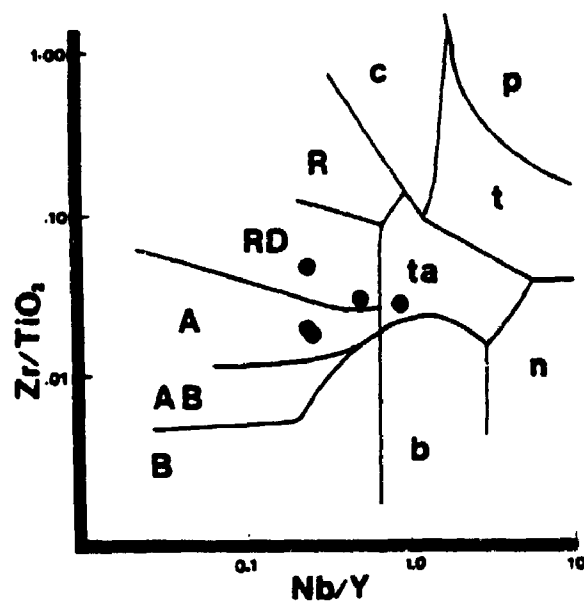
Figure 35. Lamprophyre dyke plotted on Zr/TiO$_2$ verses Nb/Y diagram (after Winchester and Floyd, 1977). Nb/Y ratios suggest that the lamprophyre is calc-alkaline (Webb and Kerricn, 1988).
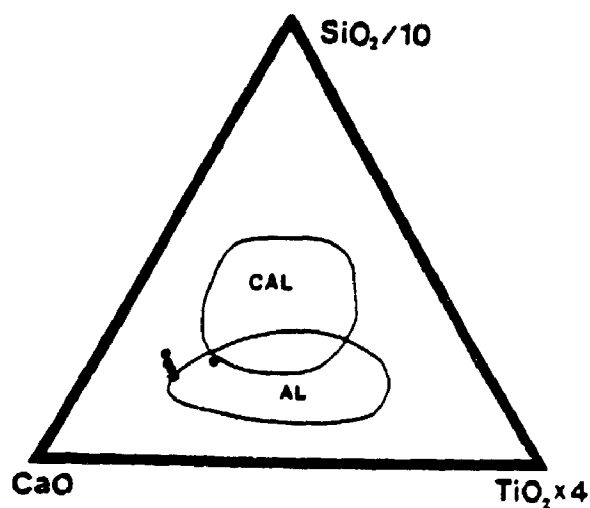
Figure 36. Lamprophyre dyke on a ternary SiO$_2$/10, CaO, and TiO$_2$ x 4 diagram plots in a CaO-rich field, possibly reflecting post-emplacement metasomatic effects (Webb and Kerrich, 1988).

and are found in mature arcs at destructive plate boundaries. Accordingly, this dyke at Yellowknife is considered to be an alkaline lamprophyre; the term shoshonitic lamprophyre is synonymous (Rock, 1986).

4.5 Discussion

The lamprophyre dyke at the NERCO-Con Mine is found adjacent, nd subparallel to, a large ore-bearing structure, the Campbell shear zone. Relative age relationships reveal that the emplacement of the lamprophyre pre-dated mineralization in the shear zone. Dyke emplacement suggests an alkaline magmatic event late in the formation of the Yellowknife greenstone belt. Nikic et al. (1980) related emplacement of the dyke to the intrusion of the Western Granodiorite, although compositionally they are unlikely to be comagmatic given the extreme LILE and LREE enrichment in conjunction with extremely high contents of Cr, V, Co, and Ni. Xenoliths within the lamprophyre dyke have yeilded zircons dated as young as 2,570 Ma, further supporting a post-Western Granodiorite age (Nikic et al., 1980; Easton, 1984).

Rock (1984) reported that some calc-alkaline lamprophyres appear to be spatially associated to granitic plutonism, and may be volatile differentiates, but as stated above, this is

ruled out in the Yellowknife, and other Archean lamprophyres, by the mafic element contents (Wyman and Kerrich, 1988, 1989). Other workers propose a deeper, upper mantle source for lamprophyre dykes, but agree that some crustal modification of the magmas takes place (Bachinski and Scott, 1980; Thompson et al., 1984). In the case of the Yellowknife lamprophyre, a depleted mantle source is indicated by low HREE and Y, in conjunction with elevated Mg numbers, and Cr, Co, and Ni abundances (Morrison, 1980; Thompson et al., 1984, Venturelli et al, 1984; Rock, 1986; Wyman and Kerrich, 1988, 1989). Moreover, such crustal modification must be restricted, given low SiO_2 contents, in conjunction with high Mg numbers, and enhanced Cr, V, Co, and Ni abundances.

There is a general consensus that alkaline mafic magmas may be generated in the mantle by low degrees of partial melting, which enriches the melt in LILE and LREE relative to high field strength elements (HFSE) such as Zr, Hf, and P. An alternative hypothesis appeals to the addition of a LILE and LREE-enriched "metasomatizing" fluid to a depleted mantle source region, as a precursor to magmatism (see Thompson et al., 1984 for a discussion).

A consistent compositional feature of the lamprophyre dyke is the troughs at Nb-Ta and Hf-Ti on extended chondrite-normalized plots. Depletions of Ta and Nb relative

to the neighbouring alteration-insensitive elements Th and La has been attributed to two possible processes. First, the incorporation of sediments, which carry a signature of Ta-Nb and Ti depletions, into the source region; or second, stabilization of a Ti-phase in the source region which preferentially retains Ta and Nb relative to Th and La. Possible causes of Nb-Ta and Ti retention in the mantle sources of lamprophyres and other arc magmas are beyond the scope of this thesis; the subject has been reviewed by Ryerson and Watson (1988) Alkaline mafic magmas from ocean islands and continental rifts show extreme LILE and LREE enrichment, but no normalized Ta-Nb and Ti depletions, whereas subduction-related shoshonitic lamprophyres possess these Ta-Nb and Ti depletions. Accordingly the Yellowknife lamprophyre is a feature interpreted as an analogue of a Phanerozoic mature-arc shoshonite.

Depletions of Sr relative to Ce and Nd on normalized spidergrams have been observed in tholeiitic ocean island andesites, and has been attributed to extreme assimilation fractional crystallization (AFC) processes. A similar Sr depletion observed in subduction-related magmas, has been related to sialic contamination, either at the source, through the incorporation of pelagic muds or other material, or during ascent (Thompson et al., 1984). The incorporation of partially resorbed sialic xenoliths within the lamprophyre at

Yellowknife indicates that some crustal contamination of the magma must be assumed, although as argued above, such contamination or AFC must be limited, and accordingly the relative Sr depletion is likely a source characteristic.

Irrespective of the causal mechanism, there is a clear empirical relationship whereby all Phanerozoic arc magmas possess LILE- and LREE-enrichment with normalized depletions of Nb, Ta, and Ti (Ellam and Hawkesworth, 1987). This relationship extends to Phanerozoic alkaline mafic magmas that feature Nb, Ta, and Ti depletions and are uniquely associated with destructive plate margins, specifically mature arcs developed in a transpressional regime, undergoing local transtension (Thompson et al., 1984).

Notwithstanding uncertainties in the details of plate tectonics in the Proterozoic and Archean, these distinctive geochemical characteristics suggest that Archean and younger lamprophyres arise from the same general processes. Accordingly, the environment of the lamprophyre genesis is not implied to be exactly analogous to plate tectonic processes in Phanerozoic arcs; rather it is suggested that some aspects of the subduction zone processes are reproduced in the Archean lamprophyre source region, namely, a depleted mantle source, metasomatically enriched in LILE and LREE by subduction processes, with low degrees of partial melting triggered by

decompression following collision, uplift, and erosion. The significance of the lamprophyre then, may be as a tectonic "probe" of the crust-mantle conditions under which gold deposits were also formed, albeit the two reflecting different processes and depths (cf. Wyman and Kerrich, 1988, 1989).

The geometric similarities, and spatial and temporal association of the lamprophyre dyke and the Campbell shear zone must be addressed. Lamprophyre dykes are relatively abundant in mesothermal gold camps, and in fact may host ore in some deposits (McNeil and Kerrich, 1986). It is likely that for the most part this association reflects the mutual localization of both lamprophyres and gold deposits near large trans-crustal fractures, that may be terrain boundaries in a geodynamic regime of oblique plate convergence (Wyman and Kerrich, 1988, 1989). Lamprophyre dykes require structures communicating with the upper mantle, and the gold deposits require structures to tap either metamorphic fluids (Kerrich, 1983, Watson and Kerrich, 1983), magmatic fluids (Burrows and Spooner, 1986, Mason and Melnik, 1986), or mixtures of both. A translithospheric fracture could conveniently account for the presence of both lamprophyre dykes and gold deposits.

In summary, the lamprophyre dyke at Yellowknife appears to be a shoshonitic lamprophyre, emplaced late in the volcanic-plutonic history of the Yellowknife greenstone belt. It post-

dates intrusion of the Western Granodiorite (2,620 ±8 Ma) and pre-dates mineralization in the Campbell Shear Zone. The dyke occupies a pre-existing structure, which is likely why it is so closely associated with the Campbell shear zone. The dyke signifies that the Yellowknife greenstone belt was underlain by a sialic crust at ≈ 2.6 Ga, through which mantle derived alkaline magmas intruded, prior to the formation of the gold deposits.

CHAPTER 5

GEOCHEMISTRY

5.1 Introduction

An analysis of the metasomatic alteration associated with gold
mineralization within the Yellowknife Greenstone Belt requires
an understanding of the primary lithogeochemistry, and a
number of secondary geochemical processes. These include: (1)
low temperature interaction between the erupting basalts and
seawater; (2) contact metamorphic effects between the basalts
and intrusions, (3) metasomatism associated with development
of the shear zones prior to development of mineralization, (4)
effect of the mineralizing event itself, and (5) superimposed
effects from recent surface fluid-related alteration.

This chapter review data from the literature considering the
above mentioned processes. Statistical, and empirical
analysis of the data defines covarying suites of elements that
are thought to be indicative of these processes. Thus
defined, these trends are then examined for spatial
distributions to determine where each processes may have
acted.

Data for identifying primary geochemical trends at Yellowknife
are provided from the literature and samples collected by the
writer. Samples collected by the writer were selected to

139

avoid visible alteration, such as obvious quartz veining, silicification, and/or sericitization. This study is limited to rocks from the Kam Group, as they host all of the principal gold deposits within the volcanic stratigraphy of the Yellowknife Greenstone Belt, and are the precursor lithology of the schists.

Information on secondary processes is primarily based upon samples collected by the writer, and this forms the bulk of this chapter. Geochemical data are interpreted with the aid of multi-level statistical analyses. Initially, univariate data are used as screens, to characterize the distribution of the data, then several multivariate analyses are conducted. The focus is on the gold-mineralizing process, and the data are reviewed in light of current research in this field.

The data are considered using a principal component analysis, a multivariate analytical technique that has been described by others (Nichol, 1968, 1973; May, 1974; Dumitriu et al., 1979; Davies, 1985). Aspects are summarized in Appendix 4.

Subpopulations identified in this study have common enrichments and depletions of elements. Correlations in each subpopulation will be different from each other, and from the population as a group. The data from this multivariate analysis is presented in Appendix 4.

5.2   Previous Geochemical Work

Host Rocks

The Kam Group, and the overlying Banting Group volcanic rocks have been extensively studied (Boyle, 1961; Baragar, 1966; Baragar and Goodwin, 1969; Condie and Baragar, 1974; Jenner et al., 1981; Cunningham, 1984; Goodwin, 1988; Cunningham and Lambert, 1989). The Burwash Group, and the plutons within and bounding the Yellowknife Greenstone Belt have been considered by other workers (Drury, 1971; Jenner et al., 1981; Atkinson, 1988; Atkinson and van Breeman, 1990; Atkinson and Fyfe, 1991).

The chemical composition of the Kam Group has been estimated by workers over the past 3 decades, as summarized on Table 7. Petrogenetic studies using major element discriminants (AFM, Jensen Cation Plots) reveal general tholeiitic enrichment trends within the Kam Group (Baragar, 1966; Condie and Baragar, 1974; Webb, 1983; Cunningham, 1984; Goodwin, 1988; Cunningham and Lambert, 1989). Significant differences in interpretation of the trace element and REE data exist, and may in part be due the incorporation of altered rocks in the data, (Jenner et al., 1981; Cunningham, 1984; Goodwin, 1988; Cunnningham and Lambert, 1989). Cunningham (1984) and Cunningham and Lambert (1989) employed Hughes' (1973) igneous spectrum screen to exclude altered rocks from their discrimant diagrams, and determined that the Kam Group is dominated by

TABLE 7

	Brown (1949)	Baragar 1966)	Goodwin (1988)	Cunningham and Lambert (1989)
Basalt		49	62	65
Basaltic Andesite			17	27
Quartz basalt		6		
Massive Andesite	43	27*	8*	17*
Pillowed Andesite	42			
Variolitic Andesite	11			
Latite		3		
Dacite	3	8	13	2
Quartz dacite		7		
Tuff/cherty tuff	1			

* includes all varieties of andesite

Estimated composition of the Yellowknife volcanic belt from various workers

ocean floor basalts; a few samples are low K tholeiites.

A magma source consistent with partial melting of an undepleted peridotite is suggested, and using additional data from the Banting Group which has arc affinities, a tectonic model, of ensialic rifting related to a mantle hot spot followed by subduction and arc formation is proposed (Cunningham and Lambert, 1989). It is recognized that this model is not too dissimilar to a backarc basin model suggested by others (Helmstaedt and Padgham, 1986a, 1986b). Specific models will be discussed in Chapter 8.

Shear zones at Yellowknife were determined to have formed by metasomatic and tectonic processes (Boyle, 1961; Henderson and Brown, 1966). Mass balance studies reveal that such a transformation requires additions of volatiles (H_2O, S, CO_2), and K, variable gains or losses in Ca, Fe, and Mg, and losses in Na (Boyle, 1961; Osatenko, 1971; Kerrich et al., 1977; Webb, 1984; Richards et al., 1991). Auriferous zones and attendant carbonatization, silicification, sulfidation, and sericitization and may have been superimposed upon the structurally prepared schists in prolate ellipsoidal domains that constitute orebodies. These would then represent a later metasomatic event, including absolute gains of Si, CO_2, K, Au, Ag, S, As, Sb, Te. Aluminum, Ti, Zr, Hf, V, and Th behaved isochemically (Kerrich et al., 1981; Kerrich and Fyfe, 1988).

Alternatively, the development of gold mineralization may represent part of a process that included the development of the chlorite schists (N. Duke, pers com., 1992), although this may be inconsistent with the structural observations presented in Chapter 3. This chapter attempts to document relative gains or losses of major and trace elements in the chlorite-carbonate schists that may be attributable to; (1) primary variations within the host rocks, (2) variations related to shear zone development, (3) ore-related metasomatic events, and (4) other geochemical processes active within the shear zones.

Mineralization is known to post-date schist formation, and the ore-forming fluids are known to have been voluminous, and focused within the shear zones (Kerrich and Allison, 1978; Kerrich and Fyfe, 1981; Kerrich, 1983; Kerrich et al., 1984; Colvine et al., 1988; Duke et al., 1990). The design philosophy of this experiment was an attempt to identify a geochemical signature in the chlorite schists of proximal gold mineralization, given that the schists present a much larger target than the orebodies within them.

5.3 Sample Collection and Preparation

Two hundred samples of chlorite-carbonate schist have been collected, with careful exclusion of samples containing quartz

and/or carbonate veining, or abundant sericite. Samples were collected from drifts and crosscuts within the NERCO-Con Mine, outside of gold orebodies, extending over an area more than 1,800 m long from a depth ranging from 700 m to more than 1,550 m below surface. An additional 21 samples of chlorite-carbonate schist were collected from the Campbell shear zone outside of the NERCO-Con Mine area, 3,000 m to the south, from the Giant Yellowknife Mine area 9,000 m to the north, and from a shear zone barren of ore marginal to the Campbell shear zone to the east. Non-ore samples were chosen to minimize the extreme chemical variability common to most ore samples. The drifts are approximately 60 m apart ve tically, and may or may not lie within the Campbell shear zone. Crosscuts are driven near orebodies, near shafts and winzes, or to access specific areas of the mine. Samples from diamond drill holes supplement the data in areas where development within the shear zone is limited. Additionally, auriferous quartz veins and the immediate wall rocks have been analyzed from several stopes in the Campbell shear zone, and compared to data from the Con, Negus and Rycon, and Giant shear zones.

Sample spacing is not regular, with samples 2 to 200 m apart, depending on location within the mine. Ten samples were collected in duplicate to ascertain local variations, and 10 samples were analyzed in duplicate to check for analytical reproducibility.

Samples were subdivided into four different suites based on field examination, and were designated as follows: (1) basalt, (2) chlorite schist, (3) sericite schist, or (4) quartz vein. These samples were then submitted to XRay Assay Laboratories for standard whole rock and selected trace element analysis by XRF, and ICP MS. Portions of each sample were retained for reference. The coarse crush and powders from this work were retained for further analysis (see Chapter 6). The data are presented in Appendix 4.

Data from several geochemical studies at Yellowknife are also considered, and these have been analyzed for different suites of elements using various analytical techniques. As such, all of the different data sets may not be directly comparable. Data collected by R. Kerrich, B. Gates, D. Myers, H. Osatenko, and D. Jardine, are used where possible (Tabulated in Appendix 4).

The analytical treatment of the samples is described in Appendix 1. The accuracy and precision of an analysis is discussed where appropriate.

5.4 Host Rocks

Previous workers in Yellowknife determined the Kam Group volcanics to be primarily subalkaline and tholeiitic in composition (Figures 37, 38, 39; Baragar, 1966; Jenner et al., 1981; Webb, 1983; Cunningham, 1984; Bullis et al., 1986; Goodwin, 1988; Cunningham and Lambert, 1989). The location of sample traverses has been shown in Chapter 2, Figure 5). The Kam Group has been separated into two populations from geochemical considerations; a Lower Kam Group (Chan and Crestaurum Formations) and an Upper Kam (Yellowknife Bay Formation) separated by the dominantly dacitic Townsite Formation (Baragar, 1966; Baragar and Goodwin, 1969; Condie and Baragar, 1974; Jenner et al., 1981; Cunningham, 1984; Goodwin, 1988; Cunningham and Lambert, 1989). Baragar (1966) considered the Lower and Upper Kam Groups to represent the products of two tholeiitic magmatic cycles, each culminating in a more intermediate to felsic event. Goodwin's (1988) sults confirm this, revealing $FeO_{total}/FeO_{total}+MgO$ ratios changing from 0.68 to 0.76 in cycle 1, and 0.64 to 0.59 in cycle 2, and introducing a third cycle from the rocks south of Kam Point with $FeO_{total}/FeO_{total}+MgO$ ratios of 0.68. This cycle had been sampled and is recognized from Baragar's data, but not described as distinct (Baragar, 1966; Goodwin, 1988). Rocks from this third cycle were not sampled, and thus not recognized in later work (Cunningham and Lambert, 1989).

5.4.1 Lower Kam Group

Univariate data for the Lower Kam Group (Chan and Crestaurum Formations) are summarized on Table 8. Individual major and trace elements from the Lower Kam Group generally possess a bimodal arithmetic distribution typical of two end-member populations.

Results of a principal component analysis are presented in Figures 40, 41, 42.

Trend 1 (Component 1)

A principal feature in these rocks appears to be a trend towards MgO depletion and TiO_2, Zr, and Y enrichment. This is accompanied by a less prominent trend of Fe_2O_3, Na_2O and P_2O_5 enrichment and K_2O depletion. This would appear to resemble a trend towards magmatic differentiation along a tholeiitic trend. The lack of influence on SiO_2, Al_2O_3, and CaO contents indicates that feldspar crystallization did not play an important role in this trend. Similarly, TiO_2-V diagrams suggest that fractionation of pyroxene, or possibly garnet is implicated in the development of the Kam Group (Cunningham and Lambert, 1989). These geochemical trends are characteristic of some tholeiitic basalts, expressing only moderate iron concentration (Kuno, 1984), and thus fractionating magnetite is not implicated in the petrogenesis of these rocks (Cunningham and Lambert, 1989).
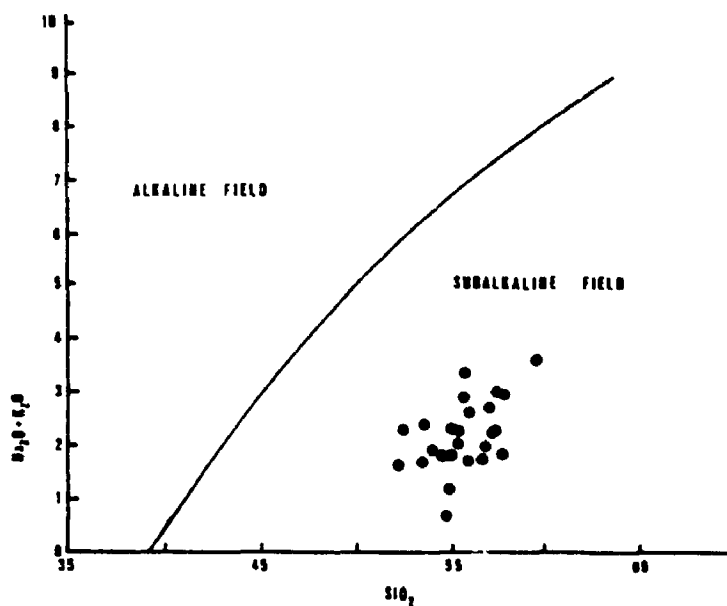
Figure 37 Kam Group basalts plotted on a total alkalies verses SiO₂ diagram using the discriminant line of Irvine and Baragar (1971), characterize them as subalkaline (Webb, 1984)
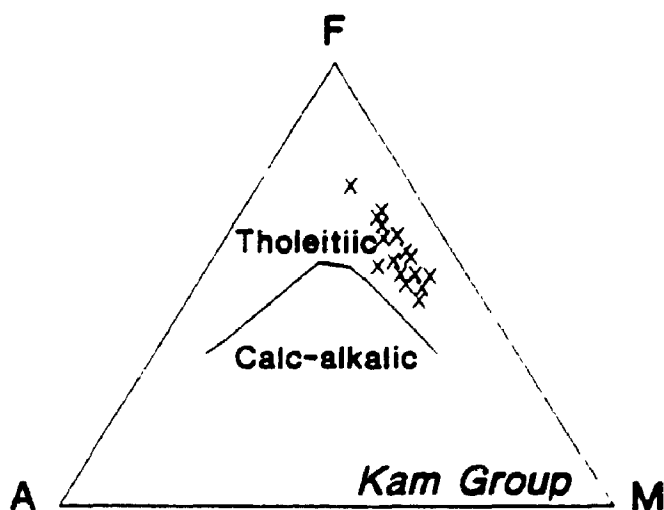
Figure 38. Kam Group basalts plotted on ternary AFM diagram illustrate the tholeiitic nature of these volcanic rocks (Cunningham and Lambert, 1989).
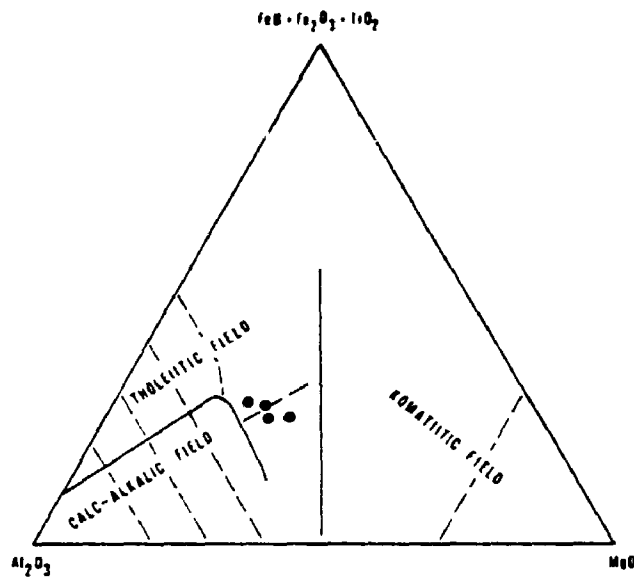
Figure 39. Kam Group basalts plotted on ternary Jensen
          Cation Plot reveal them to be dominantly
          tholeiitic basalts with Fe/Mg ratios near unity
          (Bullis et al., 1987).

TABLE 8
SUMMARY TABLE, Lower Kam Group

	Log/Ar	Mode	Mean	Std	Pop
SiO_2	Arith	51	48.7	1.2	24.5
		54	50.5	1.0	46.5
			53.8	0.6	28.9
Al_2O_3	Arith	13.8	11.9	1.3	5.6
		14.4	14.2	0.5	86.9
		14.8	15.8	n.6	7.5
TiO_2	Arith	1.1	1.0	0.15	82.6
		1.7	1.5	0.26	17.4
Fe_2O_3	Arith	14.0	13.2	1.9	100
MgO	Arith	7.5	7.3	1.0	100
CaO	Arith	11.0	10.2	1.4	100
K_2O	Arith	0.3	0.24	0.09	52.8
		0.7	0.65	0.11	47.2
Na_2O	Arith	2.2	1.88	0.24	63.3
		3.3	3.03	0.49	36.7
MnO	Arith	0.24	0.22	0.04	66.2
		0.30	0.30	0.04	33.8
S	Log	0.04	0.038	-0.029 +0.050	81.5
			0.108	-0.067 +0.174	18.5
P_2O_5	Arith	0.06	0.057	0.006	30.0
		0.11	0.099	0.005	56.1
		0.16	0.146	0.019	13.9
Ba	Log	10	19.3	-7.8 +48.0	95.8
Nb	Arith	2	1.87	0.77	87.6
		5	4.72	0.47	12.4
Zr	Arith	75	52	1.5	6.6
			71	4.8	69.5
			96	17.1	23.9
Y	Arith	23	24	3.0	88.3
		27	34	3.7	11.7
Sr	Arith	140	128	26.6	100
Rb	Log	2.5	6.7	-2.7 +16.5	100

Summary table for the univariate distribution of major and minor elements within basalts of the Lower Kam Group. Data are characterized as logarithmically or arithmetically distributed (Log/Arith), the modes are indicated, the arithmetic mean of various populations are given along with respective standard deviations (Std) as determined from probability plots. The percentage of the total population represented by each subpopulation is presented as Pop. Data from Cunningham (1984).

Yellowknife, NWT
Principal Component Analysis
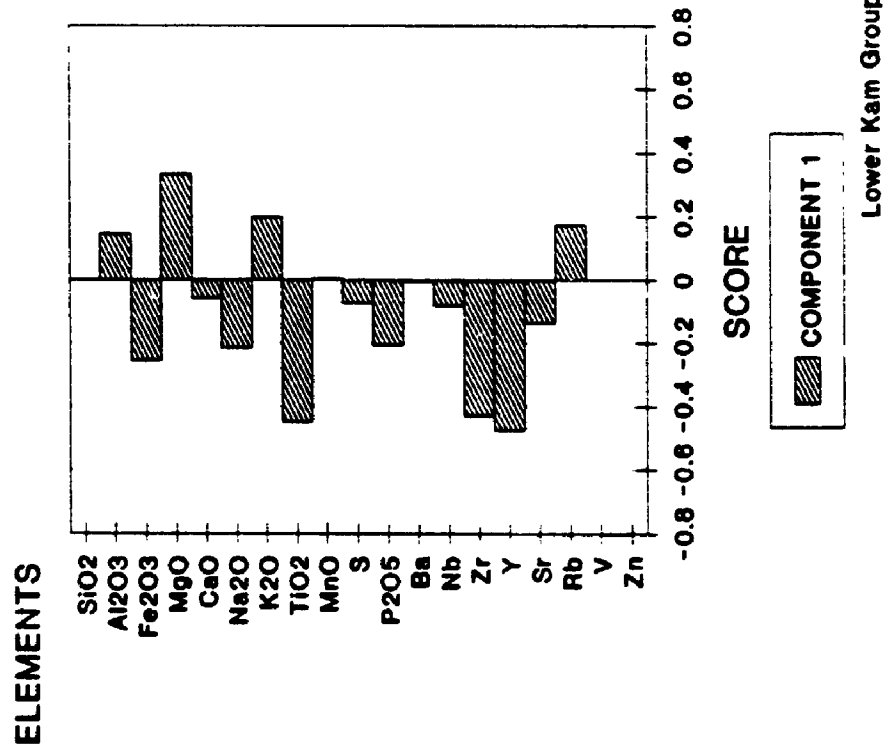
Yellowknife, NWT
Principal Component Analysis

Figure 40. Bar chart illustrating the PC1 and PC2 element scores from a principal component analysis on the Lower Kam Group basalts.

Figure 41. Bar chart illustrating the PC3 and PC4 element scores from a principal component analysis on the Lower Kam Group basalts.

Yellowknife, NWT
Principal Component Analysis

Yellowknife, NWT
Principal Component Analysis

Figure 42. Bar chart illustrating the PC5 and PC6 element scores from a principal component analysis on the Lower Kam Group basalts.

Trend 2 (Component 2)

Less prominent features identified in this data set from the Lower Kam Group is a CaO depletion coupled with enrichment of K_2O, Ba, and Nb, and to a lesser extent Na_2O and Rb. This suite of elements would appear to characterize a trend towards enriched incompatible elements at the expense of compatible elements. The exclusion of MgO and Sr depletions or TiO_2, P_2O_5, Zr, and Y enrichments suggests that this process may have been affected by feldspar, but not pyroxene or apatite fractionation. Inasmuch as Ti, Zr, Y, and Nb are relatively insensitive to alteration, these trends are considered to be magmatic (Drury, 1979; Jenner et al., 1981; Kerrich, 1981, 1986, 1989b; Goodwin, 1988; Cunningham and Lambert, 1989.

A similar trend was observed for the Townsite Formation by Cunningham and Lambert (1989) from REE plots (Yb vs La/Sm_n), which indicated only minor garnet or hornblende involvement, and thus implicated magnetite and presumably plagioclase fractionation. They also included pyroxene fractionation as a possible mechanism to explain the geochemical trends observed within the Townsite Formation on general grounds. The Townsite Formation is composed of calc-alkaline dacite breccias, tuffs, massive and pillowed dacites, and minor andesites, and is forms the top of the Lower Kam Group (Helmstaedt and Padgham, 1986a; Bullis, 1983; Cunningham and

Lambert, 1989).

Trend 3 (Component 3)

A calc-alkaline differentiation trend, of SiO_2, Al_2O_3, Nb, and P_2O_5 enrichments and Fe_2O_3, and MnO depletions is apparent as a minor trend within the Lower Kam Group rocks. Calc-alkaline trends characterize the more intermediate to felsic component of the Kam Group, and have been recognized within the Kam Group before (Baragar, 1966; Webb, 1983; Cunningham, 1984; Goodwin, 1988; Cunningham and Lambert, 1989). Sulphur depletions recognized here, may be related to the abundance (or lack thereof) of iron in the rock.

Trend 4 (Component 4)

Other less apparent trends, identified during multivariate analyses are characterized by Fe_2O_3, and MgO depletion, with CaO, Ba, and Rb enrichment, interpreted as trends that may typify localized granophyric domains within the Lower Kam Group, richer in feldspar than the surrounding basalts.

Trend 5 (Component 5)

A minor trend towards Sr, Rb, Ba, and S enrichment with MnO, Na_2O, and Al_2O_3 depletion may characterize local metasomatic domains.

5.4.2 Upper Kam Group

Univariate data for the Upper Kam Group (Yellowknife Bay Formation) are summarized on Table 9. This is a much more heterogeneous sample population than that recognized in the Lower Kam Group.   However, certain other features are consistent with Goodwin's (1984) interpretation that the Upper Kam Group represents a distinct population, separate from that of the Lower Kam Group. Goodwin (1984) based his conclusion on a clustering of data on a Ni-Sr plot (Figure 43).   The invariant progression of Sr over a wide range of Ni in rocks from the Lower Kam Group is interpreted to represent fractional crystallization proce: es from a magma with > 300 ppm Ni and restricted Sr (90 - 150 ppm) concentrations. This contrasts to the extensive scatter of Sr verses Ni in the Upper Kam Group, indicative of a partial fusion process from a mantle source (Goodwin, 1988).   Cunningham and Lambert (1989) however, reviewed these results, and together with new data (excluding altered samples), concluded that Lower and Upper Kam Group samples are similar, and infer partial melting of an undepleted mantle source for both Lower and Upper Kam Groups. The calc-alkaline Townsite Formation is interpreted to bᵢ an undepleted siliceous volcanic (USV), and a normalized Yb verses La/Sm discriminant diagram suggests the Townsite Formation has a chemistry controlled by anhydrous phases, excluding garnet, with pyroxene-controlled fractionation trends (Cunningham and Lambert, 1989).

The only major elements expressing a more complex distribution than a unimodal population trend is TiO_2 and Na_2O. The Na_2O distribution is likely due to hydrothermal processes, and has been screened out of Cunningham's (1984) and Cunningham and Lambert's (1989) data sets. The bimodal distribution of TiO_2 coincides with bimodal trends in critical trace elements Zr and Y, and to a lesser extent Nb and Rb. This is considered below.

The results of a principal component analysis of these data are presented in Figures 44, 45, 46.

Trend 1 (Component 1)

A significant trend toward Fe_2O_3, TiO_2, P_2O_5, Zr, and Y enrichment with less pronounced MnO and Na_2O enrichment and CaO depletion and notably invariant SiO_2, Al_2O_3, and MgO contents is very similar to the tholeiitic differentiation trend observed in rocks from the Lower Kam Group, as concluded by other studies (Cunningham, 1984; Cunningham and Lambert, 1989). The lower MgO concentrations in the Upper Kam Group (mean $\approx 6.7 \pm 1.8$ wt %) relative to the Lower Kam Group (mean $\approx 7.3 \pm 1.0$ wt %) may account for this trend being less pronounced, or alternatively, interpreted as a contaminated tholeiitic trend (Goodwin, 1988). The differentiation trend corresponds to a tholeiitic differentiation trend analogous to that of Kuno's (1984) moderate iron concentration tholeiite.

TABLE 9

SUMMARY TABLE, Upper Kam Group

	Log/Ar	Mode	Mean	Std	Pop
SiO_2	Arith	53	52.3	1.8	100
Al_2O_3	Arith	14.5	14.2	1.1	100
TiO_2	Arith	1.0	0.9	0.21	65.1
		1.8	1.7	0.18	34.9
Fe_2O_3	Arith	14.0	12.8	1.9	100
MgO	Arith	8.0	6.7	1.8	100
CaO	Arith	10.0	9.7	1.9	100
K_2O	Log	0.2	0.23	-0.09 +0.11	100
Na_2O	Arith	2.0	0.5	0.12	6.7
		4.5	2.0	0.45	73.1
			4.2	0.45	20.2
MnO	Arith	0.24 0.30	0.24	0.05	100
S	Log	0.04	0.04	-0.031 +0.053	100
P_2O_5	Log	0.10 0.23	0.11	-0.055 +0.215	100
Ba	Log	10	18.8	-4.28 +82.5	100
Nb	Log	0	1.79	-1.09 +2.94	86.2
		2	9.05	-5.27 +15.6	13.8
Zr	Log	60	65.5	-51.1 +84.0	72.2
		80	151	-120 +191	27.8
Y	Log	20	23.1	-18.9 +28.3	64.9
		25	43.6	-37.8 -50.3	35.1
		42.5			
Sr	L .	95	43	-35.4 +52.2	5.3
		125	111	-81.9 +151	86.5
			346	-283 +425	8.2
Rb	Log	2.5	1.45	-1.0 +2.2	41.4
		10	10.4	-4.2 +26.2	58.6
		30			

Summary table for the univariate distribution of major and minor elements within basalts of the Upper Kam Group. Presentation is a s per Table 8. Data from Cunningham (1984).
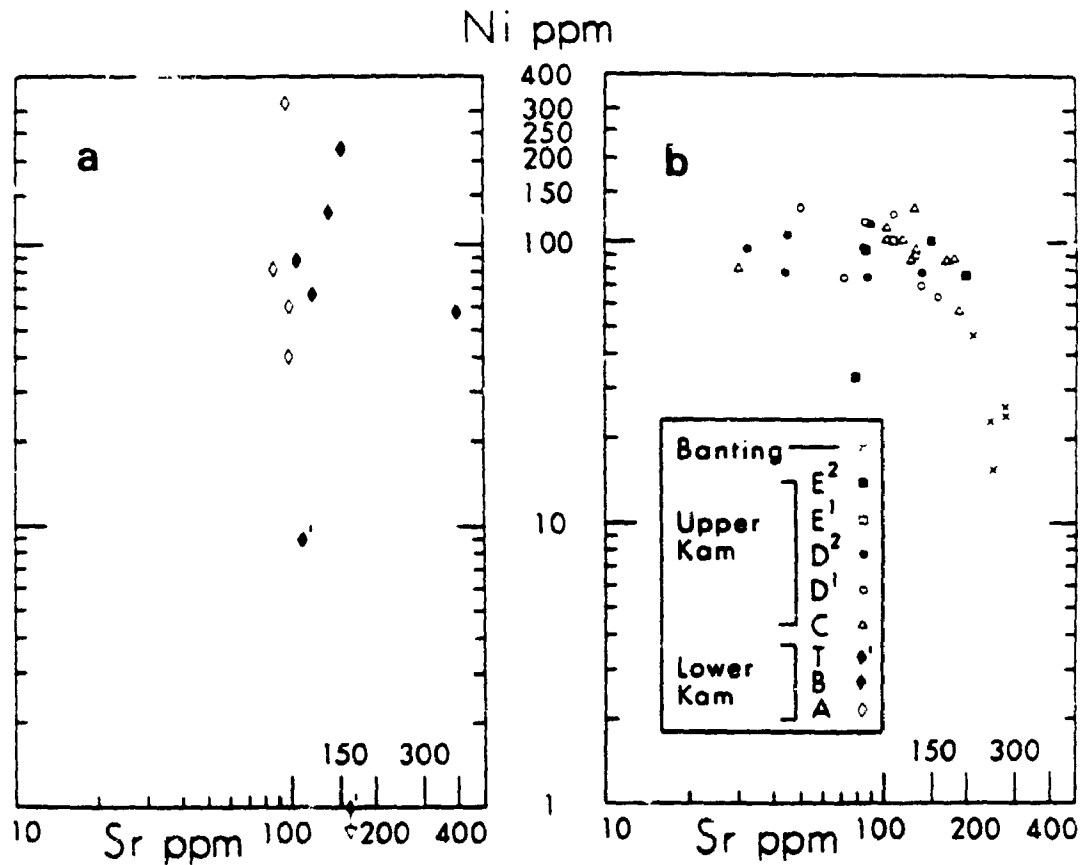
Figure 43. Lower and Upper Kam Groups plotted on a Sr verses Ni diagram showing limited Sr variance over a broad range of Ni for the lower Kam Group, but a large variance in Sr over similar Ni values for the upper Kam Group (Goodwin, 1988).

Yellowknife, NWT
Principal Component Analysis

ELEMENTS

SiO2
Al2O3
Fe2O3
MgO
CaO
Na2O
K2O
TiO2
MnO
S
P2O5
Ba
Nb
Zr
Y
Sr
Rb
V
Zn

SCORE

-0.8 -0.6 -0.4 -0.2 0 0.2 0.4 0.6 0.8

Upper Kam Group

[ ] COMPONENT 2

Yellowknife, NWT
Principal Component Analysis

ELEMENTS

SiO2
Al2O3
Fe2O3
MgO
CaO
Na2O
K2O
TiO2
MnO
S
P2O5
Ba
Nb
Zr
Y
Sr
Rb
V
Zn

SCORE

-0.8 -0.6 -0.4 -0.2 0 0.2 0.4 0.6 0.8

Upper Kam Group

[ ] COMPONENT 1

Figure 44. Bar chart illustrating the PC1 and PC2 element
scores from a principal component analysis on the
Upper Kam Group basalts.

Yellowknife, NWT
Principal Component Analysis

Yellowknife, NWT
Principal Component Analysis

Figure 45. Bar chart illustrating the PC3 and PC4 element scores from a principal component analysis on the Upper Kam Group basalts.

Yellowknife, NWT
Principal Component Analysis

Yellowknife, NWT
Principal Component Analysis
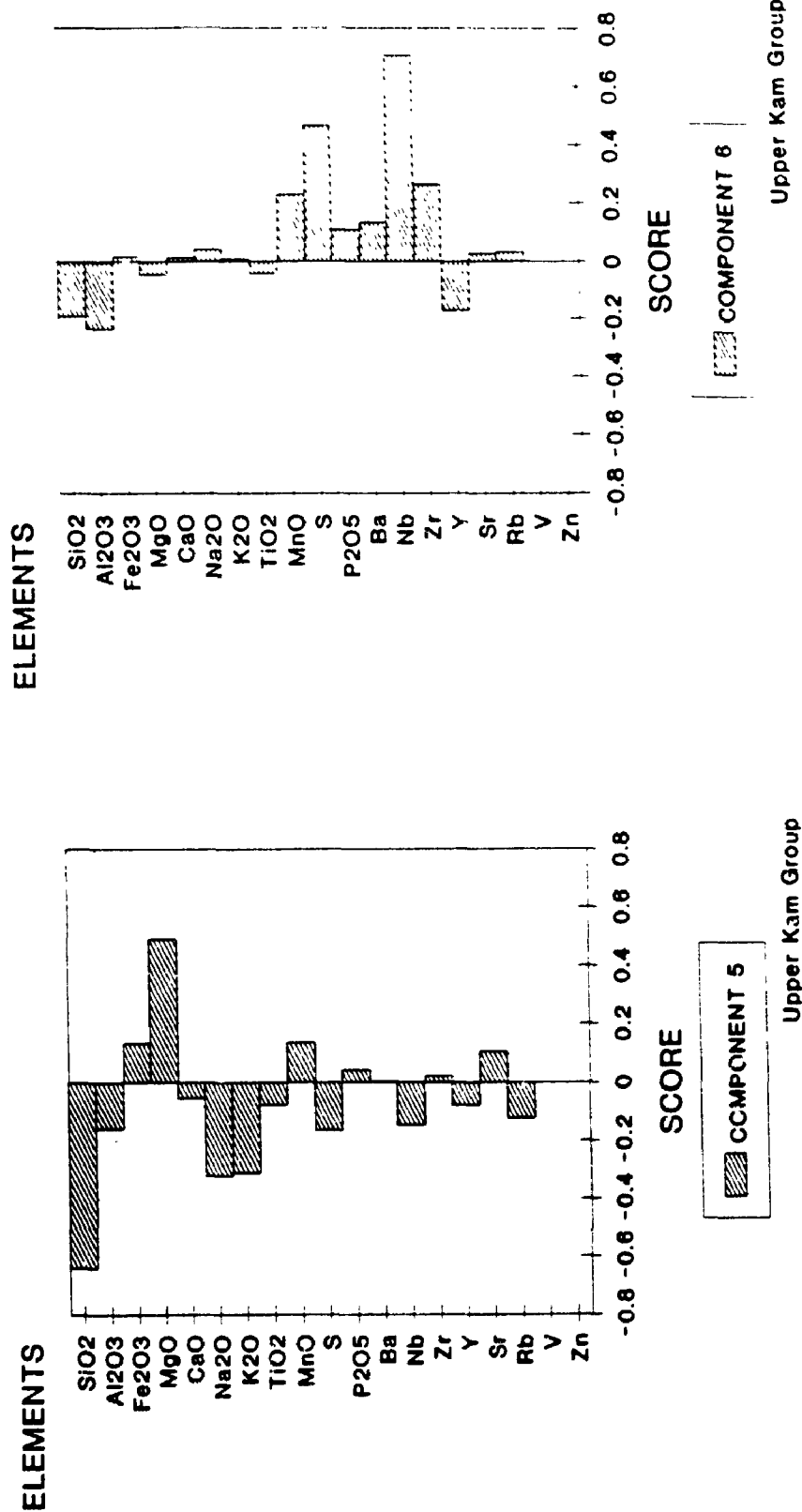
Figure 46. Bar chart illustrating the PC5 and PC6 element scores from a principal component analysis on the Upper Kam Group basalts.

Trend 2   (Component 2)

Another significant feature of the Upper Kam Group recognized from this data set is characteristic Al_2O_3, K_2O, Ba, and Rb, and to a lesser extent Sr, Fe_2O_3, S and P_2O_5 enrichment concomitant with Na_2O, and lesser Nb depletions. This trend would appear to be similar to a magmatic differentiation trend featuring enrichment of alkali-feldspar relative to plagioclase. The depletion of Nb is likely related to the trend to alkali-enrichment, or to some independent, unrecognized metasomatic process. Enrichment of P_2O_5 without CaO enrichment suggests either that apatite is not involved in this process, or that there is an equivalent depletion of another CaO-bearing phase. Similar trends have been noted by Thompson et al. (1984) which have been related to processes involving crustal contamination of more mafic magmas. Crustal contamination of a tholeiitic magma has been proposed before as a process to account for the geochemistry of the Upper Kam Group rocks (Baragar, 1966; Jenner et al., 1981; Cunningham, 1984; Goodwin, 1988; Cunningham and Lambert, 1989).

Trend 3   (Component 3)

A minor trend identified within the Upper Kam Group, represented by enrichments in MgO, K_2O, and Rb, and to a lesser extent SiO_2, and MnO, accompanied by a depletion in CaO and Sr, and to a lesser degree, Al_2O_3, would appear to be a metasomatic alteration trend of the type alluded to by

Armstrong (1991). An alteration assemblage in the hanging wall basalts of the Con Shear Zone, favouring muscovite, rare high-MgO chlorite, alkali- feldspar, quartz, ankerite-dolomite (near his type 2 mineralization) is associated with an ore-related metasomatic event. Further examination of the sample locations from Cunningham's (1984) data from the Upper Kam Group confirms this association to mineralized centres. The recognition of mineralization-related metasomatism within the host basalts external to the shear zones, has been identified by others (Gates, 1979; Webb, 1984).

Trend 4 (Component 4)

Subtle trends identified though a multivariate analysis of the data include SiO_2, Fe_2O_3, CaO, S, and less important MgO enrichments coupled with K_2O, and less significant Na_2O, Ba, and Rb depletions, interpreted as a feature similar to what is empirically related to quartz+carbonate+sulphide veining.

Trend 5 (Component 5)

MgO depletion with SiO_2, Na_2O, K_2O, enrichment is similar but not identical to that related with the local granophyric domains within the basalts as identified in samples from the Lower Kam Group.

5.4.3 Schists

The schists form the immediate host rocks for all of the

economically exploitable gold mineralization at the NERCO-Con and Giant Mines at Yellowknife. It is clear that the schists have been derived from the Kam Group basalts. The major orebodies occur where the schists cross-cut rocks of the Upper Kam Group (Padgham, 1990). Boyle (1961), Jardine (1974), Myers (1977, 1978), Osatenko (1971), Webb (1984), Duke et al. (1991), Gates (1979), Duke et al. (1990), Armstrong (1991), and Duke and McDonald (1991) all describe the evolution from undeformed, relatively unaltered rocks of the Kam Group to chlorite schist, and ultimately auriferous sericite schists + auriferous quartz veins in the Con, Campbell, or Giant shear zones. These transformations have been described as complex hydrothermal alterations invo_ving one or more aqueous fluids, ultimately implicating the fluids responsible for the gold mineralization (Boyle, 1961; Kerrich and Allison, 1978).

This section describes the geochemistry of "typical" chlorite, and sericite schists, and attempts to characterize the chlorite schists in terms of a statistical treatment of their geochemistry. Geochemical t.ends are recognized, and an attempt is made to assign each trend to a geologically recognizable event. Previous discussions have characterized the major geochemical events that may be identified in the relatively unaltered host rocks, and the quartz veins are considered below. Presumably, aspects from both end-members (basalt and auriferous quartz vein) will be recognized in the

chlorite schist which is spatially and temporally, and geochemically intermediate between the two extremes.

The "average" Kam Group basalt (Boyle, 1961; Myers, 1978; Cunningham, 1984; Goodwin, 1985), chlorite schist (Boyle, 1961; Osatenko, 1971; Myers, 1978; this study), sericite schist (Boyle, 1961; Osatenko, 1971; Jardine, 1974; Myers, 1978), and mineralized quartz vein (Boyle, 1961; Osatenko, 1971; Jardine, 1974; Myers, 1978; this study) is presented below.

<u>Avera' analysis</u>

	Kam basalt	chlorite schist	sericite schist	mineralized quartz
SiO_2	49.60	45.60	38.19	88.20
TiO_2	1.09	1.14	0.82	0.13
Al_2O_3	13.86	12.80	16.26	5.76
Fe_2O_3	12.64	10.94	10.15	2.29
MgO	7.11	6.55	5.77	0.90
MnO	'.21	0.13	0.17	0.04
CaO	10.50	9.50	11.02	2.40
K_2O	0.36	0.83	2.82	0.30
Na_2O	2.16	1.07	0.29	0.30
P_2O_5	0.09	0.20	0.21	0.05
S	0.14	0.37	2.54	0.45
Total	**97.76**	**89.13**	**88.24**	**100.82**
Au	0.009	0.007	1.61	23.7
Ag	0.6	1.6	12.2	9.1
As	8	1,149	1,840	190
Hg	0.024	0.028	0.151	0.071
Sb	10	21	53	46
V	283	492	-	96
Cr	303	107	-	67
Co	26	32	-	24
Ni	82	81	75	42
Cu	68	79	88	53
Pb	9	4	36	106
Zn	67	96	175	113
Rb	10	24	28	-
Sr	121	136	47	88
Y	24	-	-	-
Z1	74	68	-	-
Nb	2	-	-	-
Ba	130	152	209	156
Ga	-	15	-	-

Major oxides are reported in weight %
Minor and trace elements are reported in ppm

Trends identified in the chlorite schists are evaluated empirically for similarities with features apparent within the relatively unaltered Kam Group rocks. Those expressing

similar gains and losses identified previously for the Kam Group rocks are related to those trends. Unrecognized trends are evaluated in the following manner. First, the more alteration insensitive elements Al_2O_3, TiO_2, are examined for coherent behaviour, indicating volume gains or losses, characteristic of silicification or carbonatization. Non-coherent behavious of these elements may be interpreted as a primary magmatic trend. Second, the most mobile major elements, SiO_2, CaO, Na_2O, and K_2O are considered, along with Rb, a.ud Sr, for evidence of coherence, revealing evidence of alkali-metasomatic events, carbonatization, or alternatively, considered together with Al_2O_3, Fe_2O_3, and MgO, for magmatic differentiation trends. Lastly, Fe_2O_3, MgO, S, P_2O_5, Ba, V, and Zn are examined, in light of the above, to evaluate chalcophile/siderophile element behaviour, possible lamprophyre involvement, or other empirically defined trend.

A principal component analysis identifies the following geochemical trends (Figures 47, 48, 49).

Trend 1   (Component 1)

The principal geochemical trend identified in the chlorite schist sample population (n=153) is one of K_2O, S, As, Zn, Rb, and Ba enrichment, and Al_2O_3, Fe_2O_3, and Na_2O depletion. All other elements are shown to be essentially invariant. These correspond to a trend from unaltered Kam Group basalt to

mineralized quartz veining plus sericite schist. Some diagnostic elements, such as Au and Ag were not included in this analysis. It would be preferable to check these elements to confirm this interpretation.

Trend 2 (Component 2)

A second trend observed within the schist data is characterized by TiO_2, As, and Zn enrichment, and SiO_2, K_2O, Na_2O, Rb, and Sr depletion. The other elements included in this analysis are nearly invariant. These trends also reflect the changes involved in the transition from a basalt to a chlorite schist with alkali-metasomatism. Arsenic and Zn are traditionally related to rocks proximal to gold mineralization. Potassium and Rb are generally coherent in ore-related metasomatic events at Yellowknife, and commonly enriched in the sericite schists associated with gold mineralization, and depleted in the chlorite schists adjacent to the sericite schists (Webb, 1984; Rye, 1987).

It is possible that this trend relates to incorporation of lamprophyre in the schists (see Chapter 3), as the elements expressing the greatest variance here are some of those that account for the greatest geochemical variance between lamprophyre and basalts or chlorite schist analyses. However, incorporation of lamprophyre should result in enrichments of TiO_2, MgO, V, and P_2O_5, and this is not seen. There is also a

Yellowknife, NWT
Principal Component Analysis
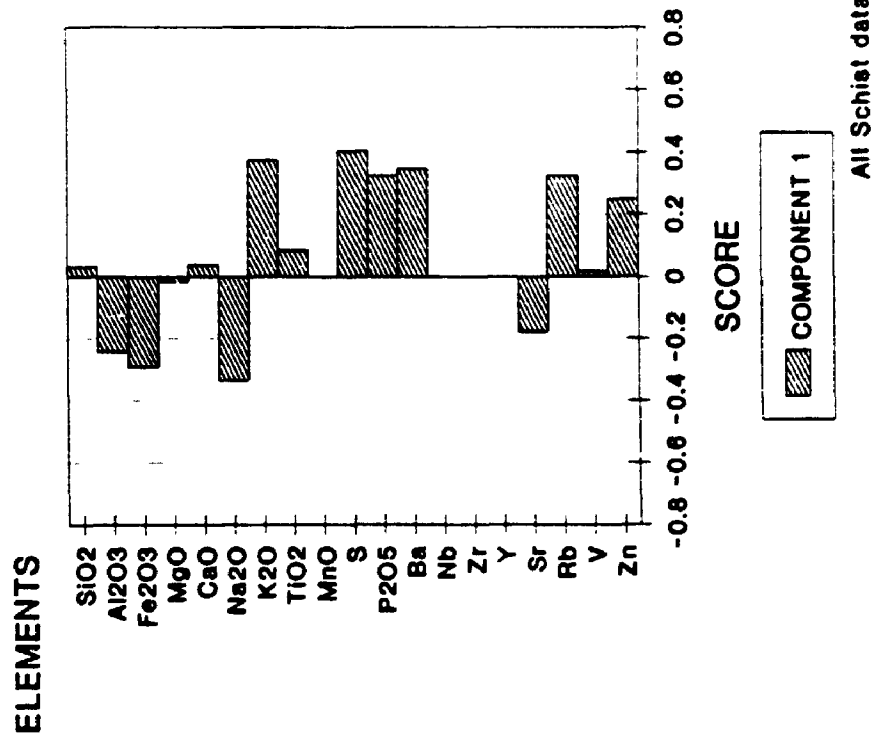
Yellowknife, NWT
Principal Component Analysis
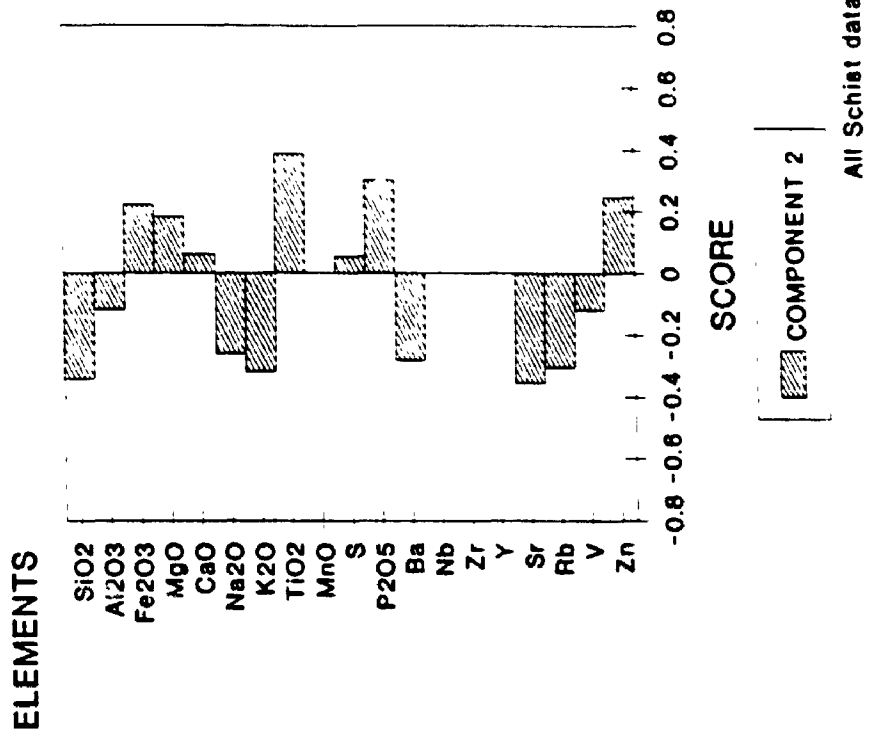
Figure 47. Bar chart illustrating the PC1 and PC2 element scores from a principal component analysis on the chlorite-carbonate schist.

Yellowknife, NWT
Principal Component Analysis
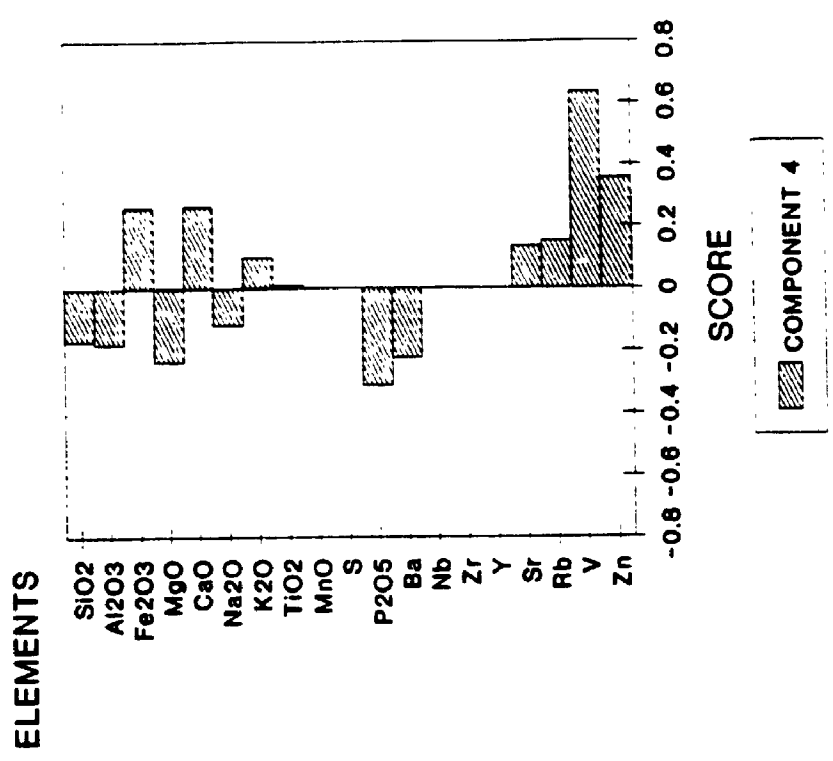
ELEMENTS

SiO2, Al2O3, Fe2O3, MgO, CaO, Na2O, K2O, TiO2, MnO, S, P2O5, Ba, Nb, Zr, Y, Sr, Rb, V, Zn

SCORE

-0.8 -0.6 -0.4 -0.2 0 0.2 0.4 0.6 0.8

All Schist data

COMPONENT 4

Yellowknife, NWT
Principal Component Analysis

ELEMENTS

SiO2, Al2O3, Fe2O3, MgO, CaO, Na2O, K2O, TiO2, MnO, S, P2O5, Ba, Nb, Zr, Y, Sr, Rb, V, Zn

SCORE

-0.8 -0.6 -0.4 -0.2 0 0.2 0.4 0.6 0.8
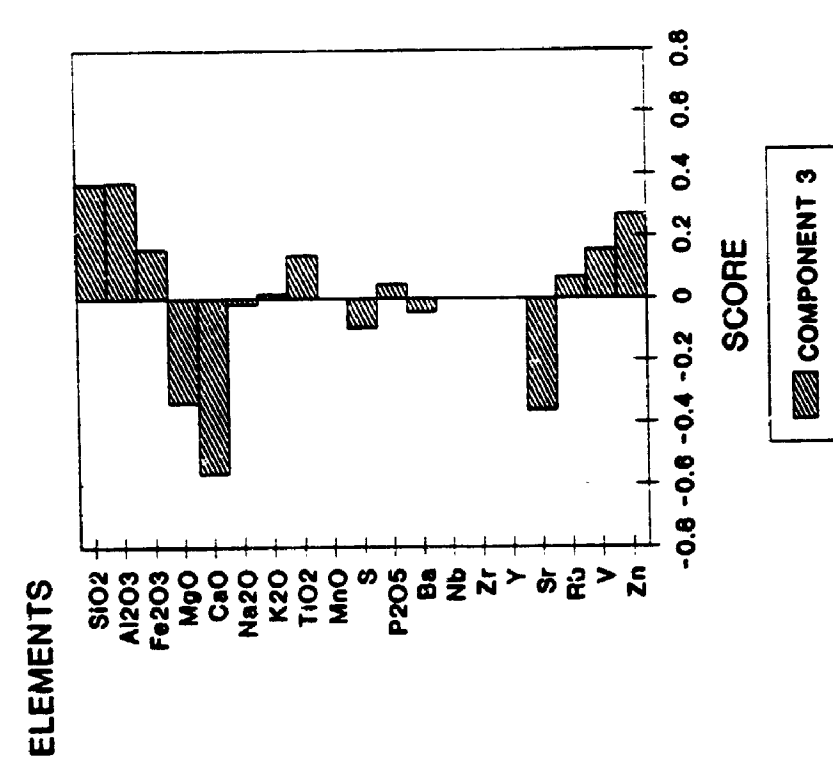
All Schist data

COMPONENT 3

Figure 48. Bar chart illustrating the PC3 and PC4 element scores from a principal component analysis on the chlorite-carbonate schist.
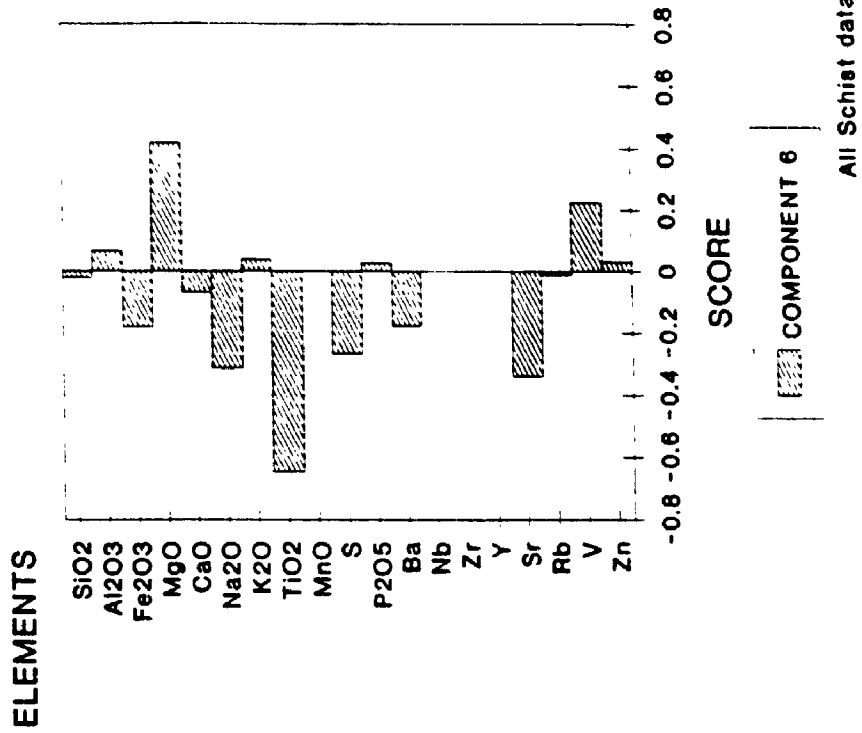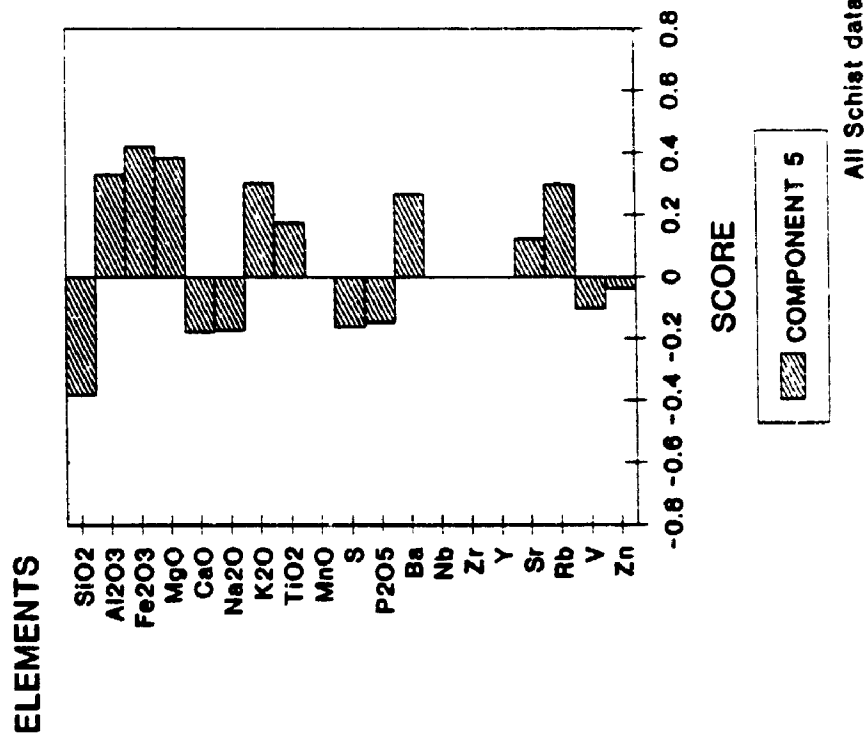
Figure 49. Bar chart illustrating the PC5 and PC6 element scores from a principal component analysis on the chlorite-carbonate schist.

similarity between this trend and the trend identified previously within rocks from the Upper Kam Group and interpreted to be indicative of local granophyre development. There are similar relative gains and losses for all elements associated with this trend, with the exception of TiO_2, P_2O_5, and Sr.

Trend 3   (Component 3)

The third largest amount of variance within the schist data set, is characterized by SiO_2, Al_2O_3, and Zn enrichment and MgO, CaO, and Sr depletion.   All other elements in this analysis are invariant.   This trend is similar to a calc-alkaline differentiation trend, or alternatively, a metasomatic trend characterized by silicification accompanied by destruction and mobilization of bivalent cations (MgO, CaO, and Sr) but not Fe.   The absence of any involvement with S is consistent with the invariance of Fe.   There is no comparable trend within the Upper Kam Group, and as such, the involvement of a primary magmatic trend is considered unlikely for this component.   It is therefore considered to best represent a metasomatic process, most likely related to carbonatization of the host volcanics.   This geochemical trend reflects a metasomatic trend in the transformation from basalt to chlorite-carbonate schist.

Trend 4   (Component 4)

A fourth trend identified within the schists in... .e Fe$_2$O$_3$, CaO, V, and Zn enrichment and MgO, P$_2$O$_5$, As, and .. .. .etion, interpreted to represent part of a tholeiitic diffe.entiation trend.

Trend 5 (Component 5)

A fifth trend includes Al$_2$O$_3$, Fe$_2$O$_3$, MgO, K$_2$O, Rb, and Ba enrichment and SiO$_2$, depletion, possibly defining some involvement with a lamprophyre, or rocks proximal to mineralization (Webb, 1984; Head, 1985).

Trend 6 (Component 6)

A minor trend features MgO, and V enrichment, and TiO$_2$, Na$_2$O, S, and Sr depletions, perhaps representing a component of a magmatic differentiation trend.

None of these trends have any apparent equivalents identified within the Upper Kam Group. There is a partial correlation however between the last geochemical trend (MgO and V enrichment, and TiO$_2$, Na$_2$O, S, and Sr depletions) for the schists, and the principal geochemical trend for the Lower Kam Group (MgO depletion and TiO$_2$, Zr, and Y enrichment). It is unclear why this magmatic differentiation trend, characteristic of the Lower Kam Group basalts might be reflected within the schists hosted within Upper Kam Group volcanics. It may indicate that perhaps the Upper and Lower

Kam Groups are more similar than originally revealed (Cunningham and Lambert, 1989).

More likely, it is thought that the trend in the Lower Kam Group reflects the involvement of tholeiitic intrusions (early mafic dykes and sills), which are abundant and form an integral component of these rocks (Boyle, 1961, Henderson and Brown, 1966, Helmstaedt and Padgham, 1981), and that the schist samples were preferentially collected from material derived from intrusions, relative to the Upper Kam Group basalts. It has been recognized that the auriferous shear zones are preferentially aligned both in strike and dip to the early mafic dykes (number 8 dykes; Henderson and Brown, 1966; Webb, 1983; Hodgson, pers com., 1983; Duke et al., 1990). Further, it has been noted that the Negus and Rycon shear zones are preferentially mineralized where early mafic dykes form the host to the schist zones; elsewhere, these schist zones are barren of ore bodies (McCartney and Webb, 1986).

5.5 Quartz veins

Previous work by Jardine (1974), Myers (1977, 1978), Osatenko (1971), Head (1985), Webb (1983), Webb (1984), and Boyle (1961) is compilled, and presented together with new work. Results reveal that some elements are normally below detection levels for quartz vein samples, or are essentially invariant. These elements have been excluded from further analysis. The

table below summarizes these elements specifically excluded from this study.

ELEMENT	AVE RANGE	SOURCE
Li	5-25 ppm	Boyle (1961)
Ti	1-3 ppm	Boyle (1961)
	0-0.14 ppm	Head (1985)
Ba	<20 ppm	Boyle (1961)
Sr	<20 ppm	Boyle (1961)
B	<20 ppm	Boyle (1961)
C	<20 ppm	Boyle (1961)
Cr	<20 ppm	Boyle (1961)
Mn	1-10 ppm	Boyle (1961)
Be	0-1.5 ppm	Head (1985)
Bi	0-8 ppm	Head (1985)
Mo	0-4 ppm	Head (1985)

On the basis of these data, the quartz vein samples from Yellowknife were analyzed for a restricted suite of elements, in an attempt to select those that, (a) showed some correlation with mineralization based on previous work, and (b) showed a significant variance. A third criterion, economics and ease of analysis was considered, as some of these data were acquired as part of a privately funded exploration program.

All of the elements are log-normally distributed with bimodal or trimodal populations. One mode, for Au, Ag, Pb, and Sb is at or near detection limits.

Strong correlations between all of the elements considered

(Au, Ag, Cu, Pb, Zn, As, Sb) was obtained, except for Au/Zn, ranging from r=0.100 (Au/Zn) to r=0.638 (Au/As; n=500, r_{95}=0.168).

Principal component analysis of these data reveals geochemical trends expressed graphically in Figures 50, 51, 52 and discribed below.

Trend 1 (Component 1)

The most significant trend recognized is characterized by extreme Au, Ag, As, and Sb enrichments, with less intense Cu, Pb, and Zn enrichments. This trend would best be described as the gold mineralization trend, as it emphasises the critical suite of elements empirically associated with the known orebodies in Yellowknife (Boyle, 1961; Henderson and Brown, 1966; Webb, 1984; Head, 1985). It also reveals a partial separation of Au (and Ag, As, Sb) from the base elements Cu, Pb, Zn, a feature recognized in many Canadian Precambrian-gold deposits (Kerrich and Hodder, 1982). This aspect appears to be in contrast to the empirical relationship that the best mineralized quartz veins at the NERCO-Con Mine commonly contain sphalerite, galena, and trace sulphosalts. Sphalerite and galena are also common indicators of high-grade ore shoots at the McIntyre-Hollinger and Dome mines in Timmins (Hodgson and Troop, 1984).

Trend 2   (Component 2)

Another trend present within the quartz samples is characterized by Zn and Cu enrichment and a relative depletion in Au, and to a lesser extent, Sb.   This would appear to be the corollary to the first component, described above; base metal enrichment and Au depletion.

Trend 3   (Component 3)

Also recognized is a trend toward Pb and Sb enrichment and Ag depletion. Less significant Cu depletion is also apparent in this suite of samples. This describes a second, base metal-rich association, distinct from the Cu+Zn-rich suite described above.

Trend 4   (Component 4)

Other features identified from the quartz data include Ag and Pb enrichment and Cu and Sb depletion, characteristic of Ag-rich galena zones, in otherwise barren (of gold) quartz veins. Falck and Atkinson (1991) described a trend in silver mineralization that transgresses the strike of the greenstone belt and is apparently unrelated to the other elements (Au, As, Co, Fe, Mo, Ni, Zn, Mn, Pb, and Cu) from their suite of 400 samples.   They mention, however, that Pb has a distribution roughly correlating to the spatial distribution of Ag, elevated at The Ptarmigan Mine, on the east-side of Yellowknife Bay, east of Yellowknife at Burwash Point, and at

Yellowknife, NWT
Principal Component Analysis
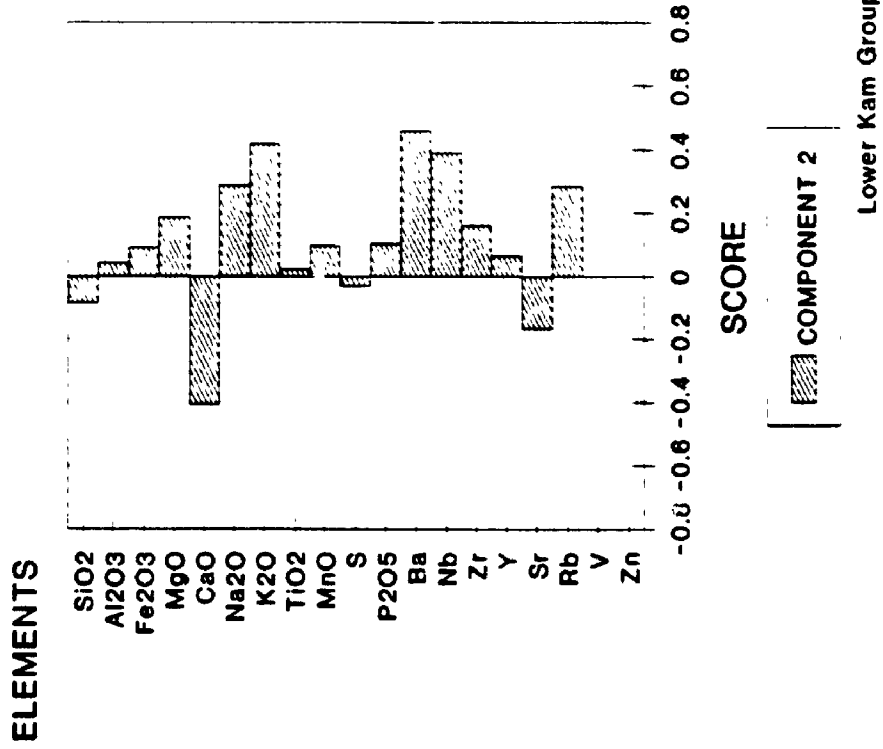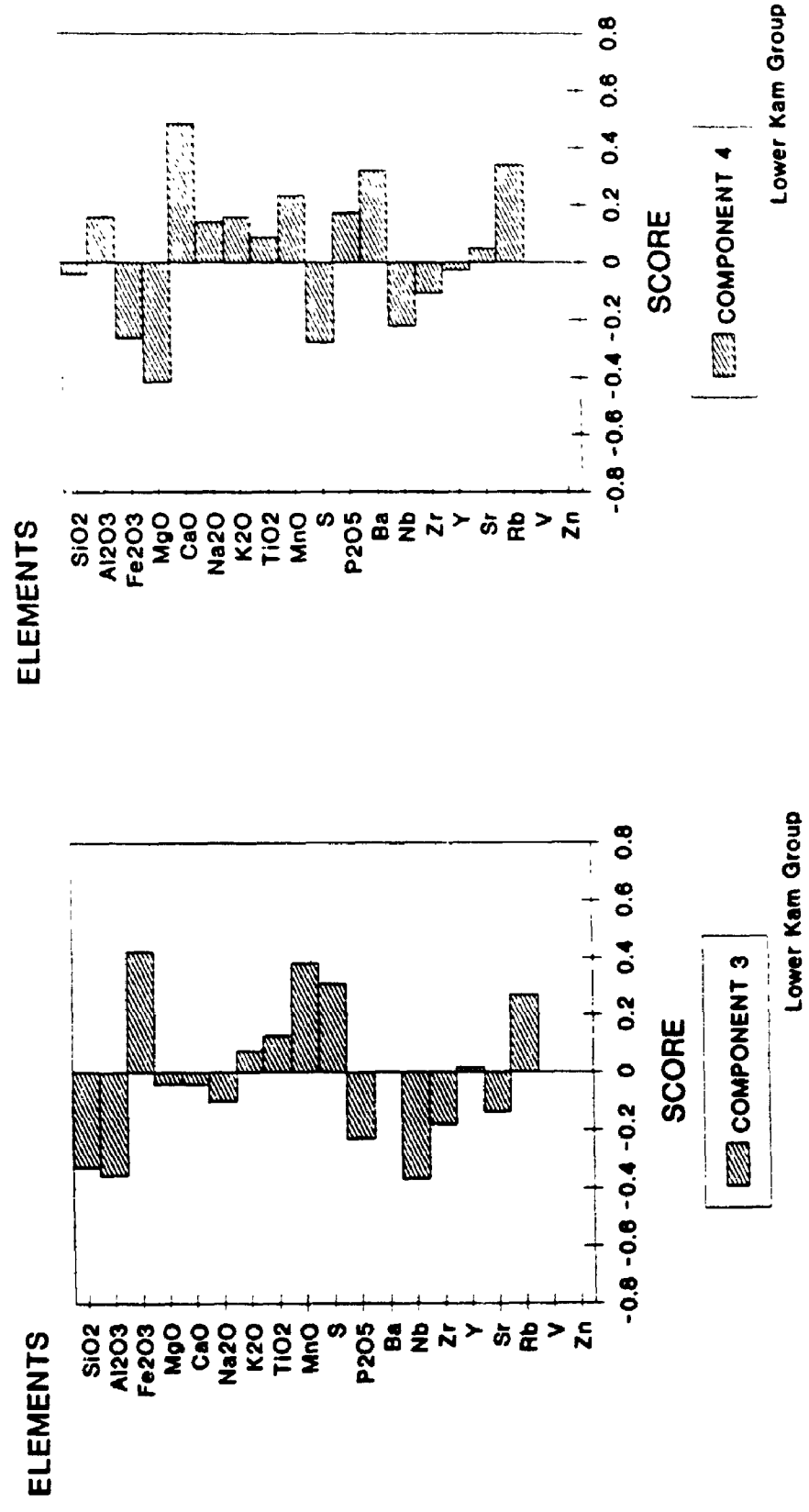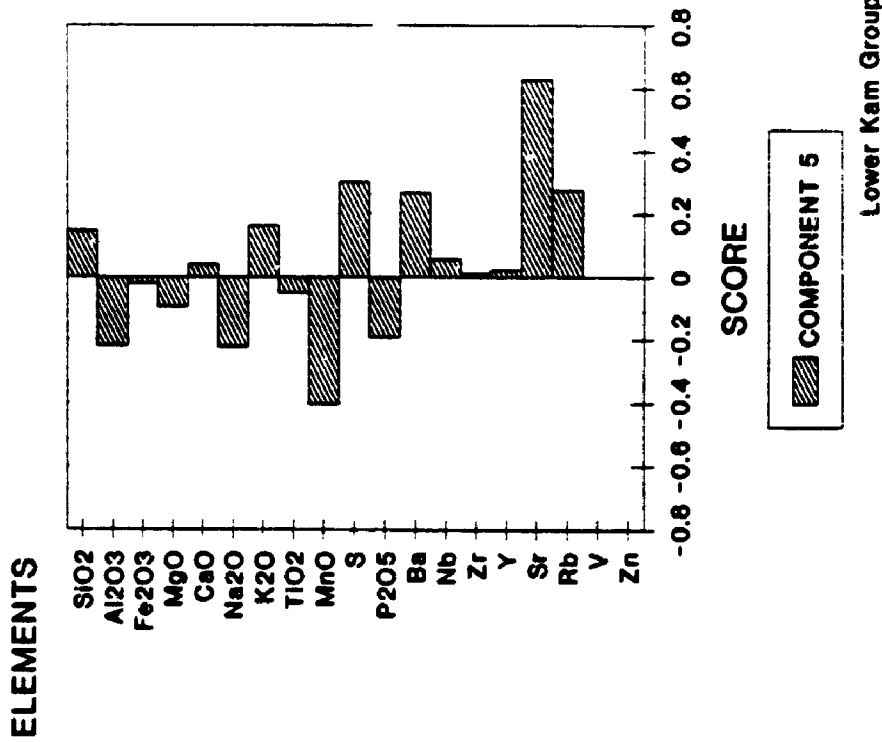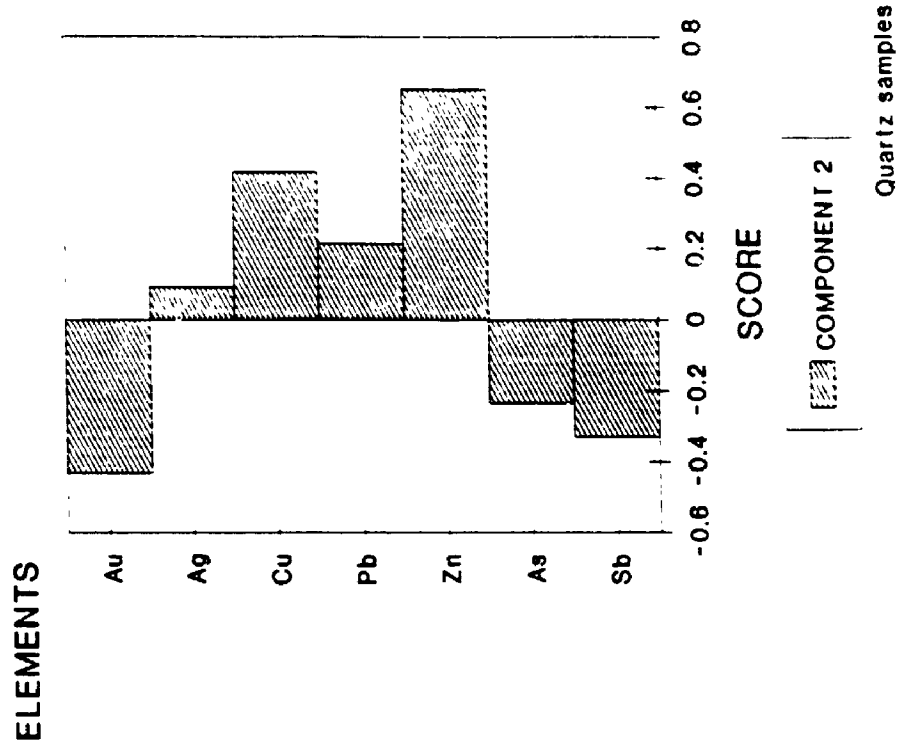

Yellowknife, NWT
Principal Component Analysis
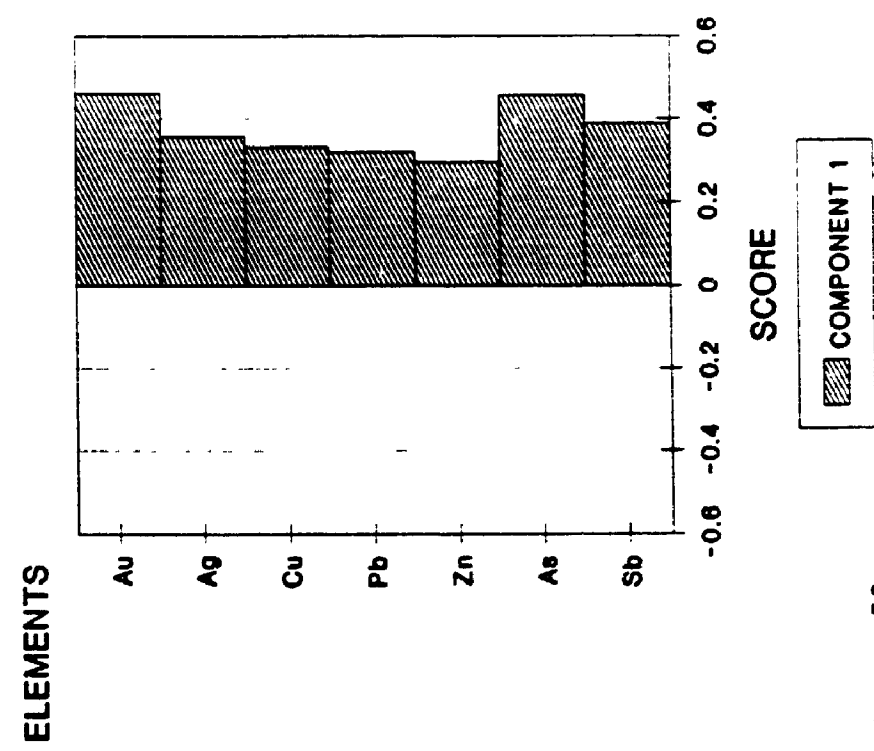
Figure 50.

Bar chart illustrating the PC1 and PC2 element scores from a principal component analysis on the quartz samples.

Yellowknife, NWT
Principal Component Analysis

Yellowknife, NWT
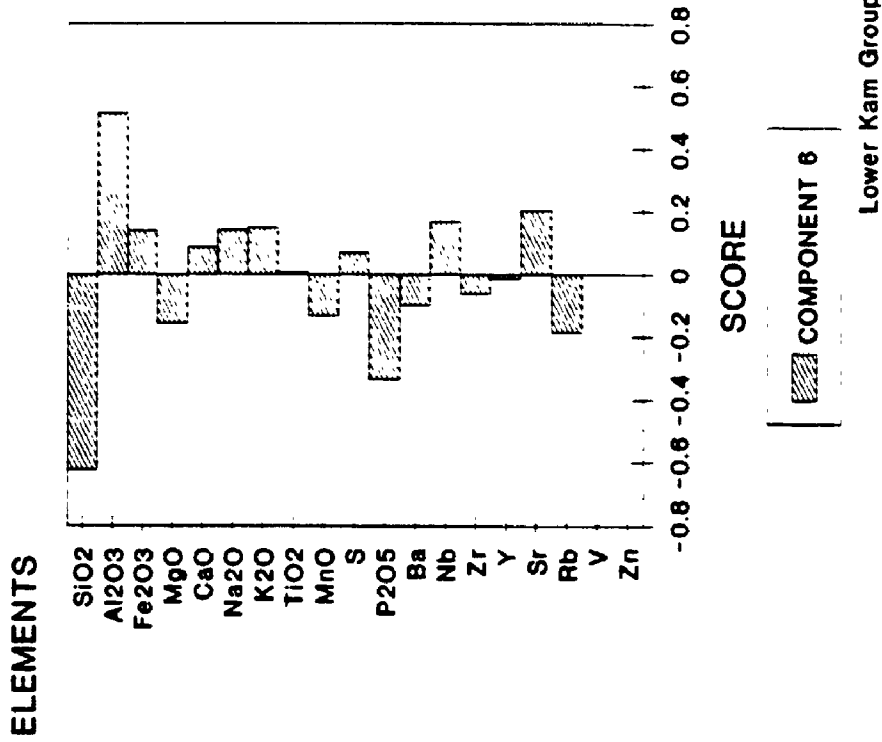### Principal Component Analysis
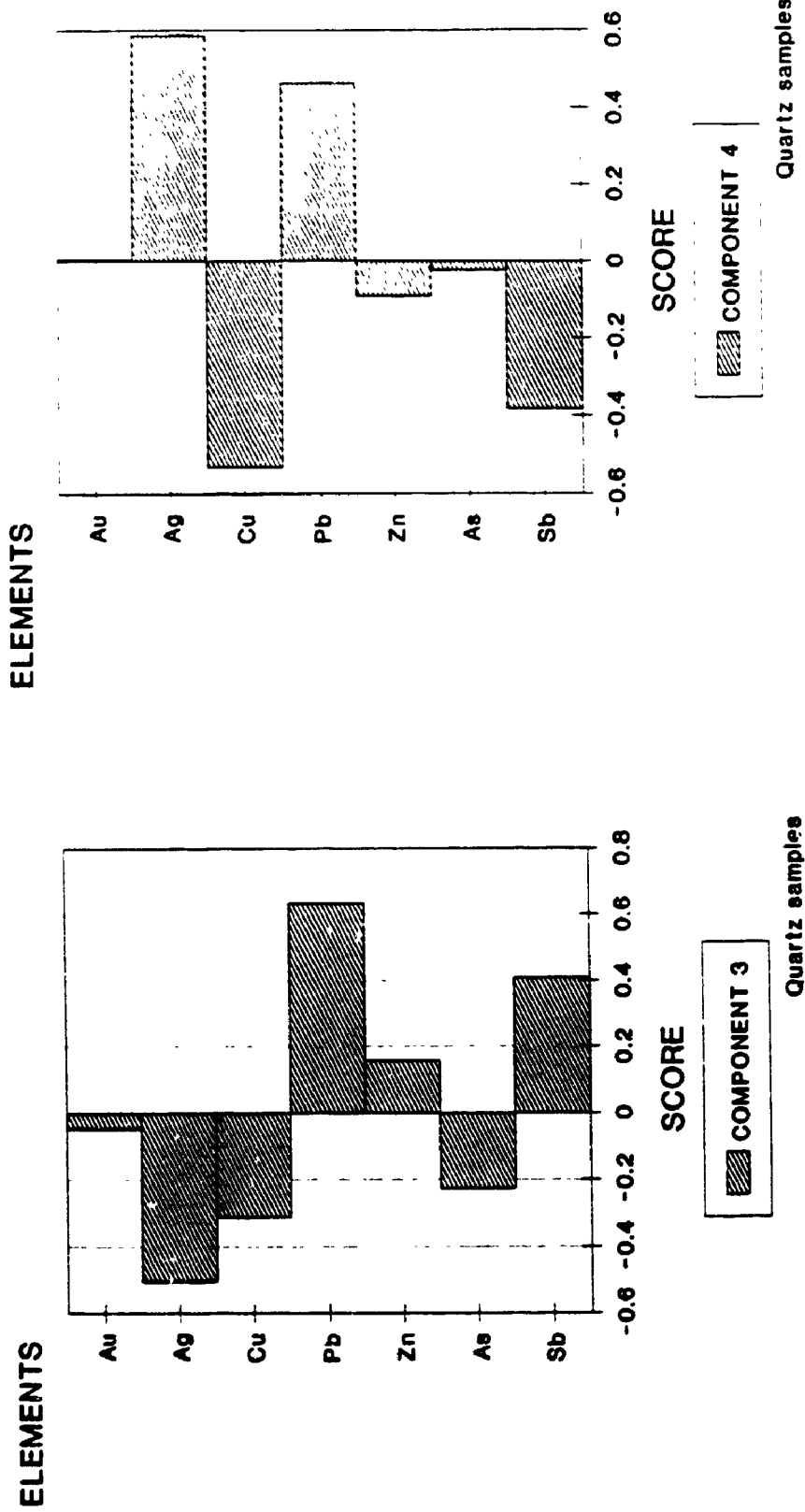
Figure 51. Bar chart illustrating the PC3 and PC4 element scores from a principal component analysis on the quartz veins.
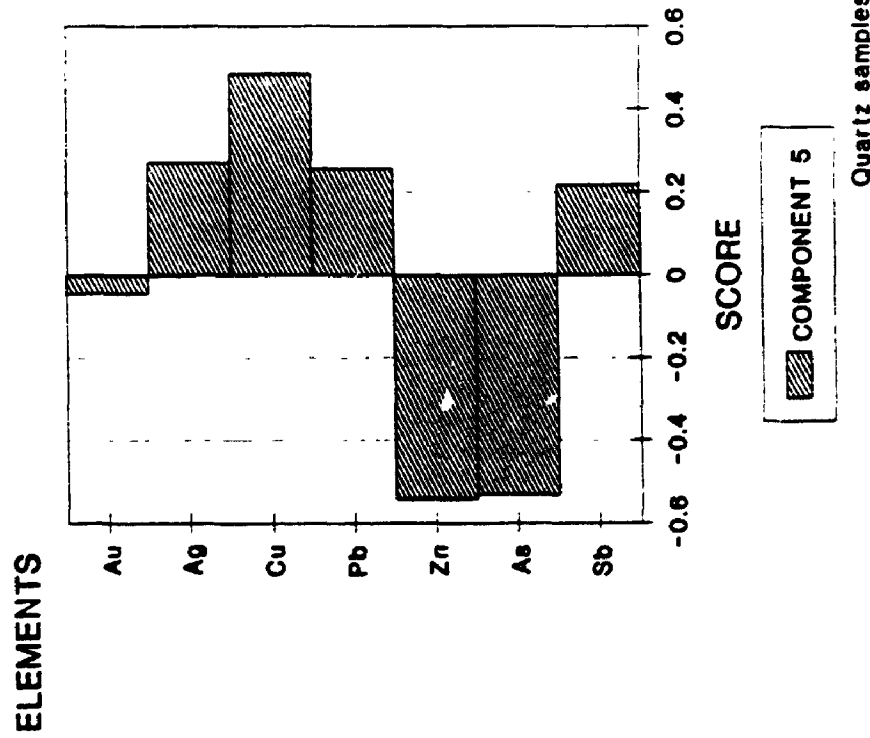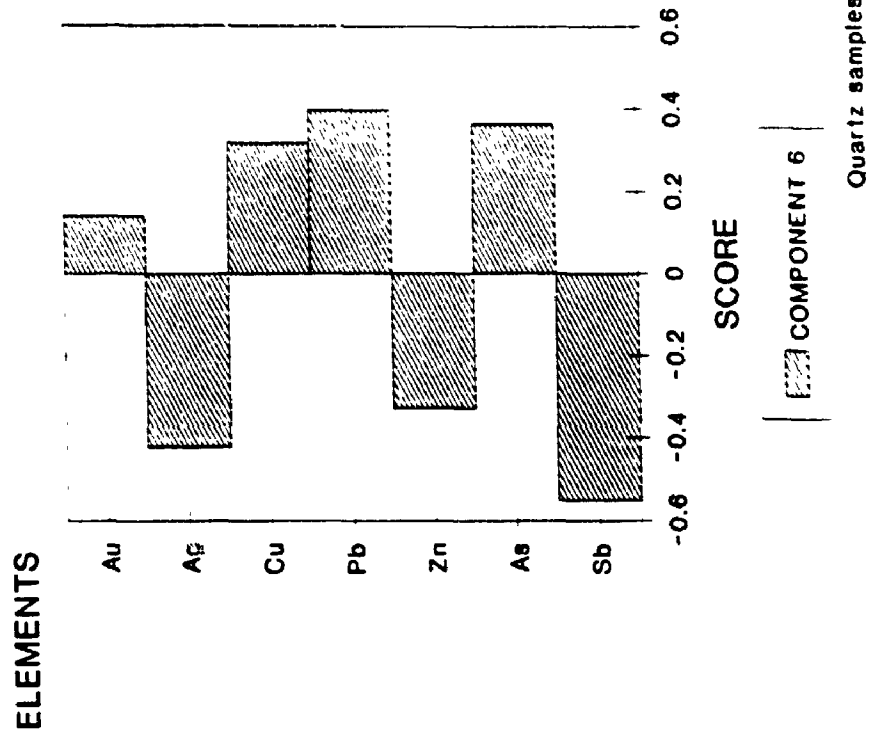
Figure 52. Bar chart illustrating the PC5 and PC6 element scores from a principal component analysis on the quartz veins.

Homer Lake, 20 km north of Yellowknife, describing a transgressive, somewhat east-west trend.

Trend 5   (Component 5)

A minor trend of Cu enrichment and Zn and As depletion is apparent from the data, and may be related to Falck and Atkinson's (1991) trend of Cu-rich showings which they related to the major Proterozoic faults.

Trend 6   (Component 6)

Arsenic enrichments, with Sb, Ag and Zn, and Au depletions characterize a population of arsenopyrite-rich zones that are essentially barren (of gold), commonly recognized at both the NERCO-Con and Giant gold mines.   An arsenic-rich event which, although related to a gold mineralizing event, accounts for a minor amount of gold compared to a galena-sphalerite event (Falck and Atkinson, 1991; Falck, 1990).   The trends identified from these data suggests the existence of several arsenic-rich events, some of which are unrelated to gold mineralization.

5.6 Interpretation

Five to six distinctive geochemical trends can be recognized from the least altered basalts from each the Lower and Upper Kam Groups. Aspects from all of these trends can be observed in the field, and most had been recognized and documented by

other workers using different techniques (Boyle, 1961; Jenner et al., 1981; Cunningham, 1984; Cunningham and Lambert, 1989).

Geochemical differences between the undeformed basalt and the extensive chlorite-carbonate schist zones had formerly been characterized, as had some of the differences between the chlorite-carbonate schists, sericite-carbonate schists, and auriferous quartz veins (Boyle, 1961, 1979; Osatenko, 1971; Jardine, 1974; Myers, 1978; Webb, 1984; Head, 1985). This study assumed that some of the geochemical variation in the chlorite-carbonate schist is attributable to differences inherited from precursor rocks, as noted in other camps (Davies et al., 1982; Hodgson and Troop, 1984; McNeil and Kerrich, 1986; Skwarnecki, 1989). The identification of lamprophyre within the Campbell Shear Zone indicates that these inherited differences are significant. Similar assumptions might apply to geochemical variations identified within the sericite-rich schists, and perhaps to the quartz veins.

Previous studies on ore-related metasomatism have identified geochemical trends that are generally consistent between Archean gold camps, with diagnostic suites of elements that may characterize specific gold camps, or types of gold camps (Boyle, 1979; Fyon and Crocket, 1982; Davies et al., 1982; Kerrich and Hodder, 1982; Kerrich, 1983, 1989a, 1989b, 1990;

Fyfe and Kerrich, 1984; Kerrich and Watson, 1984; Keith, 1984; Hodgson and Troop, 1988; Hodgson, 1990; Leitch, 1990; Phillips, 1990; Ridley, 1990). Significant volatile addition is ubiquitous in most mesothermal gold deposits, as are enrichments of Cu, Ag, Zn, Cd, B, Pb, As, and Sb, and variable enrichments of Se, Te, Cr, Mo, W, Co, and Bi (Boyle, 1979).

Wall rock alteration varies with metamorphic grade and host lithotype, but commonly noted alteration assemblages in greenschist-hosted deposits include, chlorite, sericite, carbonate, sulphide and quartz. Relative gains and/or losses of major and trace elements within the wall rocks peripheral to the gold-bearing quartz veins are extremely dependant upon the geochemistry of the host rocks, and the changes are rarely coherent (Kerrich and Watson, 1984; Head, 1985; McCartney and Webb, 1986). Geochemical incoherence requires spatial considerations to be incorporated. For example, Fe, Mg, K, Rb, Zn, S, As, Ba, and CO_2, characteristically enriched in the altered wall rocks adjacent to auriferous quartz-carbonate veins relative to wall rocks more distal to mineralization, are found to contain lower gold values than those in immediate contact with the quartz vein. Here SiO_2 (and Au) enrichment reflects increased silicification (Head, 1985; Appendix 4). Mass balance requirements however, will elevate Fe, Mg, K, Rb, Zn, S, As, Ba, and CO_2 concentrations in the more silicified rocks, such that there will be an apparent depletion in the

Fe, Mg, K, Rb, Zn, S, As, Ba, and CO_2 concentrations in the adjacent, altered wall rocks.

5.6.1 Spatial Distribution

A subset of the chlorite schist data set, exclusively from the Campbell Shear Zone is considered here. The subset includes stable isotope data, reported in Chapter 6, and ICP AE data for Co, and Ni. A second multivariate analysis was completed on this data set, independent of the other chlorite schist samples. Similar, although slightly enhanced metasomatic trends are determined (Appendix 4).

Single element plots revealing distribution trends within the Campbell Shear Zone, the sample locations, the distribution of stopes and ore-reserves within the Campbell Shear Zone are presented in Appendix 4. Figures 53, 54, 55 reveal the principal trends determined from multivariate analysis.

Data Presentation

Individual samples are coded for longitude and elevation. The data are krigged onto orthogonal grids, with nodes at 100' (32.5 m) intervals, using the 10 closest points in a quadrant search, with a radius of 1,000' (325 m). This is plotted on a vertical plane approximating the hanging wall surface of the Campbell Shear Zone.

The major elements show distributions of K_2O enrichment, and SiO_2, Al_2O_3, Na_2O depletions, with variable, TiO_2, Fe_2O_3, MgO, and CaO, and LOI gains and losses, proximal to mineralization. Trace elements are distributed in a more complex pattern. P_2O_5, Ni, Sr, Zr, and Y are all significantly enriched south of latitude 18,000, below elevation 1,000. This corresponds to where the Campbell Shear Zone cross-cuts a lamprophyre dyke. These elements are consistently enriched in the lamprophyre dyke relative to all other rocks in the Yellowknife Greenstone Belt (see chapter 4). P_2O_5, Sr, and Ga are also enriched near latitude 19,000 and elevation 1,200. It is not known what this represents, as there has been nothing noted in this area to account for this anomaly.

Cobalt and Ni are extremely enriched in an elongate, south plunging domain, 2,000' by 1,000' (650 m x 325 m) centred at latitude 20,000 and elevation 1,800. A second domain, roughly of the same dimensions, open in all directions but closed to the surface is located centred at latitude 22,500 and elevation 3,000. These two domains precisely coincide with the 102 and 103 ore zones respectively. Moderately enhanced Co is associated with the 100 and 101 ore zones, whereas enhanced Ni concentration is only associated with portions of each of these ore zones.

A domain anomalously enriched in Cu extends from the upper

Yellowknife, NWT
Principal Component Analysis

Campbell Shear Zone

COMPONENT 1

Yellowknife, NWT
Principal Component Analysis
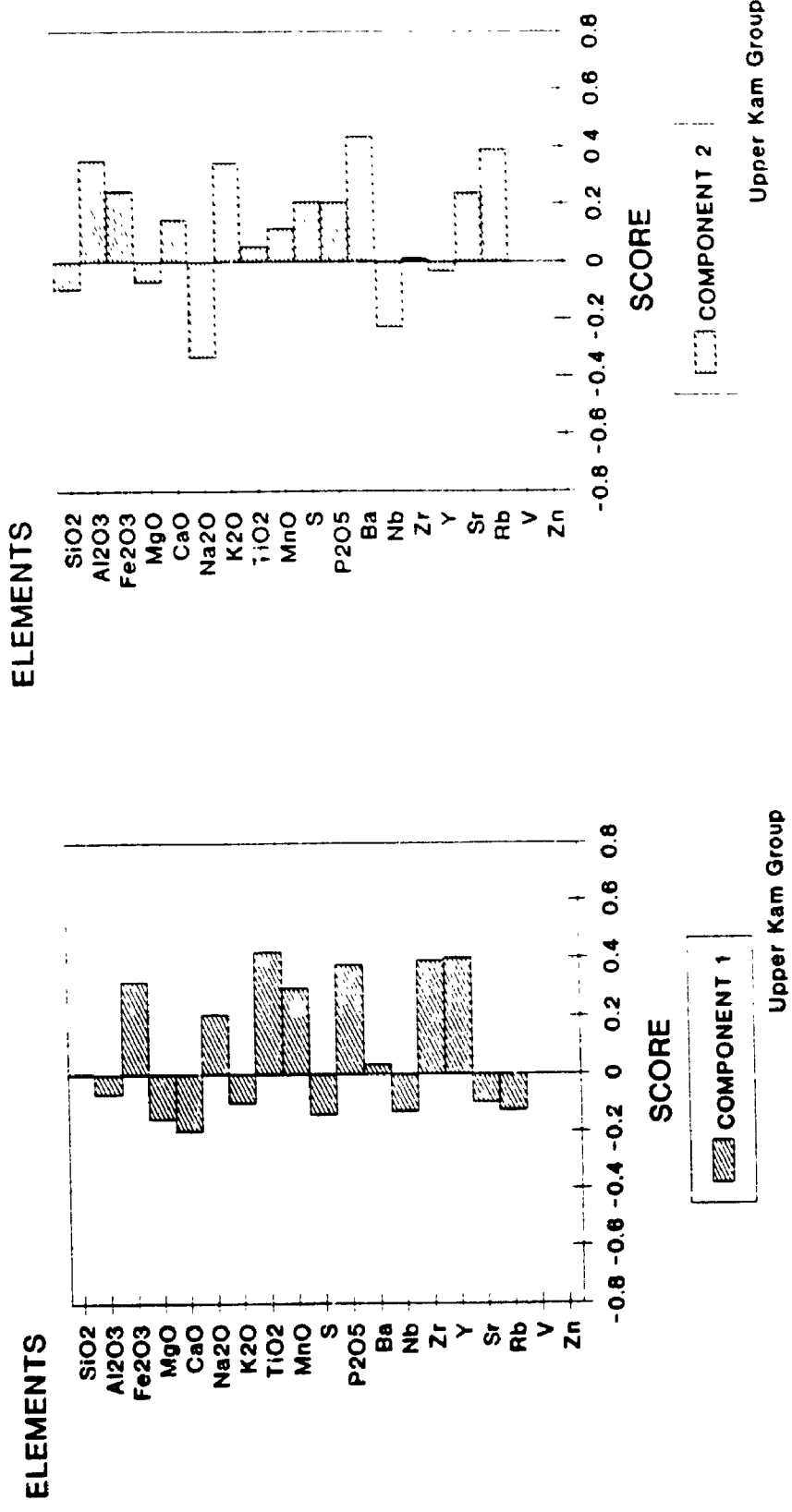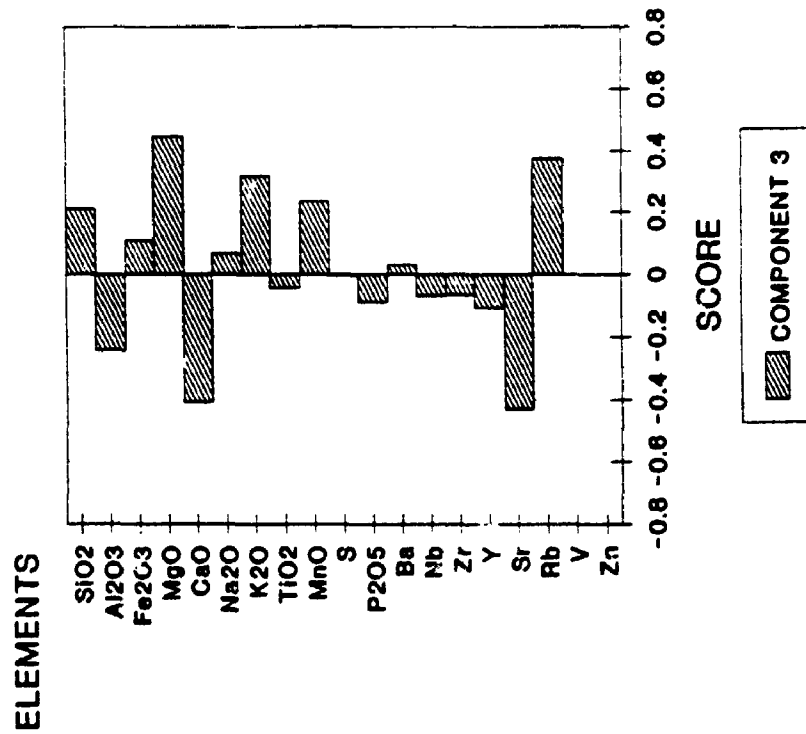

Campbell Shear Zone
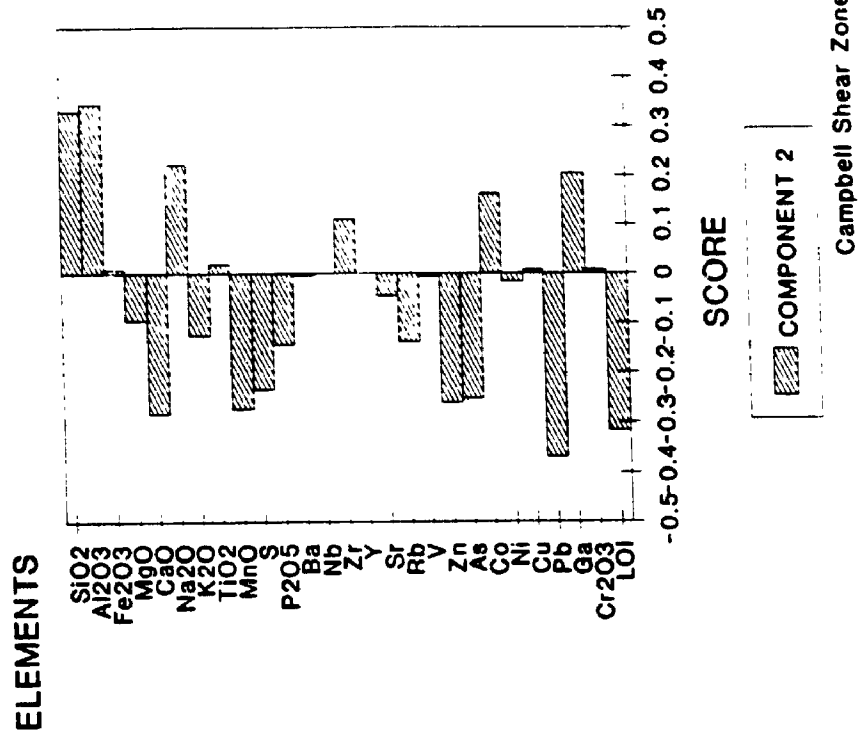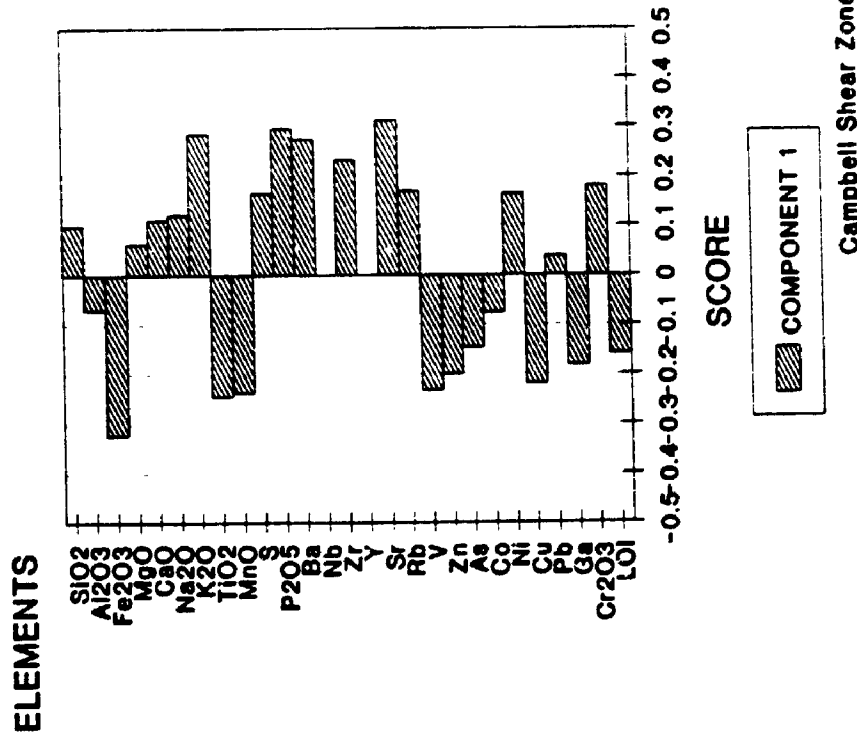
COMPONENT 2

Figure 53. Bar chart illustrating the PC1 and PC2 element scores from a principal component analysis on the chlorite schist samples.

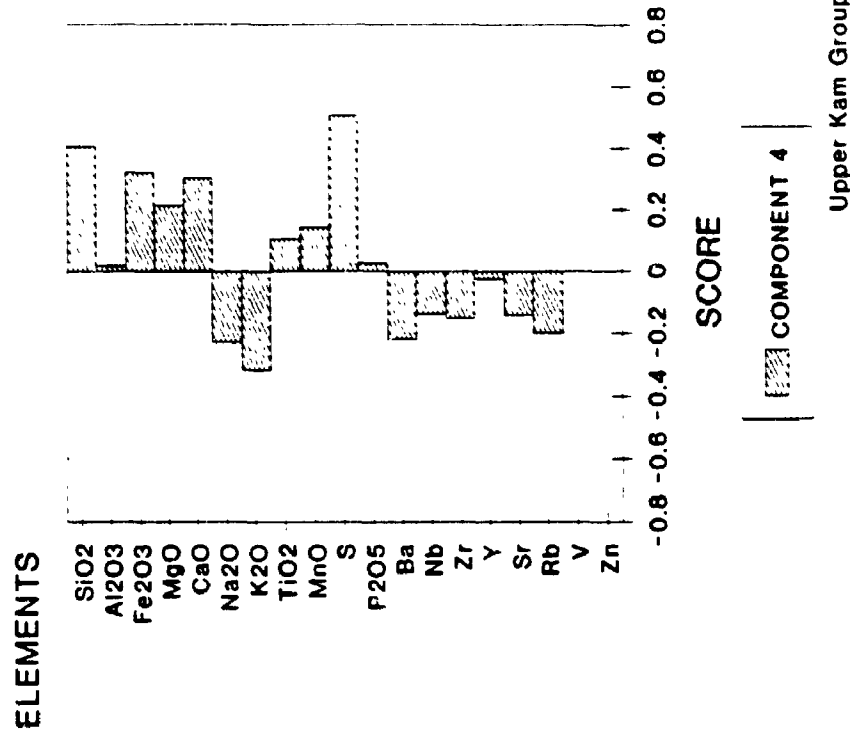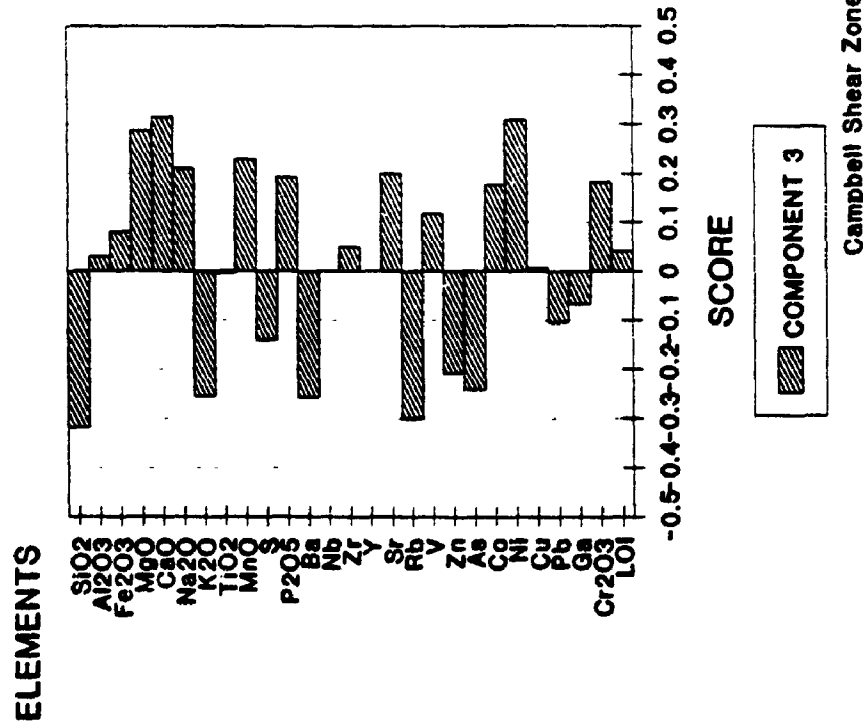## Yellowknife, NWT
Principal Component Analysis
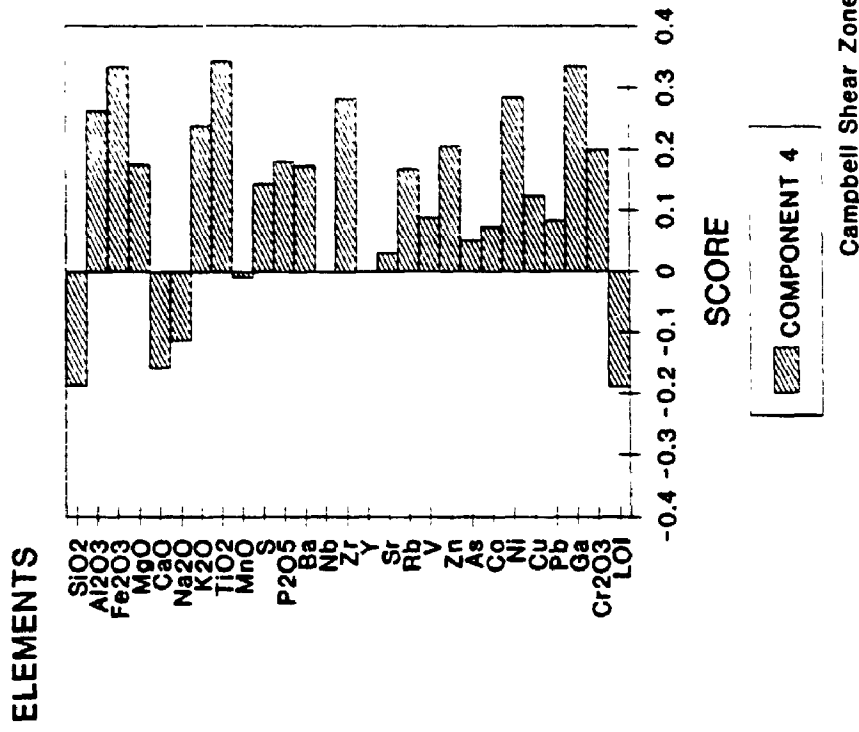
Figure 54. Bar chart illustrating the PC3 and PC4 element scores from a principal component analysis on the chlorite schist samples.

Yellowknife, NWT
Principal Component Analysis

ELEMENTS

SCORE

Campbell Shear Zone

COMPONENT 6

Yellowknife, NWT
Principal Component Analysis
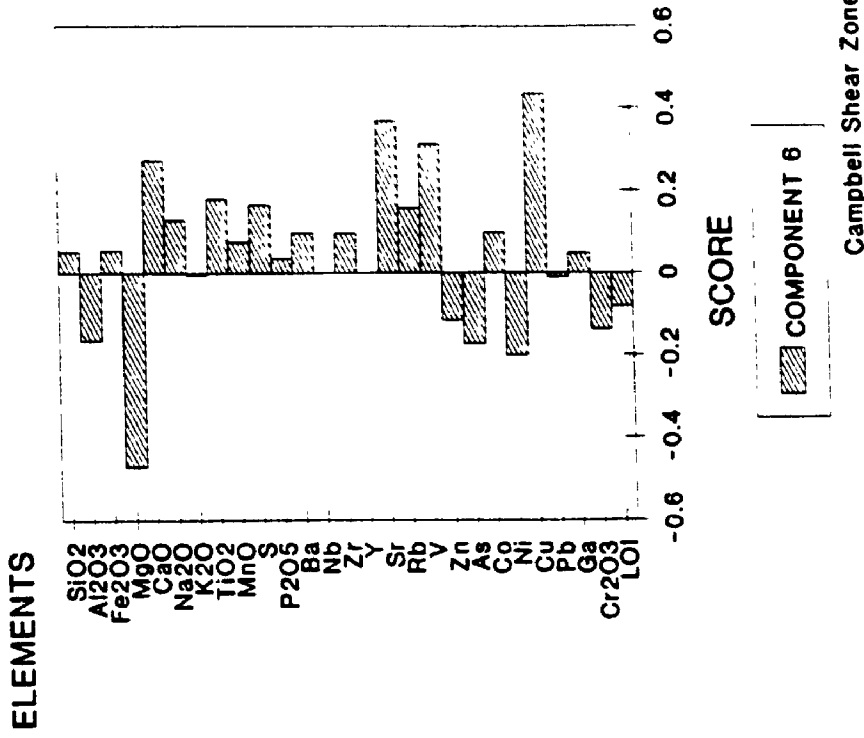
ELEMENTS

SCORE

Campbell Shear Zone
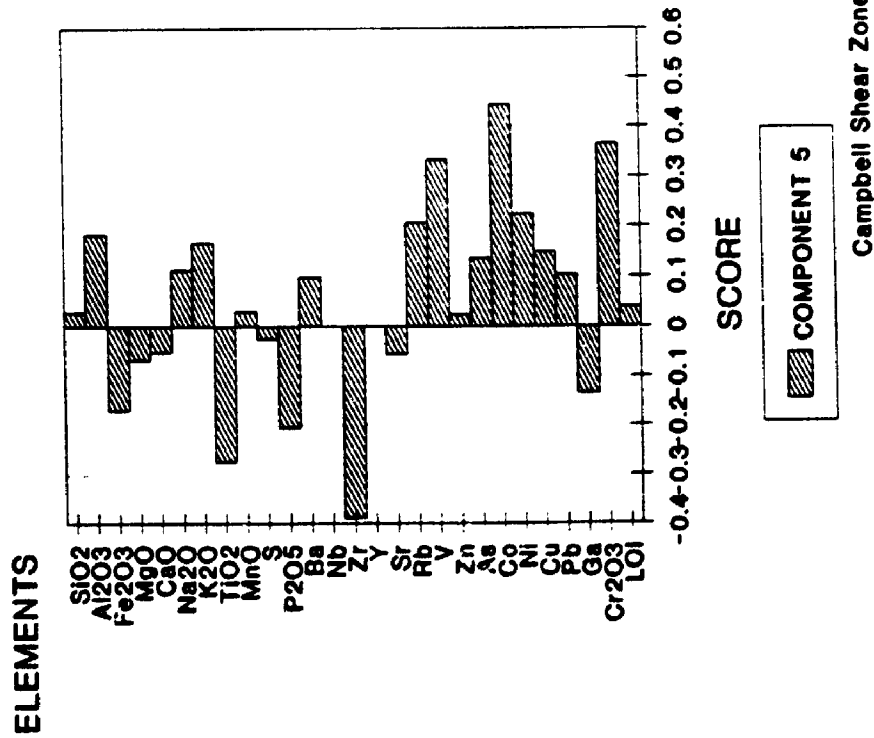
COMPONENT 5

Figure 55. Bar chart illustrating the PC5 and PC6 element scores from a principal component analysis on the chlorite schist samples.

levels of the Campbell Shear Zone in the south, down to the north in a zone 4,000' (1,230 m) long and 1,000' (325 m) to 3,000' (925 m) wide. A similarly enriched domain occurs near latitude 21,500 above elevation 3,000. Domains anomalously depleted in Cu appear to coincide with the 102, and portions of the 100 and 103 ore zones.

Zinc concentrations in the chlorite schists possess a moderately north-plunging trend, coincident with, but less intense than that expressed by Cu. Elsewhere, Zn is moderately enriched proximal to the 103, 101, and portions of the 100 ore zone. Chlorite schists proximal to the 102 ore zone are generally depleted in Zn relative to the rest of the shear zone.

Rubidium distributions correspond to the distribution of the ore zones in a general way. Significant Rb enrichments are found centred at the south-end of the 103, and 101 ore zones, and near the top and central portions of the 102 ore zone, and to depth beneath the 101 ore zone.

Yttrium is moderately enriched in the rocks adjacent to the 103 and 101 ore zones, and significantly enriched in the schists adjacent to the deeper portion of the 102, and the northern portion of the 100 ore zones.

Sulphur and As are enriched in the chlorite schists adjacent to the 101 and 103 ore zones. Sulphur is also significantly enriched in the rocks adjacent to the deeper portions, and to the north of the 102 ore zone, and in a domain above the 100 ore zone.

Chlorite schists, anomalously enriched in Pb occur at latitude 19,200 below elevation 800. This trend is projected into an area where there are no samples, and is an artifact of the griding program, and accordingly may not be real.

The primary trends recognized in the analysis of all of the schist samples described previously in this chapter also reveal distributions that aid the interpretation of the single element plots.

Principal component analysis of these data are presented in Figures 56, 57, 58. Similar analyses including all chlorite schist data are presented in Appendix 4.

Principal trend one (PT1) reveals peak scores in the rocks adjacent to the 103, top of the 102, and portions of the 101 ore zones. Distinct moderate north-plunging trends can be discerned from this plot.

The second principal trend (PT2) is clearly related to chlorite

schist derived from lamprophyre, and is strongly enhanced at depth to the south.

The third trend (PT3) recognized in the chlorite schists reveals an irregular distribution, that is moderately enhanced proximal to the 101, 102, and 103 ore zones.

Principal trend 4 (PT4) scores are moderately to strongly depleted adjacent to the 102 ore zone, but otherwise is irregularly distributed in the Campbell Shear Zone.

A fifth trend (PT5) is clearly coincident with mineralization within the Campbell Shear Zone, and are positive adjacent to all of the known ore zones within the shear zone. An unusual near vertical discontinuity exists to depth in the south, near latitude 17,000.

5.7 Discussion

Geochemical trends have been used to interpret the nature of the rocks at Yellowknife, and by extension, the environment of deposition (Baragar, 1966; Baragar and Goodwin, 1969; Condie and Baragar, 1974; Cunningham, 1984; Cunningham and Lambert, 1989). Tholeiitic differentiation trends dominate, characterized by Fe_2O_3, Na_2O, P_2O_5, MnO, TiO_2, Zr, and Y enrichment, concomitant with MgO, CaO, and K_2O depletion.
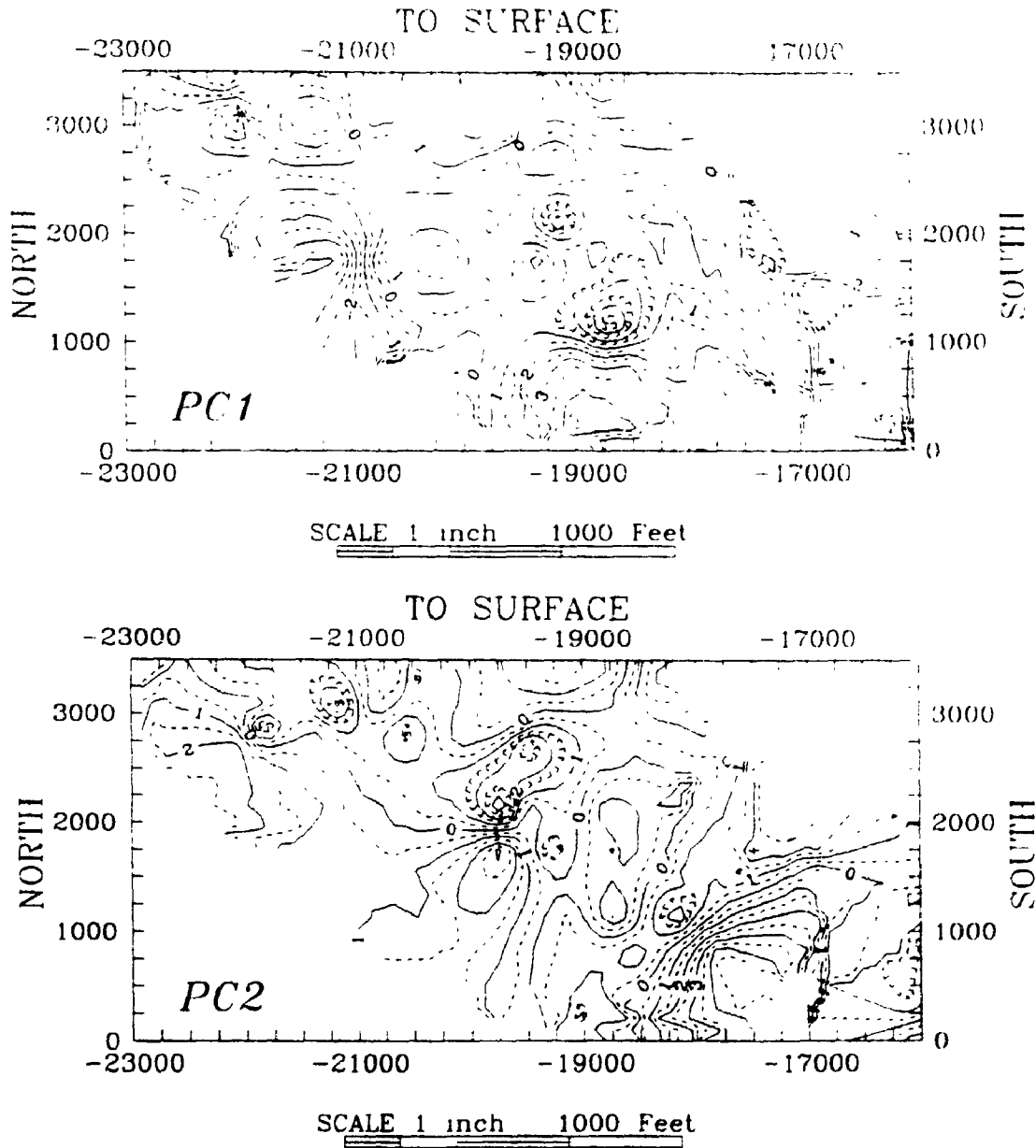
Figure 56. Longitudinal section of the Campbell Shear Zone
revealing the distribution of PC1 and PC2 scores.
The location of sample locations, and ore zones
in the Campbell Shear Zone are shown in Appendix
3.

CAMPBELL SHEAR ZONE
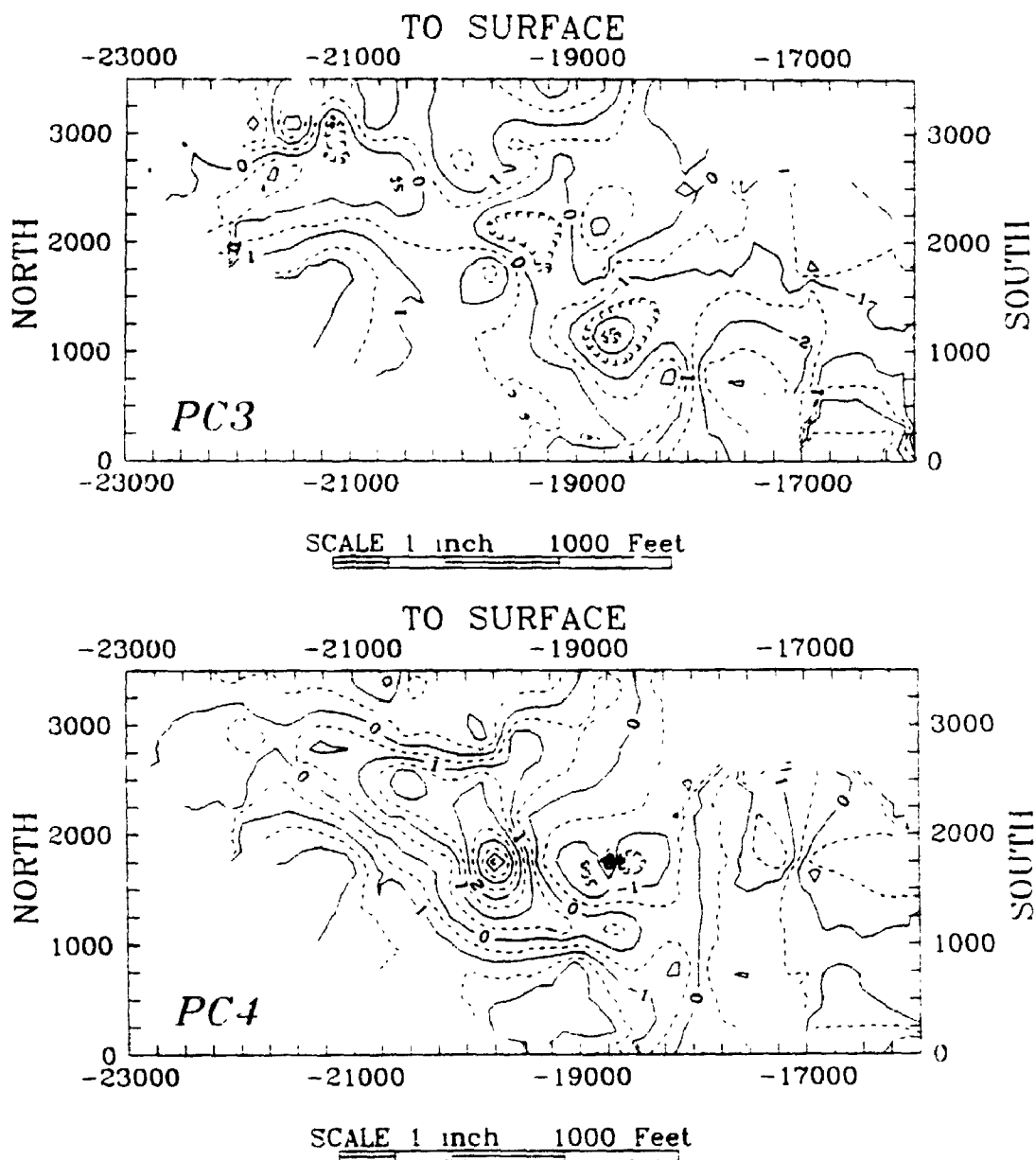
Figure 57. Longitudinal section of the Campbell Shear Zone revealing the distribution of PC3 and PC4 scores. The location of sample locations, and ore zones in the Campbell Shear Zone are shown in Appendix 3.

CAMPBELL SHEAR ZONE

TO SURFACE

PC5

SCALE 1 inch   1000 Feet

TO SURFACE

PC6

SCALE 1 inch   1000 Feet
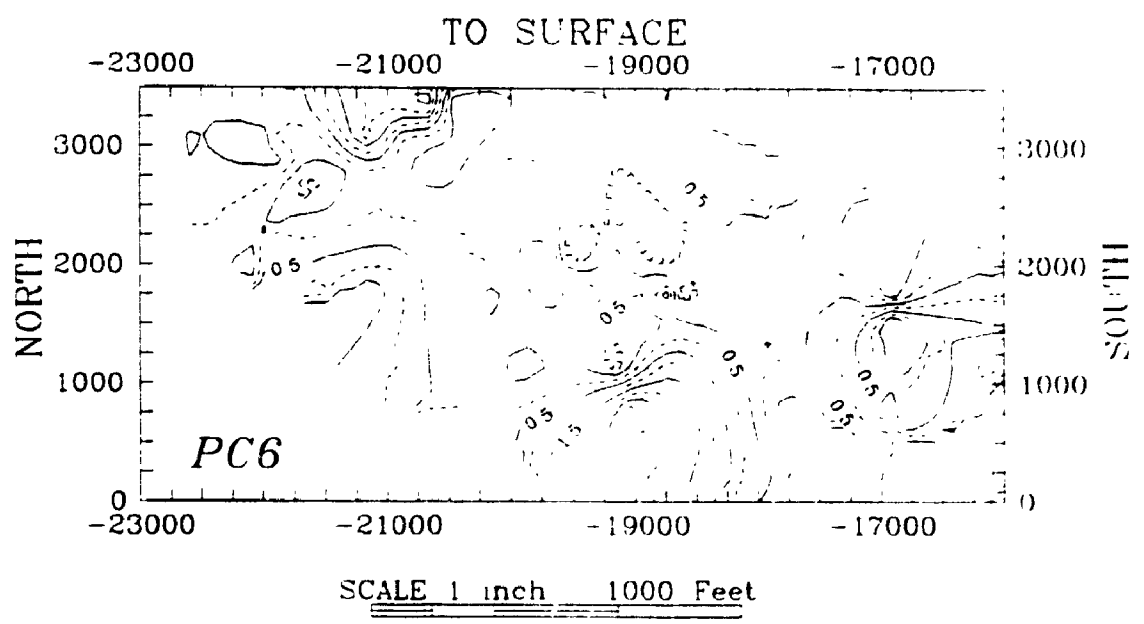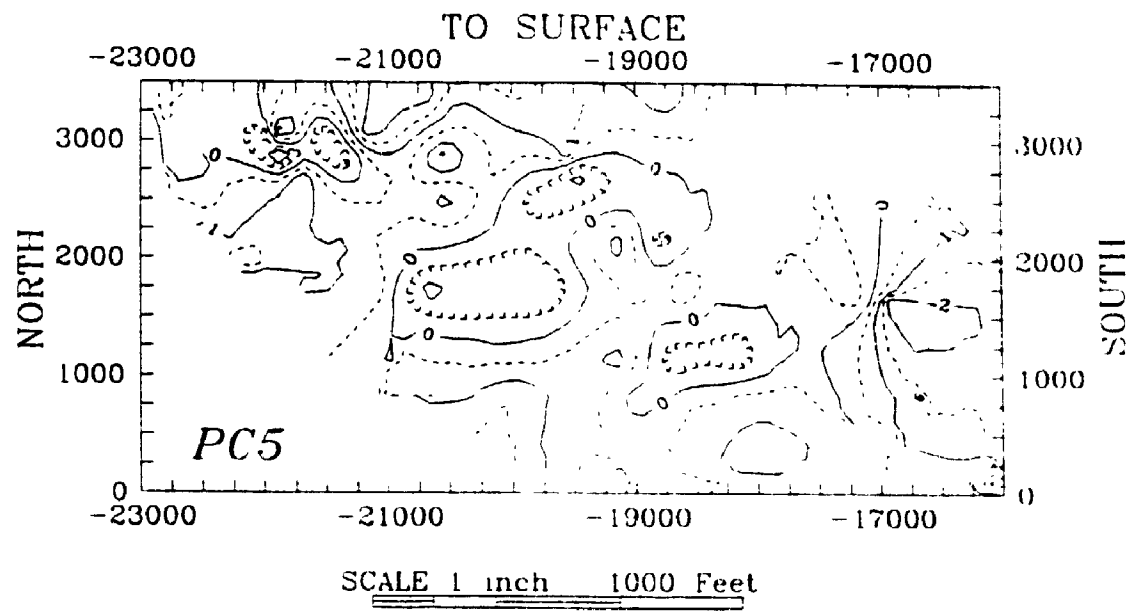
Figure 58. Longitudinal section of the Campbell Shear Zone
revealing the distribution of PC6 and PC5 scores.
The location of sample locations, and ore zones
in the Campbell Shear Zone are snown in Appendix
3.

Minor calc-alkaline trends can be discerned from the data, indicated by SiO_2, Al_2O_3, K_2O, P_2O_5, Ba, Rb, Sr, and S enrichments with concomitant Fe_2O_3, MnO, and Na_2O depletions.

Secondary processes have acted on these rocks, and certain types of geochemical alteration can be inferred from the data, including early, synvolcanic spilitization, later alteration related to regional metamorphism, at least one ore-related metasomatic event, and other, pre-, and post-, mineralization metasomatic events (Boyle, 1961; Osatenko, 1971; Harrigan and Maclean, 1976; Kerrich and Fyfe 1981; Webb, 1984, Head, 1985; Duke et al., 1990; Armstrong, 1991). Each subsequent geochemical alteration to the rocks overprints and modifies preceding events.

The recognition of a lamprophyre signature in the chlorite schists of the Campbell Shear Zone, although not unexpected is new, and similar to observations made in the Abitibi belt (McNeil and Kerrich, 1986), and some of these lamprophyre-derived schists at Yellowknife host ore-grade mineralization.

Past work has identified geochemical anomalies for Ca, Na, K, As, and CO_2 that are spatially displaced relative to Au at the Macassa Mine (Kerrich and Watson, 1984); K, Na, Fe, As, S, Co, and Ni relative to Au at the NERCO-Con Mine (Head, 1985; Webb, 1986), and Na, K, and Au at the Kerr Addison Mine (Kishida and

Kerrich, 1987). Geochemical anomalies for these elements are spatially related to gold mineralization and may occur proximal to, but generally are not juxtaposed with gold mineralization. As such, these elements may erroneously reveal positive or negative correlation coefficients with Au (Kerrich and Watson, 1984; Kishida and Kerrich, 1987).

Major and trace elements do not react coherently across the shear zones in Yellowknife (Boyle, 1961; Kerrich, 1983; Webb, 1984; Head, 1985). For example, SiO_2, K, As and S, and to some extent Ba shows significant depletions adjacent to enriched areas, and Al and Na are enriched adjacent to depleted domains (see Appendix 4). This association of relatively depleted domains adjacent to relatively enriched domains has been recognized before, evidence of which led to lateral diffusion theories (Boyle, 1961). Mass balance calculations reveal many of the depletions are apparent, due to a dilutive effect of the more mobile constituents in the rock such as SiO_2, CO_2, H_2O (Kerrich, 1983).

Head (1985) studied a number of drill sections through the Campbell Shear Zone, and documented trends empirically related to mineralization. Some of these sections are included in Appendix 4. Major and trace elements behaved differently in the basalt, chlorite-carbonate schist, sericite-carbonate schist, and quartz veins, as would be expected. Some evidence

of closed system behaviour is apparent in the alkali elements as has been identified in Timmins (Webb, 1984; Head, 1985; Rye, 1986). Anomalies are in the order of a standardized variation of 1 to 1.5σ. This suggests that longitudinal anomalies <1.5σ may be related to lateral differences across the shear zone rather than differences along the shear zone. However, sampling was restricted to chlorite schists external to known orebodies, and as such, a variation >0.5σ is considered significant.

Auriferous quartz veins are enriched in SiO_2, S, Au, Ag, As, Hg, Sb, Pb, Zn, and Ba and depleted in TiO_2, Al_2O_3, Fe_2O_3, MgO, MnO, CaO, K_2O, Na_2O, V, Cr, Ni, Cu, Rb, Sr, Y, and Zr relative to the host basalts. It is significant that the auriferous quartz contains relative depletions in S, Ag, Hg, Sb, As, and Zn relative to sericite schists, as these common indicator elements. Thus it becomes critical to only consider one lithotype in these comparisons, otherwise correlations dependant upon primary compositions might be interpreted as correlations characteristic of hydrothermal processes. Shear zone-hosted gold mineralization in Yellowknife is associated in general with a relative K_2O, S, As, Zn, Rb, and Ba enrichment, and Al_2O_3, Fe_2O_3, and Na_2O depletion in the chlorite schists adjacent to ore zones. Single element plots reveal locally enhanced Rb, S, Co, Ni, and As in the chlorite schists associated with most of the ore zones, whereas Zn, Cu, and

possibly Pb enrichments coincide only with some of the ore zones within the Campbell Shear Zone. These trends are consistent with that recognized in other Archean mesothermal gold deposits (Boyle, 1979).

A multielement approach, as applied in volcanogenic base metal exploration, initially developed from empirical data, and evolved to be incorporated in genetic models (Franklin et al., 1975; Riverin and Hodgson, 1980; Armor and Nichol, 1983; Parslow, 1987). The data presented here, recognizing the gross geochemical transformation from basalt, to chlorite-carbon te schist, to sericite-carbonate schist, to auriferous quartz vein focuses on the chlorite schists as the most aerially extensive host-rock, next to the Kam Group basalts, that may be related to, or host mineralization. The chlorite schists are an inhomogeneous lithotype, retaining geochemical signatures of all precursor rocks and alterations imposed upon them.

The transformation from basalt to chlorite-carbonate schist included absolute additions of volatiles (H_2O, S, CO_2), and K, Ba, Rb, and Zn, variable gains or losses in SiO_2, MnO, Ca, Fe, and Mg, and losses in Na (Boyle, 1961; Osatenko, 1971; Webb, 1984; this study). These elements are not evenly distributed within the shear zones, and are redistributed, or suffer gains or losses in subsequent metasomatic events, including the gold

mineralizing event.

Spatial distribution plots suggest relative (and to some extent absolute) gains in Al_2O_3, Fe_2O_3, MgO, K_2O, Ba, Rb, S, Co, Ni, As, Zn, Cu, and perhaps Pb, and losses in SiO_2, CaO, and Na_2O within the chlorite-carbonate schists adjacent to mineralization. The clear spatial relationship between the first principal trend for the chlorite schist data, and the distribution of orebodies within the Campbell Shear Zone is striking, inasmuch as the chlorite schist samples did not possess any macroscopic evidence of mineralization or alteration. The application of this technique for mineral exploration at Yellowknife appears to be two fold: (1) potentially mineralized shear zones, or portions of shear zones may be indicated in apparently unaltered chlorite schists, and (2) the nature of a potential ore zone defined above, may be infered from the trace element pattern in the alteration halo.

Processes responsible for metasomatic changes that are superimposed upon the chlorite schists during gold mineralization are compatible with fluids implicated in most Archean mesothermal gold deposits. Enhanced Co and Ni concentrations associated with gold mineralization, although not unknown, were formerly not well documented in Yellowknife (Breakey, 1975; Boyle, 1978).

There is some suggestion that the alteration peripheral to the ore zones expresses different geochemical anomalies (Co, Ni, Cu, S, As) which may be a reflection of the refractory nature of the gold ore in these areas (see Appendix 2). The 103, and the upper portions of the 102 ore zones contain refractory ores; gold that cannot be recovered by conventional cyanidation processes (Breakey, 1975). Studies on refractory ore from the Campbell, Con, and Giant shear zones indicate that these ores generally possess similar or only slightly elevated As, CO_2, contents compared to non-refractory ore from the Campbell Shear Zone. Ore mineralogy in the Campbell Shear Zone includes pyrite, arsenopyrite, pyrrhotite, sphalerite, chalcopyrite, tetrahedrite, freibergite, bournonite, boulangerite, jamesonite, madocite, ullmanite, gudmanite, aurostibite, galena, bismuth tellurides, hessite, and native, Bi, Sb, Pb, and Au (Breakey, 1975).

Temporal evolution of the mineralizing fluids progressed from Fe and As rich through Zn and Cu rich, to Au, Pb, Bi, and Sb rich (Breakey, 1975; Falck, 1990). The transition from refractory ore to free-milling ore in the Campbell Shear Zone is accompanied by a decrease in the abundance of sulfosalts, and a variable decrease in the total arsenopyrite content of the ores (Breakey, 1975).

Studies on arsenopyrite-rich ores from roasting and non-

roasting ores determined four principal modes of gold occurrence within these samples: (1) native gold or electrum in silicate or carbonate gangue, not included or in contact with sulphides or sulfosalts, (2) native gold or electrum, in contact with a sulphide or sulfosalt, either external to, along a grain contact, or in a penetrating fracture in the sulphide or sulfosalt, or (3) native gold or electrum totally encapsulated within a sulphide or sulfosalt, excluding mode 2, or (4) gold contained in a sulphide or sulfosalt species as an essential component (as in aurostibite) or as a contaminant to a sulphide or sulfosalt (Appendix 2; Webb, 1985).

The first two modes are characteristic of free-milling ore, whereas the last two modes are characteristic of refractory ore at Yellowknife. Interestingly, arsenopyrite was never observed to contain mode 3 gold, despite showing clear replacement textures of pyrite containing mode 3 gold (Webb, 1985). The suggestion that some of the arsenopyrite is related to a later, post-mineralization event is consistent with observed mineralogical and geochemical studies at Yellowknife (Breakey, 1975; Webb, 1985; Ransom, pers com., 1985; Falck, 1990; this study). This would account for the different geochemical trends and distributions observed in the Campbell Shear Zone, such as a general gold/arsenic correlation (4700 level haulage, Appendix 4), but apparent lack of gold/arsenic correlation throught the Campbell Shear Zone (see longitudinal sections, Appendix 4; Jardine, 1976).

CHAPTER 6

STABLE ISOTOPE GEOCHEMISTRY

6.1 Introduction

The gold orebodies at Yellowknife consist of weakly to intensely deformed quartz-carbonate veins and silicified zones within ductile shear zones (Boyle, 1961; Kerrich and Alison, 1977; Allison and Kerrich, 1978; Webb, 1983; Bullis et al., 1987). Sericite is commonly present in, or peripheral to, mineralization. Calcite and Fe-dolomite are ubiquitous in or near auriferous quartz veins, and together form extensive zones of alteration around the orebodies. This chapter addresses the nature of the ore-forming hydrothermal fluids responsible for precipitating the gold-bearing quartz veins, using stable isotopes.

In principle, the stable isotopes of H and O can provide information on the origin of hydrothermal fluids (seawater, magmatic, meteoric, or metamorphic), and the temperature and minimum water/rock ratio at the site of vein formation. Carbon isotopes may constrain the source of carbon in an ore-fluid, the Eh and pH during carbonate precipitation, and possible conditions of CO_2 unmixing (for reviews, see Taylor, 1974; Ohmoto and Rye, 1979; Ohmoto, 1986; Taylor, 1987).

This chapter represents comprehensive sampling for stable

isotope analysis in the NERCO-Con Mine. Limited data were previously reported from Yellowknife (Kerrich and Fyfe, 1984; Kerrich, 1986). Fractionation factors for O are taken from O'Neil et al. (1969), Sheppard and Schwarcz (1970), Matthews and Katz (1977), Matsuhisa et al. (1979), Wesolowski and Ohmoto (1986), and Rossenbaum and Sheppard (1986), and for C, by Sharma and Clayton (1965), Robinson and Clayton (1969) and Deines et al. (1974).

6.1.1 Sample Design

Samples of chlorite-carbonate schist were collected from the ore-bearing Campbell Shear Zone. Additional samples were collected from the Campbell Shear Zone outside of the NERCO-Con Mine area, ≈3 km to the south, from the Giant Yellowknife Mine ≈10 km to the north, and from a shear zone barren of ore marginal to the Campbell Shear Zone (100 Shear Zone). These are a subset of the sample population collected for the major and trace element analysis as described in Chapter 5. The samples were analyzed for the oxygen and carbon isotope compositions of calcite and coexisting Fe-dolomite. Samples collected by R. Kerrich supplement this, and carbonate and silicate data from these samples are used for comparison. Systematic isotope patterns are described, interpreted, and compared with examples from the literature.

Two hundred samples of chlorite carbonate schist were collected, as described in chapter 5, and a total of 66 samples met the mineralogical criteria outlined in that chapter, and yielded sufficient CO_2 for isotopic analysis from the Campbell Shear Zone. These samples span a horizontal distance of 2,200 m and a vertical distance of 1,200 m. Eight samples from the Giant Yellowknife mine were collected to determine regional differences in the chlorite carbonate schists. Six samples of late carbonate veining, and 11 other non-ore-related carbonate alteration were analyzed for comparative purposes. A total of 91 samples were analyzed for carbon and oxygen isotopic composition of the carbonates.

6.1.2 Sample Preparation

Sample preparation and data collection is described in detail in Appendix 1. Pulverized samples retained from whole rock and trace element analysis were reacted with 100% H_3PO_4 at 25°C for 2 hr for the extraction of calcite (McCrea, 1950). The residue was then reacted at 50°C for 24 hr for the extraction of Fe-dolomite. The resultant CO_2 was collected; some CO_2 attributed to calcite is undoubtably due to some Fe-dolomite, and the reverse is likely, however, absolute contributions have been determined to be minimal (Kerrich, 1990; Pleydell et al., 1990).

6.2 Data treatment

The data were reduced to values relative to PDB in the case of carbon, and SMOW in the case of oxygen, using the UWO1 calcite standard ($\delta^{18}O$ = +13.0 SMOW, $\delta^{13}C$ = +2 PDB), the AGS standard ($\delta^{18}O$ = 9.6 SMOW) and the TS Lst standard ($\delta^{18}O$ = 28.65 SMOW and $\delta^{13}C$ = 1.95 PDB). Fractionation factors of 1.01025 and 1.01110 are used for calcite and Fe-dolomite CO_2 respectively (Kyser, 1987).

The data was analyzed at the University of Western Ontario on an IBM 4341 series mainframe computer using SAS (Statistical Analysis System) software. Univariate statistics, and correlations of the data were determined and input into an IBM - compatible PC, using programs designed by Davies (1973) and modified by the writer. The spatial data are krigged, to accommodate data clustering using SURFER (Golden Graphics, 1990), plotted using TOPO, and SURF (Golden Graphics, 1990) to provide topographic or isometric plots, GRAPHER (Golden Graphics, 1986) to provide XY plots, 123 (Lotus, 1991) and HARVARD GRAPHICS (Harvard Graphics, 1990) for histograms, and PPLOT for probability plots (Stanley, 1987).

6.3 Oxygen Isotopes

6.3.1 Carbonates

a) General features

Ninety-one chlorite carbonate schist samples from Yellowknife were analyzed: $\delta^{18}O$ values are reported in Appendix 4.

The data from all of Yellowknife appears to be arithmetically distributed, and at least two populations of carbonates can be deduced from the data (Figures 59 and 60). A strongly depleted population of calcite (< 7.0 permil) exists from these data and is not present in Fe-dolomite from the same rocks. The Campbell Shear Zone data exhibits a similar bimodal distribution of $\delta^{18}O$ values, with some evidence of a smaller ^{18}O-enriched population (Figures 61 and 62). The strongly ^{18}O-depleted calcite population observed in the all Yellowknife samples is not present in the Campbell Shear Zone sub-population. The more ^{18}O-depleted calcite and Fe-dolomite populations (mean $\delta^{18}O$ ~9.1 and 8.0 permil respectively) account for 70 and 60% of the data from the Campbell Shear Zone respectively.

b) Mine distribution

Figures 63 and 64 reveal a general enrichment of ^{18}O for both calcite and Fe-dolomite in the shallower, nearer surface levels relative to the deeper levels of the Campbell Shear Zone. Figures 65 and 66 are longitudinal sections of the Campbell Shear Zone, and illustrate a more complex

distribution of $\delta^{18}O$ values in carbonates from the chlorite carbonate schists, including a lateral component to the general trend of ^{18}O-enrichment towards surface.

6.3.2 Silicates

Thirty quartz, one albite, one muscovite, one scheelite, one tourmaline, and seven chlorite samples, analyzed at the University of Saskatchewan in Saskatoon, and from previously published data (Kerrich and Fyfe, 1986) are considered below. The samples were collected from auriferous quartz veins from the Con and Campbell Shear Zones, and from quartz veins exposed on surface in the Yellowknife Greenstone Belt.

Quartz $\delta^{18}O$ values range from +10.6 to +13.1 permil and have modes at +11.0 and +11.6 permil (Figure 67). Samples with quartz having $\delta^{18}O$ values near +11.0 are generally found in the surface samples whereas those from the more ^{18}O-enriched population are dominated by samples collected from the Campbell Shear Zone. There is no depth-related trend in the $\delta^{18}O$ values of the quartz from the Campbell Shear Zone over 1,000 m, although the most ^{18}O-depleted quartz (+9.0 ± 0.5 permil) within the Campbell Shear Zone occurs at elevations >500 m below surface (elevation 3,300′ (Figure 68).

One sample of mineralized quartz-tourmaline vein material from

stope 5177M yielded tourmaline with a $\delta^{18}O$ of +7.9. A sample of ore from stope 4773L yielded quartz, muscovite, and scheelite separates with $\delta^{18}O$ values of +10.8, +7.4, and +3.8 permil respectively. These mineral pair fractionations correspond to calculated temperatures ranging of 310° ±20°C, 390° ±15°C, and 509° ±48°C. The extreme temperature estimates represent mineral pairs involving muscovite, which may be out of equilibrium with the quartz and scheelite (see Chapter 7). This may be due to the enhanced suseptability of ^{18}O reequilibration in muscovite relative to quartz and scheelite. The calculated temperature of 390° ±15°C is in general agreement with previous estimates and is therefore considered reliable (O'Neil and Taylor, 1969; Breakey, 1975; Matsuhisa et al., 1979; Wesolowski and Ohmoto, 1986; Kerrich and Fyfe, 1988b).

Chlorite separates from chlorite-carbonate schists collected from the Campbell Shear Zone exhibit a wide range in the $\delta^{18}O$ values (+2.6 to +12.1 permil), and have no apparent domainal distribution, although this is difficult to properly assess with only 7 samples.

6.4 Carbon Isotopes

6.4.1 General features

211

Yellowknife, NWT
Chlorite Schist Geochemistry

n=86

618O from calcite (per mil, SMOW)

Figure 59.

Yellowknife, NWT
Chlorite Schist Geochemistry

n=90

618O from Fe-dol (per mil, SMOW)

Figure 60.

Histogram of the δ18O values of calcite extracted Histogram of the δ18O values of Fe-dolomite from chlorite-carbonate schists at Yellowknife, extracted from chlorite-carbonate schists at with modes near 8.2 and 11.2 permil. Yellowknife, with modes near 9.0 and 10.5 permil.

Yellowknife, NWT
Chlorite Schist Geochemistry

δ18O from Fe-dolomite (per mil, SMOW)

n=66, CSZ

Data from UWO

Figure 62. Histogram of the δ¹⁸O values of Fe-dolomite extracted from chlorite-carbonate schists in the Campbell shear zone, with modes near 9.0 and 11.0 permil.

Yellowknife, NWT
Chlorite Schist Geochemistry

δ18O from calcite (per mil, SMOW)

n=66, CSZ

Data from UWO

Figure 61. Histogram of the δ¹⁸O values of calcite extracted from chlorite-carbonate schists in the Campbell shear zone, with modes near 8.3 and 11.0 permil.
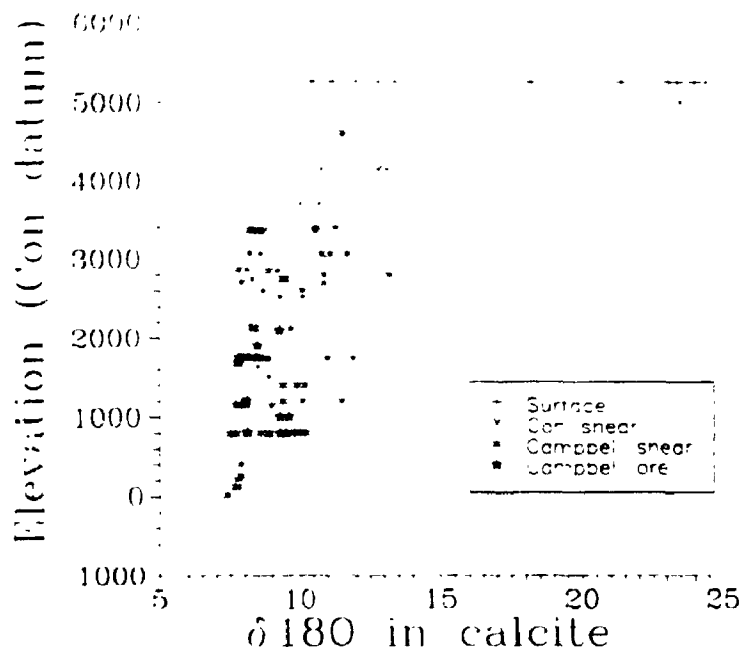
Figure 63. Plot of $\delta^{18}O$ values for calcite from chlorite-carbonate schists in the Campbell Shear Zone verses depth. Notice the increased enrichment of ^{18}O at shallower elevations.
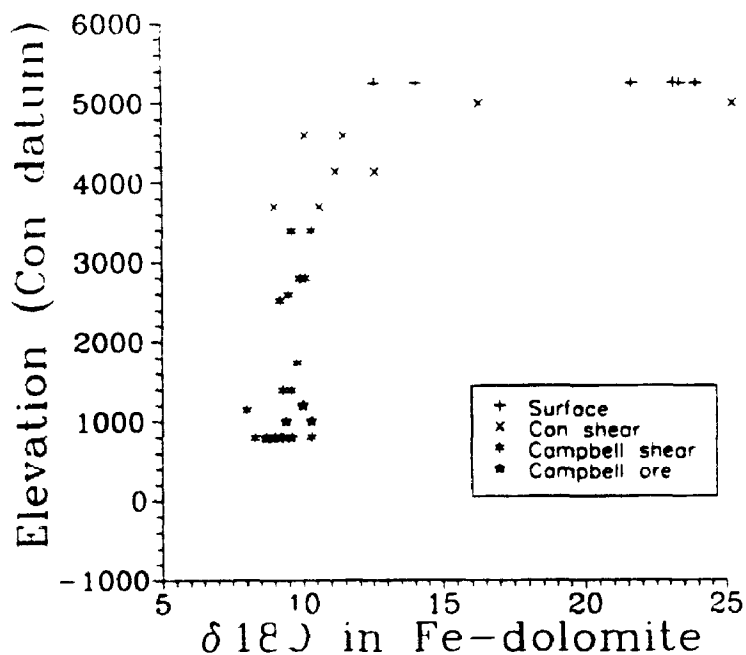
Figure 64. Plot of $\delta^{18}O$ values for Fe-dolomite from chlorite-carbonate schists in the Campbell Shear Zone verses depth showing a similar distribution as for calcite.

CAMPBELL SHEAR ZONE

TO SURFACE

$\delta^{18}O$ Calcite
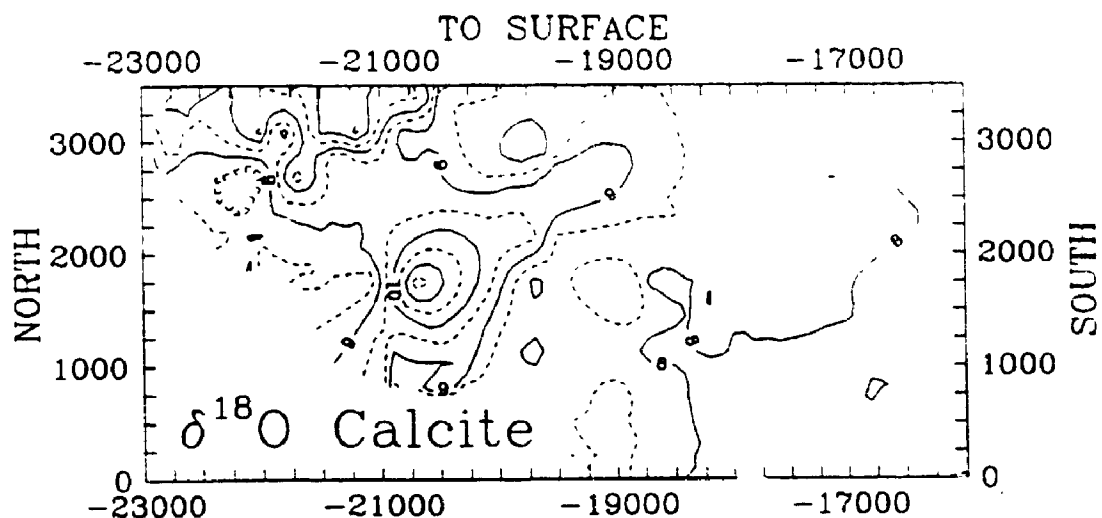
Figure 65. Longitudinal section of the Campbell Shear Zone revealing the distribution of $\delta^{18}O$ values for calcite in chlorite-carbonate schists showing an irregular distribution, with an enriched domain near latitude 20,800.

TO SURFACE
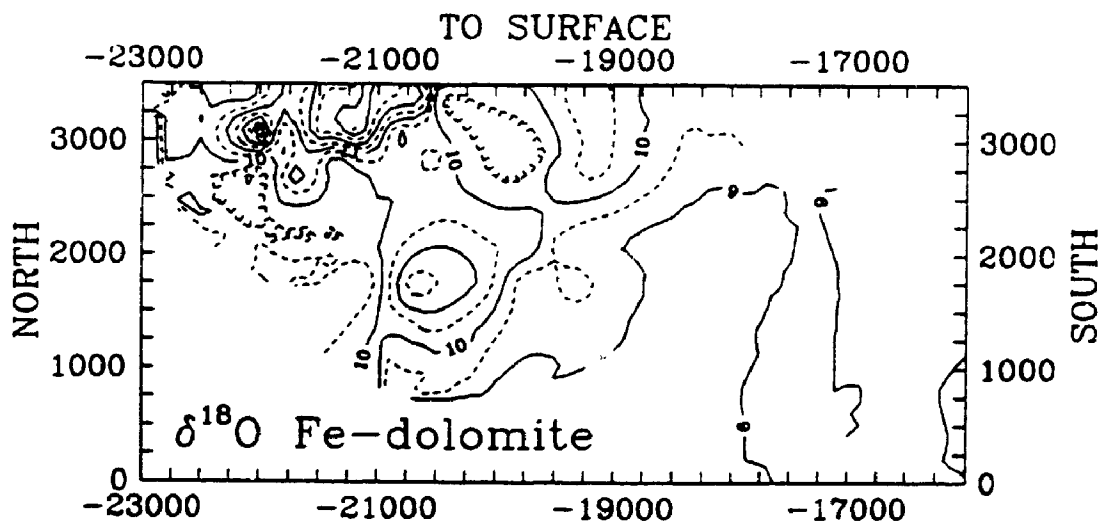
$\delta^{18}O$ Fe-dolomite

Figure 66. Longitudinal section of the Campbell Shear Zone revealing the distribution of $\delta^{18}O$ values for Fe-dolomite in chlorite-carbonate schists. Domains of enrichment occur near latitude 20,800, and at shallower elevations north of latitude 21,000.
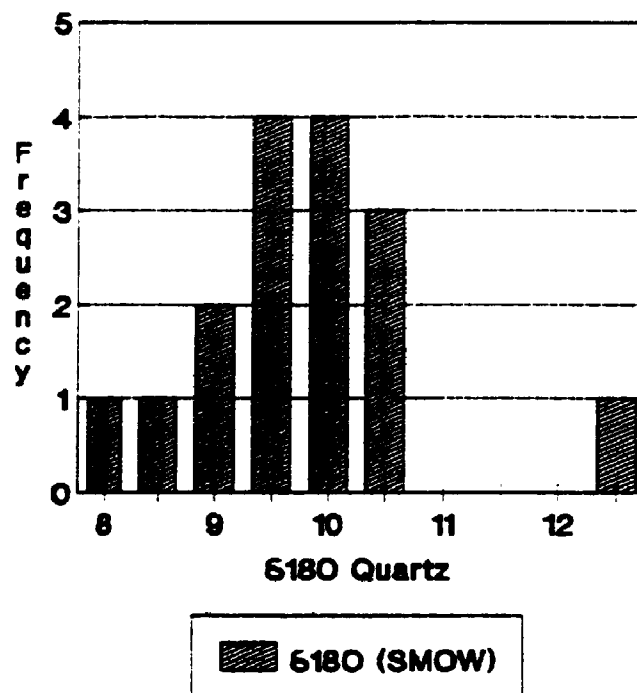
Figure 67. Histogram of the $\delta^{18}O$ values of quartz extracted from chlorite-carbonate schists in the Campbell Shear Zone
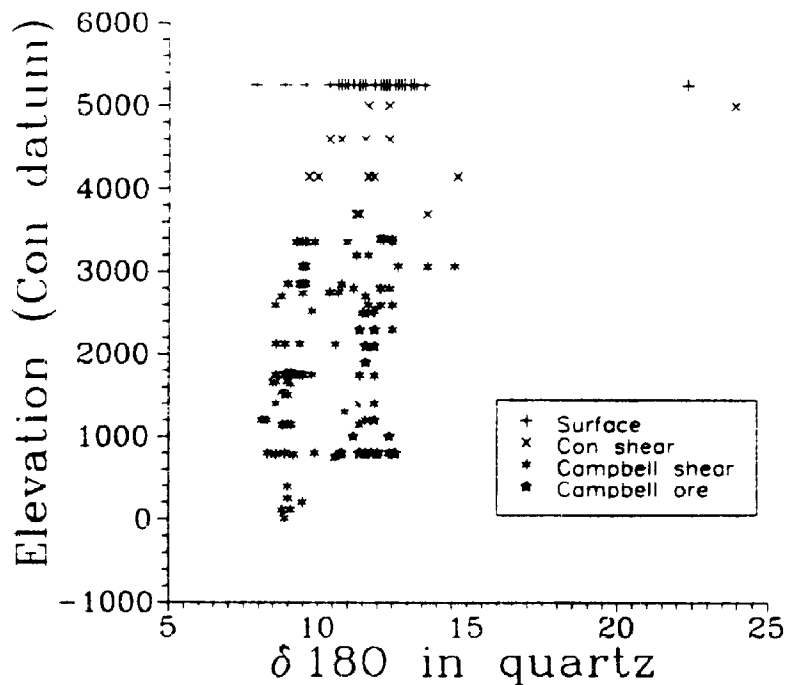
Figure 68. Plot of $\delta^{18}O$ values for quartz from chlorite-carbonate schists in the Campbell Shear Zone verses depth revealing a fairly consistent variance with depth. Also note the clustering of $\delta^{18}O$ in ore samples, near 12.0 permil within a much more variable schist population.

Ninety-one chlorite carbonate schist samples were analyzed; $\delta^{13}C_{(PDB)}$ values for calcite and coexisting Fe-dolomite are reported in Appendix 3.

The populations of the Yellowknife carbonates approximate unimodal arithmetic distributions with a total range of $\delta^{13}C$ values from -6.5 to -0.6 permil, except for an apparent deficiency of samples with $\delta^{13}C$ values between -3.8 and -2.8 permil in calcite. The majority of the Campbell Shear Zone carbonates span a narrower range, between -6.0 and -2.1 per mil for calcite, and -6.5 and -2.8 for Fe-dolomite (Figures 69 and 70). A second population of calcite with a mean $\delta^{13}C$ around -5.2 is suggested, and probability plots (Figures 71 and 72) support this interpretation. There is a population of $\delta^{13}C$-depleted carbonates with calculated $\delta^{13}C$-means of -4.4 and -4.1 permil for calcite and Fe-dolomite respectively, and a second population of more $\delta^{13}C$-enriched calcite is indicated with a mean of -2.5 per mil.

6.4.2 Mine distribution

Figures 73 and 74 reveal no obvious depth-related distribution of the $\delta^{13}C$-values of the carbonates. However, longitudinal sections of the Campbell Shear Zone reveal a domainal distribution of ^{13}C-enriched ($\delta^{13}C_{calcite}$=-2.5, $\delta^{13}C_{Fe-dolomite}$=-3.5) and ^{13}C-depleted ($\delta^{13}C_{calcite}$=-4.5, $\delta^{13}C_{Fe-dolomite}$=-5.0) zones

(Figures 75 and 76). A broad domain of δ^{13}C-enrichment in calcite (> -2.5 permil), and in Fe-dolomite (>-3.5 permil) is centred at latitude 20,300 and elevation 2,700, and latitude 20,500 and elevation 2,400 respectively. There are associated domains of relatively δ^{13}C-depleted carbonates (δ^{13}C$_{calcite}$=-4.5, δ^{13}C$_{Fe-dolomite}$=-5.0) peripheral to these zones, located 2,200 feet to the south, and 2,000 feet to the north, and below the δ^{13}C-enriched domains.

6.5 Observations

Plots of δ^{18}O calcite verses δ^{18}O Fe-dolomite (Figure 77) illustrate the close correlation about a calcite - Fe-dolomite fractionation of $\approx$+1 permil over a wide range of absolute values. The largest consistent calcite - Fe-dolomite fractionation is from the lamprophyre dyke at the NERCO-Con Mine, at $\approx$+3 permil (3 samples).

A plot of δ^{13}C calcite verses δ^{13}C Fe-dolomite, reveals some scatter about the 1:1 regression line (Figure 78). The bulk of the scatter is towards the negative Δ calcite - Fe-dolomite field. Figures 79 and 80 illustrate the samples plotted in δ^{13}C verses δ^{18}O space, with the fields of three principal reservoirs shown for reference. A general trend of ^{18}O-

enrichment, and to a lesser degree ^{13}C-enrichment can been observed in samples collected at shallower elevations.

Oxygen isotope compositions of quartz - Fe-dolomite pairs from Yellowknife are plotted on Figure 81. Five samples from the Campbell Shear Zone range from Δ quartz - Fe-dolomite = +1.6 to +4.4 permil with an average of +2.8 permil. Five samples from the Con Shear Zone reveal a wider range, from Δ quartz - Fe-dolomite = -13.5 to +2.5 permil, in a highly skewed population favouring the more positive fractionations. Two samples collected from surface have a quartz - Fe-dolomite fractionation of -12.0 and -0.6 permil. Quartz - calcite pairs reveal a similar distribution, with samples collected from deeper mine workings containing more positive fractionations (Figure 82).

Eight chlorite - carbonate pairs from Yellowknife are plotted on Figure 83. Chlorite - Fe-dolomite fractionations range from -6.3 to +4.1, and average -3.2 permil. Chlorite - calcite fractionations range from -10.0 and +3.1 permil, and average -4.6 permil.

6.6 Interpretation

a) Oxygen isotopes

The $\delta^{18}O$ values of hydrothermal minerals is dependant upon the $\delta^{18}O$ of aqueous mineralizing fluids, and the temperature of the system for equilibrium reactions (Taylor, 1974). The bimodal distribution of the $\delta^{18}O$ values of both the calcite and the Fe-dolomite from all samples from Yellowknife, and the Campbell Shear Zone implicates two different fluid systems, two radically different temperature conditions, or some combination of the two. The majority of the carbonate data from Yellowknife is from the depleted population. There is some evidence of a smaller population of more intensely ^{18}O-depleted Fe-dolomite with a calculated mean of +6.3 ± 0.9 permil.

The Campbell Shear Zone data has a similar distribution, exclusive of the most ^{18}O-depleted Fe-dolomite population. Calcite exhibits differences of between 4 to 9 permil between the two populations, and would require temperature differences in the order of 350 to 570°C if they are assumed to have precipitated from a fluid with a $\delta^{18}O$ of +7.5 to +8.2 permil (Kerrich, 1983). If on the other hand, two fluids are invoked, and the dominant population is assumed to have formed at temperatures between 320 and 450°C (Breakey, 1975; Kerrich, 1983), then the primary fluid had a $\delta^{18}O$-value of +5.5 to +6.0 permil.

Yellowknife, NWT
Chlorite Schist Geochemistry

δ13C from Fe-dolomite (per mil, PDB)

Data from UWO

n=66, CS2

Figure 70.

Histogram of the $\delta^{13}C$ values of Fe-dolomite extracted from chlorite-carbonate schists in the Campbell shear zone, distributed similarly to the calcite separates.

Yellowknife, NWT
Chlorite Schist Geochemistry

δ13C from Calcite (per mil, PDB)

Data from UWO

n=68, CS2

Figure 69.

Histogram of the $\delta^{13}C$ values of calcite extracted from chlorite-carbonate schists in the Campbell shear zone, revealing a general unimodal distribution.
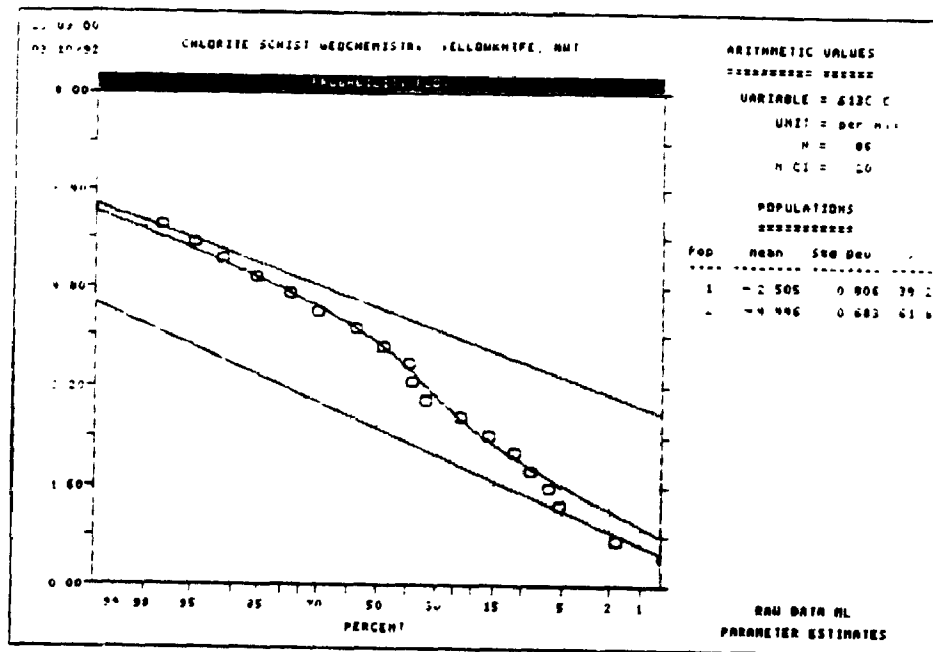
Figure 71. Probability plot of $\delta^{13}C$ in calcite extracted from chlorite-carbonate schist from the Campbell Shear Zone.
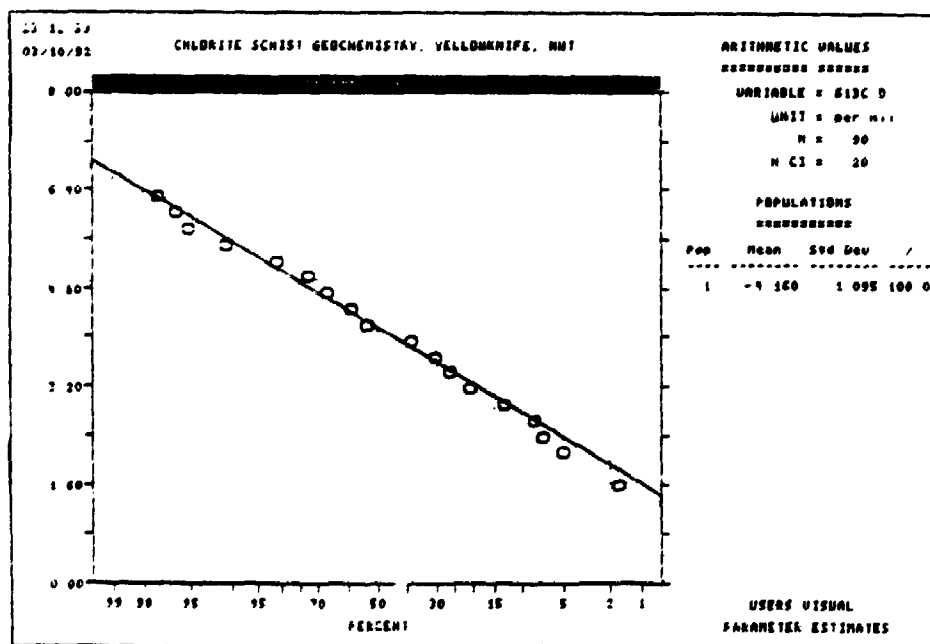
Figure 72. Probability plot of $\delta^{13}C$ in Fe-dolomite extracted from chlorite-carbonate schist from the Campbell Shear Zone.
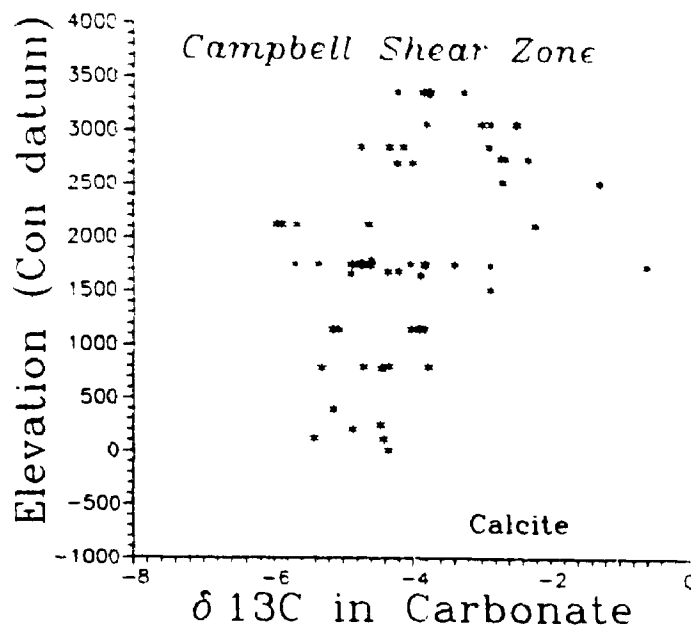
Figure 73. Plot of δ¹³C values for calcite from chlorite-carbonate schists in the Campbell Shear Zone verses depth revealing no consistent trend, although a significantly broader range of δ¹³C is apparent near elevation 2,000
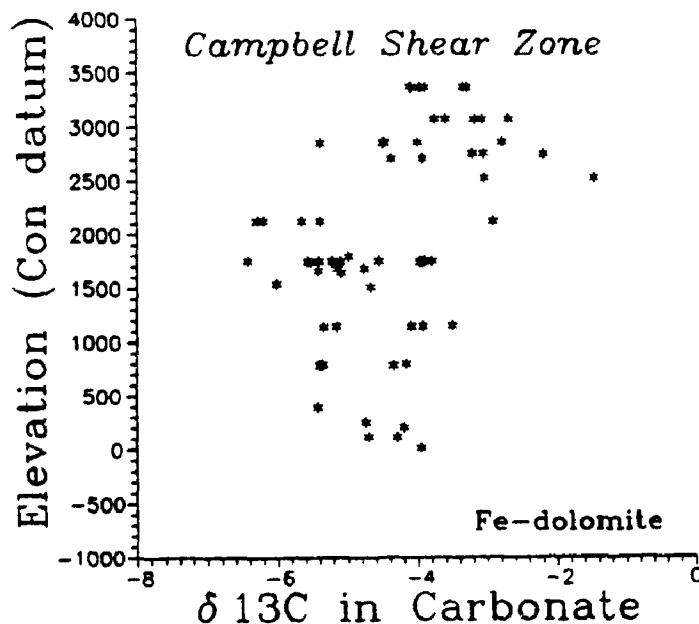
Figure 74. Plot of δ¹³C values for Fe-dolomite from chlorite-carbonate schists in the Campbell Shear Zone verses depth reveals a similar trend as that in calcite, with an apparent extension of the range of ¹³C composition near elevation 2,000.

CAMPBELL SHEAR ZONE
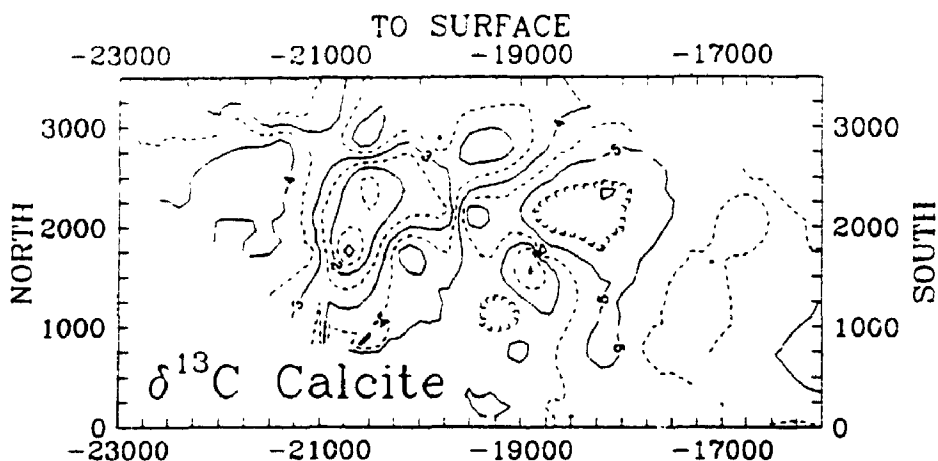
Figure 75. Longitudinal section of the Campbell Shear Zone revealing the distribution of $\delta^{13}C$ values for calcite in chlorite-carbonate schists. A domain enriched in ^{13}C is apparent near latitude 20,800 adjacent to a depleted domain centred at latitude 18,500.
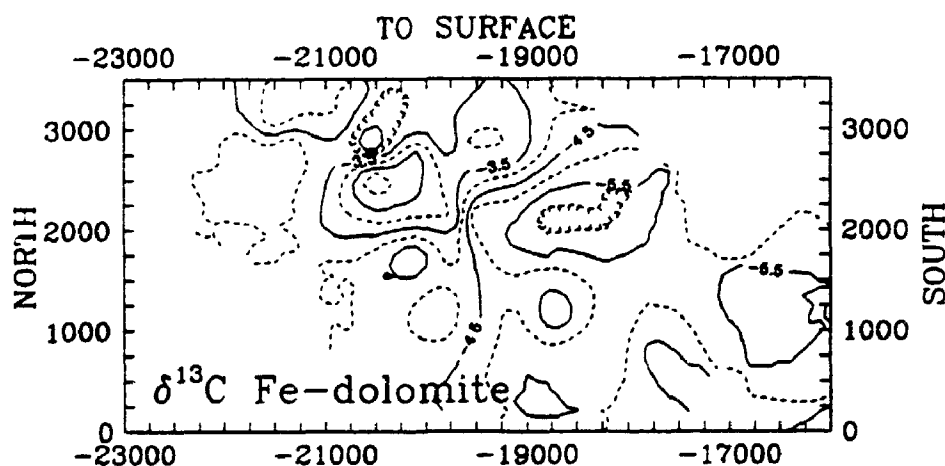
Figure 76. Longitudinal section of the Campbell Shear Zone revealing the distribution of $\delta^{13}C$ values for Fe-dolomite in chlorite-carbonate schists. A paired depletion/enrichment domain is noted, centred near latitude 19,500.
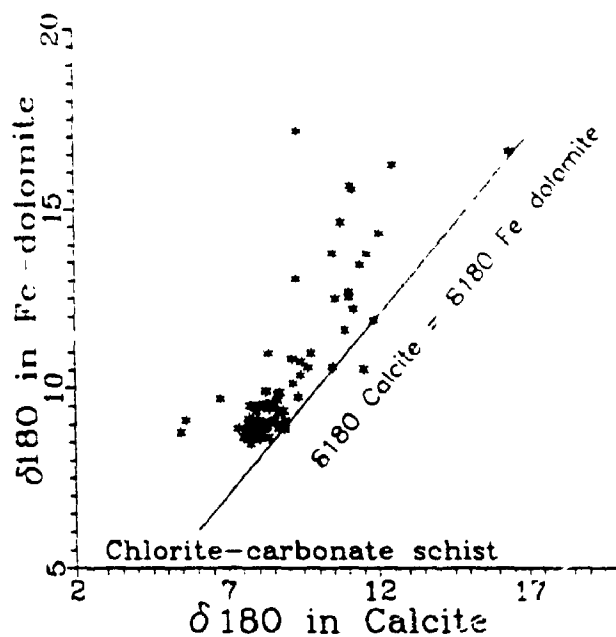
Figure 77. Plot of $\delta^{18}O_{calcite}$ − $\delta^{18}O_{Fe-dolomite}$ pairs coexisting from chlorite-carbonate schists of the Campbell Shear Zone.
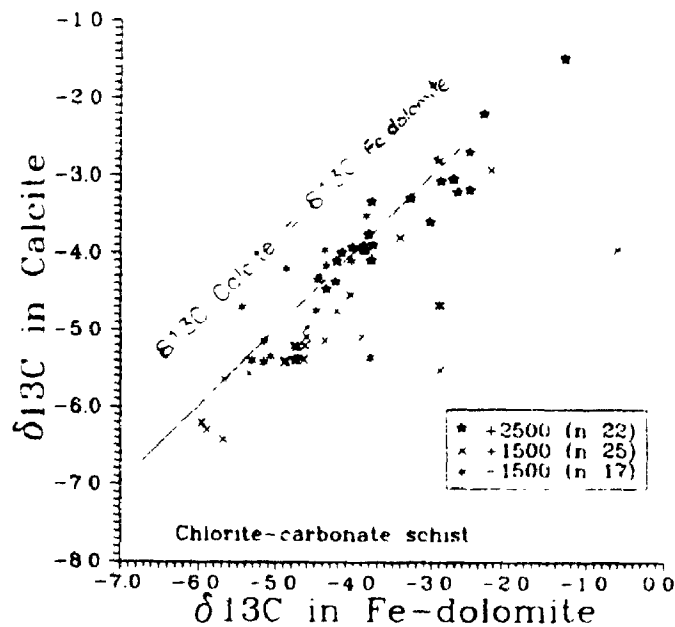
Figure 78. Plot of $\delta^{13}C_{calcite}$ − $\delta^{13}C_{Fe-dolomite}$ pairs coexisting from chlorite-carbonate schists of the Campbell Shear Zone. Most sample cluster near isotopically identical carbonates.
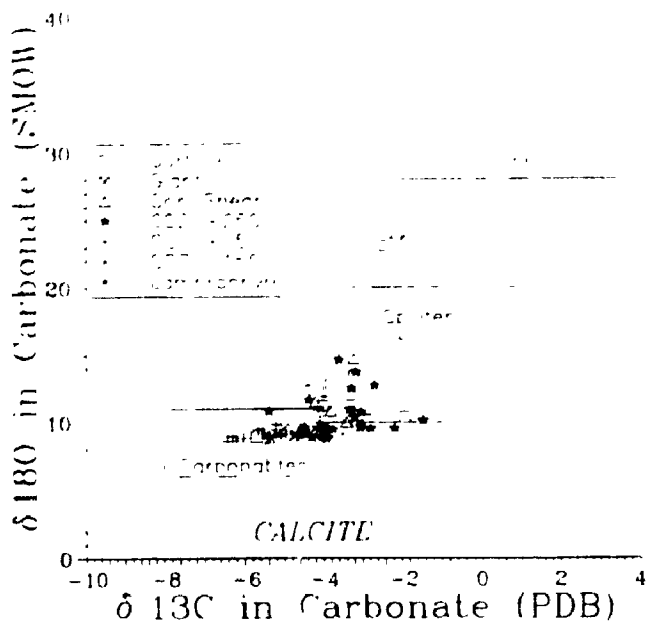
Figure 79. Plot of $\delta^{13}C_{calcite}$ verses $\delta^{18}O_{calcite}$ from chlorite-carbonate schists of the Campbell Shear Zone, with three principal reservoirs shown for reference (after Kerrich, 1989). There is a sharp cut-off for $\delta^{18}O$ values near +8.5.
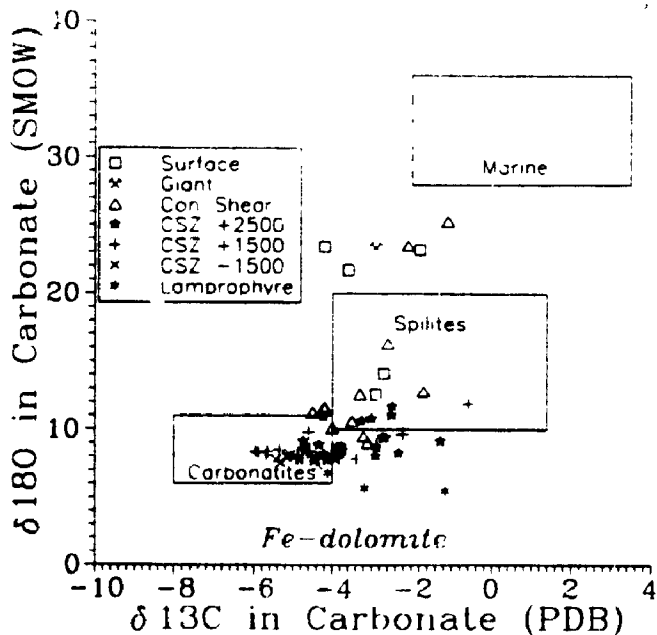
Figure 80. Plot of $\delta^{13}C_{Fe-dolomite}$ verses $\delta^{18}O_{Fe-dolomite}$ from chlorite-carbonate schists of the Campbell Shear Zone, with three principal reservoirs shown for reference (after Kerrich, 1989). The only samples with $\delta^{18}O$ values > +7.5 are those from the lamprophyre dyke.
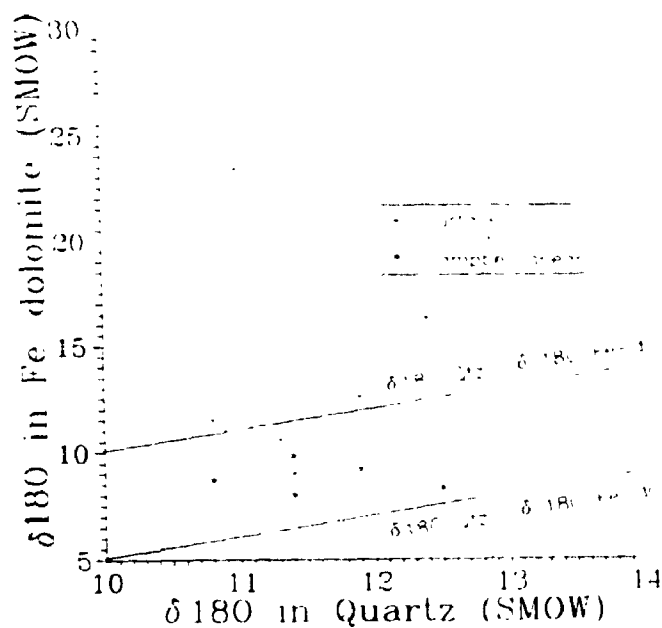
Figure 81. Plot of $\delta^{18}O_{quartz} - \delta^{18}O_{Fe-dolomite}$ pairs coexisting from chlorite-carbonate schists show samples from the Campbell Shear Zone to be constrained to Δ Qtz-Fe-dol 0 to -5, however, other samples range to positive fractionations.
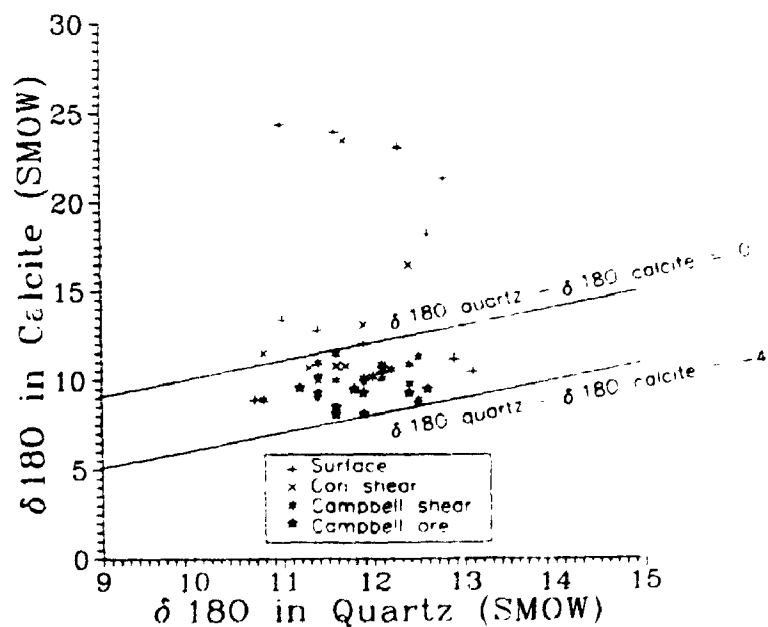
Figure 82. Plot of $\delta^{18}O_{quartz} - \delta^{18}O_{calcite}$ pairs coexisting from chlorite-carbonate schists from the Campbell Shear Zone cluster between Δ Qtz-Cal of 0 to -4, whereas samples from shallower structures posses positive fractionations .
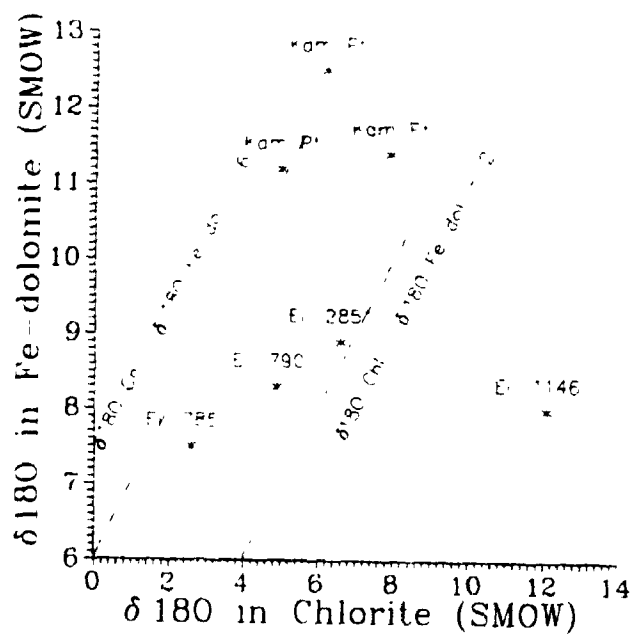
Figure 83. Plot of $\delta^{18}O_{chlorite}$ - $\delta^{18}O_{carbonate}$ pairs coexisting from chlorite-carbonate schists of the Campbell Shear Zone produce negative fractionations except for one sample (El 1,146) at elevation 1,146. Samples are coded for elevation relative to the NERCO-Con Mine coordinates, with surface at ≈5,300 feet.

If the second, more ^{18}O-enriched carbonate population is attributed to re-equilibration of the primary carbonates by secondary fluids or surface-related processes, then marine waters ($\delta^{18}O$ ~ -1.0 (Kerrich and Hodder, 1982; Kerrich, 1983)) may be considered. This may have occurred at geologically reasonable temperatures of between 150 and 180°C, using fractionation factors reported by Freidman and O'Neil (1977). Fritz and Frape (1982) described some hypersaline brines ($\delta^{18}O$ -14.4) from the deeper levels of the NERCO-Con Mine, and deduced a parent fluid with $\delta^{18}O$ values of -10 ±3. These Ca-chloride brines could have equilibrated with the more ^{18}O-enriched calcites and Fe-dolomites at temperatures of 30 - 70°C.

Quartz $\delta^{18}O$ values are bimodally distributed, indicative of two isotopic populations of quartz. The more ^{18}O-depleted population is largely constrained to samples collected external to the Campbell Shear Zone, and may be due to fluids of a different composition, temperature, or more likely, due to domains of low fluid/rock ratios. The $\delta^{18}O$ of quartz may be buffered by the wall rocks in domains where there is a low fluid/rock ratio. Within the Campbell Shear Zone, quartz $\delta^{18}O$ values are normally distributed and unbuffered by the host rocks, indicative of high fluid/rock ra (Kerrich, 1983; Kerrich and Fyfe, 1988; Relf, 1987). The most ^{18}O-depleted

quartz within the Campbell Shear Zone is generally located in the deeper-levels, where the structure is narrower (Bullis et al., 1988), and temperatures are here interpreted to have been higher by 20 to 40°C (Kerrich and Fyfe, 1988a).

O'Neil (1987) has shown that reequilibration of isotopic ratios in most minerals at low temperature by diffusion is kinetically inhibited, and that reequilibration requires some solution/precipitation process. Disequilibrium mineral-pair fractionations, including negative Δ quartz - feldspar values has been used by Kerrich and Hodder (1982), Kerrich (1983), Kishida and Kerrich (1987) and others to identify low temperature resetting of primary isotopic values in Archean mesothermal gold deposits. The correlation of increasingly negative quartz - carbonate fractionations in samples collected at shallow depths (Figures 81 and 82) attests to the selective ^{18}O-enrichment of the isotopically more easily reset carbonates relative to quartz, and supports the involvement of a late, lower temperature fluid (< 300°C (Clayton et al., 1968; O'Neil. 1987; Kerrich, 1987)).

A single ore-sample from stope 4783L provided quartz, muscovite, and scheelite separates, yielding quartz-mineral fractionations shown on Table 10. These mineral pair fractionations correspond to calculated best estimate temperatures of 390° ±15°C from fluids of $\delta^{18}O$ +5.5 ± 0.2,

using the fractionation constants of Wesolowski and Ohmoto (1986), Matsuhisa et al. (1979), and O'Neil and Taylor (1969).

The $\delta^{18}O$ values of chlorite separates are erratic, likely due to the impure nature of the mineral separates, stemming from the ultrafine-grained mineral aggregates (<100 m) present in the chlorite schists. This impurity was confirmed by optical means and X-ray diffraction. Accordingly, the chlorite separates are not considered further.

b) Carbon isotopes

The $\delta^{13}C$ values of hydrothermal carbonates is dependant upon the $\delta^{13}C_{RC}$ of the fluid, the C-bearing species involved, and the temperature, Eh, and pH of the fluids (Ohmoto and Rye, 1977).

The unimodal distribution of the $\delta^{13}C$ values of calcite and Fe-dolomite in both the Yellowknife and the Campbell Shear Zone data sets implicates a single carbon reservoir. The hydrothermal fluids likely had characteristics attributable to most Archean gold deposits, as summarized by numerous authors (Kerrich and Hodder, 1982; Kerrich, 1983; Burrows et al., 1986; Perring et al., 1987; Golding et al., 1987; Colvine et al., 1988). For the estimated Eh and pH of the ore-forming fluids at the NERCO-Con Mine, $\delta^{13}C_{carbonate} \approx \delta^{13}C_{H2CO3\ apparent} \approx \delta^{13}C_{fluid} \approx -4$ (cf. Ohmoto and Rye, 1979; Kerrich, 1987). $\delta^{13}C$

TABLE 10

Mineral-pair fractionations and calculated temperatures

MINERAL PAIR	$\Delta^{18}O$	TEMPERATURE
quartz-muscovite	3.4±0.2	310 +20/-22
quartz-scheelite	7.0±0.2	390 +14/-15
musc-sch	3.6±0.2	509 +44/-53

musc = muscovite
sch = scheelite

Calculations are estimates of 1000 $\ln_{\alpha\ qtz-min}$ using $\Delta_{qtz-min}$

Estimates using muscovite may be erroneous due to later resetting of muscovite to more enriched $\delta^{18}O$ values, as such, the quartz-scheelite temperature estimate is preferred.

values of $\approx$-4 are systematically depleted compared to marine water or marine carbonate of most ages ($\delta^{13}C \approx 0 \pm 2$), and enriched relative to most magmatic or mantle carbon alone where $\delta^{13}C \approx$-6 $\pm$ 2 (Taylor, 1986; Kyser, 1986). The $\delta^{13}C_{fluid}$ value of -4 is consistent with mixtures of two or more of the following reservoirs; marine carbonate, spilitic carbonate, reduced carbon, magmatic carbon, and mantle carbon, but any such mixing must have been remarkably uniform. Rather, the uniformity of the hydrothermal carbonate's δ^{13C} values implies a homogenous carbon source, such as average crustal carbon which is -5 $\pm$2 permil, and absence of regional fluctuations in Eh between the CO_2/CH_4 buffer.

The distinct, domainal distribution of the $\delta^{13}C$ data from the unimodal population sets is not attributable to temperature, depth, variations in host lithologies, or proximity to mineralization, given the uniformity of $\delta^{18}O_{quartz}$ values, but may be related to local perturbations in the pH and Eh conditions. There is an empirically determined correlation between the domains of $\delta^{13}C$-enriched and $\delta^{13}C$-depleted carbonates in the host schists and the sulphide mineralogy of the adjacent orebodies within the Campbell Shear Zone.

Breakey (1975) differentiates stopes where pyrite dominates over pyrrhotite from those where the reverse is true (Figure

84). Pyrite is more abundant than pyrrhotite in the stopes at shallower elevations and at the middle latitudes, whereas pyrrhotite dominates in the deeper stopes, and those located to the north and south (Breakey, 1975).

Trends in the isocompositional distribution of sphalerite coincide, and parallel the distribution of pyrite verses pyrrhotite dominated stopes (Breakey, 1975, Figure 85). Contours of the weight percent iron in sphalerite reveal low iron sphalerite at shallower elevations, and a rapid increase in iron content to depth from < 1.5 wt % to > 6.0 wt % over a vertical distance of 200 m. The stability fields of pyrite, pyrrhotite, and magnetite in f_{O_2} verses pH space at 350°C, reveals the f_{O_2}-dependence of the pyrite:pyrrhotite stability field under these conditions at neutral to acidic pH. Also shown is the f_{O_2}-dependence of the iron content of sphalerite under these conditions (Rye and Ohmoto, 1979; from Hayba et al., 1985; Walsh et al., 1988, Figure 86).

Stable carbon isotope fractionation is extremely sensitive to oxidation conditions near the CO_2/CH_4 buffer, due to the large fractionations between oxidized and reduced carbon species in solution (Rye and Ohmoto, 1973). Calcite precipitating within the calcite field would generally be depleted in $\delta^{13}C$ relative to calcite forming within the pyrrhotite stability field, all other variables held constant (Figure 87). However, [13]C-

enriched carbonates are present adjacent to pyrite-dominated orebodies, whereas ^{13}C-depleted carbonates occur proximal to pyrrhotite-dominated orebodies, near the boundary between these two types of orebodies. The shifts of ^{13}C-enrichment or depletion is the opposite of that predicted assuming Eh-controlled fractionations, however, it is thought that a more complex fractionation process occurs during a degassing or devolatilization episode.

During CO_2 unmixing, H_2, N_2, CH_4, CO_2, H_2S, and NH_3 may partition into the vapour phase (Henley et al., 1984). Generally, the least soluble gasses should fractionate towards the gas phase, whereas the more soluble species should fractionate towards the liquid phase. Thus, during a degassing episode, there is a preferential partitioning of ^{13}C depleted, reduced carbon species towards the vapour phase, causing a concomitant ^{13}C-enrichment of residual oxidized species in the liquid phase. Additionally, in a CH_4, H_2S-bearing, CO_2-rich system, this could cause a concomitant shift towards more oxidizing conditions in the residual aqueous fluid after degassing of the CH_4 (Henley et al., 1984; Drummond and Ohmoto, 1985). Therefore, it is likely that a degassing event caused both a more oxidizing environment, characterized by pyrite dominating over pyrrhotite, as well as ^{13}C-enriched carbonates due to preferential partitioning of δ^{13}C-depleted CH_4 into the vapour
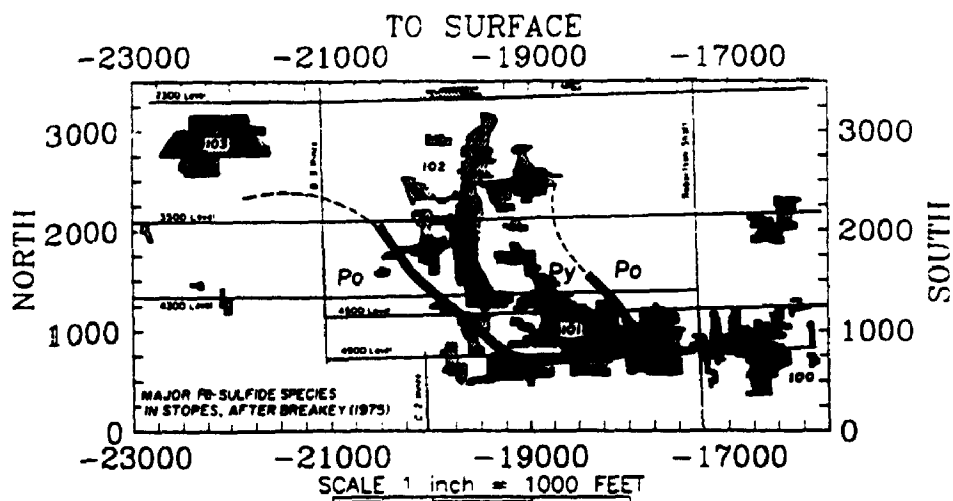
Figure 84. Longitudinal section of the Campbell Shear Zone revealing line separating pyrite dominated stopes from those where pyrrhotite dominates. This line is nearly coincident with the separation of the ^{13}C-depleted from ^{13}C-enriched carbonates.
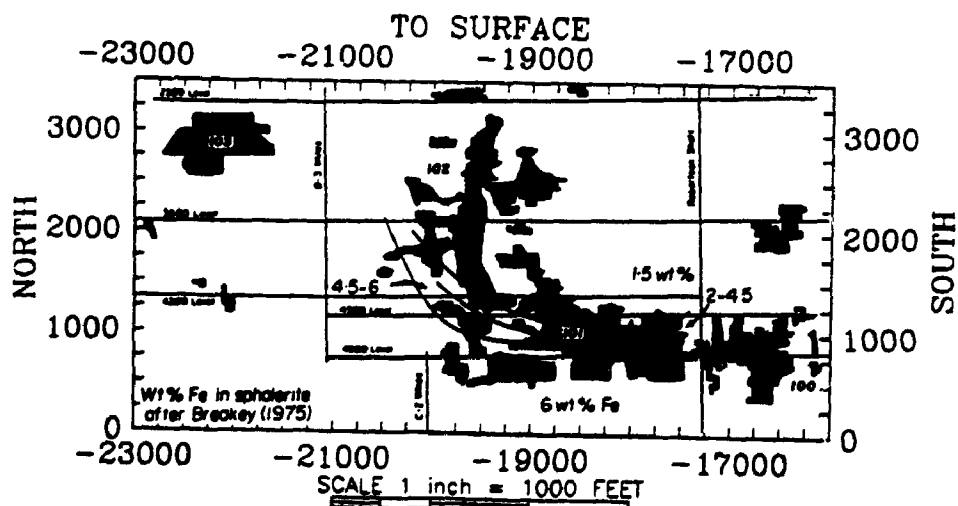
Figure 85. Longitudinal section of the Campbell Shear Zone showing isocompositional lines for sphalerite to be nearly coincident with the pyrite/pyrrhotite fields defined on Figure 84.
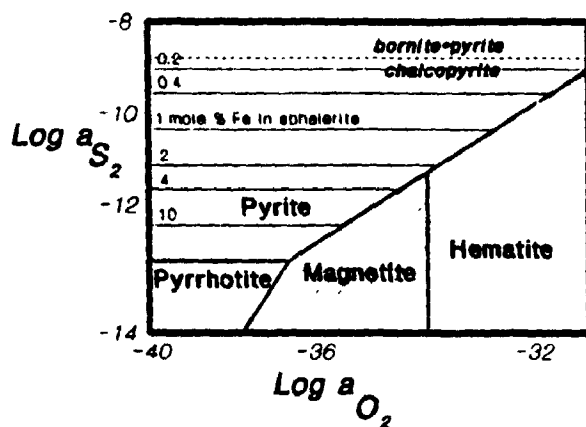
Figure 86. f_{O_2} - pH diagram at 300°C, $P_{fluid} = P_{total}$, illustrating the relationship between oxygen fugacities and the iron composition in sphalerite, after Taylor (1974).
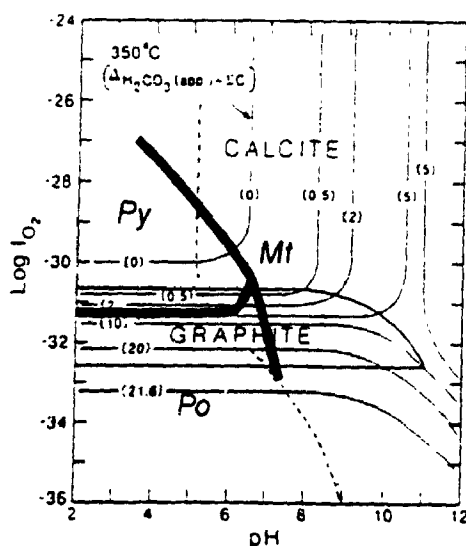
Figure 87. f_{O_2} - pH diagram showing the stability fields of pyrite, pyrrhotite, magnetite, and hematite, and the ^{13}C fractionation of calcite from aqueous fluids. Note the significant changes in ^{13}C fractionations at the pyrite/pyrrhotite stability transition. Figure after Taylor (1987)

phase.

6.7 Discussion

The extremely erratic nature of the gold mineralization within vein-hosted deposits is mirrored by the structure, mineralogy and geochemical characteristics of these deposits. As such, any generalizations, such as Breakey's (1975) characterization of stopes as pyrite-dominated or pyrrhotite-dominated is fraught with exceptions on all scales. The correlations and conclusions arrived at herein should be considered as general features of the Yellowknife gold deposits, and these conform in a general way to other Archean mesothermal gold camps.

6.7.1 CO_2 Unmixing

Recent discussions on the interpretation of the stable isotope systematics of mesothermal gold deposits has primarily focused on the source of the fluid or fluids implicated in the formation of deposits (Kerrich, 1977, 1983, 1987; Kerrich and Fyfe, 1984; Burrows et al., 1986; Golding et al., 1987; Perring et al., 1987). Several authors have reported evidence of CO_2 or CO_2 plus CH_4 immiscibility in fluid inclusions associated with gold mineralization in Archean terrains (Smith et al., 1984; Wood et al., 1986; Ho, 1987; Walsh et al., 1988) Localized redox and pH shifts have been attributed to this

type of degassing or boiling events (Drummond and Ohmoto, 1985; Walsh et al., 1988).

Work by Kerrich et al. (1978), Mortenson and Cameron (1988) and by Cameron (1988a,1988b), has recognized the local redox state of the mineralizing fluids as a major influence in the dissolution, transportation, and deposition of gold in Archean systems, and specifically fluid pressure fluctuations in the seismic-aseismic transition as promoting CO_2 unmixing. Computer simulations on the H_2O-CO_2 miscibility gap and fluid speciation, pH conditions, and mineral precipitation/dissolution using a reaction-path model reveals significant pH and log f_{O2} shifts related to devolatilization as pressure decreases on the system (Bowers, 1991). A significant observation from this work was the restriction of pyrite precipitation to initial solutions of either low ionic strength (0.1 m verses 0.5 m) or low chloride concentrations (0.05 m verses 0.5 m), and that gold precipitation from a complex system (H, O, S, C, Cl, Na, K, Ca, Mg, Al, Si, Fe, Zn, Pb, Ag, Cu, $\dot{r}$u) occurred in experiments with elevated oxygen fugacities (f_{O2} = -33 verses -35.3) (Bowers, 1991). Simpler systems (H, O, S, C, Cl, Na, K, Ca, Si, Fe, Au) revealed gold precipitation occurring over a restricted range of pressures, generally coinciding with an abrupt change in f_{O2}, which increases rapidly demarking the termination of gold precipitation (Bowers, 1991).

The work presented here has primarily focused on defining the stable isotope characteristics of the mineralizing fluids that altered the greenschist-amphibolite facies tholeiitic basalts of the Kam Group and deposited auriferous quartz lodes within the Campbell Shear Zone. The mineralogical and isotopic data presented significantly constrains the nature of these fluids. Archean gold deposits are thought in general, to have formed from weakly saline, near neutral pH, CO_2-rich (5-30 mole%) aqueous fluids, between 260 and 400°C, generally with P_{fluid} between 1-2 kb (Kerrich and Hodder, 1982; Kerrich, 1983; Burrows et al., 1986; Perring et al., 1987; Golding et al., 1987; Colvine et al., 1988) . Log f_{O2} of ore-fluids from most Archean gold deposits are reported to be between -33 to -29.7 (Golding et al., 1987). However, Breakey (1975) determined oxygen fugacities to be between log -43.5 to log -40.4 in the Yellowknife deposits; this estimate is thought to be low, because mineral stability constraints on sphalerite required it to have formed at temperatures below 250°C to be meaningful in a f_{O2} determination. Chary (1971) concluded on the basis of sericite-quartz-carbonate buffer assemblages that the pH of the mineralizing fluids would be fixed within the range of 6.0 to 6.5, in consensus with most other workers.

The extreme concentration and erratic distribution of gold within the mineralized quartz veins in Yellowknife requires depositional processes capable of generating sporadically extreme physical and/or chemical gradients. The uniformity of

$\delta^{18}O$ quartz values indicates that excursions of temperature or a two fluid system were unlikely to be responsible for the gold deposition. However, the siting of orebodies in dilational sites signifies that fluid pressure fluctuations, as discussed by Kerrich and Allison (1977), and Allison and Kerrich (1978), with attendant gas unmixing may have played a critical role in shifting the Eh and pH, and/or destabilizing gold-sulphur complexes, such as to force precipitation of gold. These ideas are fully consistent with the models of Sibson et al. (1988, 1990) who considered Archean mesothermal gold deposits to have formed in the brittle-ductile, or seismogenic zone, accompanied by pronounced fluctuations of fluid pressure.

The distribution of $\delta^{18}O$ values seems to be consistent with two fluid reservoirs, the first related to the ore-forming event with $\delta^{18}O \approx +5$ to $+6$ at around 350 to 400°C, and the second event related to a later fluid, probably meteoric or marine water ≤ 0 permil) at around 150 to 180°C. The single carbon reservoir of ≈ -4 permil was sporadically affected by volatile degassing, causing shifts in the oxygen fugacity of the mineralizing fluids, partitioning of CH_4 to the vapour phase, and a ^{13}C-enrichment of the carbonates subsequently precipitated. Walsh et al. (1988) interpreted their type 1 and 2 fluid inclusions as indicative of a degassing event, attributable to a CO_2 plus CH_4 devolatilization event at the Pamour Number 1 Mine in the Porcupine Camp, Ontario. Fyon et

al. (1983) and Ho (1987) interpreted the presence of CH_4 in auriferous quartz veins to be related to the reduction of the fluids proximal to carbonaceous sediments, rather than being a primary component of the ore-bearing fluids.

The lack of a second $\delta^{13}C$ signature in carbonates containing reset $\delta^{18}O$ values indicates that the second fluid was H_2O-rich and C-poor, and in general, carbonates are more resistant to resetting of C than O isotopes. The hypersaline brines described by Fritz and Frape (1982) appear to be likely candidates for this second fluid, however the distribution of ^{18}O-enriched fluids in shallow domains precludes the involvement of these brines which presently occur at greater depths.

The domainal distribution of carbonates with distinctly different $\delta^{13}C$ values, proximal to mineralization possessing mineralogical evidence of differing Eh conditions, within geochemically identical host-rocks suggests that CO_2-CH_4 unmixing may be responsible for these features. This process could also account for the concentration of gold mineralization in this area (cf. Bowers, 1991). The deviation of the redox conditions in Yellowknife was transient, and the carbonates deposited peripheral to the ^{13}C-enriched carbonates reveals an influence of the ^{13}C-depleted vapours, such that in total, the $\delta^{13}C$-composition of the carbonates exist as a unimodal population.

CHAPTER 7

INCREMENTAL ARGON-ARGON AGE DATING

7.1 Introduction

This chapter examines the relative and absolute age relationships of the gold mineralization, and other events in the development of the Yellowknife Greenstone Belt. The hydrothermal event that generated gold-bearing quartz veins within the shear zones at Yellowknife involved absolute addition of K, reflected in the growth of new, hydrothermal muscovite and paragonitic-muscovite from alkali-feldspar and chlorite (Osatenko, 1971; Webb, 1984; Armstrong, 1991). Muscovite is cotemporal and cogenetic with the main ore paragenesis of quartz, sericite, pyrite, arsenopyrite, sphalerite, galena, and sulfosalts, and consequently this mineral is a suitable candidate for age determination (Breakey, 1975).

Incremental argon age data on the ore-related metasomatic event is presented. The results are interpreted within the context of this and other Archean gold camps, and geochronological constraints on the timing and possible source reservoirs for the gold mineralization in Yellowknife are considered.

Mineralization

Boyle (1961) determined that the shear zones formed by the deformation and concurrent metasomatic alteration of the host rocks. Greenschist-amphibolite facies tholeiitic basalts were transformed in the Campbell Shear Zone to a greenschist assemblage of chlorite + quartz + albite + carbonate schist. Mass balance studies reveal that such a transformation requires additions of volatiles (H_2O, S, CO_2), and K, variable gains or losses in Ca, Fe, and Mg, and losses in Na (Boyle, 1961; Osatenko, 1971; Webb, 1984). The intense schistosity and lineation in the shear zone was initially imparted syn- to post- early metasomatism.

Auriferous zones and attendant carbonatization, silicification, sulfidation, and sericitization are superimposed upon the structurally prepared schists in prolate ellipsoidal domains that constitute orebodies, and likely represents a later metasomatic event, including absolute gains of Si, CO_2, K, Au, Ag, S, As, Sb, Te. Al, Ti, Zr, Hf, V, and Th behave isochemically (Kerrich et al., 1981; Kerrich and Fyfe, 1988). Gold is present in quartz veins as the native metal, and electrum, and is found in various minerals such as aurostibite, jamesonite, gudmundite, and the bismuth telluride, hedleyite. Accessory minerals include pyrite, pyrrhotite, arsenopyrite, chalcopyrite, sphalerite, galena,

bismuthinite, scheelite, tourmaline, muscovite, calcite, and Fe-dclomite (Breakey, 1975).

7.2 Incremental Argon Age Dating

Incremental argon age-dating is described by Faure (1986), Dalrymple et al. (1981) and York (1984) and details of this method will not be addressed here.

The ratio of ^{40}Ar to ^{39}Ar in a sample is dependant upon many factors including the ^{40}K to ^{39}Ar ratio which is proportional to the age of the sample. A sample that has remained closed to argon diffusion since formation will release ^{40}Ar and ^{39}Ar in a constant ratio at each temperature increment and thus yield one age date. In contrast, a sample that has been affected by a thermotectonic event of sufficient magnitude to permit some argon loss will yield a disturbed apparent age spectra. Under some conditions incremental argon age-dating can provide one with a thermotectonic history of a sample using potassium-argon systematics if two or more minerals with different blocking temperatures are analyzed. Unfortunately, muscovite is the only K-bearing phase in the gold-quartz veins. A thermotectonic or fluid event could conceivably reset the entire sample spectrum, yielding erroneously low age estimates if that age is interpreted as the time of formation.

Two samples of muscovite-bearing quartz vein were collected from the NERCO-Con Mine, from orebodies within the Campbell shear zone. Sample DRW1 was obtained from stope 5168M, a conventional stope accessed from the 5100 level at mine elevation 585 feet, south of the Robertson shaft, centred at latitude 16,800. The stope was recognized as having abundant coarse-grained hydrothermal muscovite within mineralized quartz-carbonate veins. Chalcopyrite was the common sulphide species present in the stope at this elevation. This muscovite was analyzed on the University of Western Ontario microprobe and was found to be a slightly phengitic muscovite. An ICP-MS analysis of a separate of this muscovite is reported in Appendix 4.

Sample DRW2 was collected from the fine-grained sericite alteration zone peripheral to an auriferous quartz vein in stope 5191M, a conventional stope at mine elevation 660 feet, located north of the Robertson shaft, centred at latitude 19,100 and accessed from the 5100 level. Small tan-coloured patches of gangue, referred to as sericite-rich patches are abundant in and around auriferous quartz veins in this area. The white micaceous mineral was hosted in a dark vitreous-appearing quartz vein with 7% Fe-dolomite, 1% tourmaline, and 1% pyrrhotite and arsenopyrite. The mica formed as a hydrothermal alteration product of dark-green chlorite, and is referred to as sericite alteration. It is ubiquitous around

auriferous quartz veins, extending up to several tens of metres away from mineralized quartz veins, and is rarely if ever associated with unmineralized quartz veins. Sericite-rich patches were hand-picked from the quartz vein, crushed, screened, washed and separated on a Franz isodynamic electromagnetic separator. A smear section XRD analysis on a Rigaku Geigerflex Xray Diffractometer at the University of Western Ontario found the sample to be relatively pure muscovite. Aliquots of both muscovites were submitted to Derek York in Toronto for incremental argon age dating.

7.2.1 Results

Sample DRW1 contained 6.5% K and 0.7% Ca. The contaminating Ca-phase was likely Fe-dolomite, degassed at the lowest temperatures as indicated by the $^{37}Ar/^{39}Ar$ release pattern. The data indicates that the muscovite became closed to argon diffusion at about 2,400 Ma, and was disturbed at about 2,000 Ma. The sample remained relatively undisturbed since 2,000 Ma (Figure 88; C. Hall, pers com., 1985).

Sample DRW2 contained only 1.2% K and 8.8% Ca, and was considered severely contaminated. The Ca-rich phase was likely plagioclase, which complicated the resultant age-spectra (Figure 89). The history of this sample is

Figure 89. 'Ar/'Ar profile for DRW1, a coarse muscovite
separate form stope 5168M, in the Campbell Shear
Zone. The muscovite became closed to Ar
diffusion ca 2,400 Ma, and was reset ca 2,000 Ma.
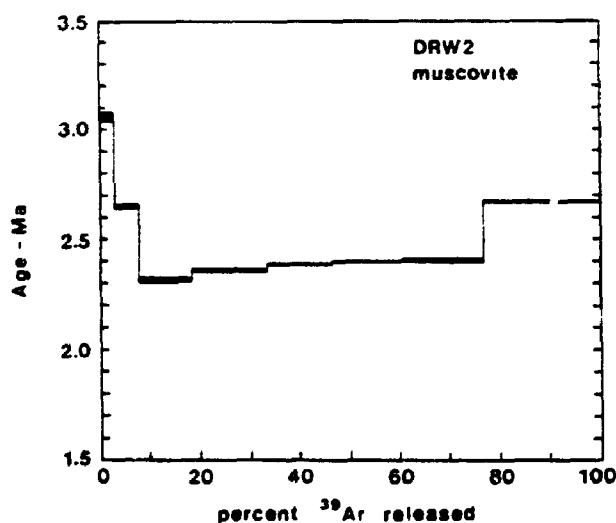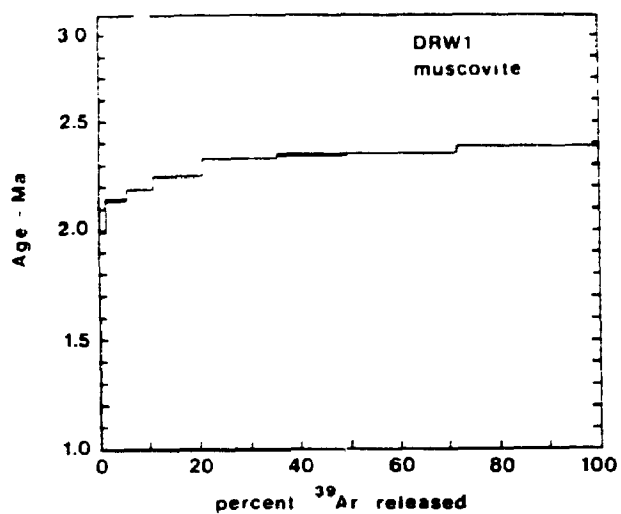
Figure 89. $^{40}Ar/^{39}Ar$ profile for DRW2, fine-grained sericite
within the alteration peripheral to an auriferous
quartz vein in stope 5191M, in the Campbell
Shear Zone. The sample is contaminated, and is
interpreted to have a profile similar to DRW1,
once Ca contamination is accounted for.

interpreted to be similar to that of DRW1 once the excess ^{40}Ar is accounted for (C. Hall, pers com., 1985).

7.3 Age relationships

Understanding of the development and mineralization of the Yellowknife Greenstone Belt has greatly advanced from constraints imposed by radiometric age determinations. The best estimates of the ages of some of the critical geological events in the development of the greenstone belt are summarized in Table 1 from Chapter 2. A review of the earlier work with cautionary notes on the interpretation of radiometric ages determined by various less robust or less well constrained methods was produced by Easton (1984).

The methods considered in this chapter include U-Pb, Rb-Sr, Sm-Nd, and K-Ar dates on whole rocks and mineral separates, as well as two incremental Ar-Ar dates on mineral separates described here. The systematics, assumptions and limitations of each method are clearly explained in detail by Faure (1986). The limitations of individual analyses will be considered where relevant, and an attempt made to synthesize this varied body of data.

The oldest rocks in the Yellowknife greenstone belt are exotic xenoliths of tonalite from the diatreme phase of the

lamprophyre dyke at the NERCO-Con Mine. The dyke was considered in some detail by Webb and Kerrich (1988). Nikic et al. (1980) reported discordant U-Pb minimum ages of 3,210 Ma from zircons extracted from the xenoliths, and discordant U-Pb minimum dates on whole rocks up to 3,300 Ma. Bibikova et al. (1986) reported Sm-Nd ages up to 3,390 Ma on whole rock samples of the same tonalite xenoliths. In both the U-Pb and Sm-Nd work, the authors recognized reset ages of around 2,600 +/- 30 Ma. The dyke also includes xenoliths providing discordant U/Pb ages as young as 2,570 Ma (Nikic et al., 1980).

Gneisses and sediments of the Dwyer Formation have ages of 2.8 Ga that structurally underlie parts of the Kam Group (U-Pb, zircon; Isachsen et al., 1991b). A felsic dyke in the Crestaurum Formation near the base of the Kam Group, has yielded a zircon U-Pb age of 2,678 +/- 8 Ma, and should be viewed as a minimum age for the Kam Group (Padgham, 1985; Helmstaedt and Padgham, 1986b). The Townsite Formation has been dated by radiometric procedures, and the apparent dichotomy in ages is addressed in chapter 3. A zircon U-Pb age of 2,683 ±5 Ma is assumed most realistic (Isachsen and Bowring, 1989). A tuff horizon within the Yellowknife Bay Formation, near the top of the Kam Group, stratigraphically above the Townsite Formation has a zircon U-Pb age of 2,688 ± 3 Ma (Isachsen and Bowring, 1989; Isachsen et al., 1991a).

The Banting Group has zircon U-Pb ages of 2,667 ± 4 Ma and 2,670 ± 14 Ma from a subvolcanic intrusive in the Ingraham Formation (Padgham, 1985; Helmstaedt and Padgham, 1986a; Isachsen and Bowring, 1989). These ages are considered to be representative of the Banting Group.

The Burwash Formation has yielded discordant minima from clastic zircons up to 2,640 Ma (Green and Baadsgaard, 1971). This date is diagnostic only of the source region.

The Western Granodiorite has been dated by various methods. Some confusion exists in the earlier work from selection of rocks from any felsic intrusive body west of Yellowknife to generate isochrons (Easton, 1985). Recent mapping and geochronological work has done much to alleviate this problem (Atkinson, 1988; Atkinson and van Breeman, 1990; Atkinson and Fyfe, 1991). Five distinct intrusive domains have been defined, based upon petrographic, geochemical, and geochronological work. Zircon U-Pb ages range from 2,634 ±5 Ma from older intrusions to 2,584 ±4 Ma to 2,525 Ma for the younger intrusions within the Western Plutonic Complex (Atkinson and van Breeman, 1990; Atkinson and Fyfe, 1991).

The Jackson Lake Formation contains granitoid boulders that have provided discordant $^{207}Pb/^{206}Pb$ minimum ages of 2,554 Ma and 2,534 Ma from zircons, and accordingly, should be viewed

as a minimum age for the boulders, and amax;mum age for the Jackson Lake Formation (Green and Baadsgaard, 1971; Easton, 1984). Other granitoid boulders have provided zircon U-Pb ages of 2,609 ±6 Ma and 2,605 ± 7 Ma (Isachsen and Bowring, 1989; Isachsen et al., 1991b).

Easton (1984) noted that many Proterozoic rocks adjacent to the margins of the Bear Structural Province, or near large northerly trending faults appeared to have reset K-Ar and Rb-Sr ages, yielding anomalous dates of less than 2,300 Ma. The predominant Proterozoic dykes in the Yellowknife area have been dated at 2,049 +/- 80 Ma using Rb-Sr isochron, or as old as 2,380 +/- 120 Ma using K-Ar methods (Gates and Hurley, 1973; Leech, 1966).

Initial retrogression likely occurred syndepositionally as a spiliti - mineral assemblage replaced the primary mineralogy of the basalts (Webb, 1984). Early prograde metamorphism is synchronous with deformation, and related to the intrusion of the Defeat Plutonic Suite (Drury, 1977; Henderson, 1985). Deformation post-dated peak metamorphism, and structures are affected by rheological differences in rocks types, including metamorphically imposed rheological differences. Subsequent intrusion of the Awrey Complex, Prosperous Lake, Stagg and Duckfish granites, and related second prograde metamorphism occurred synchronously with a second deformation, and the main

mineralizing event. The Jackson Lake Formation was likely deposited sometime, probably quite late, during this period.

Ore bodies at the NERCO-Con and Giant Yellowknife Mines in Yellowknife are confined to large shear zones which transect rocks of the Kam Group. The shear zones are coeval with late peak first metamorphism (2,620 ±8 Ma). Similar shear zones are known to offset all of the felsic dykes, and occur within the Western Granodiorite. The ore-bearing shear zones at the Giant Yellowknife Mine can be traced to the Jackson Lake Formation, which is not offset by the shear zones, and would appear to post-date the shear zones, although in places the Jackson Lake Formation appears to have been affected by some shearing (Goldstone, pers com. 1984). Mineralization is hosted within type 2 structures, and related to the second metamorphic event (2,585 Ma). Proterozoic diabase dykes (2.4 ±.2 Ga) post-date mineralization, however in places they are moderately deformed by the ore-bearing shear zones, presumably by post-dyke reactivation of the shear zones. The ore bodies at the NERCO-Con Mine have all been deformed to some extent and most have undergone extensive folding, fracturing, brecciation, and boudinage (Bullis et al., 1987).

7.4 Discussion

Once a K-bearing mineral cools below its blocking temperature,

the temperature below which diffusive argon loss is inhibited, the amount of ^{40}Ar in the sample is proportional to the amount of ^{40}K in the sample, age, and the amount of ^{40}Ar trapped at the time of formation.

The muscovite at the NERCO-Con Mine became closed to argon diffusion at $\approx$2.4 Ga and was subsequently disturbed. Muscovite is paragenetically associated with gold mineralization throughout the greenstone belt.

The Jackson Lake Formation, with a maximum age of 2,534 Ma truncates the cre-bearing shear zones at the Giant Yellowknife Mine (K. Goldstone, pers com., 1984) thus imposing a minimum mineralization age of 2,534 Ma. An independent age for gold mineralization is suggested by cross-cutting relationships west of Kam Lake and northwest of Giant Yellowknife Mines, where auriferous shear zones transect the Western Granodiorite (2,620 Ma). Atkinson and van Breeman (1990) and Atkinson and Fyfe (1991) provide further constraints, relating the gold mineralization to a complex of late Archean granite intrusions (Awrey Complex, 2,525 to 2,585 Ma) on the basis of spatial and trace element similarities. The 2,570 Ma age for a xenolith in the lamprophyre dyke which is cross-cut by the Campbell shear zone provides another independent maximum age for mineralization in Yellowknife. In summary, gold mineralization may have occurred between 2,570 and 2,534 Ma.

Gold mineralization in the NERCO-Con Mine is estimated to have formed from low salinity CO_2-charged fluids at temperatures of 300 to 400° C (Kerrich and Fyfe, 1988). Presumably the associated muscovite formed at this temperature as well, and this is confirmed by quartz-muscovite oxygen isotope temperature estimates (310°C +20/-22 °C; Chapter 6). The blocking temperature for muscovite is around 300 to 350°C, and thus the mineralization formed close to the blocking temperature of muscovite, and there should not have been protracted cooling prior to reaching the blocking temperature or the incremental Argon age profile should have revealed it (York, 1984; Lund et al., 1986).

In many Archean and younger mesothermal gold camps, mineralization is within 10 to 40 Ma of the last major magmatic events (Colvine et al., 1988). However, in the Abitibi belt, radiometric ages of 100 to 240 Ma younger than the last pre-mineralization magmatism have been recorded in the ore deposits and their host rocks. Such young ages are recorded in the U-Pb, Sm-Nd, Rb-Sr, and Ar-Ar systems (for a review, see Kerrich, 1991).

Two classes of explanation have been offered. First, that the young ages are real, and mineralization post-dated the greenstone belt by 100 to 240 Ma (Wong et al., 1989; Jemielita et al., 1988). Alternatively, the young ages have been

attributed to resetting by later deformation and/or fluid events, below the conventional blocking temperatures (Kerrich, 1991) If the first model is correct, then the Abitibi belt, and possibly the Yellowknife Greenstone Belt is an exception to the age relationships in mesothermal gold camps globally. The second model is supported by independent evidence for reactivation of the structures, and multiple fluid infiltration events that cause remobilization and selective isotopic resetting.

At Yellowknife there is clear evidence for late disturbance and reactivation of the ore-bearing shear zone as follows: (1) deformation of Proterozoic dykes where they intersect the shear zones, (2) anomalously young Rb-Sr and Pb-Pb ages relative to U-Pb zircon ages on some of the major units (Easton 1984; Henderson, 1985), (3) $\approx$2,600 Ma disturbance of the Sm-Nd systematics in the tonalite xenoliths (Biblikova et al., 1986), and (4) oxygen isotope disturbance of the quartz-carbonate and quartz-muscovite pairs in the shear zones (this study, Chapter 7).

CHAPTER 8

SUMMARY AND CONCLUSIONS

8.1 Introduction

The data presented in this thesis allows for an interpretation of the temporal and genetic evolution of the Yellowknife Greenstone Belt. It would be beyond the scope of this thesis to examine all aspects of the geology of the Yellowknife Greenstone Belt, and inasmuch as the data does not specifically exclude many alternative interpretations of these data, ambiguities and thus, controversy will exist. This thesis attempts to address certain structural, lithological, and geochemical problems that have been identified throughout this work. A review of the existing information, and new data presented in this thesis has considered 7 aspects of the geology of the Yellowknife Greenstone Belt, and the gold mineralization hosted within these rocks, and these are synthesised below.

1. **The stratigraphy** of the greenstone belt has been examined, and ambiguities and inconsistencies are documented. A sequence of volcanic rocks of intermediate to felsic composition along the north shore of Yellowknife Bay, the controversial "Banting Group", is suggested to be correlative to rocks south of Kam Point, and the later rocks are assigned to a new formation, part of the Kam Group.

2.   The structure of the Yellowknife Greenstone Belt has been considered in 3 separate structural domains in this thesis. Domains east and west of the West Bay Fault hosting brittle and brittle-ductile structures, and a third, sedimentary-dominated domain to the east containing predominantly ductile structures. Domains 1 and 2 are characterized by all of the volcanic-hosted mineralization, and abundant and intersecting type 1, 2, and 3 structures. The displacive structures within the belt are assigned to 4 types; (1) brittle syn-volcanic, (2) brittle-ductile, late first metamorphism, (3) brittle, post-first metamorphism, pre-second metamorphism, and (4) brittle, post-second metamorphism, Proterozoic faults. The 4 types of structures generally possess features diagnostic of a specific event, although reactivation obscures many temporal relationships. Economic concentrations of gold mineralization a restricted to a single type of structure, within a specific geodynamic setting.

3a.   Metamorphism witl in the Yellowknife Greenstone Belt has been related to the intrusion of the felsic plutons at the margins of, and within the Yellowknife Basin. Recent age-dating, geochemistry, and petrography, has refined the understanding of these rocks, and several generations of intrusions can be defined. The recognition cf at least three ages of major felsic intrusions within the area, and at least two prograde metamorphic events within the basin, at 2,620 and

2,585 Ma respectively suggests that similar patterns could be expected from similar rocks at Yellowknife. Evidence of two prograde metamorphic events within the Yellowknife Greenstone Belt has been presented in this thesis, on the basis of cross-cutting relationships, geological similarities to areas where two prograde metamorphic events have been documented, and general temporal constraints.

3b. Gold mineralization is hosted within type 2 structures that: (1) transect greenschist-amphibolite facies rocks, and/or parallel dyke/flow contacts, (2) are in a P-shear orientation relative to type 3 structures, and (3) are proximal to type 3 structures. Mineralization is also hosted in more westerly striking structures (R and T shears) within amphibolite-grade rocks. Quartz veins, orebodies, and ore zones all commonly reflect P-shear geometries and sense of displacements relative to their host rocks.

4. A lamprophyre dyke intrudes into the hanging wall rocks of the Campbell Shear Zone, representing a late shoshonitic magmatic event at Yellowknife. Implications for the geodynamic setting of the greenstone belt, and gold mineralization is provided by the lamprophyre, because of (1) the distinctive setting of Phanerozoic counterparts of the lamprophyre, and (2) the xenoliths of tonalite and felsic and intermediate gneiss entrained within the diatreme facies of

the dyke. The lamprophyre pre-dates mineralization, and hosts xenoliths dated as young as 2,570 Ma, providing a maximum age for mineralization.

5a. <u>Geochemistry of the host rocks</u> reveals the Kam Group to be a sequence of ocean floor or back-arc tholeiitic basalts, andesites, and tuffs, intruded by mafic dykes of similar chemistry. Early, synvolcanic spilitic alteration, of the extrusive volcanic rocks, and likely autometasomatic alteration of some of the synvolcanic intrusions is revealed. Metasomatic and dynamic alteration of the basalts syn-type 2 structure, produced chlorite carbonate schists, which retained aspects of its host rock geochemistry, including the lamprophyre dyke.

5b. <u>Geochemical anomalies related to the ore-related metasomatism</u>, for a comprehensive suite of elements in shear zone-hosted chlorite schists are found with distinctive spatial relationships to mineralization within the Campbell Shear Zone. Key examples include relative enrichments of K_2O, S, As, Zn, Rb, and Ba, and depletions of Al_2O_3, Fe_2O_3, and Na_2O, in chlorite schists proximal to gold mineralization, or K_2O enrichment, and SiO_2, Al_2O_3, Na_2O depletions, with variable, TiO_2, Fe_2O_3, MgO, and CaO, and LOI gains and losses, also related to chlorite schists proximal to mineralization. These trends, defined, in part empirically, and in part on the basis

of a multivariate analysis of data from macroscopically unaltered chlorite schist samples, clearly distinguishes mineralized portions of the Campbell Shear Zone from less mineralized portions. Some trends may dif'erentiate between differing types of mineralization within the shear zone, whereas others identify primary differences in the protoliths of the shear zone.

6. A study of <u>oxygen and carbon isotopes</u> in carbonates, and O-isotopes in silicates from the Campbell Shear Zone reveals 3 aspects of the shear zone; (1) there is a distinctive ore-forming fluid at Yellowknife, (2) gold mineralization was mediated and/or enhanced by fluid pressure fluctuations resulting in CO_2/CH_4 unmixing, and concomitant Eh/pH fluctuations, and (3) a late, low temperature, likely low CO_2 fluid infiltrated the Campbell and Con Shear Zones from surface, preferentially resetting the oxygen isotopes in the less robust minerals.

7. Lastly, a reconnaissance <u>Ar-Ar study</u> provides independent evidence of a late Archean - early Proterozoic geodynamic event that reset the Ar systematics in ore-related muscovites from a stope in the Campbell Shear Zone. However, it cannot provide a reliable estimate for the timing of mineralization.

8.2 Synthesis

Figure 90 presents a temporal framework for the development of the Yellowknife Greenstone Belt.

The Yellowknife Greenstone Belt developed in a back-arc basin, such that spreading of an oceanic crust allowed for tholeiitic basalts of the Kam Group to erupt (ca 2,680 Ma), intruded by sheeted gabbro dyke complexes (Helmstaedt and Padgham, 1986a; Cunningham and Lambert, 1989). Synvolcanic growth-faults (type 1), and less common transform faults (type 1) were brittle structures, developed at moderate to high angles, and allowed stratigraphic differences to develop across faults at successively higher stratigraphic levels (Helmstaedt and Padgham, 1986a; Fyson and Helmstaedt, 1988; Fyson, 1990). Intermediate volcanic cycles within the Kam Group reflect crustal contamination, possibly during slower spreading episodes (Goodwin, 1988; Cunningham and Lambert, 1989). Clastic sediments from an exposed continent became relatively more abundant with time, reflecting maturation of the back-arc basin (de Wit and Stearn, 1981; Helmstaedt and Padgham, 1986a).

The Banting Group was deposited circa 2,667 Ma during basin closing, reflecting a switch to calc-alkaline volcanism, with laterally discontinuous flows, and abrupt facies changes (Jenner et al., 1981; Goodwin, 1988; Bailey, 1988; Cunningham
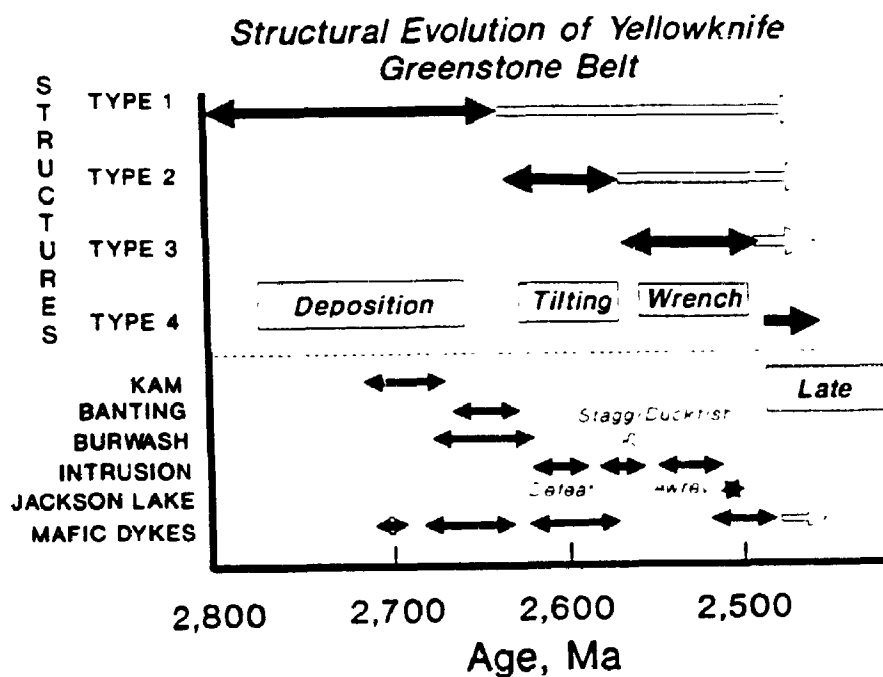
Figure 90. Time-event diagram revealing the temporal evolution of the Yellowknife Greenstone Belt. Unshaded arrows extend beyond structural periods indicating periods of reactivation.

and Lambert, 1989). The type 1 structures were reactivated during basin closure, in an oblique transpressional regime, and caused structural thickening, and lateral elongation of the volcanic sequence (Fyson, 1990). Intrusion of the Defeat Plutonic Complex (ca 2,620 Ma), and related prograde metamorphic event accompanied this event. Type 2 structures developed in this environment, syn- to post-metamorphic. Metamorphic fluids advanced up the thermal gradient and altered dilatant structures (Kerrich and Allison, 1978; Kerrich and Fyfe, 1988; Duke et al., 1990).

The Yellowknife Greenstone Belt was accreted obliquely, resulting in strike slip faulting. Lamprophyre dykes, featuring high LREE and LILE, and normalized Ta-Nb and Ti troughs intruded at this time or later: there is a compositional similarity to Phanerozoic shoshonitic rocks developed during transpressive collision. Evolved granites of the Awrey Complex and Prosperous Lake Granite, formed by anatectic melting of crustal material lowered into a rising geotherm, intruded (ca 2,585 Ma) into the sequence, and a related thermal event produced a broad, low pressure, prograde metamorphic front.

Ore-forming fluids, derived from crustal sources, accessed permeable pathways post-2,620 and pre-≈2,585 Ma, within a stress regime consistent with wrenching. In this stress

regime, these are the ductile portions of the type 2 structures in P-shear orientations relative to the type 3 structures. The type 3 structures, in D or C-shear orientation are not permeable, however, they isolate portions of the type 2 structures, allowing; (1) an additional degree of freedom for displacement, and thus (2) enhanced permeability. Pressure induced unmixing of the ore-forming fluids caused rapid Eh-shifts in the aqueous fluids, destabilizing soluble gold complexes. Subsequent/continued movement along type 2 and 3 structures deformed and displaced mineralization.

Thermally induced uplift continued, and erosion and fluviatile sedimentation deposited rocks of the Jackson Lake Formation (ca 2,534 Ma), containing boulders and cobbles of high Rb, K, U, Th, Be, Li, plutonic rocks. Diabase dykes of the Dogrib and Indin swarms intruded, into these rocks in the late Archean.

Movement along the terrane boundary fault (West Bay or Hay-Duck Fault) continued, displacing all units and structures.

8.3 Metallogenic Context

Gold mines in the Yellowknife Greenstone Belt have produced more than 435 tonnes of gold, mainly from shear zone hosted auriferous quartz veins. Mineralization is disproportionately

located within ductile shear zones that; (1) transect transitional greenschist-amphibolite facies tholeiitic basalts of the Yellowknife Bay Formation, (2) strike within 15° of north, anᵣ (3) are intersected by later cross faults. The shear zones constrained the mineralizing-fluids to a structurally defined horizon. Metasomatic alteration of the chlorite schists by ore-forming fluids extended beyond visible sericitization, silicification and quartz veining, and provides for a viable target for lithogeochemical exploration.

Basalt, chlorite schist, sericite schist, and quartz veins, are different lithotypes, and pathfinder and indicator elements for gold are not common to all of them.

APPENDIX 1

SAMPLE PREPARATION, STABLE ISOTOPE ANALYSIS

One hundred samples of chlorite carbonate schist were
collected, and sent to XRay Assay Laboratories Ltd. in Toronto
for standard whole rock and trace element analysis. The
samples were crushed and pulverized and analyzed by XRF
methods. The crushed and pulverized sample rejects were
returned to the University of Western Ontario for further
analysis. Approximately 2, 3, or 5 grams of material was
reacted with +100% phosphoric acid at 25°C according to the
method described by McCrea (1950). Digestions of 1 hour were
used for calcite extractions, and 24 hours at 50°C for Fe-
dolomite extractions on the residues from the calcite
extraction. The evolved CO_2 was dried, and collected by
freezing with liquid nitrogen, and then analyzed on a
Micromass II triple collecting mass spectrometer. Samples
containing appreciable sulphide (>1%) had the extracted
CO_2 passed through an H_2S trap prior to collection. A
representative piece of each rock sample was retained for
petrographic work.

The CO_2 attributed to calcite is expected to contain some
contribution from coexisting Fe-dolomite, and likewise, CO_2
attributed to Fe-dolomite is expected to contain minor

266

contamination from residual, unreacted calcite. In both instances the contaminating phase contributes a negligible amount of CO_2 (Kerrich, 1990; Pleydell et al., 1990).

Duplicates, submitted to check laboratory precision are shown below (Table 1) reveal average errors for $\delta^{18}O$ of 2.3% and 4.3%, and average errors for $\delta^{13}C$ of 12.6% and 3.8% for calcite and Fe-dolomite extractions respectively. The anomalously high $\delta^{13}C$ error for calcite extractions is influenced by one unusually large error (>40%), and is likely a laboratory error related to the low CO_2 production from this sample.

APPENDIX 2

The distribution of submicroscopic gold in sulfide and sulfosalt minerals in the Campbell shear zone, Con Mine, Yellowknife, N.W.T.

Introduction

Gold occurs in nature in the native state, commonly alloyed with silver, copper or platinoid metals; as sulfide or sulfosalt minerals; or in solid solutions as a contaminant in sulfide or sulfosalt minerals. The extraction of gold from natural ores normally utilizes one of golds unique properties; high specific gravity (placer ores), ability to form amalgams with mercury, solubility in oxidizing alkali cyanide solutions. However, in some instances, gold occurs in a form that precludes easy extraction utilizing any of the previously mentioned properties. This paper is concerned with a variety of gold ore from the Campbell shear zone, Con Mine, Yellowknife, N.W.T. in which submicroscopic gold occurs within sulfide and sulfosalt minerals. This type of ore is refered to as "roasting ore" in allusion to how the ore is normally treated to maximize gold recovery. "Roasting ore" is contrasted with ".ee-milling ore" which is an ore type in which the gold can be recovered by simple cyanidation. The genetic implications of the two types of ore will be speculated on, in reference to published studies.

Background

The Con Mine is located 2 km south of the city of Yellowknife, N.W.T. (Figure 1). Auriferous quartz veins are

hosted in planar domains of chlorite, sericite, carbonate schists that have been interpreted as shear zones (Boyle, 1961; Henderson and Brown, 1966; Allison and Kerrich, 1979). The shear zones can be extensive, up to 200 meters wide, in excess of 10,000 meters long, and greater than 1,800 meters deep. They transect Archean tholeiitic basalts of the Kam Formation, are erroded at an Archean unconformity surface, and intruded by Proterozoic dykes (Meyer, pers. comm.; Goldstone, pers. comm.; Henderson and Brown, 1966). Major faults, both predating and postdating the Proterozoic dykes transect the Kam Formation volcanics and associated intrusions. The most significant fault is the West Bay Fault which separates the two major gold producers in the Yellowknife area (Figure 2). Ore from the two mines is superficially similar, with a few important exceptions, notably, the Giant Yellowknife Mine produces dominantly "roasting ore" whereas the Con Mine produces dominantly "free millirg ore". Some of the early production from the Campbell shear zone was dominated by "roasting ore" but due to a zonal distribution of this ore, current production is largely all "free-milling ore".

Samples

There are five ore zones in the Campbell shear zone at the Con Mine, which along with ore type and dominant sulfide species are shown on Table 1. These five ore zones are ploted on an inclined longitudinal section which is drawn parallel to the Campbell shear zone and faces east (Figure 3). The shear zone

strikes 007 degress and dips 55 degrees to the west.

Samples were collected from the five ore zones, with detailed sampling from the 101 and 101 south fringe zones. The detailed sample locations are shown on Figure 4. Material was collected from each of the active stopes from the 101 and 101 south fringe zones, representing average ore-grade samples typical of that stope. These rocks were sent to Cominco Ltd.'s Exploration Research Laboratory for sectioning and microscopic examination. A report by McLeod (1984) outlines the basic ore suite for each sample (Appendix 1). The samples were then examined at the University of Western Ontario in an attempt to quantify the occurrence of all auriferous species by optical microscopy supplimented by scanning electron microscopy, energy dispersive x-ray analysis, and electron microprobe work.

Gold distribution

Gold occurs in various sizes, shapes and associations in the ore from the Campbell shear zone at the Con Mine. There are three important modes of gold occurrence within a somewhat continuous distribution series of gold in natural ores:

1a Native gold or electrum, not included in, or in contact with an sulfide or sulfosalt mineral.

1b Native gold or electrum, in contact with a sulfide or sulfosalt mineral, either external to, along a grain contact, or in a penetrating fracture in the sulfide or sulfosalt mineral.

2   Native gold or electrum, totally encapsulated within a sulfide or sulfosalt species, excluding gold occurring in mode 1b.

3   Gold contained in a sulfide or sulfosalt species as an
     essential component (as in aurostibite, Au Sb$_2$) or as a
     contaminant within a sulfide or sulfosalt mineral.

Gold in modes 2 and 3

Twenty nine polished thin sections were examined, and native gold or electrum was found in 23 of the sections. Gold grains down to 0.25 µm^2 are identifiable in this manner, which in a 80 mm^2 section corresponds roughly to a grade of 0.008 ounces of gold per ton.

The bulk of the gold found in mode 2 is less than 10 µm across and account for up to 100% of the gold in some sections. The gold occurs as equant grains (Plate 1) and may range up to 100 µm in diameter. No grains of gold in mode 2 are found less than 0.5 µm across, whereas the effective resolution of the scanning electron microscope using the electron backscatter detector is 0.2 µm.

In every instance when mode 2 gold is found, it is encapsulated in pyrite. No mode 2 gold is found within arsenopyrite, pyrrhotite, galena, sphalerite, chalcopyrite, or Pb + Bi + Sb sulfosalts. The mode 2 gold within pyrite appears as equant grains, randomly distributed throughout the sulfide. There is no evidence to suggest that the distribution of the gold within pyrite demarks internal crystal faces, absorbed grain boundaries, or healed fractures. The gold usually contains less than 15 wt. % impurities, although some electrum can be identified optically and confirmed using energy dispersive x-ray analysis. The most common accessory minerals with the gold included within pyrite are gangue

assemblages of quartz and carbonate. Opaque minerals included in pyrite containing mode 2 gold are galena and tetrahedrite, which are never found in contact together within the pyrite. There is one occurrence of what appears to be galena exsolving from pyrite (Plate 2a, 2b). If this is the case then this texture would suggest an anomalous crystallization temperature of $+715^{\circ}C$ (Brett and Kullerud, 1967).

Energy dispersive x-ray analysis coupled with electron microprobe analysis of pyrite, arsenopyrite, galena, tetrahedrite, sphalerite, chalcopyrite and cosalite suggest that some mode 3 gold exists within some of these sulfide and sulfosalt minerals. Pyrite was found to contain mode 2 gold, but little, if any, mode 3 gold. Arsenopyrite was found to contain no mode 2 gold, even though textural evidence shows arsenopyrite replacing pyrite containing mode 2 gold. Arsenopyrite did, however, contain mode 3 gold, although precise determinations were not calculated due to the lack of reliable standards. It appears arsenopyrite may contain mode 3 gold up to 800 ppm, and certain forms of arsenopyrite, specifically subhedral grains 30 μm long average around 400 ppm gold. Both pyrite and arsenopyrite contain significant concentrations of lead. Sphalerite was found to contain abundant gold by energy dispersive x-ray analysis (Plate 3a, 3b) which could not be confirmed using the MAC IV electron microprobe. Cosalite, a rare lead bismuth sulfide ($Pb_2 Bi_2 S_5$) is the only other mineral found to contain significant mode 3 gold in this study (Plate 4a, 4b, 4c, 4d), although Breakey (1975) found

elevated gold values in pyrrhotite, galena, gudmundite, bournonite, jamesonite, madocite, and several Bi-tellurides.

Conclusions

Previous work by Burg (1930, 1935), Kurauti (1941), Mastenitsky (1944), Boyle (1961), Callow and Worley (1965), Schwiegart (1965), Tyurin (1965), Wells and Mullens (1973) and Colvine et al. (1984) deal with the problem of identifying and interpreting very fine-grained gold in sulfides, normally pyrite, pyrrhotite, and arsenopyrite. The grains of gold are usually 10 μm^2 in size, to less than detectable using scanning electron microscopy >0.25 μm^2, and included within pyrite, pyrrhotite, or arsenopyrite with no apparent fractures to allow solutions in from external to the sulfide grain. The genesis of this texture is problematic, with two possibilities considered. Boyle (1961, 1979), Burg (1935), and others consider exsolution of gold from a metastable gold-sulfide precurser to be likely, whereas Colvine et al. (1984), Tyurin (1965) and Schwiegart (1965) postulate that coprecipitation of pyrite and gold formed these textures. Burg (1935), Kurauti (1941) and Mastenitsky (1941) produce solid solutions of gold and pyrite containing up to 2000 ppm gold, stable at elevated temperatures, whereas recent work reported by Colvine et al. (1984) suggest an upper limit of 10 ppm gold in pyrite. The textures observed in ore samples from the Campbell shear zone, Con Mine, Yellowknife do not appear to be exsolution textures, unless the grain shapes have been modified by later

deformation/remobilization.

A second, more likely provinence for the gold included in pyrite (Mode 2) texture is coprecipitation/adsorption of gold and pyrite. Wells and Mullens (1973) describe arsenical pyrite from the Carlin and Cortez Gold Mines in Nevada where submicroscopic gold is reported to occur within arsenic-rich rims in pyrite. Colvine et al. (1984) refer to Wells and Mullens' (1973) arsenical pyrite as an example of submicroscopic gold adsorbed onto pyrite due to pyrite's semiconductor properties. Colvine et al. (1984) examine pyrites microscopic properties, in an attempt to explain the presence of ubiquitous pyrite in gold deposits. They fond that gold preferentially adsorbs or plates onto the crystal faces of pyrite, in a manner more related to the electrical properties of pyrite than coincidental coprecipitation from reduced saline solutions. The semiconductive properties of pyrite vary from n-type when pure, to p-type when contaminated with arsenic. The p-n junction formed by an arsenical rim on (relatively) pure pyrite is optimal for gold adsorption.

Jean and Bancroft (1985) have examined the phenomenon of gold adsorption on sulfides and conclude that it is most likely an electrical problem in which gold is preferential adsorbed onto sulfide surfaces underlain by fractures, point, or edge dislocations (or impurity sites). Boyle (1979) reports work by Narseev and Starova on gold deposits in Kazakhstan where gold, occurring as impurities in pyrite and arsenopyrite cause point defects in the sulfide crystal lattice which is responsible for

both decreased microhardness and decrease size of the sulfide crystals. These point defects manifest themselves as areas of p-type or n-typope semiconductive sites (electron acceptors/donors). In order to reduce the free energy of the sulfide crystals the gold may migrate to sites of low chemical potential, forming blebs of gold, within sulfides containing no visible fractures.

The work done on the ore samples from the Campbell shear zone, Con Mine, Yellowknife, N.W.T. identifies gold in three modes;

type 1. Native gold or electrum, either free, or with a spatial association with sulfides

type 2. Native gold or electrum, totally encapsulated in sulfides, with no visible fracture.

type 3. Gold contained in a sulfide or sulfosalt species as an essential component or as a contaminant.

The type 2 gold occurrence is restricted to pyrite, even when textural evidence suggests later replacement of pyrite by arsenopyrite. The type 3 gold occurrence was observed in sphalerite, arsenopyrite, tetrahedrite, cosalite and reported in pyrrhotite, galena, gudmundite, bournite, jamesonite, madocite, and Bi-tellurides (Breakey, 1975).

Gold contained in arsenopyrite is of critical economic importance because of the abundance of this sulfide. Preliminary microprobe work suggests significant concentrations of gold in fine-grained subhedral to anhedral arsenopyrite, potentially to

800 ppm, although Wells and Mullens (1973) obtained gold values in arsenopyrite to 2600 ppm. At the Con Mine, with parts of some stopes averaging 1% arsenopyrite, 0.23 ounces of gold per ton of ore could be tied up with the arsenopyrite.

The elevated values of gold in sphalerite determine by energy dispersive x-ray analyses cannot be confirmed by the electron microprobe, and is probably due to peak interferences between the gold Lα line and the zinc Kβ line. Further work should be done on the more abundant refractory sulfide and sulfosalt phases to determine exact mineral compositions, a study similar to Breakey (1975) but with an emphasis towards economic implications.

REFERENCES

Allison, I. and Kerrich, R., 1979. History of deformation and fluid transport in shear zones at Yellowknife. in Proceedings of the Gold Workshop, Yellowknife, N.W.T., R.D. Morton ed., p. 202-231.

Boyle, R.W., 1961. The geology, geochemistry, and origin of the gold deposits of the Yellowknife district; Geol. Surv. Cana., Mem. 310, 193 p.

_____, 1979. The geochemistry of gold and its deposits; Geol. Suv. Can., Bull. 280, 584 p.

Burg, G.H., 1930. Die Sichtbarmachung cles feinverteilen Goles in goldhoffingen Erzen und ihre wirtschaftliche Becleutung; Mettall. Erz., v. 27, p. 333. reported in Boyle, 1979.

_____, 1935. Natur des in den Pyriten nicht sichtbar enthaltenen Goldes; Z. Prakt. Geol., v. 43, pt. 2, p. 17-26. reported in Boyle, 1979.

Callow, K.J. and Worley, B.W., 1965. The occurrence of telluride minerals at the Acupan Gold Mine, Mountain Province, Philippines; Econ. Geol., v. 60, p. 251-268.

Colvine, A.J., Andrews, A.J., Cherry, M.E., Durocher, M.E., Fyon, A.J., Lavigne, Jr., M.J., MacDonald, A.J., Marmont, S., Poulsen, K.H., Springer, J.S., Troop, D.G., 1984. An Integrated Model for the Origin of Archean Lode Gold Deposits. Ont. Geol. Suv., Open File Report 5524, 85 p.

Jean, G.E. and Bancroft, G.M., 1985. An XPS and SEM study of gold deposition at low temperatures on sulfide mineral surfaces: Concentration of gold by adsorption/reduction. Geochemica and Cosmochemica Acta, in press.

Kurauti, G., 1941. Synthetic study of gold-containing pyrite; Suiyokwai-Si, v. 10, p. 419-424. (Chem. Abst., v. 35, 3563.)

Mastenitsky, I., 1944. On some cases of formation of dipersed gold segregations in iron sulfides, C.R. Acad. Sci. USSR, Dokl., v. 14, no. 9, p. 385-388. Reported in Boyle (1979).

Schwiegart, H., 1965. Solid solution of gold in sulfides. Econ. Geol., v. 60, p. 1540-1542.

Tyurin, N.G., 1965. On finely dispersed gold in pyrite. Geol. Rud. Mestorozhd. v.7, no. 5, p. 70-75 (Engl. rev. in Econ. Geol., 1968, v. 63, p. 853.

Wells, J.D. and Mullens, T.E., 1973. Gold-bearing arsenian pyrite determined by microprobe analysis. Cortez and Carlin gold mines. Econ. Geol., v. 68, p. 187-201.
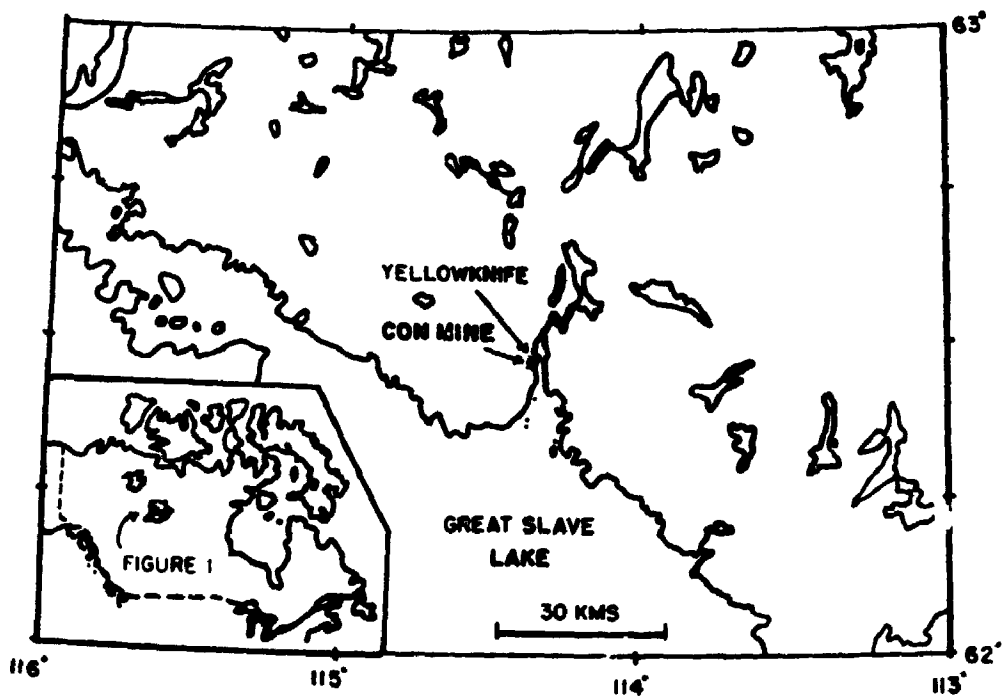
FIGURE I   Location of Yellowknife and the Con Mine
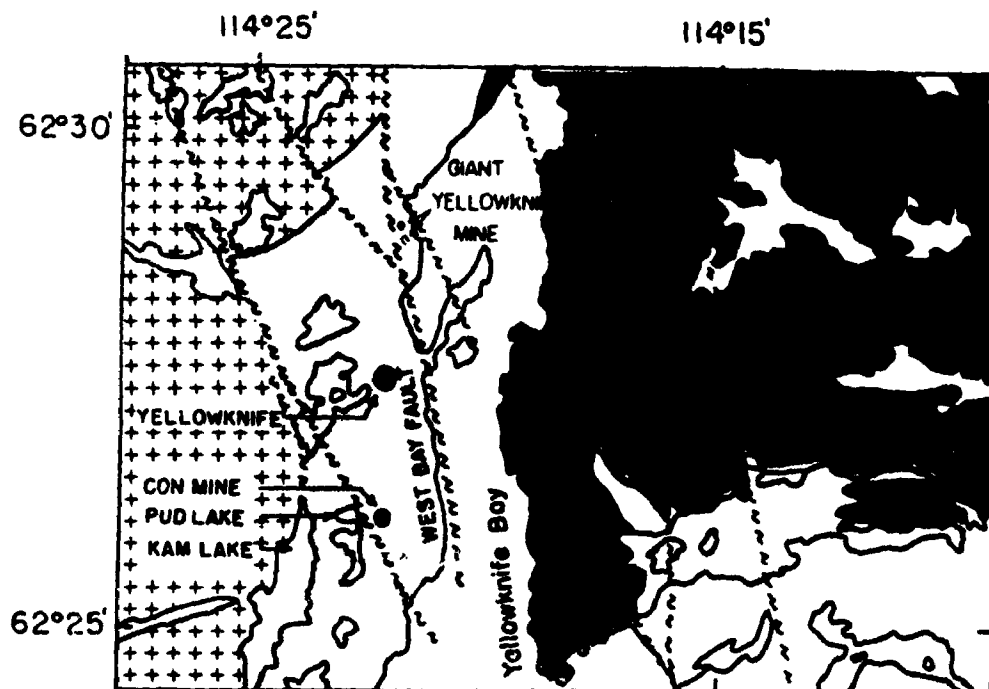
Legend:

- **Western Granodiorite** (+ + + pattern)
- **Burwash Formation** (black)
- **Jackson Lake Formation** (black)
- **Kam Formation** (white)

Map labels: 114°25′, 114°15′, 62°30′, 62°25′, GIANT YELLOWKNIFE MINE, YELLOWKNIFE, CON MINE, PUD LAKE, KAM LAKE, WEST BAY FAULT, Yellowknife Bay

Table 1

ORE ZONE	ORE TYPE	DOMINANT MINERALOGY	% SUL.
Negus zone	roasting ore	arsenopyrite pyrite	8
103 zone	roasting ore	arsenopyrite pyrite	8
102 zone	roasting ore free-milling ore	arsenopyrite pyrite	5
101 zone	free-milling ore	arsenopyrite pyrite	3
101 south-fringe zone	free-milling ore	arsenopyrite pyrite	3

CON MINE

DISTRIBUTION OF ORE ZONES
IN THE CAMPBELL SHEAR ZONE

WITH ARSENOPYRITE : PYRITE RATIOS

283

CON MINE

SAMPLE LOCATIONS

horizontal scale
feet
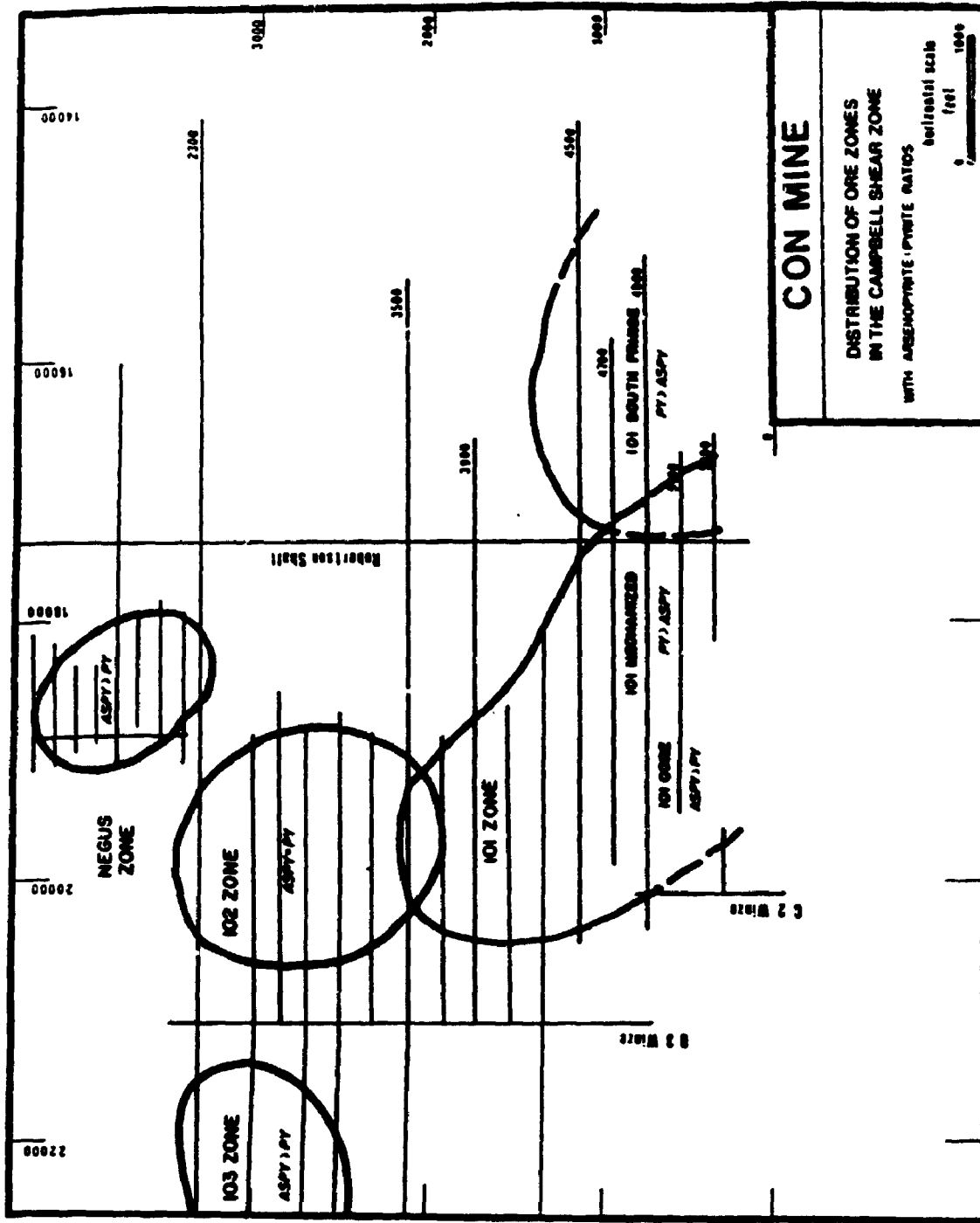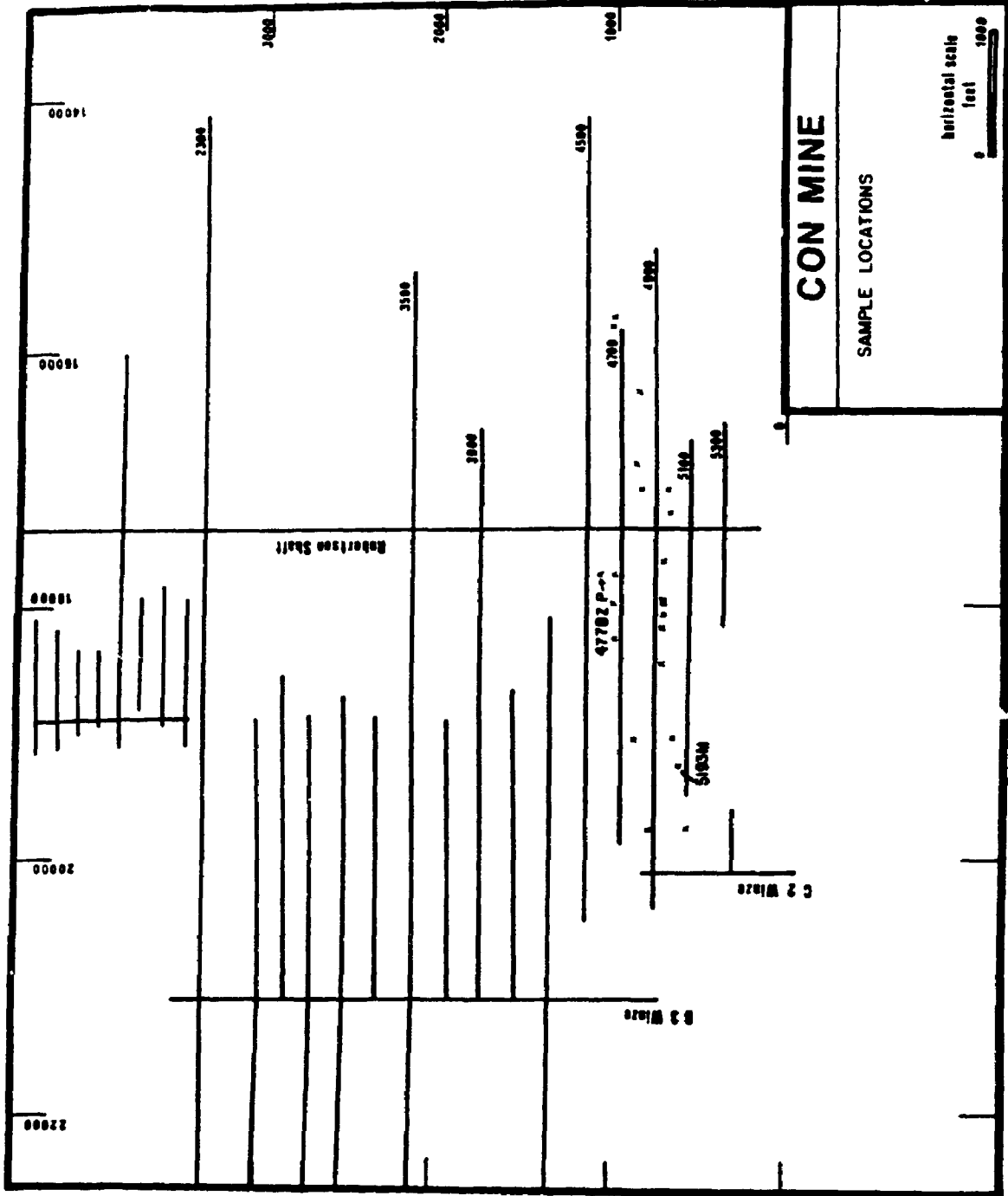
Plate 1.   Sample 284-17555 from stope 47 5

An equant grain of gold, 13 μm in diameter,
occurs as a type 2 grain of gold within pyrite.
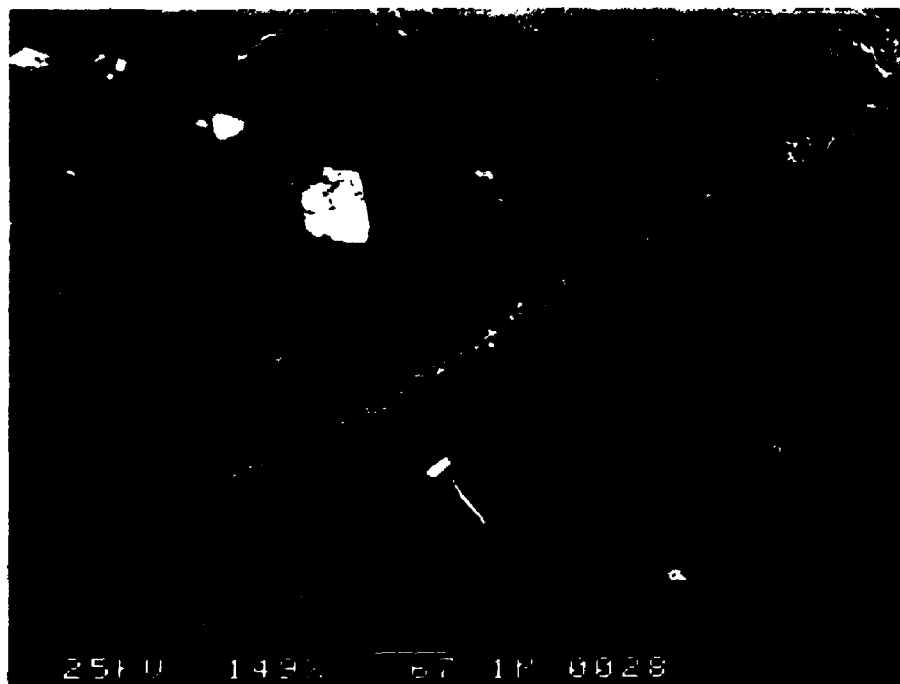
Plate 2a. Sample R84-17553 from stope 4778C pillar
A backscatter electron image of a subhedral
grain of pyrite with arsenopyrite, gold, and
galena inclusions. Location of plate 2b is shown.
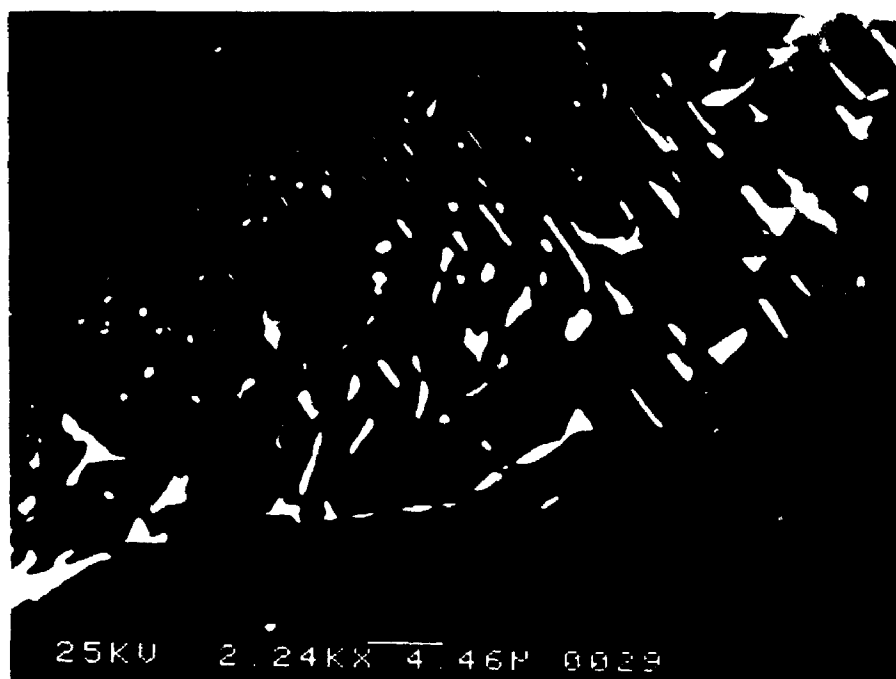
Plate 2b.   Sample r84-17553 from stope 4778Z pillar
            Close-up of galena inclusions in pyrite
            apparently showing exsolution textures.
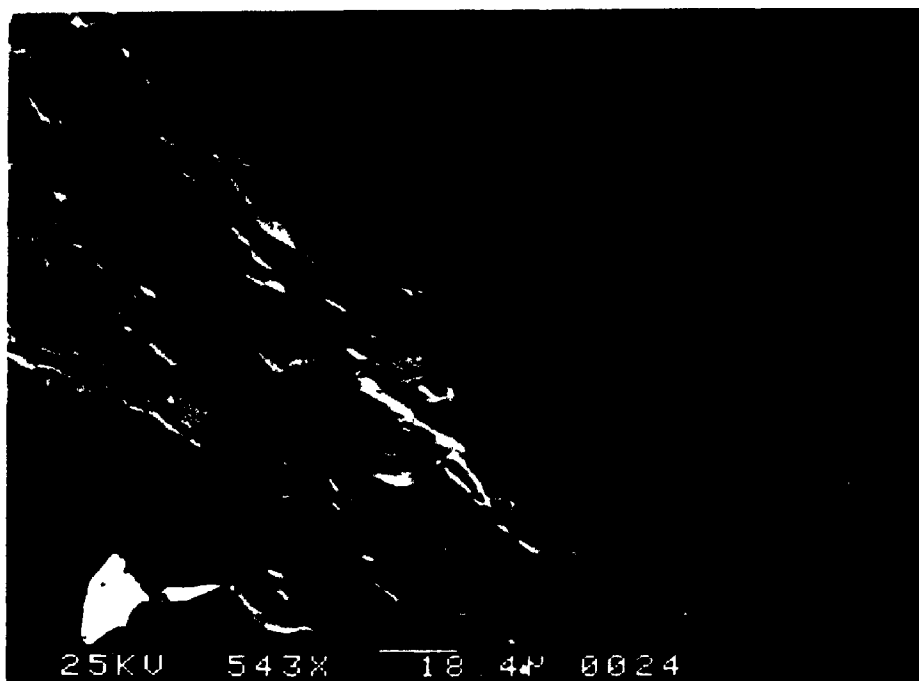
Plate 3a   Sample R84-17552 from stope 5193M

Electron backscatter image of pyrite,

sphalerite and chalcopyrite as shown on

plate 3b.
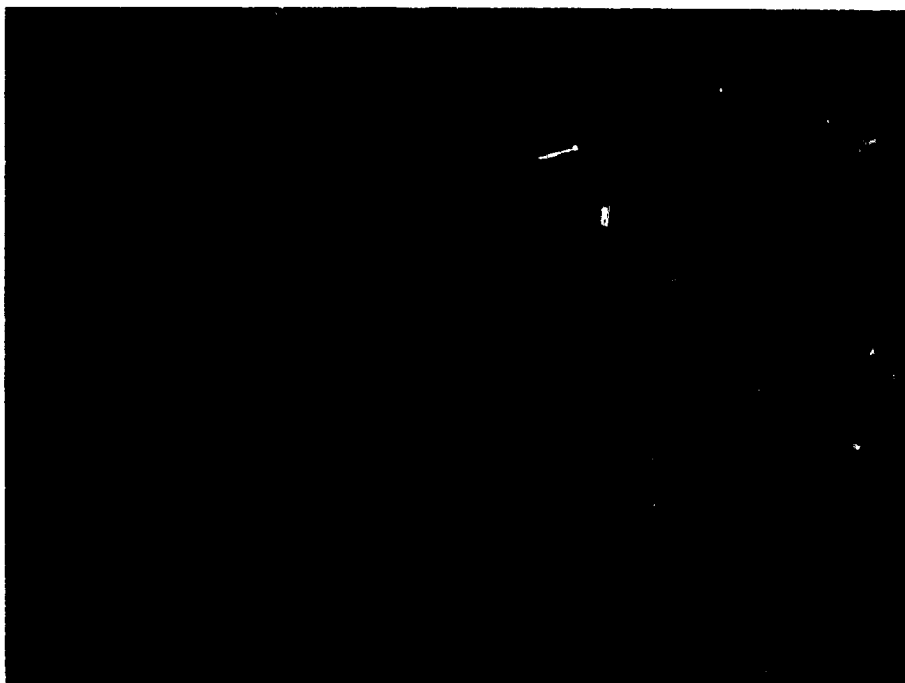
Plate 3b. Sample R84-17552 from stope 5193M

X-ray dot map on gold Lα peak showing

a concentration of gold within the sphalerite.

This concentration of gold is not confirmed

by the electron microprobe.
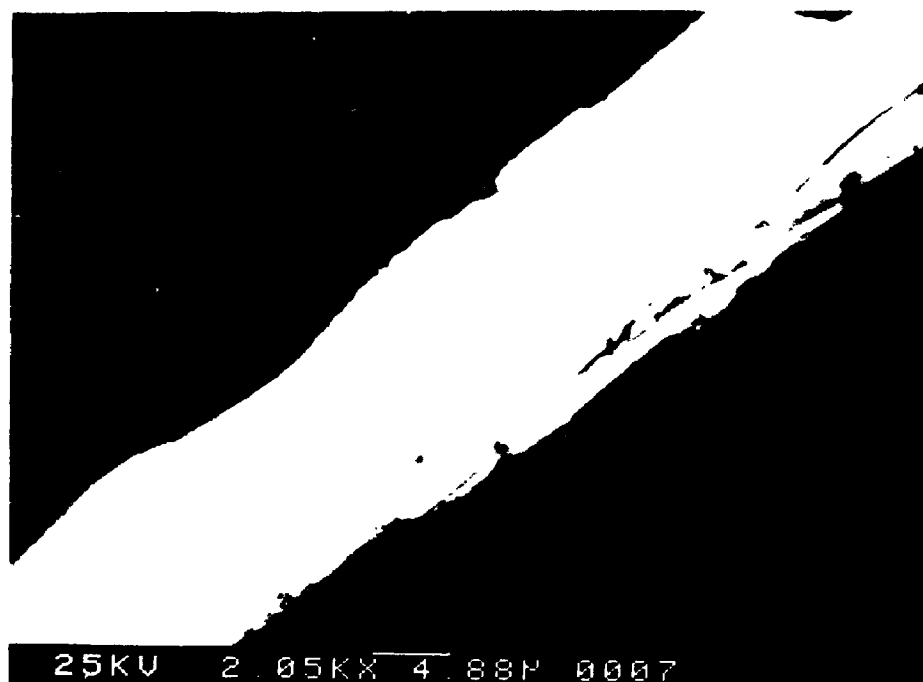
Plate 4a. Sample R84-7047, sulphide flotation concen-
trate of Con Mill tailings discharge.
Electron backscatter image of an accicular
grain of cosalite ($Pb_2 Bi_2 S_5$) as shown on
plate 4b.

Plate 4b.   Same sample as 4a.

X-ray dot map of gold Lα peak showing the distribution of gold within cosalite.
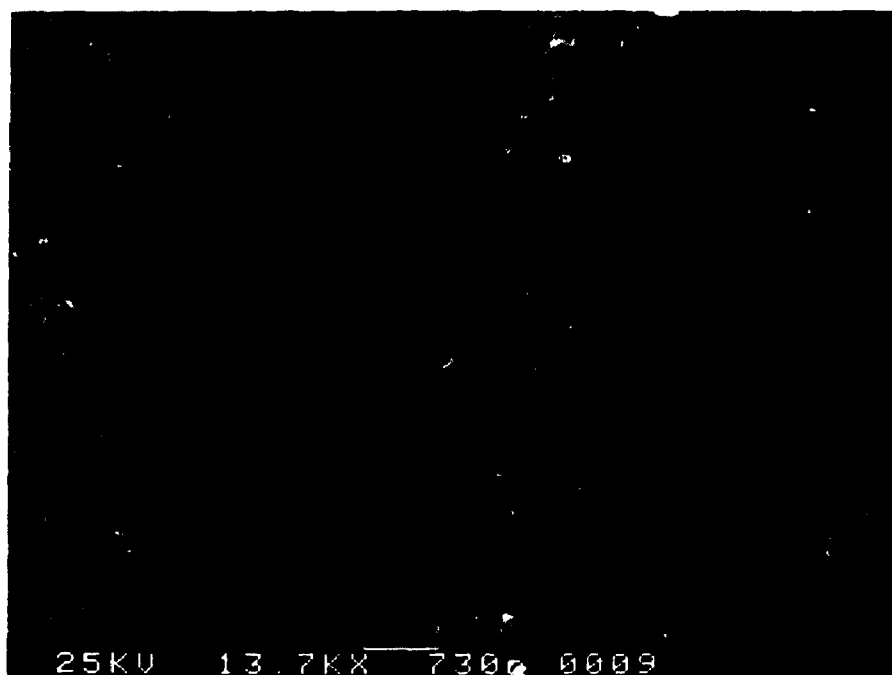
Plate 4c. Close-up of the same sample as 4a and 4b.
Close-up of a cosalite grain showing no
obvious grains of gold.

Plate 4d. Same sample as 4c.

X-ray dot map of gold Lα peak showing the
distribution of gold within calite.

APPENDIX 3

GEOCHEMICAL SAMPLING AND TREATMENT

The following analytical results for the Upper and Lower Kam Group basalts is drawn from Cunningham (1984). The distribution of individual elements is described below. The sample population is subdivided into a Lower Kam Group (n=42), representing samples collected from the Chan, and Crestaurum Formations, and an Upper Kam Group (n=30), representing samples collected from the Yellowknife Bay Formation. Samples collected from the Townsite Formation have been excluded as these rocks are essentially not present in the hanging wall or footwall of the Campbell, or Con shear zones where the majority of the schist and ore samples have been collected. The major elements were determined by Cunningham to have a precision of >1% (1σ standard deviation), and an accuracy of between 97 to 100% of the actual value. The trace elements were less well constrained, and had precisions ranging from ±1% for Sr at concentrations >50 ppm, to ±20% for Nb. The accuracy of these results is not reported.

UNIVARIATE STATISTICS

The geochemical data is examined by univariate statistical procedures, including calculations of the mean, mode, standard deviation, and plotted on histograms and probability plots in

order to characterize the data sets. The pertinent equations are as follows;

1. $x = 1/n \ \Sigma \ x_j$ sample mean

2. $s = ((1/(n-1)) \ \Sigma(x_j-x)^2)^{-2}$ standard deviation

Some of the data appeared to have log-normal distributions. These were transformed prior to statistical treatment.

Multiple populations identified on the probability plots are initially estimated manually by identifying inflection points, and by avoiding both selecting populations comprising less than 5% of the total population, while at the same time trying to limit the total number of populations involved. The former criterion is chosen because a sample set of less than 5% of the total data set (n=150 maximum) represents fewer than 8 samples, and may not be statistically valid. The latter criterion is chosen to provide for the simplest explanation or subdivision of the data set. It is recognized that this may introduce errors, and this will be considered in the discussion.

In general, there are 30 samples considered from the Lower Kam Group.

Multivariate analysis examines the correlation between variables within a sample population, or a data set, and the correlation between populations within a data set, and the correlations between data sets.   There are many ways to accomplish this type of analysis, each with restrictions on the type of data or the interpretations that can be made. One of the simplest methods of multivariate analysis is the correlation function, and a principle component analysis (PCA). These methods are well described in many elementary statistic texts.

There are three types of correlations that could be applied to these data sets, however the Pearson product moment correlation on standardized arithmetic distributions was chosen because of the number of samples involved (>30). Initially Cunningham (1983) subdivided the data empirically, based upon field observation, locations, and macroscopic characteristics.

The geochemical data has been subdivided into data sets on the basis of these observations, providing three groups; 1) basalt, 2) schist, and 3) quartz vein. Each group is then examined by itself to identify subsets, trends, and correlations, then as much as possible, correlations between each group are examined. This analysis will rely on commonly

accepted statistical approaches, but because of the nature of statistics, some errors will occur. Confidence levels will be stated where applicable in an attempt to quantify the potential errors in each analysis.

The data is standardized by conventional methods. The mean of the population is subtracted from the raw data, or logarithmic transforms of the data. This value is divided by the standard deviation of the population, providing a standardized data set with a mean of 0 and a standard deviation of 1. The Pearson correlations are determined using COR30, COR20, or COR10, PC-based software programs written in FORTRAN by the author from subprograms listed by Davis (1985), and compiled using MICROSOFT's fortran compiler, linked to an xx87 library.

A principle component analysis is made of the data sets in an attempt to quantify interrelated correlations. New variables (components) are determined from the existing variables, that correlate such that component one is aligned to describe the maximum variance in the population, component two is orthogonal to component one and describes the maximum remaining variance, and so on. This type of analysis can be imagined as a type of multidimensional scattergram with the principle components representing the major orthogonal axis of that plot.

Correlations

Thirty samples from the lower Kam group, presented by Cunningham (1983) reveal correlations consistent with a poorly differentiated basaltic sequence.

Principle component analysis

Seventeen elements are used in this analysis, with the logarithmically distributed elements transformed prior to inclusion in the data set. The variables are then standardized to a mean of 0 and a standard deviation of 1. Thirteen components account for 98% of the total variation in this data set, with the first 6 components accounting for over 76% of the total variation. The results are included, restricted to the components accounting for the greatest variance.

Principle Component 1 accounts for $\approx 25\%$ of the sample variance, and is summarized below:

POSITIVE	NEGATIVE
MgO	TiO_2
	Zr
	Y

This represents a trend of MgO enrichment, and TiO_2, Zr, and Y depletion.

Principle Component 2 accounts for ≈14% of the sample variance, and is summarized below:

<u>POSITIVE</u>	<u>NEGATIVE</u>
Ba	CaO
Nb	

This represents a trend of Ba and Nb enrichment, with a concomitant CaO depletion.

Principle Component 3 accounts for ≈13% of the sample variance, and is summarized below:

<u>POSITIVE</u>	<u>NEGATIVE</u>
Fe_2O_3	SiO_2
MnO	Al_2O_3
S	Nb

This represents a trend of Fe_2O_3, MnO, and S enrichment, with concomitant SiO_2, Al_2O_3, and Nb depletion.

Principle Component 4 accounts for ≈9% of the sample variance, and is summarized below:

<u>POSITIVE</u>	<u>NEGATIVE</u>
CaO	MgO
Ba	
Rb	

This represents a trend of CaO, Ba, and Rb enrichment with a concomitant depletion of MgO.

Principle Component 5 accounts for ≈8% of the sample variance, and is summarized below:

POSITIVE	NEGATIVE
S	MnO
Sr

This represents a trend of S and Sr enrichment and MnO depletion.

Principle Component 6 accounts for ≈8% of the sample variance, and is summarized below:

POSITIVE	NEGATIVE
Al_2O_3	SiO_2
	P_2O_5

This represents a trend of Al_2O_3 enrichment and depletion of SiO_2 and P_2O_5.

UPPER KAM GROUP

Correlations

Forty two samples collected from the upper Kam group by Cunningham (1983) reveals a more complex pattern of correlations, consistent with the univariate analysis.

Principle component analysis

Seventeen elements are used in this analysis, with the logarithmically distributed elements transformed prior to inclusion in the data set. The variables are then

standardized to a mean of 0 and a standard deviation of 1. 301

Twelve components account for nearly 98% of the total variation in this data set, with the first 6 components accounting for over 80% of the total variation.

Principle Component 1 accounts for $\approx 30\%$ of the sample variance, and is summarized below:

POSITIVE	NEGATIVE
Fe_2O_3
TiO_2
P_2O_5
Zr
Y

This represents a trend of Fe_2O_3, TiO_2, P_2O_5, Zr, and Y enrichment with no significant depletions.

Principle Component 2 accounts for $\approx 16\%$ of the sample variance, and is summarized below:

POSITIVE	NEGATIVE
Al_2O_3	Na_2O
K_2O
Ba
Rb

This represents a trend of Al_2O_3, K_2O, Ba, and Rb enrichment, with a concomitant Na_2O depletion.

Principle Component 3 accounts for $\approx 13\%$ of the sample variance, and is summarized below:

POSITIVE	NEGATIVE
MgO	CaO
K_2O	Sr
Rb	

This represents a trend of MgO, K_2O, and Rb enrichment, and a concomitant CaO, and Sr depletion.

Principle Component 4 accounts for ≈8% of the sample variance, and is summarized below:

POSITIVE	NEGATIVE
SiO_2	
CaO	
S	

This represents a trend of SiO_2, CaO, S enrichment with no concomitant depletions.

Principle Component 5 accounts for ≈7% of the sample variance, and is summarized below:

POSITIVE	NEGATIVE
MgO	SiO_2
	Na_2O
	K_2O

This represents a trend of MgO enrichment and SiO_2, Na_2O, and K_2O depletion.

Principle Component 6 accounts for ≈6% of the sample variance, and is summarized below:

POSITIVE   NEGATIVE
S
Nb

This represents a trend of S and Nb enrichment with no corresponding depletions

5.4 SCHIST SAMPLES

All of the economically exploitable gold mineralization within the Nerco Con and Giant Yellowknife Mines is hosted within schists derived from rocks of the Upper Kam Group. The schists form the immediate host rocks to these deposits. Those in immediate contact with, and commonly forming a significant proportion of the ore bodies, are dominated by a light-coloured, tan to buff sericite-rich schist, whereas the schists more removed from mineralization are dark to light-green chlorite-rich varieties. Both types of schist are arbitrary end-members of a continuous series of schists derived from metasomatically and tectonically altered Kam Group basalts.

Ninety three samples were collected and submitted to Xray Assay Laboratories for standard whole rock analysis, and are reported in this appendix. Fourteen duplicate samples were submitted to check for laboratory precision. The mean differences between duplicate samples ranged between 0.42 and 29.16% for the major exides, and 5.13 to 91.27% for the trace

elements. The trace element errors are largely due to a large number of samples at or near detection limits.

UNIVARIATE STATISTICS

The schist data is subject to a univariate statistical analysis similar to that applied to the host basalts (above).

MULTIVARIATE ANALYSIS

Multivariate statistics are determined on a data set prepared in the same manner as described in the preceding section for the host basalts.

Correlations

Samples collected by the author were annotated as to location, and collected over a period of 3 years as mine workings or diamond drill programs permitted. In total 93 samples are selected for this analysis.

Principle component analysis

Fifteen elements are used in this analysis, with the logarithmically distributed elements transformed prior to inclusion in the data set. The variables are then standardized to a mean of 0 and a standard deviation of 1. Twelve components account for nearly 98% of the total

variation in this data set, with the first 6 components accounting for over 80% of the total variation.

Principle Component 1 accounts for ≈23% of the sample variance, and is summarized below:

POSITIVE	NEGATIVE
K_2O	Al_2O_3
S	Fe_2O_3
As	Na_2O
Zn	
Rb	
Ba	

This represents a trend of K_2O, S, As, Zn, Rb, and Ba enrichment with significant corresponding depletions in Al_2O_3, Fe_2O_3, and Na_2O.

Principle Component 2 accounts for ≈17% of the sample variance, and is summarized below:

POSITIVE	NEGATIVE
TiO_2	SiO_2
As	K_2O
Zn	Na_2O
	Rb
	Sr
	Ba

This represents a trend of TiO_2, As, and Zn enrichment, with concomitant SiO_2, K_2O, Na_2O, Rb, Sr, and Ba depletions.

Principle Component 3 accounts for ≈15% of the sample

POSITIVE	NEGATIVE
SiO_2	MgO
Al_2O_3	CaO
Zn	Sr

This represents a trend of SiO_2, Al_2O_3, and Zn enrichments, and

a

concomitant MgO, CaO, and Sr depletion.

Principle Component 4 accounts for ≈11% of the sample

variance, and is summarized below:

POSITIVE	NEGATIVE
Fe_2O_3	MgO
CaO	As
V	Ba
Zn	

This represents a trend of Fe_2O_3, CaO, V and Zn enrichment with

concomitant depletions of MgO, As, and Ba.

Principle Component 5 accounts for ≈9% of the sample variance,

and is summarized below:

POSITIVE	NEGATIVE
Al_2O_3	SiO_2
Fe_2O_3	
MgO	
K_2O	
Rb	
Ba	

This represents a trend of Al_2O_3, Fe_2O_3, MgO, K_2O, Rb, and Ba

Principle Component 6 accounts for ≈6% of the sample variance, and is summarized below:

<u>POSITIVE</u>   <u>NEGATIVE</u>
MgO TiO_2
V Na_2O
                S
                Sr

This represents a trend of MgO and V enrichment with a corresponding depletion of TiO_2, Na_2O, S, and Sr.

5.5 QUARTZ

The mineralization that forms the orebodies exploited at the Nerco Con and Giant Yellowknife Mines are dominated by quartz veining and silicification, as well as by sericitization, sulfidation, and carbonatization. The quartz-rich samples were not analyzed in the same manner as the basalt and schist samples. Gold was determined by atomic absorption techniques on a fire assay preconcentration of a ½ assay ton aliquot, and the remaining elements were determined by conventional atomic absorbtion techniques. A suite of elements had been selected on the basis of previous work (Webb, 1986; Head, 1986, Meyers, 1974) as showing gross variability within the sample populations as well as revealing some correlation (either

MULTIVARIATE ANALYSIS

Data for five hundred samples is prepared in the same manner as described for the multivariate analysis of the host basalts.   These are then analyzed by COR10 for Pearson correlations, and by PCA10 to extract principle components.

Correlations

Five hundred samples of quartz were selected for correlation analysis, and all elements were found to correlate positively with each other, at the 95% confidence level.

Principle component analysis

Five hundred samples, analyzed for 7 elements each are used in this analysis.   All of the elements are logarithmically distributed and have been transformed to an arithmetic distribution.   The variables are then standardized to a mean of 0 and a standard deviation of 1.

Principle Component 1 accounts for ≈40% of the sample variance, and is summarized below:

POSITIVE	NEGATIVE
Au	
Ag	
Cu	

Pb
Zn
As
Sb

This represents a trend toward trace metal enrichment without significant corresponding depletions in the elements analysed.

Principle Component 2 accounts for ≈17% of the sample variance, and is summarized below:

POSITIVE	NEGATIVE
Cu	Au
Pb	As
Zn	Sb

This represents a trend of base metal enrichment concommittant with Au, As, and Sb depletions.

Principle Component 3 accounts for ≈14% of the sample variance, and is summarized below:

POSITIVE	NEGATIVE
Pb	Ag
Sb	Cu
	As

This represents a trend of Pb and Sb enrichments, and a concomitant Ag, Cu, and As depletion.

Principle Component 4 accounts for ≈11% of the sample variance, and is summarized below:

POSITIVE	NEGATIVE
Ag	Cu

This represents a trend of Ag and Pb enrichment with concomitant depletions of Cu and Sb.

Principle Component 5 accounts for ≈8% of the sample variance, and is summarized below:

POSITIVE	NEGATIVE
Cu	Zn
Pb	As
Sb	

This represents a trend of Cu, Pb and Sb enrichment and Zn and As depletion.

Principle Component 6 accounts for ≈6% of the sample variance, and is summarized below:

POSITIVE	NEGATIVE
Cu	Ag
Pb	Zn
As	Sb

This represents a trend of Cu, Pb, and As enrichment with a corresponding depletion of Ag, Zn, and Sb.

Principle Component 7 accounts for the remaining ~4% of the sample variance, and is summarized below:

POSITIVE	NEGATIVE
As	Au
Sb	Zn

This represents a trend of As, and Sb enrichment with a
corresponding depletion of Au and Zn.

DISCUSSION

The Kam Group basalts display multiple trends in both of the divisions (Lower and Upper groups) examined here. This was recognized by Cunningham (1984) and Goodwin (1984), and ascribed to differentiation, partial fusion, or assimilation processes. Each data set is examined, and the various trends that are recognized are described, and plausible mechanisms are proposed. It is not the intent of these chapter to propose a genetic model for the Yellowknife Greenstone Belt, rather it is to discuss the various geochemical trends identified from Cunningham's (1984) data set, and compare these results to those of other workers.

Lower Kam Group

SUMMARY

Trend	Enrichments	Depletions
1	MgO, Fe_2O_3, Na_2O, P_2O_5 K_2O	
2	K_2O, Ba, Nb, Na_2O, Rb	CaO
3	SiO_2, Al_2O_3, Nb, P_2O_5 Fe_2O_3, MnO	
4	CaO, Ba, Rb	Fe_2O_3, MgO
5	Sr, Rb, Ba, S	MnO, Na_2O, Al_2O_3
6	Al_2O_3, Sr	SiO_2, P_2O_5, Rb

Upper Kam Group

SUMMARY

Trend	Enrichments	Depletions

1	Fe_2O_3, TiO_2, P_2O_5, Zr CaO Y, Mn, Na_2O	
2	Al_2O_3, K_2O, Ba, Rb, Sr, Fe_2O_3, S, P_2O_5	Na_2O, Nb
3	MgO, K_2O, Rb, SiO_2 Mno	CaO, Sr, Al_2O_3
4	SiO_2, Fe_2O_3, CaO, S, MgO	K_2O, Na_2O, Ba, Rb
5	MgO	SiO_2, Na_2O, K_2O
6	S, Nb, Mno, Zr	Al_2O_3

Quartz veins

SUMMARY

Trend	Enrichments	Depletions
1	Au, Ag, As, Sb	
2	Zn, Cu	Au, Sb
3	Pb, Sb	Ag
4	Ag, Pb	Cu, Sb
5	Cu	Zn, As
6	As	Sb, Ag, Zn
7	As	Au

Schists

SUMMARY

Trend	Enrichments	Depletions
1	K_2O, S, As, Zn, Rb, Ba	Al_2O_3, Fe_2O_3, Na_2O
2	TiO_2, As, Zn	SiO_2, K_2O, Na_2O, Rb, Sr
3	SiO_2, Al_2O_3, Zn	MgO, CaO, Sr
4	Fe_2O_3, CaO, V, Zn	MgO, As, Ba
5	Al_2O_3, Fe_2O_3, MgO, K_2O Rb, Ba	SiO_2
6	MgO, V	TiO_2, Na_2O, S, Sr

Tag	X10313	X1170	X10315	X10319	X10312	X1187	64003	66050	66049	65027
SiO2	44.9	50.3	42.6	45.9	42.5	45.3	46.9	45.2	50.7	44.3
TiO2	1.2	0.7	1.3	1.4	1.4	0.6	1.2	1.3	1.2	1.3
Al2O3	11.2	12.5	12.5	13.9	15.6	12.6	10.9	16.2	15.8	11.4
Fe2O3	12.7	10.1	12.7	13.7	14.8	9.8	8.0	9.4	7.3	9.4
MnO	0.2	0.1	0.2	0.2	0.2	0.2	.	.	.	.
MgO	4.77	5.55	6	6.54	7.8	6.21	6.5	6.4	5.3	7.9
CaO	12.2	6.85	11.2	6.71	8.55	11.3	9.8	7.3	7	10.4
K2O	0.10	1.92	0.05	1.17	0.03	0.36	1.40	0.09	0.50	0.60
Na2O	1.14	0.34	1.89	0.33	1.00	1.93	0.40	2.90	2.70	0.10
P2O5	0.09	0.11	0.10	0.12	0.13	0.21	.	.	.	.
Cr2O3	0.005	0.005	0.010	0.005	0.010	0.005	.	.	.	.
LOI	11.9	11.4	11.9	3.4	8.3	11.4	.	.	.	.
TOTAL	100.395	100.325	100.4	99.325	100.34	99.905	85.1	88.79	90.5	85.4
S	337	603	2	961	58	892	15000	8900	3800	2200
Au	.	.	.	.	.	.	130	7	14	2
As	24	222	134	505	47	19	0	10	10	2000
V	387	308	360	417	.	314	2300	.	.	55
Cr	17	17	34	17	34	17	.	.	.	.
Co	22	36	24	30	.	37	.	.	.	.
Ni	60	72	93	71	.	65	.	.	.	.
Cu	67	32	84	136	72	58	.	.	.	.
Zn	119	191	113	201	93	72	112	90	88	100
Pb	2	2	2	4	4	2	.	.	.	.
Rb	5	80	10	30	5	10	35	10	20	20
Sr	130	120	100	30	100	110	50	140	110	40
Y	20	20	10	30	20	10	.	.	.	.
Zr	40	50	40	70	90	60	.	.	.	.
Nb	10	10	10	20	30	20	.	.	.	.
Ba	50	400	30	160	40	230	220	230	215	230
Ga	16	18	13	23	17	13	.	.	.	.
Lat	-21715	-21850	-21865	-21960	-22050	-22100	.	.	.	.
Elev	2702	2853	3066	3067	2702	3360	.	.	.	.
O18	10.92		8.18	10.80	7.90					
C13	-4.22		-3.80	-3.01	-4.00					
O18	11.62	9.59	9.46	14.63	8.76	9.57				
C13	-4.36	-4.48	-3.74	-3.58	-3.92	-3.96				

Tag	66026	65029	66025	65031	66014	65040	65145	65014	65144	65043
SiO2	40.7	45.9	41.0	42.7	43.0	49.6	46.5	45.4	44.3	47.7
TiO2	1.2	1.1	1.3	1.3	1.2	1.2	1.6	1.2	1.5	1.3
Al2O3	7.8	13.1	6.1	11.8	13.4	10.1	11.4	14.5	10.9	11.8
Fe2O3	7.0	9.3	7.2	10.1	9.4	7.4	9.8	10.3	9.2	7.9
MnO	.	.	.	.	.	.	.	.	.	.
MgO	13.1	6.2	15.1	8.3	10.3	5.4	6.7	7.4	7	6.1
CaO	13.1	8.4	14.4	9.6	8.2	9.9	7.5	5.7	9.4	11.4
K2O	1.00	0.90	2.00	0.20	0.30	1.40	0.90	1.10	1.20	0.80
Na2O	0.40	0.30	0.10	0.60	0.70	0.30	0.70	0.10	0.60	0.40
P2O5	.	.	.	.	.	.	.	.	.	.
Cr2O3	.	.	.	.	.	.	.	.	.	.
LOI	.	.	.	.	.	.	.	.	.	.
TOTAL	84.3	85.2	87.2	84.6	86.5	85.3	85.1	85.7	84.1	87.4
S	5700	400	10300	1600	700	11500	14300	18300	16100	400
Au	10	1	12		6	5	530	110	1440	
As	10	6000	10	5000	750	1000	3000	0	5000	8000
V	.	130	.	10	.	2300	.	1570	.	2650
Cr	.	.	.	.	.	.	.	.	.	.
Co	.	.	.	.	.	.	.	.	.	.
Ni	.	.	.	.	.	.	.	.	.	.
Cu	.	.	.	.	.	.	.	.	.	.
Zn	50	170	45	82	60	145	88	150	75	102
Pb	.	.	.	.	.	.	.	.	.	.
Rb	30	25	50	10	10	40	20	20	25	30
Sr	630	50	700	50	70	40	30	15	40	60
Y	.	.	.	.	.	.	.	.	.	.
Zr	.	.	.	.	.	.	.	.	.	.
Nb	.	.	.	.	.	.	.	.	.	.
Ba	610	185	500	170	150	190	255	255	255	210
Ga	.	.	.	.	.	.	.	.	.	.
Lat	.	.	.	.	.	.	.	.	.	.
Elev	.	.	.	.	.	.	.	.	.	.
O18										
C13										
O18										
C13										

Tag	65143	65025	65137	65024	65133	64025	65132	65021	65130	64012
SiO2	45.5	47.8	44.5	48.2	44.9	43.0	41.6	44.6	46.0	40.6
TiO2	1.4	1.6	1.6	1.3	1.0	1.1	2.0	1.2	1.1	1.4
Al2O3	11.8	10.8	9.9	13.0	15.0	13.8	12.1	14.3	11.9	11.7
Fe2O3	8.8	8.7	8.8	8.5	9.0	9.8	10.1	8.1	7.8	9.7
MnO	.	.	.	.	.	.	.	.	.	.
MgO	6.1	5.5	6.6	4.1	11.3	10.5	10.5	7.6	7.7	8.7
CaO	9.1	9.6	11.6	6.9	6.4	7.9	8.4	8.4	10.4	11.2
K2O	1.00	0.20	0.60	1.90	0.60	0.80	0.80	0.90	1.10	1.10
Na2O	0.90	1.50	0.70	0.30	0.40	0.10	0.20	0.80	0.60	0.10
P2O5	.	.	.	.	.	.	.	.	.	.
Cr2O3	.	.	.	.	.	.	.	.	.	.
LOI	.	.	.	.	.	.	.	.	.	.
TOTAL	84.6	85.7	84.3	84.2	88.6	87	85.7	85.9	86.55	84.5
S	13700	3100	10400	21000	900	1300	2200	5200	3000	700
Au	850	1	1160	420	1			7		1
As	5000	3000	5000	0	0	7000	7000	1000	6000	3000
V	.	225	.	1590	25	45	50	450	50	65
Cr	.	.	.	.	.	.	.	.	.	.
Co	.	.	.	.	.	.	.	.	.	.
Ni	.	.	.	.	.	.	.	.	.	.
Cu	.	.	.	.	.	.	.	.	.	.
Zn	82	105	88	135	68	75	77	165	55	125
Pb	.	.	.	.	.	.	.	.	.	.
Rb	30	10	15	45	20	30	15	35	35	30
Sr	55	90	55	40	30	20	25	65	75	25
Y	.	.	.	.	.	.	.	.	.	.
Zr	.	.	.	.	.	.	.	.	.	.
Nb	.	.	.	.	.	.	.	.	.	.
Ba	215	200	205	290	230	260	275	205	315	245
Ga	.	.	.	.	.	.	.	.	.	.
Lat	.	.	.	.		.	.	.	.	.
Elev	.	.	.	.	.	.	.	.	.	.
O18										
C13										
O18										
C13										

Tag	65129	64010	65125	65023	65124	66095	65123	65026	65122	65030
SiO2	46.8	40.9	48.0	47.6	51.0	48.5	45.3	46.5	44.3	46.1
TiO2	1.0	1.5	1.5	1.2	1.5	1.8	1.5	1.4	1.9	1.1
Al2O3	13.5	12.3	13.8	10.9	14.3	12.1	11.7	11.9	9.4	12.8
Fe2O3	8.6	10.2	8.2	6.8	7.9	8.7	9.2	9.2	9.6	10.0
MnO	.	.	.	.	.	.	.	.	.	.
MgO	8.9	6.7	5.9	5.3	4.9	4.6	8.2	5.2	7.5	7.7
CaO	7.4	10.4	7.1	11.5	4.9	7.4	9.7	9.1	12.2	7.4
K2O	0.50	1.30	2.60	0.90	2.30	0.60	0.80	0.40	0.03	0.60
Na2O	1.40	0.10	0.10	0.80	0.70	2.10	0.90	1.50	1.10	0.20
P2O5	.	.	.	.	.	.	.	.	.	.
Cr2O3	.	.	.	.	.	.	.	.	.	.
LOI	.	.	.	.	.	.	.	.	.	.
TOTAL	88.1	83.4	87.2	85	87.5	85.8	87.3	85.2	86.03	85.9
S	1400	5500	1000	8700	3300	2600	1300	2800	1500	1400
Au		11		21	7	12		2		1
As	5000	0	4000	5000	6000	30	3000	5000	1000	0
V	50	2000	70	3200	70	.	15	10	10	70
Cr	.	.	.	.	.	.	.	.	.	.
Co	.	.	.	.	.	.	.	.	.	.
Ni	.	.	.	.	.	.	.	.	.	.
Cu	.	.	.	.	.	.	.	.	.	.
Zn	65	150	75	160	85	60	85	90	85	160
Pb	.	.	.	.	.	.	.	.	.	.
Rb	15	30	75	25	80	30	30	20	10	20
Sr	80	20	15	80	30	110	50	65	60	35
Y	.	.	.	.	.	.	.	.	.	.
Zr	.	.	.	.	.	.	.	.	.	.
Nb	.	.	.	.	.	.	.	.	.	.
Ba	210	285	480	170	635	340	310	250	170	185
Ga	.	.	.	.	.	.	.	.	.	.
Lat	.	.	.	.	.	.	.	.	.	.
Elev	.	.	.	.	.	.	.	.	.	.
O18										
C13										
O18										
C13										

Tag	65121	65041	65119	65044	65118	65045	65117	64024	65079	64009
SiO2	44.2	44.2	45.2	45.8	42.3	50.2	44.3	43.5	45.3	49.4
TiO2	1.1	1.6	1.2	1.3	1.3	1.0	1.2	1.3	1.2	1.5
Al2O3	13.1	9.8	10.5	13.7	11.9	12.9	13.5	12.1	11.2	11.1
Fe2O3	9.1	8.4	8.7	8.7	10.1	6.8	9.6	10.5	8.4	9.1
MnO	.	.	.	.	.	.	.	.	.	.
MgO	8	5.7	6.6	6.6	6.9	4.7	7.9	8.7	7.8	6.1
CaO	8.7	12.1	11.4	9.7	10.4	9.4	8	8.2	10.7	8.2
K2O	0.80	0.90	1.10	1.00	0.60	1.90	0.20	0.50	0.70	1.00
Na2O	0.70	0.60	0.10	0.40	0.90	0.50	1.60	1.20	0.40	0.10
P2O5	.	.		.	.	.	.	.	.	.
Cr2O3	.	.	.	.	.	.	.	.	.	.
LOI	.	.	.	.	.	.	.	.	.	.
TOTAL	85.7	83.3	84.8	87.2	84.4	87.4	86.3	86	85.7	86.5
S	1500	3400	7000	1900	2900	21000	2200	700	2300	2000
Au		2	6	1		335			1	2
As	3000	0	1000	4000	6000	0	6000	1000	0	1000
V	10	115	1000	125	15	1350	10	10	210	240
Cr	.	.	.	.	.	.	.	.	.	.
Co	.	.	.	.	.	.	.	.	.	.
Ni	.	.	.	.	.	.	.	.	.	.
Cu	.	.	.	.	.	.	.	.	.	.
Zn	80	140	90	145	95	150	70	81	80	115
Pb	.	.	.	.	.	.	.	.	.	.
Rb	25	25	30	30	15	40	10	30	20	30
Sr	50	50	35	35	50	40	80	45	35	20
Y	.	.	.	.	.	.	.	.	.	.
Zr	.	.	.	.	.	.	.	.	.	.
Nb	.	.	.	.	.	.	.	.	.	.
Ba	260	190	260	230	260	235	230	195	190	250
Ga	.	.	.	.	.	.	.	.	.	.
Lat	.	.	.	.	.	.	.	.	.	.
Elev	.	.	.	.	.	.	.	.	.	.
O18										
C13										
O18										
C13										

Tag	65078	66094	65077	65039	65075	64026	65074	64011	65070	65028
SiO_2	47.5	40.9	49.5	48.8	44.5	41.7	59.8	44.8	48.9	52.5
TiO_2	1.1	1.7	1.1	1.3	1.4	1.3	1.2	1.2	1.0	1.2
Al_2O_3	10.2	10.6	9.7	10.4	12.1	10.9	13.3	8.6	12.9	11.7
Fe_2O_3	7.2	11.7	9.2	7.4	9.8	10.3	6.8	8.0	1.7	9.1
MnO	.	.	.	.	.	.	.	.	.	.
MgO	6	6.1	5.6	5	7	7.4	3.4	6.9	6.7	6
CaO	10.9	10.3	10.6	9.9	9.2	11.1	3.3	13.6	8.6	7.4
K_2O	1.80	0.10	1.60	1.60	0.60	0.40	1.30	1.00	0.90	0.60
Na_2O	0.10	0.80	0.20	0.40	0.20	0.80	0.60	0.10	0.90	0.20
P_2O_5	.	.	.	.	.	.	.	.	.	.
Cr_2O_3	.	.	.	.	.	.	.	.	.	.
LOI	.	.	.	.	.	.	.	.	.	.
TOTAL	84.8	82.2	87.5	84.8	84.8	83.9	89.7	84.2	81.6	88.7
S	23100	1600	23100	16200	10300	700	23100	13100	4300	2900
Au	20	8	38	110	1		22	51		
As	0	15	0	0	3000	5000	0	0	4000	8000
V	9500	.	9000	6000	125	30	1500	2900	75	10
Cr	.	.	.	.	.	.	.	.	.	.
Co	.	.	.	.	.	.	.	.	.	.
Ni	.	.	.	.	.	.	.	.	.	.
Cu	.	.	.	.	.	.	.	.	.	.
Zn	525	80	625	160	150	75	280	135	70	80
Pb	.	.	.	.	.	.	.	.	.	.
Rb	40	10	35	30	25	20	40	25	35	20
Sr	25	80	35	35	30	35	50	40	50	70
Y	.	.	.	.	.	.	.	.	.	.
Zr	.	.	.	.	.	.	.	.	.	.
Nb	.	.	.	.	.	.	.	.	.	.
Ba	180	185	180	205	180	185	260	175	340	210
Ga	.	.	.	.	.	.	.	.	.	.
Lat	.	.	.	.	.	.	.	.	.	.
Elev	.	.	.	.	.	.	.	.	.	.
O18										
C13										
O18										
C13										

Tag	65047	65015	65042	64002	65046	X10699	X10710	X1175	X10345	X1195
SiO2	51.7	48.2	42.4	48.0	47.1	48.0	73.7	55.3	43.5	47.4
TiO2	1.0	1.2	1.1	1.1	1.2	0.8	0.5	0.9	1.0	0.8
Al2O3	7.2	14.3	8.1	12.1	12.9	15.1	11.0	10.3	13.5	12.7
Fe2O3	6.1	9.4	7.8	8.3	8.4	13.0	4.7	8.5	8.8	10.1
MnO	.	.	.	.	.	0.2	0.1	0.1	0.2	0.2
MgO	6.5	7.1	4.1	6.6	6.5	8.14	1.73	3.07	7.33	5.5
CaO	14.9	5.6	16.3	8.6	10.3	9.03	2.04	10	8.52	10.3
K2O	0.50	1.20	1.40	0.08	1.00	0.18	1.59	1.27	1.26	0.45
Na2O	0.30	0.10	0.20	2.50	0.10	2.56	0.57	0.77	1.92	1.~
P2O5	.	.	.	.	.	0.07	0.09	0.08	0.10	0.09
Cr2O3	.	.	.	.	.	0.020	0.010	0.005	0.020	0.005
LOI	.	.	.	.	.	3.2	4.0	9.7	13.8	10.9
TOTAL	88.2	87.1	81.4	87.28	87.5	100.36	99.98	100.105	99.98	100.425
S	10900	7600	21000	300	4900	249	1120	127	921	0
Au	4	11	610		2	.	.	.	.	.
As	8000	0	0	9000	6000	75	48	14	68	20
V	700	2100	40	45	950	310	121	358	427	329
Cr	.	.	.	.	.	68	34	17	68	17
Co	.	.	.	.	.	52	19	14	37	39
Ni	.	.	.	.	.	131	31	34	79	63
Cu	.	.	.	.	.	123	39	65	162	79
Zn	140	160	150	86	135	53	55	48	120	66
Pb	.	.	.	.	.	2	2	2	5	5
Rb	20	30	10	10	30	20	50	50	60	20
Sr	35	10	40	85	25	150	260	150	90	110
Y	.	.	.	.	.	20	30	20	10	10
Zr	.	.	.	.	.	30	90	40	40	50
Nb	.	.	.	.	.	20	10	10	30	20
Ba	120	250	210	150	225	90	330	340	120	160
Ga	.	.	.	.	.	17	13	17	13	14
Lat	.	.	.	.	.	.	.	.	.	.
Elev	.	.	.	.	.	.	.	.	.	.
O18						11.19		7.77	16.45	8.27
C13						-1.99		-5.01	-2.62	-4.34
O18						12.21	13.17	9.06	16.63	9.91
C13						-3.13	-2.79	-4.80	-3.03	-4.13

320

Tag	X10700	X1196	X10702	X12249	X10704	X12276	X10706	X12909	X10708	X144945
SiO2	56.1	49.6	47.7	40.5	48.1	63.4	58.0	42.8	44.0	48.4
TiO2	1.0	0.7	0.8	0.8	1.5	0.6	0.8	1.3	1.1	0.6
Al2O3	19.1	12.7	15.6	10.2	13.3	15.4	13.1	13.1	11.6	13.3
Fe2O3	8.7	9.7	12.8	7.9	14.6	5.7	8.7	15.1	12.5	8.5
MnO	0.1	0.1	0.2	0.1	0.2	0.1	0.1	0.2	0.2	0.1
MgO	2.81	5.4	8.1	8.75	5.42	2.14	5.06	5.99	5.23	8.53
CaO	2.87	7.65	9.8	12.9	7.39	6.13	3.69	9.94	10	12.1
K20	2.75	1.94	0.17	3.32	0.08	0.69	1.38	0.32	0.58	1.40
Na20	2.74	0.24	2.32	2.14	2.38	4.16	1.55	0.77	0.69	2.41
P205	0.08	0.08	0.07	1.83	0.13	0.19	0.19	0.10	0.11	0.70
Cr203	0.030	0.005	0.020	0.005	0.005	0.005	0.010	0.005	0.005	0.020
LOI	4.1	12.4	2.9	6.7	7.5	1.9	7.6	10.8	14.5	3.2
TOTAL	100.28	100.545	100.48	95.115	100.515	100.305	100.2	100.385	100.525	99.24
S	328	405	0	6537	252	282	0	139	23	1484
Au	.	.	.	.	.	.	.	.	.	.
As	258	190	5	6	7	5	22	28	56	6
V	509	293	308	177	402	103	154	349	337	288
Cr	103	17	68	17	17	17	34	17	17	68
Co	161	36	49	10	41	16	12	47	20	44
Ni	147	59	140	140	39	14	64	80	63	121
Cu	38	33	110		98	23	36	142	124	38
Zn	64	145	46	91	94	52	115	84	103	22
Pb	2	2	2	9	2	2	2	2	2	2
Rb	100	80	5	110	10	20	40	20	30	40
Sr	120	80	200	4450	80	140	40	130	60	1110
Y	30	10	30	40	20	10	30	20	20	20
Zr	30	50	30	320	80	160	140	60	70	160
Nb	5	20	20	10	10	30	10	20	10	10
Ba	1050	330	80	3920	70	480	190	90	140	730
Ga	18	14	16	12	16	14	15	17	15	12
Lat	.	.	.	.	.	.	.	.	.	.
Elev	.	.	.	.	.	.	.	.	.	.
O18	10.51	9.28	11.43	6.76	9.38	8.89	12.08	8.08	11.12	
C13	-1.71	-4.21	-2.96	-4.11	-1.23	-2.88	-2.42	-5.09	-2.24	
O18	10.59	13.04	13.44	9.71	17.16	8.84	14.31	8.60	15.65	
C13	-2.02	-4.18	-3.56	-4.54	-3.31	-3.95	-2.40	-5.01	-2.63	

NERCO-Con Mine
Quartz vein samples

locn	sample number	lab	Au	Ag	Cu	Pb	Zn	As	Sb
KAM-PT	8736	C	0	0.2	65	4	31	0	0
KAM-PT	8737	C	0	0	40	2	20	0	0
KAM-PT	8738	C	65	0	18	30	40	60	0
KAM-PT	8745	C	0	0.2	2	10	42	0	0
KAM-PT	8746	C	0	0.2	0	6	33	0	0
KAM-PT	8747	C	0	0	0	0	6	0	0
KAM-PT	8752	C	0	0	15	4	36	0	0
KAM-PT	8754	C	0	0.6	115	1380	5714	15	0
KAM-PT	8757	C	0	0.2	57	58	175	10	0
KAM-PT	8758	C	0	0.4	44	38	85	10	0
KAM-PT	8759	C	10	0	1	12	30	5	0
KAM-PT	8760	C	0	0.2	44	4	377	10	0
KAM-PT	8761	C	30	0.4	446	4	28	15	0
KAM-PT	8762	C	5	0	32	6	16	0	0
KAM-PT	8766	C	5	0	11	4	29	0	0
KAM-PT	8768	C	180	0.4	13	2	16	40	0
KAM-PT	8771	C	15	0.8	12	2	26	235	0
KAM-PT	8772	C	215	0	4	2	3	795	0
KAM-PT	8773	C+	25231	5	17	150	210	2780	5
KAM-PT	8775	C	5	0	0	2	5	400	0
KAM-PT	8776	C	190	0.4	17	4	25	330	0
KAM-PT	8777	C	2400	0.4	2	0	5	1380	5
KAM-PT	8778	C	20	0.2	28	12	30	120	15
KAM-PT	8779	C	0	0	11	2	19	0	0
KAM-PT	8780	C	20	0.4	140	80	870	5	0
KAM-PT	8781	C	330	0	5	0	27	4460	0
KAM-PT	8782	C	5	0.2	14	0	35	150	0
KAM-PT	8783	C	5900	0.6	1354	10	874	30	0
KAM-PT	8786	C	30	0.4	43	0	38	1140	0
KAM-PT	8787	C	5	0	8	0	36	35	0
KAM-PT	8789	C	60	0	77	0	23	270	0
KAM-PT	8792	C	0	0.2	113	0	103	30	0
KAM-PT	8795	C	0	0	7	0	29	5	0
KAM-PT	8798	C	0	0.2	1	0	12	0	0
KAM-PT	8799	C	0	0	37	0	9	0	0
STOCK	8905	C	0	0.2	29	6	36	0	0
STOCK	8911	C	10	0.2	2	2	2	0	0
STOCK	8912	C	115	0.2	3	4	1	20	0
STOCK	8913	C	370	2.6	7	18	2	85	0
STOCK	8914	C	265	2.4	4	14	1	45	0
STOCK	8915	C	290	2	9	14	1	45	0
STOCK	8919	C	470	3	66	8	39	90	0
STOCK	8920	C	305	0.8	10	158	3	30	20
STOCK	8926	C	1500	0.8	3	0	1	630	0
STOCK	8927	C	2500	21	3	18	1	15	0
STOCK	8928	C	130	0.2	4	4	3	25	0
STOCK	8929	C	0	0.2	2	18	2	0	0
STOCK	8930	C	10000	20.6	7	22	4	125	0
STOCK	8931	C	1800	9	52	10	17	55	0

Tag	X3783	X3794	AVERAGE	Std dev
SiO2	44.3	40.8	45.96	5.92
TiO2	0.7	0.7	1.13	0.38
Al2O3	11.0	10.2	12.53	2.22
Fe2O3	9.7	8.4	10.54	2.81
MnO	0.2	0.1	0.10	0.09
MgO	9.97	9.57	6.56	1.99
CaO	11.4	11.8	9.13	2.67
K2O	2.77	4.97	0.82	0.73
Na2O	2.32	1.37	1.07	0.90
P2O5	1.03	1.36	0.13	0.29
Cr2O3	0.040	0.050	0.01	0.01
LOI	4.7	8.2	5.77	5.22
TOTAL	98.09	97.61	93.74	

S	1558	2452	3280	5388
Au	.	.	44	189
As	4	14	1375	2958
V	210	154	542	1224
Cr	137	171	23	34
Co	28	26	20	21
Ni	129	173	47	46
Cu	79	40	55	60
Zn	78	106	63	63
Pb	7	18	49	96
Rb	100	210	22	28
Sr	1060	2160	174	435
Y	20	20	25	19
Zr	210	270	43	53
Nb	10	20	11	11
Ba	1050	2880	171	414
Ga	13	12	83	113

Lat	.	.
Elev	.	.
O18	5.65	5.48
C13	-3.18	-1.16
O18	9.10	8.77
C13	-4.49	-4.31

LOWER KAM GROUP

Sample	620-10	620-20	620-30	620-40	620-50	620-60	620-70	620-50B	703-1A	703-2A
SiO2	50.07	53.44	50.39	54.37	50.21	51.04	50.13	49.75	52.12	52.45
Al2O3	13.60	15.11	13.65	13.27	14.79	14.76	15.41	14.96	13.72	14.56
Fe2O3	12.88	10.09	14.99	12.44	13.21	13.32	12.01	12.86	13.97	12.74
MgO	6.56	5.92	6.43	7.38	7.77	7.99	9.84	7.44	6.69	4.27
CaO	13.51	11.97	10.38	9.19	9.82	9.84	9.01	9.33	9.41	10.26
Na2O	2.14	2.32	1.80	1.80	2.86	1.73	1.97	4.34	2.00	3.30
K2O	0.10	0.08	0.82	0.36	0.10	0.09	0.18	0.09	0.02	0.38
TiO2	0.79	0.87	1.17	0.90	0.93	0.94	1.07	0.92	1.65	1.61
MnO	0.22	0.17	0.26	0.22	0.25	0.22	0.26	0.26	0.22	0.29
S	0.04	0.04	0.05	0.04	0.03	0.05	0.03	0.03	0.04	0.05
P2O5	0.06	0.03	0.10	0.06	0.07	0.06	0.10	0.06	0.20	0.14
TOTAL	100.05	100.04	100.04	100.03	100.04	100.04	100.01	100.04	100.04	100.05
Ba	0	0	97	0	7	0	14	5	39	13
Nb	2	1	2	1	2	0	5	1	2	0
Sr	51	39	71	63	58	57	69	58	107	94
Y	25	19	30	22	23	26	23	25	37	34
Sr	122	187	105	85	151	84	144	150	152	95
Rb	1	0	28	13	2	3	9	1	10	4

LOWER KAM GROUP

Sample	703-2C	703-3A	710-1A	710-2B	710-3B	710-5A	710-6A	710-7A	710-8A	710-9A
SiO2	52.46	48.90	52.10	52.12	52.43	52.22	52.21	56.37	54.40	54.00
Al2O3	16.33	14.49	13.70	13.56	15.44	14.06	12.16	13.30	14.39	14.49
Fe2O3	10.44	15.28	13.49	14.73	12.90	14.19	11.94	10.55	9.08	9.89
MgO	1.90	6.74	7.53	4.27	4.77	6.23	9.51	7.81	8.73	8.08
CaO	15.47	9.81	7.90	9.57	11.28	9.74	11.17	8.83	9.58	11.03
Na2O	1.69	2.59	2.49	2.80	1.61	1.72	1.57	0.80	2.55	2.07
K2O	0.08	0.24	1.39	0.40	0.23	0.19	0.40	0.86	0.30	0.26
TiO2	1.33	1.52	1.02	2.12	0.99	1.24	0.75	0.80	0.73	0.64
MnO	0.17	0.29	0.28	0.25	0.31	0.31	0.23	0.33	0.21	0.28
S	0.03	0.03	0.04	0.04	0.04	0.06	0.07	0.04	0.02	0.03
P2O5	0.14	0.14	0.09	0.17	0.05	0.10	0.05	0.04	0.04	0.84
TOTAL	100.04	100.03	100.03	100.03	100.05	100.06	100.06	99.73	100.03	101.61
Ba	5	0	140	247	28	7	32	55	10	31
Nb	1	0	3	0	0	3	2	2	2	3
Sr	88	90	77	113	58	75	53	55	57	48
Y	28	32	25	42	21	29	17	18	19	17
Sr	312	125	81	156	174	1??	159	87	118	83
Rb	1	1	44	4	2	:	13	28	7	7

LOWER KAM GROUP

Sample	710-10A	710-11A	710-12A	710-13A	803-1	803-2	803-3	803-4	803-5	803-6
SiO2	54.31	53.22	53.44	50.95	53.64	54.03	53.32	53.48	51.93	52.99
Al2O3	14.79	14.25	13.11	14.20	15.07	15.32	12.95	13.98	14.82	12.76
Fe2O3	10.01	11.73	14.43	14.06	11.57	10.95	14.70	9.64	12.27	15.04
MgO	8.12	9.15	4.64	6.20	6.53	7.98	5.49	1.98	5.01	5.63
CaO	9.22	7.81	10.05	10.41	10.53	7.10	6.65	12.81	11.24	7.29
Na2O	1.85	2.26	1.76	2.11	1.06	2.20	4.45	5.61	2.06	3.84
K2O	0.24	0.39	0.06	0.08	0.15	0.18	0.24	0.16	0.18	0.22
TiO2	1.11	0.88	1.93	1.57	1.10	1.15	1.79	1.85	1.97	1.80
MnO	0.24	0.25	0.32	0.26	0.23	0.19	0.20	0.22	0.30	0.21
S	0.05	0.03	0.03	0.04	0.05	0.03	0.05	0.05	0.03	0.05
P2O5	0.10	0.07	0.25	0.16	0.11	0.09	0.22	0.26	0.22	0.23
TOTAL	100.04	100.04	100.02	100.04	100.04	100.02	100.06	100.04	100.03	100.06
Ba	6	48	3	1	0	6	28	22	3	15
Nb	0	4	5	4	2	0	11	0	2	3
Sr	74	72	151	118	75	76	169	164	142	163
Y	24	23	52	42	25	27	52	52	42	49
Sr	171	55	103	139	131	135	385	94	87	95
Rb	7	5	0	1	0	2	3	1	0	2

LOWER KAM GROUP

Sample	003-7	003-8	003-9	015-2	015-6	015-7	015-8AB	015-9	015-10	015-11
SiO2	54.02	50.45	52.33	50.05	51.25	53.15	54.00	49.38	55.15	52.32
Al2O3	12.67	13.26	12.64	12.40	13.94	14.30	15.73	14.97	14.68	14.13
Fe2O3	13.63	15.67	14.69	18.12	14.57	11.45	13.09	13.22	13.55	11.61
MgO	4.78	6.48	5.08	5.72	7.01	7.51	8.08	7.32	8.75	7.57
CaO	12.04	10.37	10.89	9.23	7.01	7.51	8.08	7.32	8.75	7.57
Na2O	0.65	1.78	2.04	1.89	4.58	1.52	4.29	1.53	1.13	1.41
K2O	0.17	0.53	0.14	0.28	0.52	0.40	0.28	0.14	0.12	0.17
TiO2	1.63	1.17	1.74	1.86	1.53	0.71	1.44	1.10	0.94	0.88
MnO	0.20	0.20	0.23	0.28	0.34	0.17	0.14	0.22	0.20	0.21
S	0.04	0.04	0.04	0.06	0.05	0.05	0.03	0.07	0.05	0.04
P2O5	0.21	0.10	0.22	0.17	0.12	0.08	0.41	0.10	0.08	0.08
TOTAL	100.04	100.05	100.04	100.06	100.92	96.85	105.57	95.37	103.4	95.99
Ba	4	58	0	4	4	30	100	15	0	0
Nb	1	0	0	0	0	2	17	3	3	2
Sr	149	73	137	124	98	73	264	81	77	67
Y	48	30	42	41	35	20	47	31	26	23
Sr	472	101	112	113	41	137	95	235	96	147
Rb	2	14	1	2	10	9	0	0	0	0

LOWER KAM GROUP

Sample	015-12	015-13		AVG	STD
SiO2	52.06	49.76		52.31	1.73
Al2O3	12.34	17.38		14.18	1.10
Fe2O3	11.71	11.06		12.80	1.89
MgO	9.23	7.56		6.71	1.78
CaO	9.23	7.65		9.66	1.84
Na2O	1.27	2.63		2.29	1.07
K2O	1.02	2.76		0.36	0.46
TiO2	0.70	0.73		1.23	0.42
MnO	0.21	0.24		0.24	0.05
S	0.03	0.04		0.04	0.01
P2O5	0.06	0.05		0.14	0.13
TOTAL	97.86	99.86			
Ba	125	802		48	127
Nb	1	11		2	3
Sr	54	47		91	45
Y	18	17		30	11
Sr	90	118		139	80
Rb	21	92		8	16

UPPER KAM GROUP

Sample	712-1B	712-2A	712-3A	712-4A	712-5A	712-6B	712-7B	714-1B	714-2B	714-3A
SiO2	49.62	49.09	49.32	48.67	47.13	49.82	48.40	51.58	50.57	52.84
Al2O3	15.65	15.09	14.51	15.13	14.76	13.62	14.26	13.80	14.73	13.53
Fe2O3	11.63	14.01	13.39	15.63	15.99	16.33	15.75	13.29	13.42	12.70
MgO	9.11	7.11	8.33	6.22	6.27	7.41	7.67	7.26	6.42	6.27
CaO	10.53	10.88	10.89	8.70	11.47	6.66	9.24	9.42	10.80	9.33
Na2O	1.74	1.82	1.89	2.95	2.03	3.76	2.63	2.48	1.97	3.51
K2O	0.71	0.60	0.10	0.63	0.22	0.09	0.34	0.76	0.64	0.27
TiO2	0.77	1.08	1.16	1.57	1.63	1.85	1.21	1.05	1.09	1.16
MnO	0.19	0.24	0.31	0.36	0.34	0.30	0.39	0.27	0.28	0.28
S	0.05	0.10	0.05	0.04	0.03	0.03	0.03	0.04	0.05	0.03
P2O5	0.05	0.10	0.10	0.14	0.16	0.17	0.10	0.10	0.10	0.12
TOTAL	100.05	100.12	100.05	100.04	100.03	100.04	100.02	100.05	100.07	100.04
Ba	29	23	12	89	29	6	23	19	53	5
Nb	1	0	0	1	0	1	0	0	1	3
Zr	50	66	73	100	112	127	73	76	80	89
Y	22	24	27	32	34	39	30	23	25	28
Sr	93	109	113	148	111	80	109	112	160	107
Rb	25	17	3	14	3	1	7	30	14	3

UPPER KAM GROUP

Sample	714-4A	714-5BC	716-1A	716-2B	716-3A	725-1A	725-1BC	725-2B	725-3	725-3C
SiO2	50.98	54.46	53.77	53.74	53.54	49.81	50.9˜	50.93	54.28	48.72
Al2O3	14.06	11.37	13.66	13.66	13.77	14.10	13.93	13.87	16.41	14.60
Fe2O3	13.76	11.16	10.99	11.58	12.38	13.56	13.57	14.06	8.89	14.80
MgO	7.50	8.36	8.64	7.67	7.35	6.54	6.33	6.81	4.72	8.25
CaO	8.62	8.48	8.23	9.57	9.90	12.05	10.64	10.72	11.05	9.38
Na2O	2.66	4.64	2.14	2.32	1.62	2.08	2.85	2.11	3.25	2.02
K2O	0.88	0.23	1.52	0.27	0.21	0.46	0.31	0.02	0.22	0.75
TiO2	1.13	0.96	0.80	0.88	0.94	1.09	1.10	1.16	0.99	1.14
MnO	0.29	0.28	0.19	0.25	0.23	0.20	0.20	0.20	0.16	0.24
S	0.03	0.04	0.03	0.03	0.05	0.03	0.02	0.05	0.06	0.04
P2O5	0.11	0.06	0.06	0.05	0.06	0.10	0.10	0.11	0.05	0.09
TOTAL	100.02	100.04	100.03	100.02	100.05	100.02	100.02	100.04	100.08	100.03
Ba	40	0	245	12	7	11	11	9	10	18
Nb	5	2	2	2	4	2	0	3	2	0
Zr	93	69	62	67	75	71	69	74	60	66
Y	27	25	22	21	24	26	29	30	24	24
Sr	101	88	108	99	128	179	154	145	146	161
Rb	35	4	18	5	2	5	3	2	3	14

UPPER KAM GROUP

Sample	725-4A	725-5	730-1A	730-2A	730-3A	730-4	730-5A	730-5B	730-6A	730-7
SiO2	50.83	49.39	52.88	5.18	49.88	51.04	46.98	50.70	54.67	52.13
Al2O3	14.90	14.39	14.60	14.32	14.20	13.72	14.83	13.41	14.39	14.07
Fe2O3	12.98	14.69	11.01	10.58	11.89	13.68	16.84	12.43	13.79	12.43
MgO	7.01	7.94	7.96	6.91	9.73	7.35	8.21	6.99	6.58	7.05
CaO	10.93	9.42	10.50	10.43	11.5.	10.31	9.05	13.38	12.23	10.52
Na2O	1.73	2.11	1.69	2.21	1.58	1.76	2.08	1.30	3.54	1.80
K2O	0.36	0.67	0.33	0.25	0.10	0.63	0.54	0.54	0.47	0.64
TiO2	1.01	1.08	0.76	0.81	0.79	1.08	1.06	0.94	1.03	1.02
MnO	0.19	0.22	0.22	0.22	0.24	0.33	0.32	0.21	0.27	0.23
S	0.05	0.05	0.05	0.03	0.05	0.08	0.21	0.16	0.09	0.04
P2O5	0.07	0.10	0.06	0.09	0.05	0.10	0.09	0.10	0.10	0.10
TOTAL	100.06	100.06	100.06	51.03	100.05	100.08	100.21	100.16	107.16	100.03
Ba	0	7	16	22	1	46	42	43	7	25
Nb	1	0	1	3	5	3	2	2	2	1
Zr	69	67	72	84	53	78	71	69	74	71
Y	27	27	22	23	17	25	21	23	23	22
Sr	122	153	143	180	132	128	134	116	163	124
Rb	5	12	8	5	3	13	15	11	3	9

Sample	AVG	STD
SiO2	49.40	8.47
Al2O3	14.24	0.84
Fe2O3	13.24	1.82
MgO	7.33	0.99
CaO	10.16	1.34
Na2O	2.34	0.75
K2O	0.46	0.30
TiO2	1.08	0.24
MnO	0.26	0.06
S	0.05	0.04
P2O5	0.09	0.03
TOTAL		
Ba	29	44
Nb	2	1
Zr	75	16
Y	26	4
Sr	128	26
Rb	10	8

locn	sample number	lab	Au	Ag	Cu	Pb	Zn	As	Sb
NEG-DDH	3758	B	583	3	75	5	34	2200	5
NEG-DDH	3759	B	651	1	174	5	76	1700	5
NEG-DDH	3771	B	446	1	151	5	1	7200	10
NEG-DDH	3937	B	446	1	76	16	58	10000	32
NEG-DDH	3939	B	103	1	35	5	2	84	5
NEG-DDH	3940	B	206	1	107	20	529	4050	5
NEG-DDH	3944	B	127871	32	216	40	3	3950	13
NEG-DDH	3946	B	17652	22	104	102	62	1100	90
KAM-PT	4001	C	15	0	0	4	4	0	0
KAM-PT	4002	C	0	0	118	0	5	0	0
KAM-PT	4015	C	10	0	38	30	6	20	0
KAM-PT	4103	C	0	0.6	48	300	1816	5	0
KAM-PT	4104	C	0	0	33	4	80	10	0
KAM-PT	4107	C	0	0	10	0	12	0	0
KAM-PT	4110	C	0	0	33	8	?7	30	0
KAM-PT	4114	C	0	0	121	52	64	0	0
STOCK	4116	C	4090	1	5	8	5	15	0
STOCK	4117	C	0	0	2	0	1	0	0
STOCK	4118	C	0	0	2	6	1	0	0
STOCK	4120	C	0	0	14	8	16	0	0
STOCK	4121	C	30	0	78	28	16	115	0
STOCK	4122	C	0	0	12	56	3	5	5
STOCK	4123	C	0	0	25	0	3	5	0
STOCK	4124	C	0	0	3	2	2	15	0
STOCK	4126	C	0	0	5	0	3	0	0
STOCK	4127	C	0	0	5	2	3	10	0
STOCK	4129	C	0	0	6	2	16	5	0
STOCK	4130	C	0	0	53	6	34	5	0
STOCK	4131	C	0	0	4	4	12	0	0
STOCK	4132	C	5	0	20	0	6	5	0
STOCK	4133	C	0	0	204	0	9	0	0
STOCK	4134	C	0	0	5	0	9	0	0
STOCK	4137	C	0	0	17	8	29	10	0
STOCK	4140	C	0	0	8	6	92	5	0
STOCK	4141	C	0	0	3	10	4	0	0
STOCK	4143	C	0	0	56	6	47	5	0
STOCK	4144	C	0	0	94	52	93	15	0
NEG-S	4502	B	69	0.02	17	5	73	50	5
NEG-S	4503	B	69	0.02	128	5	1	20	6
NEG-S	4504	B	69	0.02	2050	5	42	40	5
NEG-S	4505	B	69	0.02	41	5	18	20	5
NEG-S	4506	B	69	0.02	120	262	671	20	5
NEG-S	4507	B	69	0.02	15	5	32	20	5
NEG-S	4508	B	69	0.02	10	5	40	20	5
NEG-S	4509	B	69	0.02	10	5	11	20	5
NEG-S	4513	B	69	0.04	4	5	20	30	5
NEG-S	4515	B	69	0.04	12	5	34	10	5
NEG-S	4525	B	69	0.04	38	5	25	10	5
NEG-S	4526	B	69	0.04	4	5	16	20	5

NERCO-Con Mine
Quartz vein samples

locn	sample number	lab	Au	Ag	Cu	Pb	Zn	As	Sb
NEG-S	4528	B	69	0.04	10	32	109	80	5
NEG-S	4529	B	69	0.04	3	5	24	16	5
NEG-S	4532	B	103	0.02	10	5	15	128	5
NEG-S	4535	B	103	0.02	37	5	27	110	5
NEG-S	4537	B	103	0.02	11	5	20	78	5
NEG-S	4538	B	103	0.02	3	5	9	14	5
NEG-S	4540	B	103	0.02	7	5	15	18	5
NEG-S	4544	B	103	0.02	4	5	9	10	5
NEG-S	4546	B	103	0.02	12	5	21	10	5
NEG-S	4548	B	103	0.02	7	5	23	20	5
NEG-S	4549	C	60	0.8	3417	104	3450	25	5
NEG-S	4550	C	0	0.2	35	0	31	10	0
NEG-S	4551	C	0	0.2	108	2	121	0	0
KAM-LK	4562	C	55	0.6	257	12	55	55	0
KAM-LK	4563	C	1450	0.2	19	2	19	210	0
KAM-LK	4569	C	10	0	21	0	12	10	0
KAM-LK	4570	C	5	0	274	0	14	0	0
KAM-LK	4571	C	20	0.2	18	12	55	100	0
KAM-LK	4572	C	0	0.2	7	0	18	5	0
KAM-LK	4575	C	0	0	3	4	13	5	0
KAM-LK	4576	C	0	0.4	0	2	28	15	0
KAM-LK	4577	C	1350	1.4	312	8	22	820	0
KAM-LK	4580	C	40	0.2	446	8	195	40	0
KAM-LK	4583	C	1550	0.8	39	4	18	195	0
KAM-PT	4585	C	8800	10.4	110	3618	5145	2300	165
KAM-PT	4586	C	250	0.2	8	90	163	25	0
KAM-PT	4587	C	210	0.2	11	36	49	190	5
KAM-PT	4588	C	20	0.2	0	14	32	15	0
KAM-PT	4589	C	15	0	11	38	47	0	0
KAM-PT	4590	C	55	0	6	6	26	0	0
KAM-PT	4591	C	315	1.4	6	10	5	225	0
KAM-PT	4592	C	3300	0.2	0	4	5	5870	5
KAM-PT	4595	C	310	0.4	32	56	1488	215	0
KAM-PT	4596	C	1100	0.2	3	6	676	905	0
KAM-PT	4597	C	595	0.2	22	16	125	805	0
KAM-PT	4599	C	45	0	11	2	22	30	0
KAM-PT	4600	C	0	0	0	12	29	5	0
NEG-DDH	5045	B	960	7	151	5	91	2100	21
NEG-DDH	5046	B	5999	16	251	30	88	5100	6
NEG-DDH	5047	B	1783	9	130	46	59	10000	28
PUB-GRD	5601	B	309	1	87	5	18	1500	5
PUB-GRD	5602	B	69	1	32	5	12	52	5
PUB-GRD	5604	B	274	1	115	5	39	2300	5
PUB-GRD	5606	B	53480	138	1120	143	188	2950	35
PUB-GRD	5607	B	179294	3	45	5	8	7	1200
PUB-GRD	5608	B	14158	1	25	9	27	7800	5
PUB-GRD	5609	B	274	1	253	5	133	224	5
PUB-GRD	5612	B	69	1	39	8	34	134	5
PUB-GRD	5615	B	206	1	50	5	44	250	5

locn	sample number	lab	Au	Ag	Cu	Pb	Zn	As	Sb
PUD-GRD	5617	B	206	1	14	5	14	505	5
PUD-GRD	5618	B	411	1	9	5	20	770	5
PUD-GRD	5619	B	69	1	22	5	9	120	5
PUD-GRD	5620	B	480	4	104	58	24	570	14
N-R-TC	5621	B	69	2	107	14	58	110	16
N-R-TC	5622	B	40453	22	87	52	127	220	11
N-R-TC	5623	B	549	5	42	12	32	305	6
N-R-TC	5624	B	1474	6	57	178	104	120	5
N-R-TC	5625	B	61707	32	12	106	21	735	34
N-R-TC	5626	B	29140	5	38	5	12	490	5
N-R-TC	5627	B	181694	57	168	5	22	80	37
N-R-TC	5629	B	2194	1	23	5	2	21	2400
N-R-TC	5630	B	651	1	27	5	15	5	5
N-R-TC	5631	B	686	1	8	5	56	10	5
N-R-TC	5632	B	69	1	15	5	29	10	5
N-R-TC	5633	B	103	1	11	5	15	5	5
N-R-TC	5634	B	69	1	940	5	52	10	5
N-R-TC	5635	B	103	1	730	13	87	10	5
N-R-TC	5636	B	103	1	47	5	41	5	5
N-R-TC	5637	B	69	1	13	5	7	10	5
N-R-TC	5638	B	69	1	137	5	38	25	5
N-R-TC	5639	B	69	1	11	5	11	20	5
STOCK	5640	C	190	0.2	25	222	1951	25	0
STOCK	5641	C	5	0.2	12	116	196	25	0
STOCK	5642	C	1800	1.6	37	10	17	45	0
STOCK	5645	C	0	0.2	54	4	9	0	0
STOCK	5651	C	0	0.2	5	4	5	0	0
STOCK	8701	C	0	0	0	2	76	5	0
STOCK	8702	C	0	0	3	0	5	5	0
STOCK	8703	C	20	0.2	18	24	19	5	0
STOCK	8704	C	0	0	3	0	10	0	0
STOCK	8706	C	0	0	0	0	3	5	0
STOCK	8708	C	0	0	0	2	2	0	0
STOCK	8710	C	0	0	30	0	6	5	0
STOCK	8711	C	210	1.4	1166	312	842	45	0
STOCK	8712	C	0	0	58	8	22	0	0
STOCK	8716	C	0	0	38	6	9	10	0
STOCK	8717	C	0	0	4	0	3	0	0
STOCK	8719	C	110	0	3	0	7	0	0
STOCK	8720	C	0	0	6	0	18	5	0
STOCK	8721	C	0	0	10	0	9	0	0
STOCK	8722	C	15	0	41	2	9	5	0
STOCK	8723	C	35	0	7	8	6	0	0
STOCK	8724	C	0	0	1	4	2	0	0
STOCK	8725	C	0	0	5	4	23	0	0
STOCK	8726	C	10	0	3	0	3	0	0
STOCK	8727	C	5	0	1	0	4	0	0
STOCK	8728	C	20	0	12	10	14	0	0
KAM-PT	8735	C	0	0	6	0	9	0	0

locn	sample number	lab	Au	Ag	Cu	Pb	Zn	As	Sb
KAM-PT	8736	C	0	0.2	65	4	31	0	0
KAM-PT	8737	C	0	0	40	2	20	0	0
KAM-PT	8738	C	65	0	18	30	40	60	0
KAM-PT	8745	C	0	0.2	2	10	42	0	0
KAM-PT	8746	C	0	0.2	0	6	33	0	0
KAM-PT	8747	C	0	0	0	0	6	0	0
KAM-PT	8752	C	0	0	15	4	36	0	0
KAM-PT	8754	C	0	0.6	115	1380	5714	15	0
KAM-PT	8757	C	0	0.2	57	58	175	10	0
KAM-PT	8758	C	0	0.4	44	38	85	10	0
KAM-PT	8759	C	10	0	1	12	30	5	0
KAM-PT	8760	C	0	0.2	44	4	377	10	0
KAM-PT	8761	C	30	0.4	446	4	28	15	0
KAM-PT	8762	C	5	0	32	6	16	0	0
KAM-PT	8766	C	5	0	11	4	29	0	0
KAM-PT	8768	C	180	0.4	13	2	16	40	0
KAM-PT	8771	C	15	0.8	12	2	26	235	0
KAM-PT	8772	C	215	0	4	2	3	795	0
KAM-PT	8773	C+	25231	5	17	150	210	2780	5
KAM-PT	8775	C	5	0	0	2	5	400	0
KAM-PT	8776	C	190	0.4	17	4	25	330	0
KAM-PT	8777	C	2400	0.4	2	0	5	1380	5
KAM-PT	8778	C	20	0.2	28	12	30	120	15
KAM-PT	8779	C	0	0	11	2	19	0	0
KAM-PT	8780	C	20	0.4	140	80	870	5	0
KAM-PT	8781	C	330	0	5	0	27	4460	0
KAM-PT	8782	C	5	0.2	14	0	35	150	0
KAM-PT	8783	C	5900	0.6	1354	10	874	30	0
KAM-PT	8786	C	30	0.4	43	0	38	1140	0
KAM-PT	8787	C	5	0	8	0	36	35	0
KAM-PT	8789	C	60	0	77	0	23	270	0
KAM-PT	8792	C	0	0.2	113	0	103	30	0
KAM-PT	8795	C	0	0	7	0	29	5	0
KAM-PT	8798	C	0	0.2	1	0	12	0	0
KAM-PT	8799	C	0	0	37	0	9	0	0
STOCK	8905	C	0	0.2	29	6	36	0	0
STOCK	8911	C	10	0.2	2	2	2	0	0
STOCK	8912	C	115	0.2	3	4	1	20	0
STOCK	8913	C	370	2.6	7	18	2	85	0
STOCK	8914	C	265	2.4	4	14	1	45	0
STOCK	8915	C	290	2	9	14	1	45	0
STOCK	8919	C	470	3	66	8	39	90	0
STOCK	8920	C	305	0.8	10	158	3	30	20
STOCK	8926	C	1500	0.8	3	0	1	630	0
STOCK	8927	C	2500	21	3	18	1	15	0
STOCK	8928	C	130	0.2	4	4	3	25	0
STOCK	8929	C	0	0.2	2	18	2	0	0
STOCK	8930	C	10000	20.6	7	22	4	125	9
STOCK	8931	C	1800	9	52	10	17	55	0

locn	sample number	lab	Au	Ag	Cu	Pb	Zn	As	Sb
STOCK	8932	C	10000	17.4	17	8	18	15	0
STOCK	8934	C	1100	1.4	16	18	124	5	0
STOCK	8936	C	210	0.2	4	12	11	5	0
STOCK	8937	C	310	0.2	21	226	85	10	0
STOCK	8938	C	65	0.2	45	16	62	35	0
STOCK	8939	C	0	0.2	10	14	16	0	0
STOCK	8940	C	40	0.2	111	10	13	35	0
STOCK	8941	C	300	0.2	56	0	22	3965	5
STOCK	8942	C	<550	1.8	112	0	33	310	0
STOCK	8943	C	100	0.2	7	10	22	50	0
STOCK	8945	C	2600	0.2	59	6	9	1660	0
STOCK	8946	C	7100	1.4	62	6	1	4740	0
STOCK	8947	C	110	0.2	19	4	6	65	0
STOCK	8948	C	20	0.2	3	8	2	15	0
STOCK	8949	C	0	0.2	26	10	1	10	0
STOCK	8950	C	0	0.2	4	4	3	5	0
STOCK	8953	C	0	0.2	26	2	19	0	5
STOCK	8954	C	0	0.2	36	2	11	0	0
STOCK	8955	C	0	0	6	4	3	0	0
STOCK	8956	C	0	0	4	2	4	5	0
STOCK	8957	C	0	0	10	8	17	5	5
STOCK	8961	C	15	0	5	4	4	10	5
STOCK	8962	C	170	0	134	4	7	20	0
STOCK	8963	C	95	0	41	6	24	15	0
STOCK	8964	C	30	0	5	10	2	25	0
STOCK	8965	C	5	0	4	8	9	0	5
STOCK	8966	C	10	0	8	2	4	0	5
STOCK	8968	C	0	0	12	0	32	0	0
STOCK	8974	C	0	0.6	20	118	38	15	0
STOCK	8977	C	0	0.2	9	20	15	5	0
STOCK	8978	C	0	0.2	5	6	8	0	0
STOCK	9401	C	0	0.5	4	6	26	11	0.4
STOCK	9403	C	35	0	26	0	9	5	0
STOCK	9406	C	65	0.4	47	0	15	195	0
KAM-PT	9408	C	0	0	4	0	4	5	0
KAM-PT	9413	C	0	0.2	201	0	104	125	5
KAM-PT	9414	C	0	0.8	164	240	273	30	0
KAM-PT	9417	C	0	0	5	0	11	0	0
KAM-PT	9419	C	90	1.6	78	10	8	375	0
KAM-PT	9420	C	620	0.2	4	0	2	335	0
KAM-PT	9423	C	0	0	2	0	10	5	0
KAM-PT	9426	C	0	0.2	78	18	166	85	0
KAM-PT	9428	C+	525129	200	348	0	79	1865	10
KAM-PT	9430	C+	24614	4.2	18	6	5	30	0
KAM-PT	9431	C	1100	0.2	3	2	2	5	0
KAM-PT	9432	C	550	0.4	73	10	45	10	5
KAM-PT	9434	C	210	0	4	0	27	55	5
KAM-PT	9435	C	55	0.6	33	0	30	25	5
KAM-PT	9438	C	900	0.4	2	0	11	35	5

locn	sample number	lab	Au	Ae	Cu	Pb	Zn	As	Sb
KAN-PT	9440	C	2650	0	2	8	2	80	0
KAN-PT	9442	C	140	0	30	6	8	10	5
KAN-PT	9444	C	540	0.2	14	4	9	185	5
KAN-PT	9445	C	230	0.4	68	8	21	690	5
KAN-PT	9447	C	290	0.4	7	6	13	0	5
KAN-PT	9449	C	30	0	13	12	9	120	5
KAN-PT	9451	C	45	0	5	8	3	10	0
KAN-PT	9452	C	35	0	14	6	6	20	0
KAN-PT	9454	C	15	0	3	6	2	5	0
KAN-PT	9455	C	0	0	19	6	7	50	0
KAN-PT	9456	C	90	0	0	12	14	290	5
KAN-PT	9459	C	700	0	2	0	13	185	0
KAN-PT	9464	C	0	0.5	22	6	82	5	0.4
KAN-PT	9469	C	210	0.2	155	12	14	105	5
KAN-PT	9470	C	20	0	91	0	4	30	5
KAN-PT	9472	C	65	5	9999	0	14	115	10
KAN-PT	9473	C	50	0.2	1748	0	49	175	5
KAN-PT	9474	C	140	0.2	9999	12	20	75	5
KAN-PT	9476	C	0	0.2	354	0	451	20	0
KAN-PT	9479	C	145	0.4	987	10	32	305	0
KAN-PT	9481	C	5	0.2	83	0	12	15	0
KAN-PT	9482	C	0	0.2	29	44	287	0	5
KAN-PT	9486	C	0	0.2	74	8	17	20	5
KAN-PT	9487	C	0	0.2	47	30	101	5	0
KAN-PT	9488	C	35	0.2	19	4	17	140	0
KAN-PT	9489	C	70	0.2	4	0	9	1210	10
KAN-PT	9491	C	0	0.2	9	18	89	100	0
KAN-PT	9494	C	0	0.5	40	4	44	1200	0.3
KAN-PT	9496	C	40	1	57	222	2090	480	0
KAN-PT	9497	C	60	0	7	4	34	95	0
KAN-PT	9498	C	0	0	5	4	15	0	0
KAN-PT	9499	C	0	0	26	0	18	5	0
PUB-GRD	9503	B	514	0.31	11	11	19	1260	5
PUB-GRD	9504	B	69	0.07	80	34	253	40	5
PUB-GRD	9505	B	994	0.32	200	13	177	1400	5
GRACE	9506	B	69	1	15	367	164	36	5
GRACE	9507	B	69	0.21	6	154	347	16	5
GRACE	9510	B	69	0.02	275	6	30	38	5
STOCK	9511	B	103	0.61	673	5	11	16	5
STOCK	9512	B	69	0.02	16	5	19	12	5
STOCK	9514	B	69	0.07	103	5	17	16	5
STOCK	9516	B	69	0.02	17	11	10	12	5
STOCK	9517	B	69	0.02	20	5	33	16	5
STOCK	9518	B	69	0.02	19	5	25	8	5
STOCK	9519	B	69	0.02	2	5	4	12	5
STOCK	9521	B	69	0.02	14	9	16	16	5
STOCK	9522	B	69	0.05	48	6	29	92	5
STOCK	9523	B	69	0.02	29	5	44	16	5
STOCK	9524	B	69	0.02	1	5	3	8	5

locn	sample number	lab	Au	Ag	Cu	Pb	Zn	As	Sb
STOCK	9527	B	1611	0.47	34	43	141	52	5
STOCK	9530	B	206	0.06	320	14	36	72	5
STOCK	9532	B	69	0.02	9	5	10	16	5
STOCK	9533	B	69	0.02	7	5	55	10	5
STOCK	9535	B	446	0.02	109	16	21	38	5
STOCK	9537	B	69	0.02	10	5	10	20	5
STOCK	9538	B	69	0.04	89	7	19	36	5
STOCK	9539	B	69	0.02	8	5	7	10	5
STOCK	9540	B	69	0.02	32	7	62	26	5
STOCK	9541	B	69	0.02	7	5	7	12	5
STOCK	9542	B	69	0.02	5	5	6	8	5
STOCK	9543	B	69	0.02	15	5	37	16	5
STOCK	9544	B	69	0.06	137	5	92	26	5
STOCK	9545	B	69	0.02	30	5	58	16	5
STOCK	9546	B	69	0.02	51	5	28	16	5
STOCK	9549	B	69	0.02	18	7	77	16	5
STOCK	9552	B	69	0.02	11	5	33	20	5
STOCK	9553	B	69	0.02	39	5	29	10	5
STOCK	9555	B	69	0.02	22	5	52	20	5
STOCK	9556	B	69	0.02	10	5	20	16	5
STOCK	9558	B	69	0.02	5	5	13	10	5
STOCK	9559	B	309	0.04	12	5	53	550	5
STOCK	9560	B	137	0.04	61	5	95	980	5
STOCK	9561	B	1234	0.39	72	24	79	780	5
STOCK	9562	B	69	0.02	9	5	24	20	5
STOCK	9563	B	171	0.31	351	5	45	25	5
STOCK	9564	B	69	0.02	15	5	46	16	5
STOCK	9566	B	1131	0.04	8	5	32	30	5
STOCK	9567	B	69	0.02	5	5	22	16	5
STOCK	9571	B	69	0.02	9	5	25	16	5
STOCK	9572	B	69	0.02	10	5	23	10	5
STOCK	9573	B	69	0.02	18	5	20	14	5
STOCK	9574	B	69	0.02	7	5	19	10	5
STOCK	9575	B	411	0.02	10	5	29	1050	5
STOCK	9576	B	69	0.02	7	8	50	20	5
STOCK	9577	B	4868	0.82	10	5	16	200	5
STOCK	9579	B	1885	0.14	38	5	41	40	5
STOCK	9582	B	69	0.02	20	5	23	10	5
STOCK	9584	B	69	0.02	4	5	26	10	5
STOCK	9585	B	69	0.03	76	5	118	72	5
STOCK	9586	B	823	0.1	69	5	40	20	5
STOCK	9587	B	69	0.19	11	107	263	20	5
STOCK	9588	B	69	0.03	2	5	18	20	5
STOCK	9589	B	69	0.02	23	5	38	32	5
STOCK	9590	B	69	0.04	18	5	81	110	5
STOCK	9591	B	69	0.02	19	5	16	10	5
STOCK	9592	B	69	0.02	5	5	38	10	5
STOCK	9593	B	514	0.46	18	7	42	700	5
STOCK	9595	B	69	0.02	19	5	49	30	5

locn	sample number	lab	Au	Ag	Cu	Pb	Zn	As	Sb
STOCK	9596	B	69	0.12	13	5	33	70	5
STOCK	9598	C	0	0	11	4	12	0	0
PUD-GRD	9601	B	69	1	60	5	38	10	5
PUD-GRD	9602	B	69	1	12	5	11	15	5
PUD-GRD	9603	B	69	0.02	17	5	17	16	5
PUD-GRD	9604	B	69	0.02	12	5	14	24	5
PUD-GRD	9605	B	69	0.02	7	5	8	18	5
NEG-S	9607	B	2743	3.2	62	5200	2750	2920	4200
NEG-S	9609	B	103	0.04	46	48	56	48	5
NEG-S	9610	B	69	0.02	18	23	29	16	5
NEG-S	9617	B	69	0.02	66	8	16	16	5
NEG-S	9625	B	69	0.1	15	41	184	6	5
NEG-S	9631	B	69	0.02	9	5	39	40	5
NEG-S	9632	B	69	0.02	14	8	27	28	5
NEG-S	9634	B	69	0.02	25	8	22	32	5
NEG-S	9635	B	69	0.02	15	11	57	76	5
NEG-S	9637	B	69	0.02	34	13	29	24	5
NEG-S	9638	B	69	0.9	295	380	352	24	5
NEG-S	9640	B	69	0.13	27	39	13	88	5
NEG-S	9645	B	69	0.02	29	11	8	150	5
NEG-S	9652	B	69	0.04	17	67	45	38	5
NEG-S	9653	B	69	0.02	11	8	7	26	5
NEG-S	9656	B	69	0.02	28	5	11	14	5
NEG-S	9657	B	69	0.02	22	7	19	40	5
NEG-S	9658	B	69	0.02	9	7	9	12	5
NEG-S	9659	B	137	0.02	35	9	4	740	5
NEG-S	9661	B	69	0.02	29	5	31	46	5
NEG-S	9663	B	69	0.02	41	5	60	50	5
NEG-S	9664	B	69	0.02	28	5	96	48	5
NEG-S	9665	B	69	0.04	21	46	240	30	5
NEG-S	9666	B	480	0.35	19	5	31	560	5
NEG-S	9668	B	69	0.29	24	5	38	310	5
NEG-S	9669	B	1714	0.03	19	5	19	1140	5
NEG-S	9670	B	857	0.07	23	5	28	820	5
NEG-S	9672	B	69	0.02	15	5	29	30	5
NEG-S	9676	B	69	0.02	5	5	25	26	5
NEG-S	9677	B	69	0.02	17	9	120	70	5
NEG-S	9678	B	69	0.02	16	5	53	60	5
NEG-S	9679	B	103	0.29	1920	5	104	50	5
NEG-S	9681	B	69	0.25	6	5	32	20	5
NEG-S	9683	B	69	0.02	25	5	38	30	5
NEG-S	9685	B	69	0.02	13	140	926	60	5
NEG-S	9686	B	69	0.02	38	5	49	40	5
NEG-S	9687	B	69	0.02	10	5	24	20	5
NEG-S	9689	B	69	0.24	153	36	126	54	5
NEG-S	9690	B	69	0.02	568	5	20	20	5
NEG-S	9691	B	69	0.02	11	5	25	20	5
NEG-S	9693	B	69	0.02	138	5	46	20	5
NEG-S	9694	B	69	0.02	18	5	16	18	5

NERCO-Con Mine
Quartz vein samples

locn	sample number	lab	Au	Ag	Cu	Pb	Zn	As	Sb
NEG-S	9696	B	69	0.02	8	5	73	68	5
NEG-S	9699	B	69	0.02	429	5	15	18	5
NEG-S	9700	B	69	0.02	26	5	98	1450	5
N-R-TC	9801	B	69	0.02	18	6	11	8	5
N-R-TC	9802	B	69	0.02	7	5	15	10	5
N-R-TC	9805	B	69	0.02	9	8	7	12	5
N-R-TC	9806	B	69	0.14	18	24	113	16	5
N-R-TC	9807	B	69	0.02	8	6	11	20	5
N-R-TC	9810	B	69	0.28	1	9	23	2	5
KAM-PT	9811	C	25	0	8	0	11	215	0
KAM-PT	9814	C	0	0	4	0	5	0	0
KAM-PT	9817	C	0	0	3	0	11	5	0
KAM-PT	9822	C	40	0	17	2	122	385	0
KAM-PT	9823	C	35	0	69	2	32	660	5
KAM-PT	9824	C	175	0	46	4	94	535	0
KAM-PT	9826	C	0	0	9	0	6	50	0
KAM-PT	9828	C	30	0	14	0	27	160	0
KAM-PT	9830	C	0	0	5	0	54	0	0
KAM-PT	9833	C	735	0.4	29	16	42	1275	0
KAM-PT	9835	C	5	0	5	0	61	25	0
PUD-GRD	9901	B	69	1	18	11	37	25	5
PUD-GRD	9902	B	69	1	9	5	11	30	5
PUD-GRD	9903	B	137	1	12	5	12	30	5
PUD-GRD	9904	B	171	1	15	5	32	50	5
PUD-GRD	9905	B	69	1	60	5	37	75	5
PUD-GRD	9906	B	69	1	12	5	13	20	5
PUD-GRD	9911	B	69	1	36	5	32	20	5
PUD-GRD	9913	B	69	1	8	5	16	30	5
PUD-GRD	9914	B	69	1	67	5	16	30	5
PUD-GRD	9915	B	69	1	16	5	8	10	5
PUD-GRD	9917	B	69	1	47	5	23	30	5
PUD-GRD	9918	B	69	1	102	5	41	25	5
PUD-GRD	9919	B	69	1	32	5	34	45	5
???????	9920	B	69	1	30	5	19	25	5
N-R-TC	9922	B	1500	0.65	18	7	7	128	31
N-R-TC	9923	B	57936	2.1	89	34	49	76	35
N-R-TC	9924	B	103	0.24	11	5	12	48	5
N-R-TC	9925	B	206	0.1	88	18	65	16	5
N-R-TC	9926	B	69	0.03	36	28	74	16	5
N-R-TC	9931	B	3805	3.7	25	12	13	240	17
N-R-TC	9932	B	18992	4.6	260	161	78	160	290
N-R-TC	9933	B	240	0.14	13	5	15	12	5
N-R-TC	9935	B	69	0.03	86	5	33	8	5
N-R-TC	9937	B	69	0.02	38	8	17	32	5
N-R-TC	9938	B	59	0.03	88	16	24	12	5
N-R-TC	9940	B	69	0.02	16	5	19	8	5
N-R-TC	9943	B	69	0.06	36	46	47	20	5
N-R-TC	9946	B	103	0.02	4	8	13	28	5
N-R-TC	9947	B	69	0.02	7	5	1	16	5

NERCO-Con Mine
Quartz vein samples

locn	sample number	lab	Au	Ag	Cu	Pb	Zn	As	Sb
N-R-TC	9948	B	69	0.02	4	8	14	28	5
N-R-TC	9949	B	69	0.08	99	5	35	12	5
N-R-TC	9950	B	69	0.02	70	5	9	10	5
N-R-TC	9951	B	69	0.02	10	8	13	16	5
N-R-TC	9954	B	69	0.02	42	12	12	12	5
N-R-TC	9956	B	69	0.02	12	12	26	20	5
N-R-TC	9958	B	69	0.02	8	5	9	8	5
N-R-TC	9959	B	137	0.02	9	12	9	1280	5
M-R-TC	9960	B	69	0.02	11	13	8	216	5
N-R-TC	9961	B	69	0.12	241	7	11	154	5
N-R-TC	9963	B	69	0.15	8	10	7	88	5
M-R-TC	9965	B	69	0.02	10	7	13	48	5
N-R-TC	9966	B	69	0.02	12	6	24	40	5
N-R-TC	9967	B	69	0.02	23	14	203	40	5
N-R-TC	9968	B	69	0.02	6	5	14	28	5
N-R-TC	9969	B	69	0.02	32	5	53	48	5
N-R-TC	9970	B	69	0.02	3	5	37	12	5
M-R-TC	9971	B	69	0.02	7	5	12	16	5
N-R-TC	9972	B	69	0.02	6	5	7	22	5
N-R-TC	9973	B	69	0.9	8	5	44	12	5
M-R-TC	9974	B	69	0.02	7	5	4	16	5
N-R-TC	9975	B	69	0.02	8	5	24	8	5
M-R-TC	9976	B	69	0.02	12	5	8	14	5
M-R-TC	9979	B	69	0.02	17	255	18	12	5
N-R-TC	9980	B	69	0.02	19	5	12	8	5
N-R-TC	9981	B	69	0.02	7	5	6	10	5
N-R-TC	9982	B	69	0.02	13	11	48	6	5
N-R-TC	9983	B	69	0.02	1	5	14	4	5
N-R-TC	9984	B	69	0.02	6	5	8	6	5
M-R-TC	9987	B	69	0.02	14	5	10	2	5
N-R-TC	9988	B	69	0.02	5	13	38	8	5
N-R-TC	9989	B	69	0.02	9	5	18	4	5
N-R-TC	9991	B	69	0.02	8	10	12	4	5
A-R-TC	9995	B	69	0.02	6	5	11	12	5
N-R-TC	9996	B	69	0.02	10	5	19	10	5
N-R-TC	9997	B	69	0.02	11	5	3	8	5
M-R-TC	9998	B	69	0.02	55	6	16	12	5
N-R-TC	9999	B	69	0.02	12	5	35	16	5
N-R-TC	10000	B	69	0.02	23	5	12	14	5
N-R-TC	9999	B	69	0.02	12	5	35	16	5
M-R-TC	10000	B	69	0.02	23	5	12	14	5

CAMPBELL SHEAR ZONE, LONGITUDINAL SECTION

TO SURFACE

SOUTH

NORTH

Sample Locations

SCALE 1 inch   1000 FEET

3200   2400   1600   800   0

-16000   -17000   -18000   -19000   -20000   -21000   -22000   -23000

X14405
X14800

X10307   X10300X10301
X1185   X1184X1182X116X180
X144808
X412X4128 X412X412X412X

X418X413X13X134

X1170X1171   X1178X1178X1177
X1172   X1178
X10310 X10311
X10313
X144910
X1187

Pearson Correlation Coefficients

n=30

Lower Kae Group, Data from Cunningham (1994)

From CO020

	SiO2	Al2O3	Fe2O3	MgO	CaO	Na2O	K2O	TiO2	MnO	S	P2O5	Ba	Nb	Zr	Y	Sr	Rb
SiO2	1	-0.114	-0.475	0.009	-0.041	-0.127	-0.159	-0.066	-0.194	-0.107	0.191	-0.019	0.063	0.161	0.004	0.045	-0.109
Al2O3	-0.114	1	-0.451	0.035	0.039	0.055	0.104	-0.276	-0.122	-0.276	-0.047	0.014	0.205	-0.178	-0.319	-0.017	-0.208
Fe2O3	-0.475	-0.451	1	-0.182	-0.194	0.055	-0.095	0.547	0.243	0.325	-0.066	-0.040	-0.065	0.356	0.521	0.010	-0.002
MgO	0.009	0.035	-0.182	1	-0.534	-0.254	0.208	-0.082	-0.061	-0.123	-0.170	0.023	0.207	-0.421	-0.613	-0.324	0.194
CaO	-0.041	0.039	-0.194	-0.534	1	-0.171	-0.292	0.074	-0.047	-0.123	0.110	-0.237	-0.351	-0.060	0.017	0.221	-0.108
Na2O	-0.127	0.055	0.055	-0.254	-0.171	1	-0.005	0.287	-0.010	-0.054	0.222	0.225	0.277	0.463	0.443	-0.125	0.048
K2O	-0.159	0.104	-0.095	0.208	-0.292	-0.005	1	-0.285	0.130	0.008	-0.173	0.463	0.306	-0.229	-0.308	-0.204	0.506
TiO2	-0.066	-0.276	0.547	-0.082	0.074	0.287	-0.285	1	0.175	0.122	0.272	0.062	0.001	0.761	0.919	0.172	-0.222
MnO	-0.194	-0.122	0.243	-0.061	-0.047	-0.010	0.130	0.175	1	0.047	0.035	0.128	-0.247	-0.169	-0.003	-0.349	0.108
S	-0.107	-0.276	0.325	-0.129	-0.123	-0.054	0.008	0.122	0.047	1	-0.155	-0.049	-0.122	0.015	0.127	0.009	-0.010
P2O5	0.191	-0.047	-0.066	-0.170	0.110	0.222	-0.173	0.272	0.035	-0.155	1	0.163	0.270	0.437	0.349	-0.012	-0.115
Ba	-0.019	0.014	-0.040	0.023	-0.237	0.225	0.463	0.662	0.128	-0.049	0.163	1	0.303	0.146	0.659	0.033	0.499
Nb	0.063	0.205	-0.065	0.207	-0.351	0.277	0.306	0.001	-0.247	-0.122	0.270	0.303	1	0.477	0.205	0.093	-0.160
Zr	0.161	-0.178	0.356	-0.421	-0.080	0.463	-0.229	0.761	-0.169	0.015	0.437	0.146	0.477	1	0.891	0.174	-0.334
Y	0.004	-0.319	0.521	-0.613	0.017	0.443	-0.308	0.919	-0.003	0.127	0.349	0.659	0.205	0.891	1	0.245	-0.290
Sr	0.045	-0.011	0.010	-0.324	0.221	-0.125	-0.204	0.172	-0.348	0.005	-0.012	0.033	0.093	0.174	0.245	1	-0.093
Rb	-0.109	-0.208	-0.002	0.194	-0.108	0.048	0.506	-0.222	0.108	-0.019	-0.115	0.499	-0.160	-0.334	-0.290	-0.093	1

CAMPBELL SHEAR ZONE DATA
PROCESSED BY PCA25 (Webb, 1988)

Chlorite-carbonate schist saamples
n=90

Pearson Correlation Matrix

	SiO2	TiO2	Al2O3	Fe2O3	MnO	Na2O	MgO	CaO	K2O	Na2O
SiO2	1	-0.1992	0.0641	-0.2259	-0.4396	0.2341	-0.2614	-0.4734	0.0522	0.2341
TiO2	-0.1992	1	0.1204	0.8012	0.2801	-0.1509	-0.1745	-0.2967	-0.0955	-0.1509
Al2O3	0.0641	0.1204	1	0.2392	-0.3103	0.1931	0.3268	-0.4455	-0.0194	0.1931
Fe2O3	-0.2259	0.8012	0.2392	1	0.2517	-0.3213	-0.0153	-0.4354	-0.1245	-0.3213
MnO	-0.4396	0.2801	-0.3103	0.2517	1	0.1044	-0.0030	0.2245	-0.2869	0.1044
Na2O	0.2341	-0.1509	0.1931	-0.3213	0.1044	1	-0.1716	0.0892	-0.5094	1.0000
MgO	-0.2614	-0.1745	0.3268	-0.0153	-0.0030	-0.1716	1	-0.2451	-0.2704	-0.1716
CaO	-0.4734	-0.2967	-0.4455	-0.4354	0.2245	0.0892	-0.2451	1	0.0552	0.0892
K2O	0.0522	-0.0955	-0.0194	-0.1245	-0.2869	-0.5094	-0.2704	0.0552	1	-0.5094
Na2O	0.2341	-0.1509	0.1931	-0.3213	0.1044	1.0000	-0.1716	0.0892	-0.5094	1
P2O5	-0.3875	-0.0057	-0.1768	-0.1076	-0.0618	0.0101	0.1395	0.4570	-0.1310	0.0101
LOI	-0.4839	-0.2007	-0.4887	-0.2677	0.1766	-0.2619	-0.0488	0.3339	0.0920	-0.2619
S	-0.0223	0.0588	-0.0496	0.0581	-0.0324	-0.0918	-0.3263	0.1495	0.3591	-0.0918
As	-0.1112	0.1021	-0.1973	0.1445	0.1555	-0.2897	-0.0159	-0.1561	0.3180	-0.2897
Co	0.2522	-0.2974	0.2376	-0.3610	-0.1346	0.2677	0.2342	-0.2173	-0.1804	0.2677
Ni	-0.3519	-0.0372	0.1700	-0.2426	0.0410	0.1491	0.3987	0.2444	-0.1853	0.1491
Cu	0.1019	0.3068	-0.0467	0.2869	0.1974	0.0792	-0.5447	-0.0087	0.1357	0.0792
Zn	-0.0643	0.5184	0.0400	0.5119	0.2839	-0.1970	-0.1529	-0.4833	0.1866	-0.1970
Pb	-0.1044	0.1396	-0.0553	0.1066	0.1467	-0.1340	-0.1306	-0.0917	0.2654	-0.1340
Rb	0.0177	-0.0180	-0.0994	-0.0173	-0.1581	-0.3449	-0.3701	0.0239	0.7188	-0.3449
Sr	-0.2411	-0.1468	-0.1270	-0.2638	0.0521	0.2674	-0.2412	0.6526	-0.0430	0.2674
Y	-0.1469	0.5084	0.1481	0.4722	0.0281	-0.1802	0.2218	-0.2417	-0.1661	-0.1802
Zr	-0.1961	0.4495	0.2487	0.3477	-0.1096	-0.0009	0.2104	-0.0127	-0.1676	-0.0009
Ba	0.2200	-0.0367	0.1290	-0.0195	-0.2007	-0.3264	-0.0765	-0.1288	0.6034	-0.3264
Ga	-0.0897	0.5553	0.2586	0.5720	0.0006	-0.2533	0.0342	-0.3267	0.0854	-0.2533

EIGAN VALUES

EIGEN	EV	ZVAR	CUMZ
1	4.727	18.907	18.907
2	3.694	14.777	33.684
3	3.085	12.341	46.024
4	2.584	10.336	56.360
5	2.340	9.359	65.719
6	1.446	5.786	71.505
7	1.202	4.809	76.314
8	0.976	3.904	80.217
9	0.860	3.440	83.657
10	0.719	2.874	86.532
11	0.562	2.247	88.779

CAMPBELL SHEAR ZONE DATA
PROCESSED BY PCA25 (Webb, 1988)

Chlorite-carbonate schist saamples
n=90

12	0.525	2.099	90.878
13	0.429	1.716	92.594
14	0.401	1.605	94.199
15	0.345	1.379	95.578
16	0.274	1.097	96.675
17	0.214	0.857	97.532
18	0.187	0.749	98.280
19	0.163	0.651	98.931
20	0.089	0.354	99.285
21	0.067	0.267	99.552
22	0.061	0.244	99.796
23	0.046	0.183	99.979
24	0.005	0.021	100.000

PRINCIPAL COMPONENT MATRIX

	1	2	3	4	5	6	7	8	9	10
SiO2	-0.025	-0.096	0.433	-0.186	-0.097	-0.041	0.285	0.240	0.130	0.096
TiO2	0.292	0.267	-0.074	-0.112	0.118	-0.191	-0.173	0.098	0.060	-0.025
Al2O3	0.034	0.224	0.281	0.002	-9.219	0.128	-0.410	-0.172	-0.273	0.055
Fe2O3	0.334	0.254	-0.015	-0.025	0.109	-0.242	-0.069	-0.066	-0.003	0.078
MnO	0.034	0.073	-0.215	-0.058	0.436	-0.014	-0.087	-0.463	0.092	-0.053
Na2O	-0.277	0.140	0.146	-0.351	0.156	0.138	-0.074	-0.011	-0.189	-0.206
MgO	-0.069	0.223	0.047	0.438	-0.108	0.204	0.030	-0.343	-0.035	0.116
CaO	-0.213	-0.139	-0.427	-0.104	-0.045	-0.092	-0.026	-0.072	-0.134	-0.039
K2O	0.205	-0.346	-0.033	0.020	-0.268	0.102	-0.190	0.49	-0.111	0.051
Na2O	-0.277	0.140	0.146	-0.351	0.156	0.138	-0.074	-0.011	-0.189	-0.206
P2O5	-0.103	0.178	-0.376	-0.011	-0.201	0.215	0.140	0.346	-0.002	0.109
LOI	-0.973	-0.226	-0.228	0.288	0.254	-0.078	-0.162	0.140	0.192	-0.234
S	0.147	-0.089	-0.159	-0.300	-0.210	0.267	0.160	-0.131	0.095	-0.157
As	0.235	-0.133	-0.055	0.074	0.170	0.367	0.241	-0.102	-0.387	0.020
Co	-0.198	0.017	0.247	0.107	-0.008	0.258	-0.304	0.038	0.544	-0.188
Ni	-0.194	0.176	-0.159	0.179	-0.043	0.213	-0.406	0.172	-0.113	0.328
Cu	0.142	-0.056	-0.029	-0.393	0.143	-0.090	-0.230	0.036	0.129	0.601
Zn	0.334	0.031	0.041	-0.038	0.279	0.278	-0.092	0.104	0.118	-0.099
Pb	0.209	-0.066	-0.089	-0.138	0.063	0.553	-0.001	-0.026	0.180	0.054
Rb	0.175	-0.326	-0.028	-0.028	-0.126	-0.012	-0.375	0.207	-0.051	-0.212
Sr	-0.183	-0.022	-0.286	-0.297	-0.216	-0.085	-0.165	-0.180	0.110	-0.146
Y	0.177	0.337	-0.094	0.014	-0.152	-0.014	0.120	0.046	0.333	-0.154
Zr	0.077	0.346	-0.157	0.104	-0.339	0.033	0.068	-0.018	0.057	-0.035
Ba	0.164	-0.216	0.122	-0.048	-0.329	-0.104	-0.092	-0.476	0.101	-0.028
Ba	0.288	0.193	0.014	0.040	-0.050	-0.033	-0.128	0.203	-0.286	-0.419

PRINCIPAL COMPONENT ANALYSIS

CAMPBELL SHEAR ZONE DATA
PROCESSED BY PCA25 (Webb, 1988)

Chlorite-carbonate schist samples
n=90

| Tag	1	2	3	4	5	6	7	8	9	10
I144911	1.898	-0.233	-1.768	0.087	-1.234	-1.129	-1.391	-1.748	-0.860	0.758
I144913	-2.448	0.448	-0.520	-1.516	-3.393	0.152	-0.456	-0.516	0.026	0.110
I144914	-3.297	0.475	-1.655	-2.469	-3.553	0.659	0.576	-1.345	-1.070	1.201
I144915	1.795	1.445	-0.111	-1.086	-0.836	-1.304	1.453	-1.057	1.281	0.857
I144910	-0.292	-1.577	-0.906	0.393	-1.556	-0.594	0.250	0.390	-0.370	-0.350
I144912	-2.278	-1.163	1.170	-0.436	-0.344	-0.373	-0.656	0.088	-1.610	-0.097
I144301	-0.072	-1.809	0.340	-1.440	-1.096	-1.766	0.735	0.749	0.056	-0.077
I144902	-0.549	-0.565	-1.168	0.479	-2.732	0.090	-0.843	-0.598	1.045	-0.160
I144906	-3.124	0.891	-1.593	-0.052	-2.119	2.001	0.634	-0.390	1.204	-0.105
I144904	-0.486	-0.484	-0.473	-0.281	0.208	-0.477	-0.174	-0.133	0.271	-0.240
I144905	-1.747	-2.391	-1.064	1.688	0.497	-0.911	-0.677	0.432	0.361	0.961
I144903	-2.011	-2.153	-1.063	1.414	0.686	-0.414	-0.069	0.167	0.204	0.875
I1180	2.574	4.776	-3.037	1.025	0.830	-1.620	-0.419	1.451	0.200	0.106
I1181	1.103	1.269	0.432	-1.231	0.787	-0.126	-0.011	0.157	-0.346	-0.615
I10301	1.721	-2.774	-1.087	-0.406	-0.876	-0.541	-0.221	0.008	-0.215	-0.303
I1190	-0.739	-2.157	-0.203	-0.673	0.360	0.767	-0.493	-0.554	0.971	-0.682
I4134	0.992	0.944	0.323	-0.645	0.156	-0.589	-0.806	-0.132	0.210	-0.158
I1182	3.271	-1.519	-1.142	-0.305	0.475	1.615	0.402	-0.862	-1.761	0.015
I4119	1.008	1.483	-0.575	-1.618	0.638	-0.994	1.367	-0.260	0.298	-0.601
I10303	-1.792	0.553	0.439	1.311	-0.804	0.201	0.058	-1.085	0.780	-3.358
I10304	-2.746	3.098	-6.580	0.478	-0.966	2.509	1.460	3.495	-0.162	0.651
I4120	-0.180	1.051	-0.803	-0.898	1.682	-0.560	0.575	-0.304	-0.791	-0.118
I4121	0.604	0.797	0.156	-0.893	0.382	-0.247	-1.099	-0.323	0.258	-0.206
I4122	-1.862	-0.028	0.110	0.302	1.376	-0.340	-1.328	0.473	-0.538	-0.335
I41238	3.410	-0.957	-0.752	-0.311	0.112	1.078	-0.650	-0.214	0.630	0.144
I4123A	0.148	2.591	2.452	4.891	-0.135	0.694	1.151	-0.800	-0.359	0.641
I1191	-3.039	0.887	1.459	0.906	1.286	0.526	0.158	0.169	0.872	0.237
I4124	4.045	0.976	-0.397	-0.369	-0.690	1.310	-0.055	-0.239	0.386	-0.150
I4133	0.629	1.354	1.415	-0.528	-0.828	-1.644	-1.497	1.150	0.866	-0.141
I144907	0.323	0.874	0.277	-1.662	0.787	-0.452	0.308	-0.527	-0.449	-1.049
I144908	0.645	0.784	-0.132	-1.684	0.129	-0.817	0.255	-0.929	-0.172	0.040
I1184	3.755	-0.922	0.206	-2.482	-0.235	3.354	-0.338	0.664	0.574	0.311
I4132	-1.933	-0.638	-0.642	-0.402	1.389	-0.352	-0.541	-0.317	0.036	-0.029
I10305	0.404	-0.596	-0.809	0.939	1.280	-1.390	-1.250	-0.344	-0.508	0.688
I1177	1.747	-1.487	-0.251	0.707	-0.396	-1.170	1.203	0.490	0.405	0.071
I1192	-0.418	1.898	2.245	-0.736	0.730	-0.587	0.901	-0.041	-0.205	0.030
I4125	2.506	-1.935	-0.663	-0.709	0.118	0.271	0.196	0.129	0.323	0.040
I1178	1.145	-3.208	1.308	1.261	-1.322	-0.105	1.013	1.026	-0.001	-0.423
I4131	0.840	0.664	-0.867	0.030	0.075	-1.889	-0.417	0.219	1.587	-0.640
I1176	-1.695	-0.253	0.098	1.762	1.184	-0.260	-0.720	0.208	-0.663	-0.916
I4130	-0.383	-4.026	-1.058	2.027	-0.229	0.929	-1.618	0.971	-0.313	-0.116
I4126	-0.080	3.496	1.988	5.112	-1.038	0.902	1.133	-0.957	0.714	0.255
I1173	-1.922	0.560	1.284	-1.311	0.359	0.057	0.375	-0.241	0.794	-0.849
I10311	0.398	-1.456	1.384	2.015	-0.683	-0.112	0.243	-0.092	0.253	1.662

CAMPBELL SHEAR ZONE DATA
PROCESSED BY PCA25 (Webb, 1988)

Chlorite-carbonate schist saamples
n=90

X10307	0.069	2.002	0.469	0.327	0.348	-0.715	-1.006	0.056	1.915	0.296
X1185	-0.505	1.534	0.769	-1.466	1.527	-0.108	0.677	-0.235	-1.005	0.338
X1193	-2.002	0.115	1.198	-0.899	1.535	-0.519	0.129	0.437	-1.192	-0.210
X1179	-1.800	0.292	1.644	-0.134	0.637	0.316	0.430	0.731	-0.842	-0.214
X4127	2.085	1.113	0.620	0.263	-0.836	-0.721	0.433	1.027	0.637	0.804
X10310	-0.267	0.952	-0.732	2.784	1.327	-0.267	-1.650	-0.395	-0.194	1.280
X1194	-2.467	-0.705	0.686	-0.053	1.123	-0.860	0.012	-0.251	0.650	0.455
X1172	0.069	-1.892	0.046	.494	-0.798	-0.865	-0.206	-0.478	0.353	-0.397
X1186	-1.067	1.323	1.304	..844	2.196	3.153	-1.952	-0.733	1.612	0.293
X4128	1.034	0.407	1.295	-0.566	-1.197	0.503	0.594	-0.413	-2.597	-0.008
X10318	-1.482	0.708	1.388	-0.113	1.373	-0.292	0.627	0.473	-0.325	-0.577
X4129	-4.078	0.976	2.232	-2.485	0.804	1.723	-1.440	1.310	-0.903	-0.324
X10314	2.076	-3.473	-1.377	0.224	2.422	2.292	2.710	-2.007	0.009	0.188
X1171	1.163	0.138	-0.017	1.160	-1.200	-0.376	-1.226	0.390	-0.686	0.039
X10317	1.771	-0.761	2.918	-0.251	-1.179	-0.065	0.075	1.237	0.500	1.580
X10313	-0.138	0.123	-1.171	-0.501	1.563	-1.192	1.553	-0.093	0.053	-0.407
X1170	1.993	-2.771	0.865	1.078	-2.128	0.724	-0.161	1.058	-0.220	-1.181
X10315	-1.131	0.272	-0.605	-0.061	2.321	-0.254	0.349	0.094	-1.196	0.548
X10319	3.986	0.209	0.426	0.615	-0.597	0.739	0.078	0.829	-0.609	-0.383
X10312	0.729	2.336	0.084	0.256	0.503	0.176	0.523	-0.787	-0.330	0.395
X1187	-1.905	-0.878	0.192	-0.522	-0.197	0.257	0.736	-0.682	0.157	-0.451

<u>SINGLE ELEMENT PLOTS</u>

Individual elements analyzed from the chlorite schist data set from the Campbell Shear Zone are plotted on inclined net diagrams, simulating a 3 dimensional image. These distributions are described in the Chapter 5 of the thesis, and are presented here for convenience.

The data has been gridded onto an orthogonal grid with nodes every 32.5 m, using a quadrant search for the ten nearest samples, within a 325 m radius which are krigged to obtain a best estimate for that node.

Distribution of orebodies, stopes, and reserve blocks within the Campbell Shear Zone. Some of the mine workings are projected onto this longitudinal section for reference.
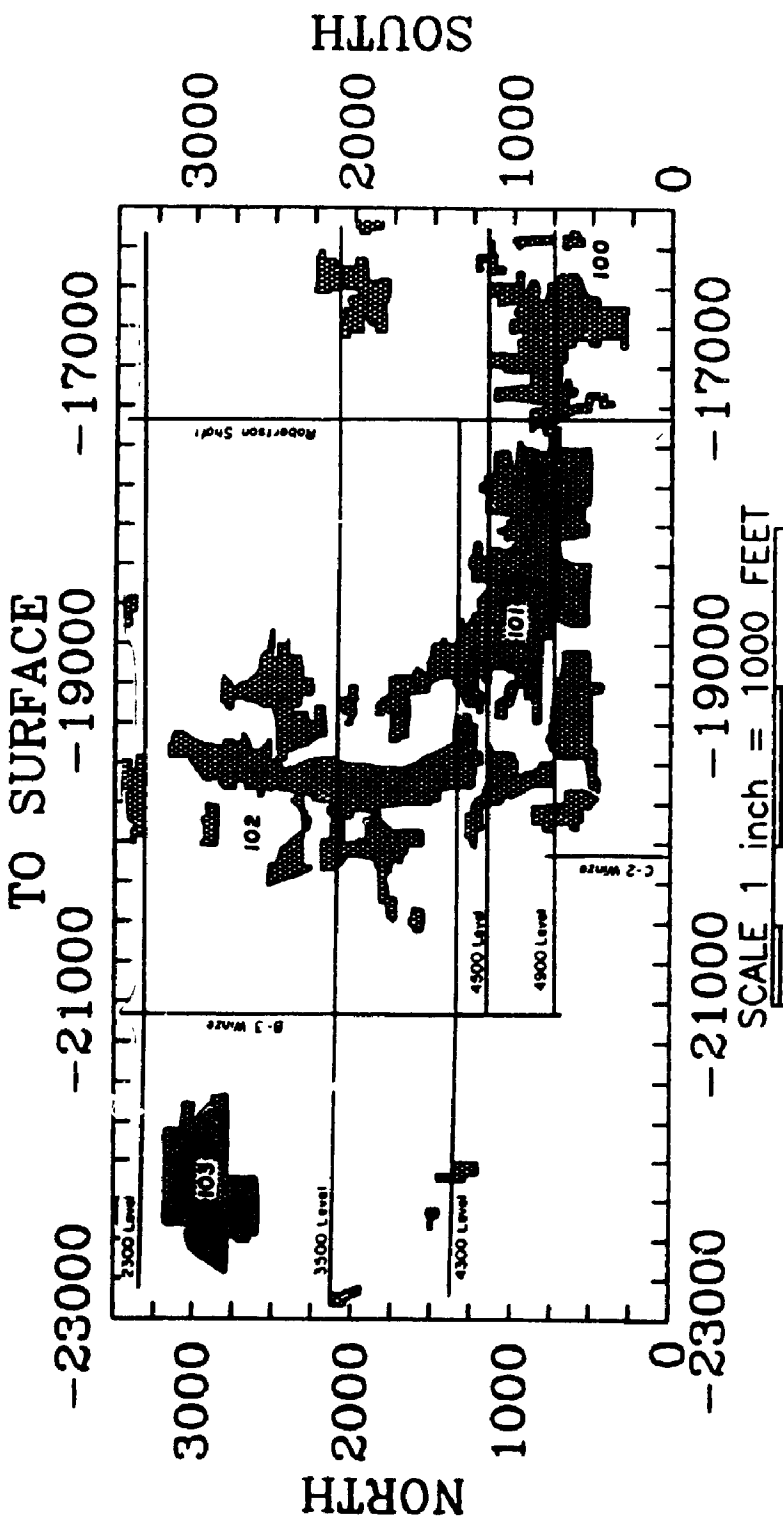
CAMPBELL SHEAR ZONE, LONGITUDINAL SECTION
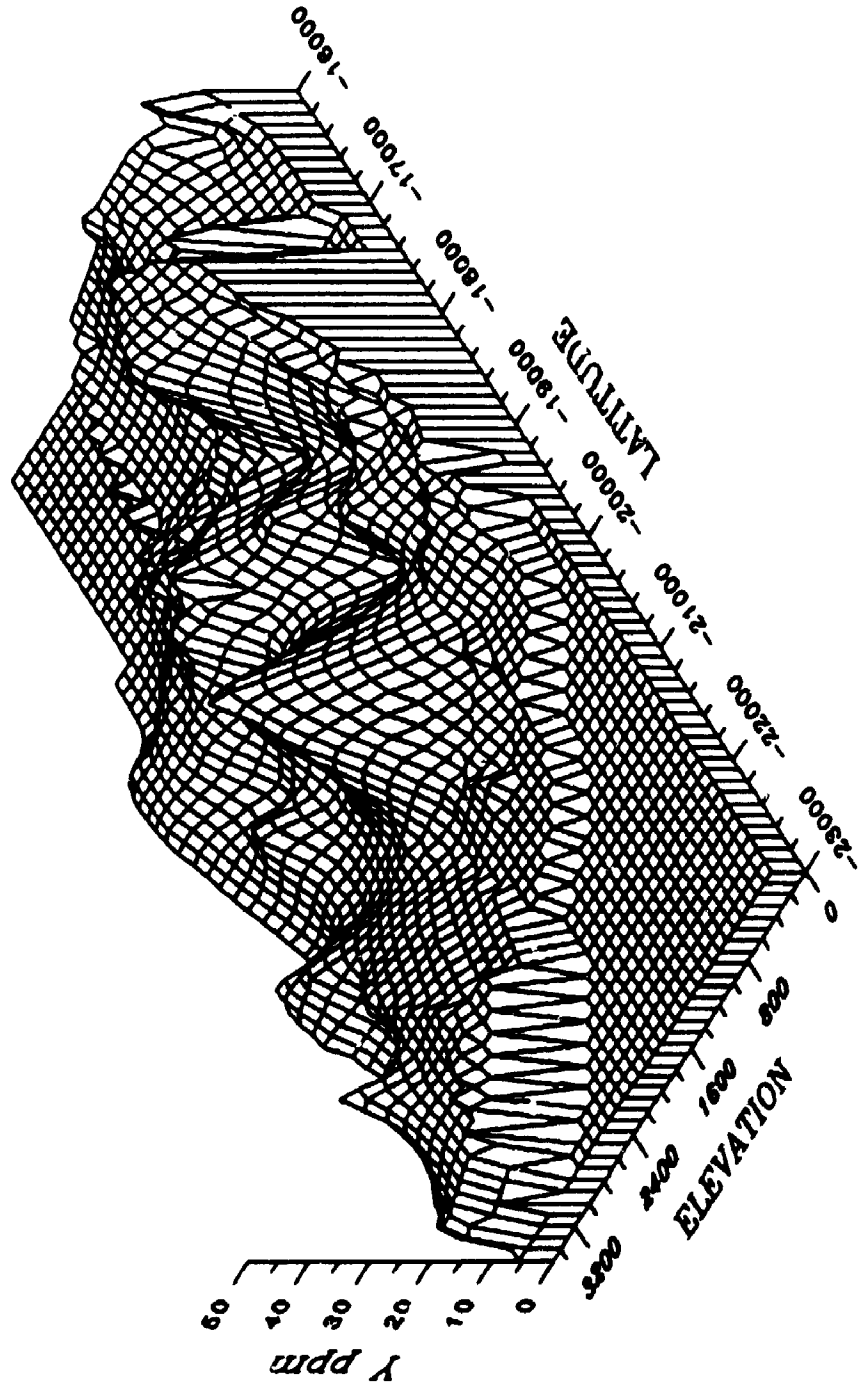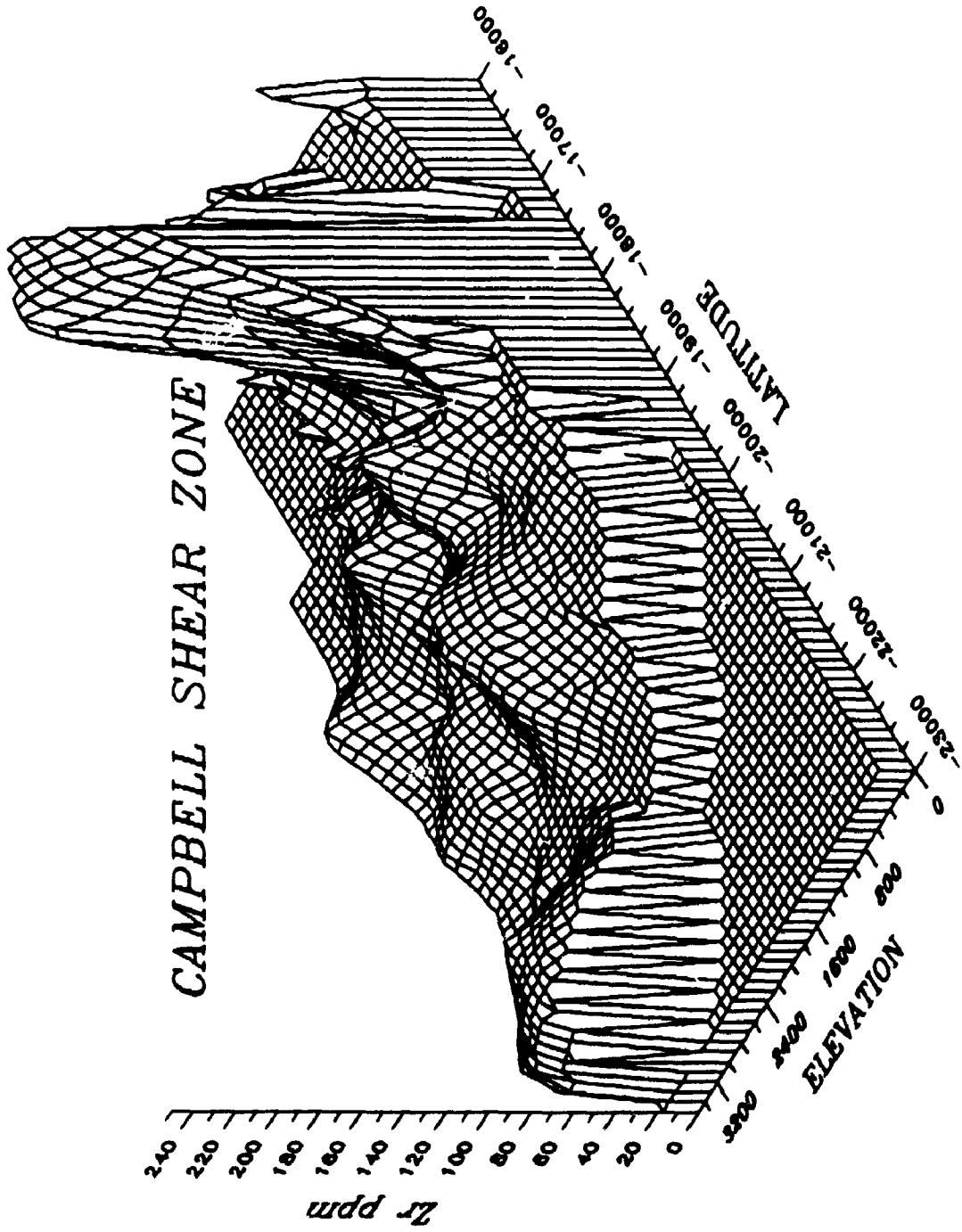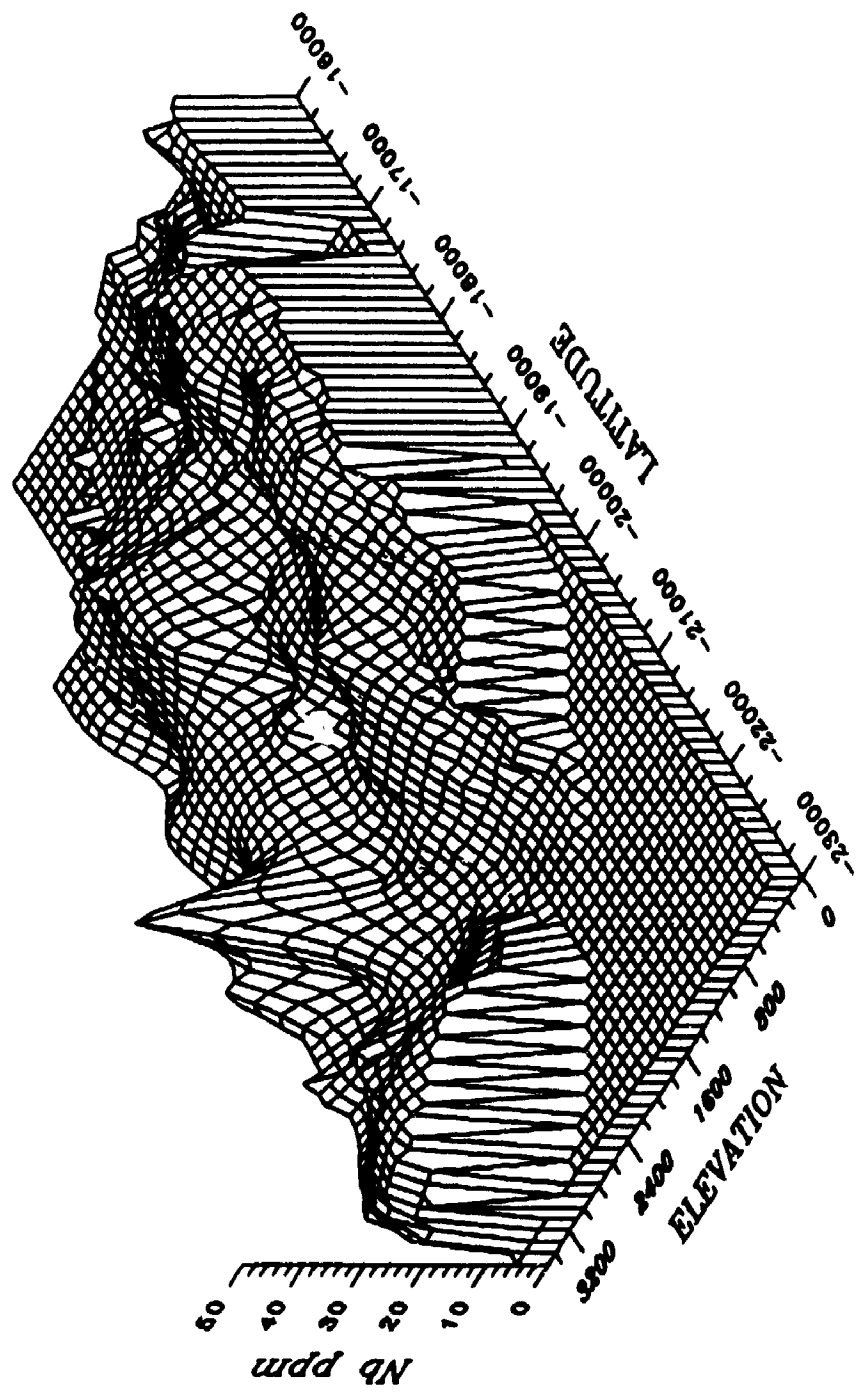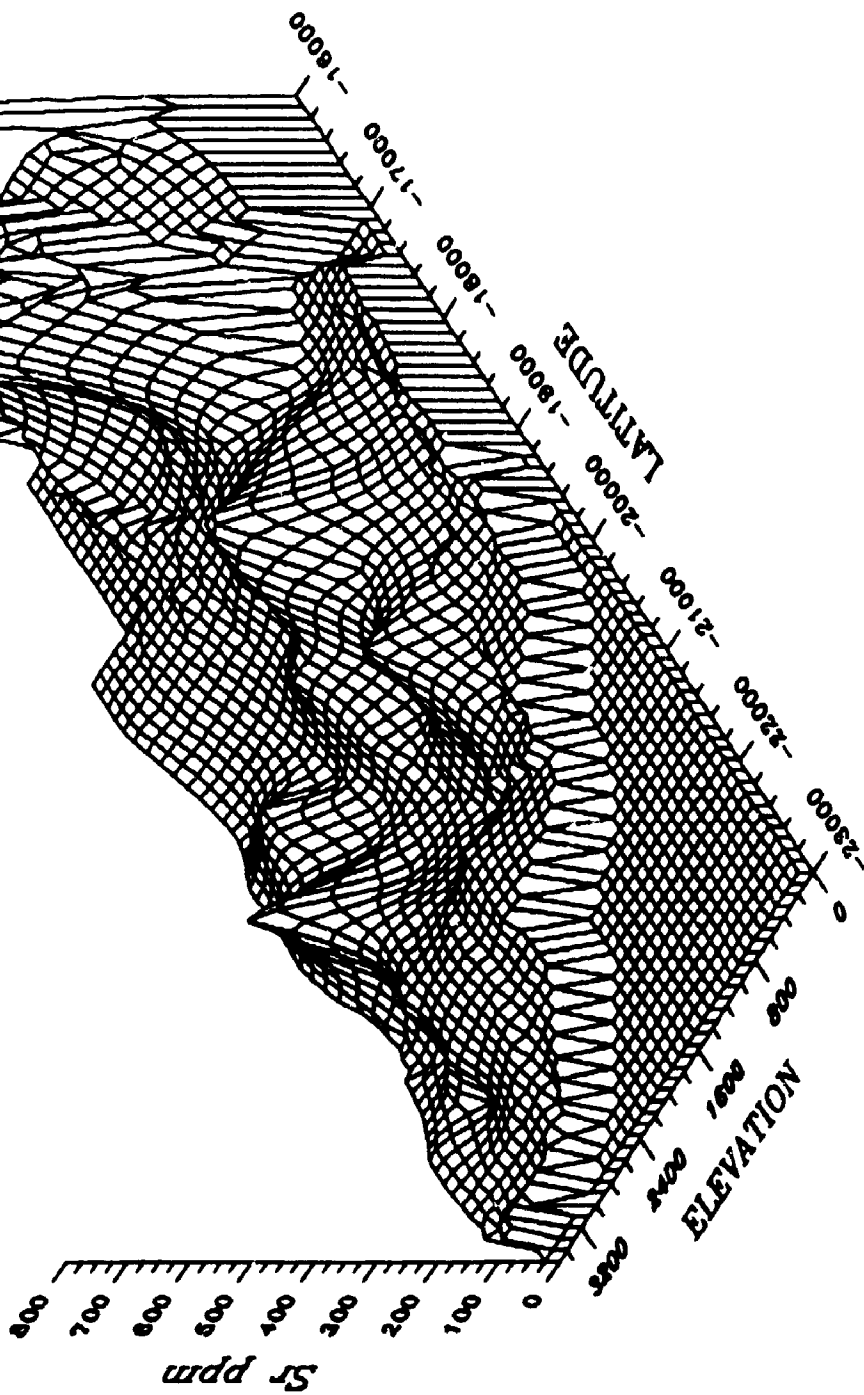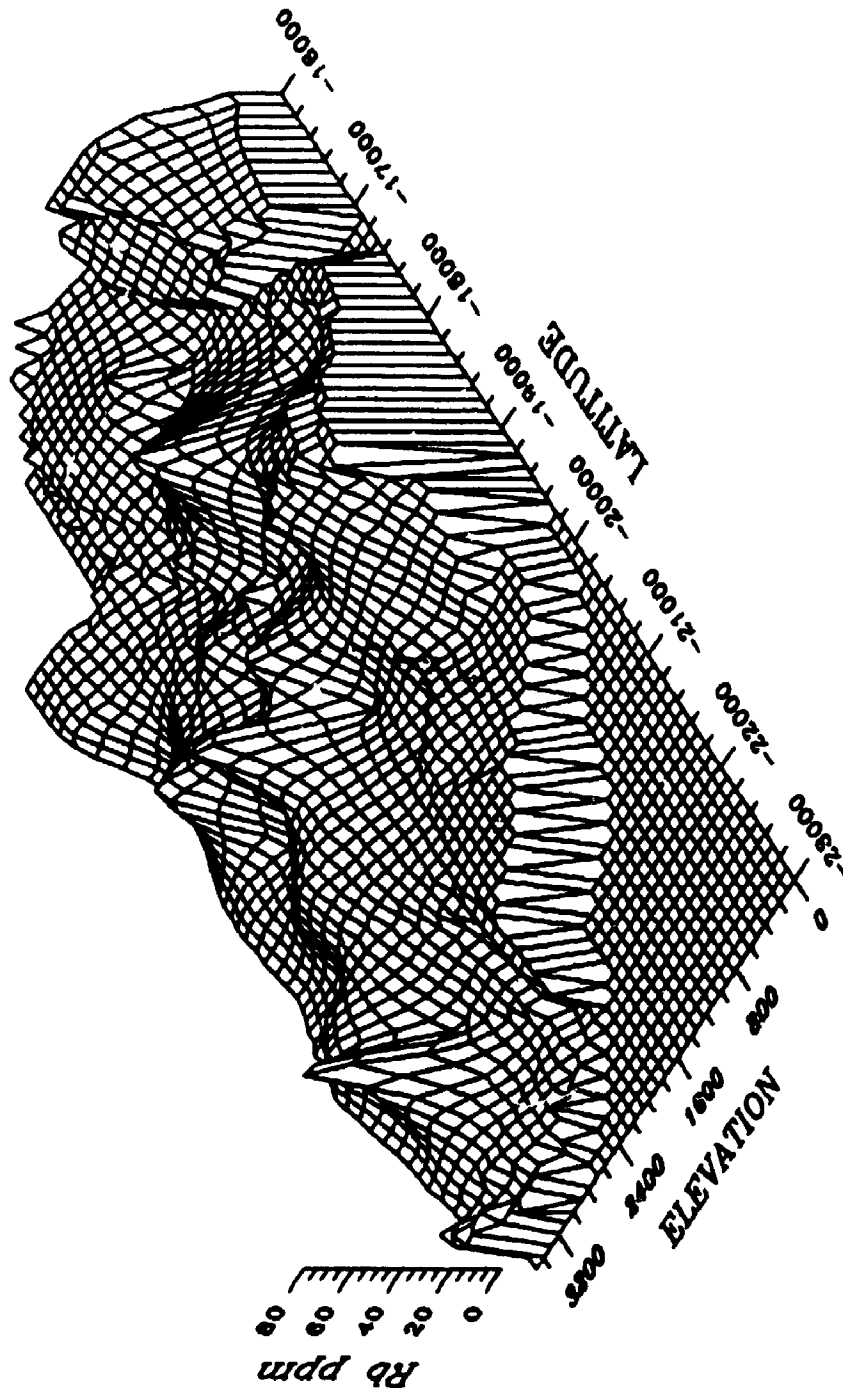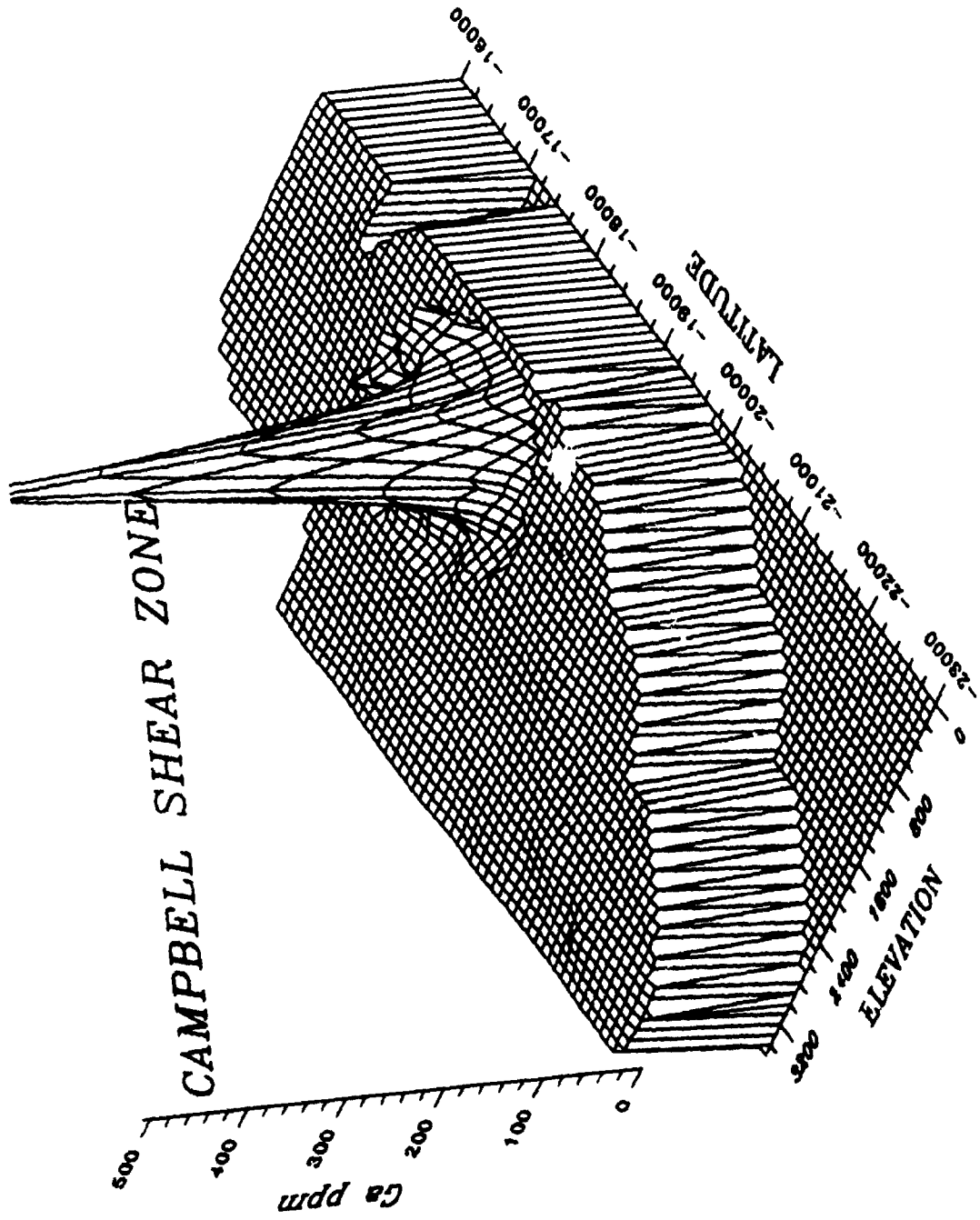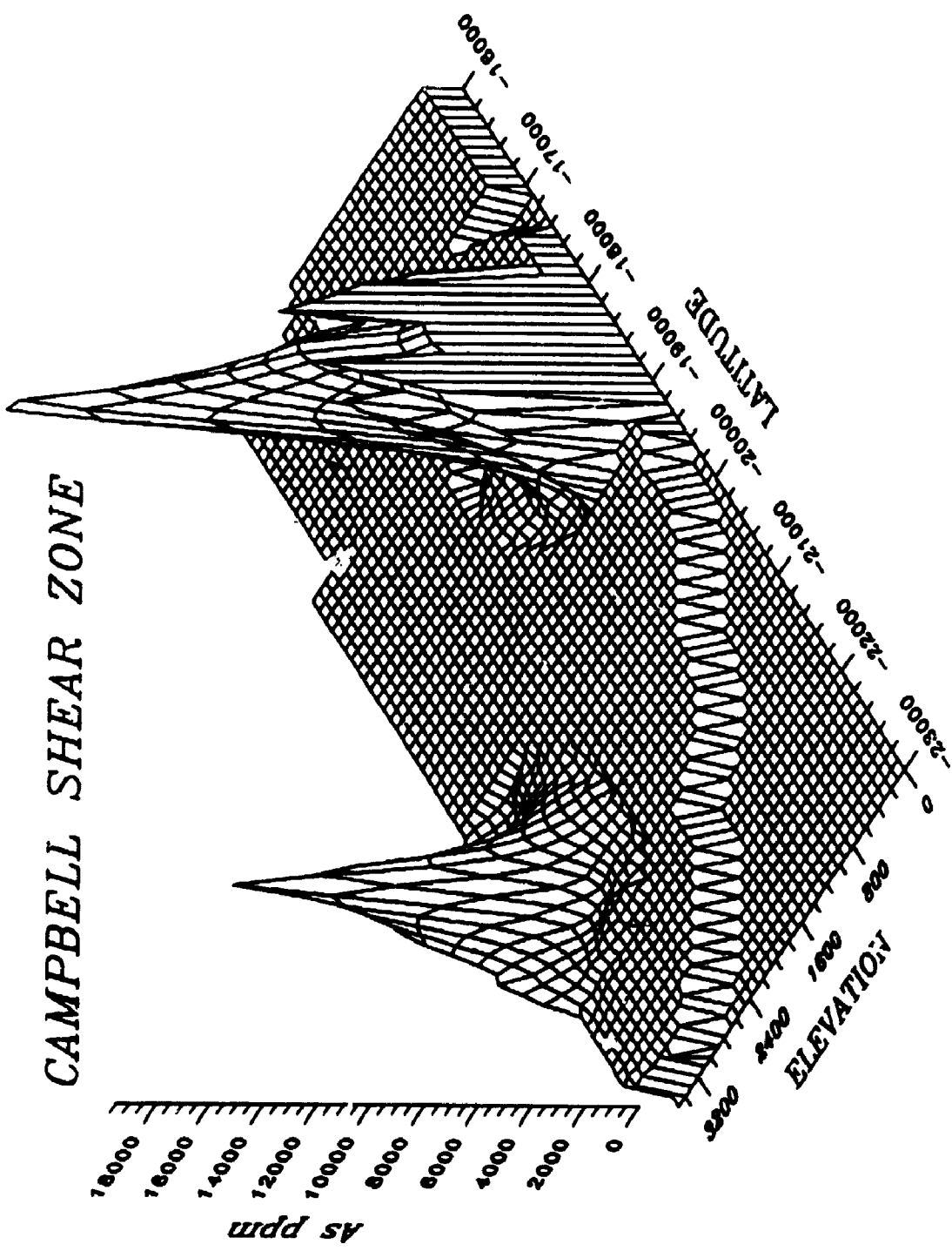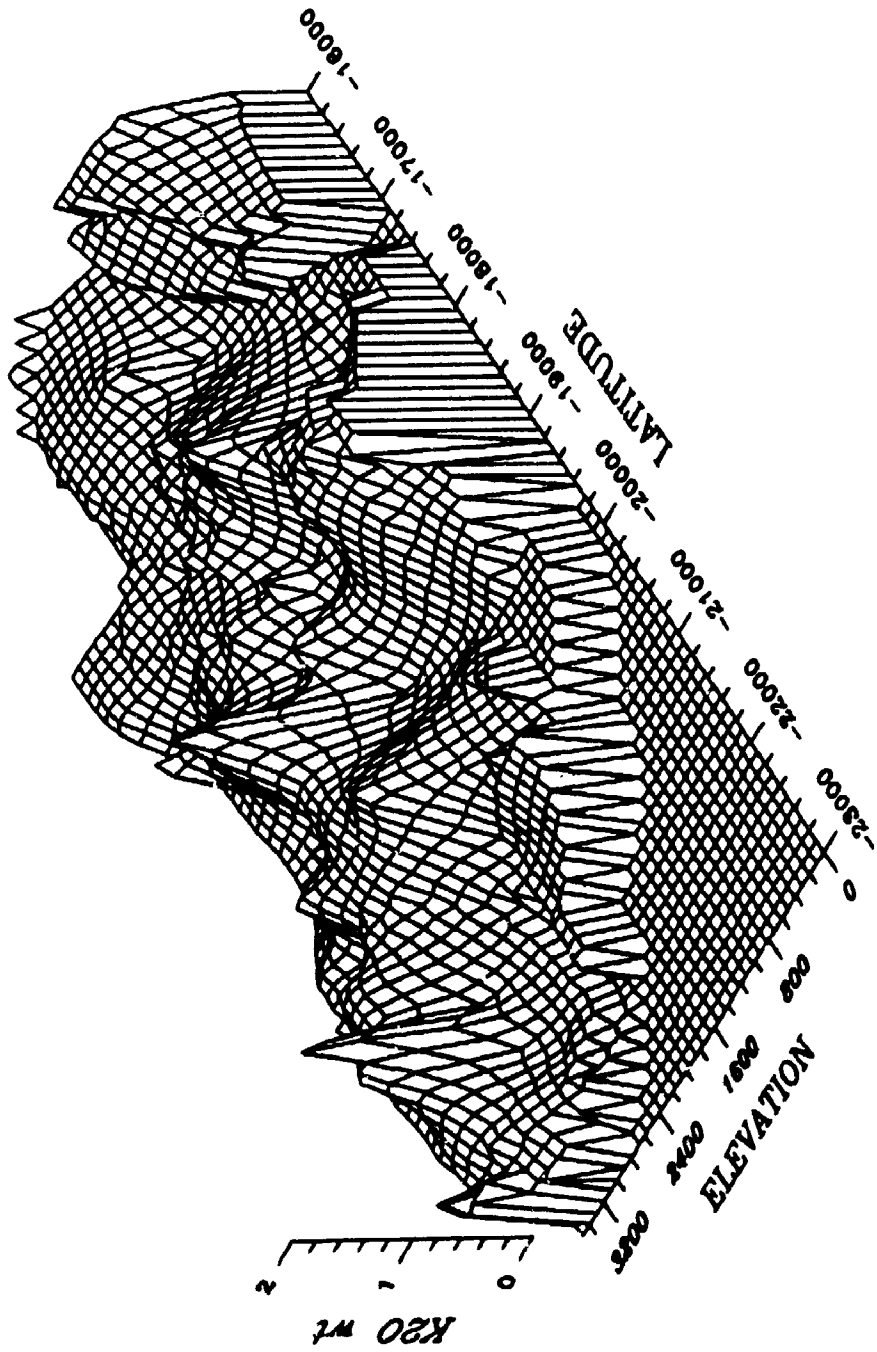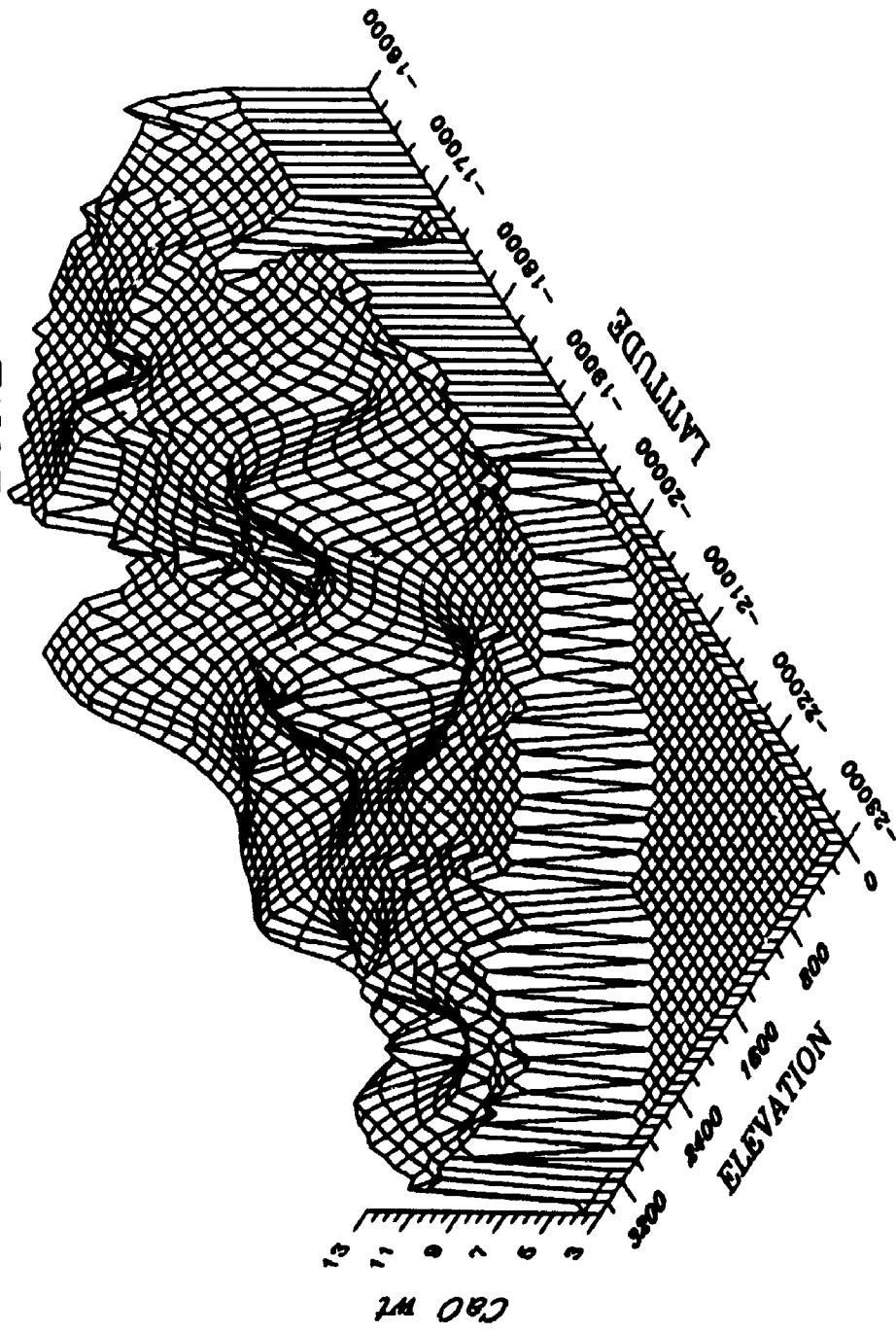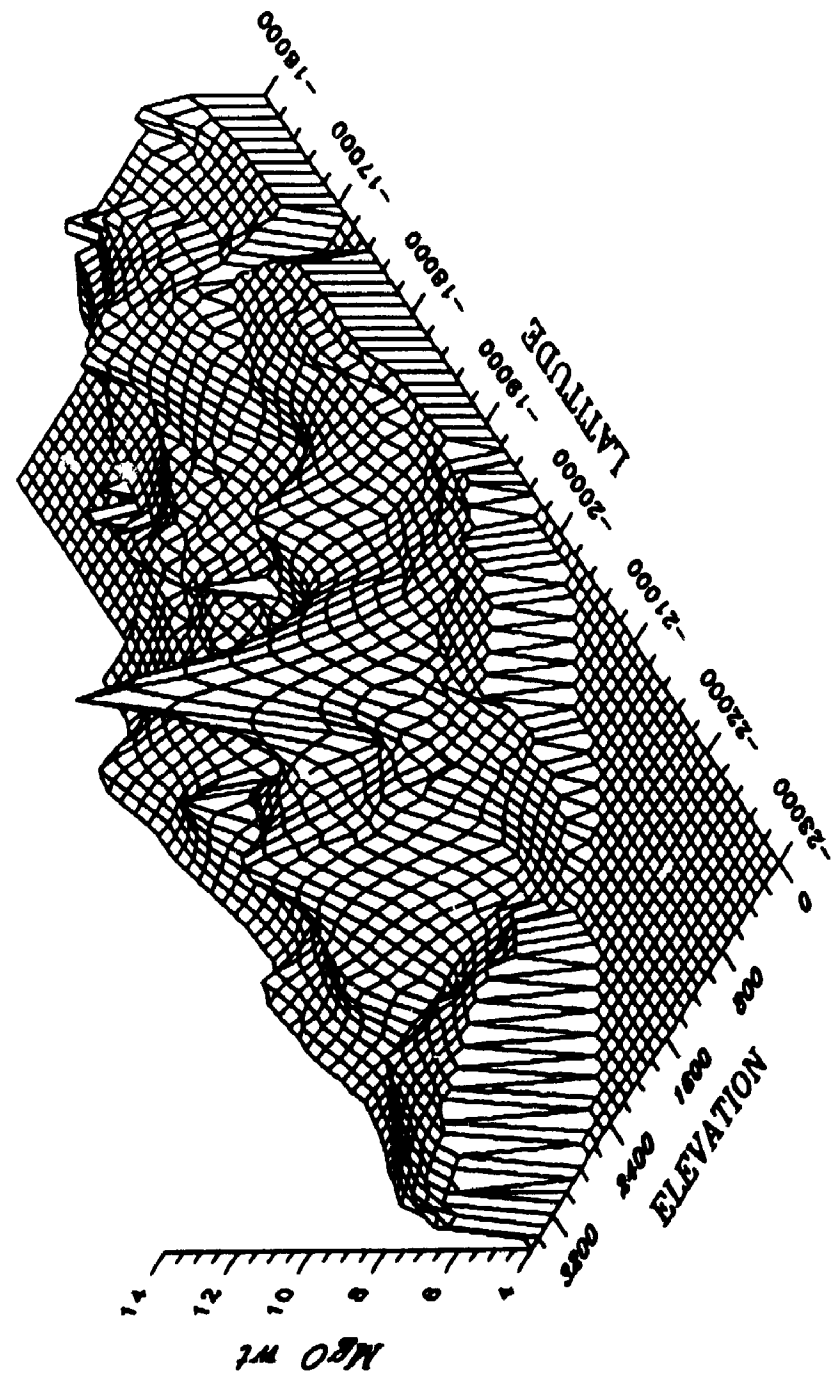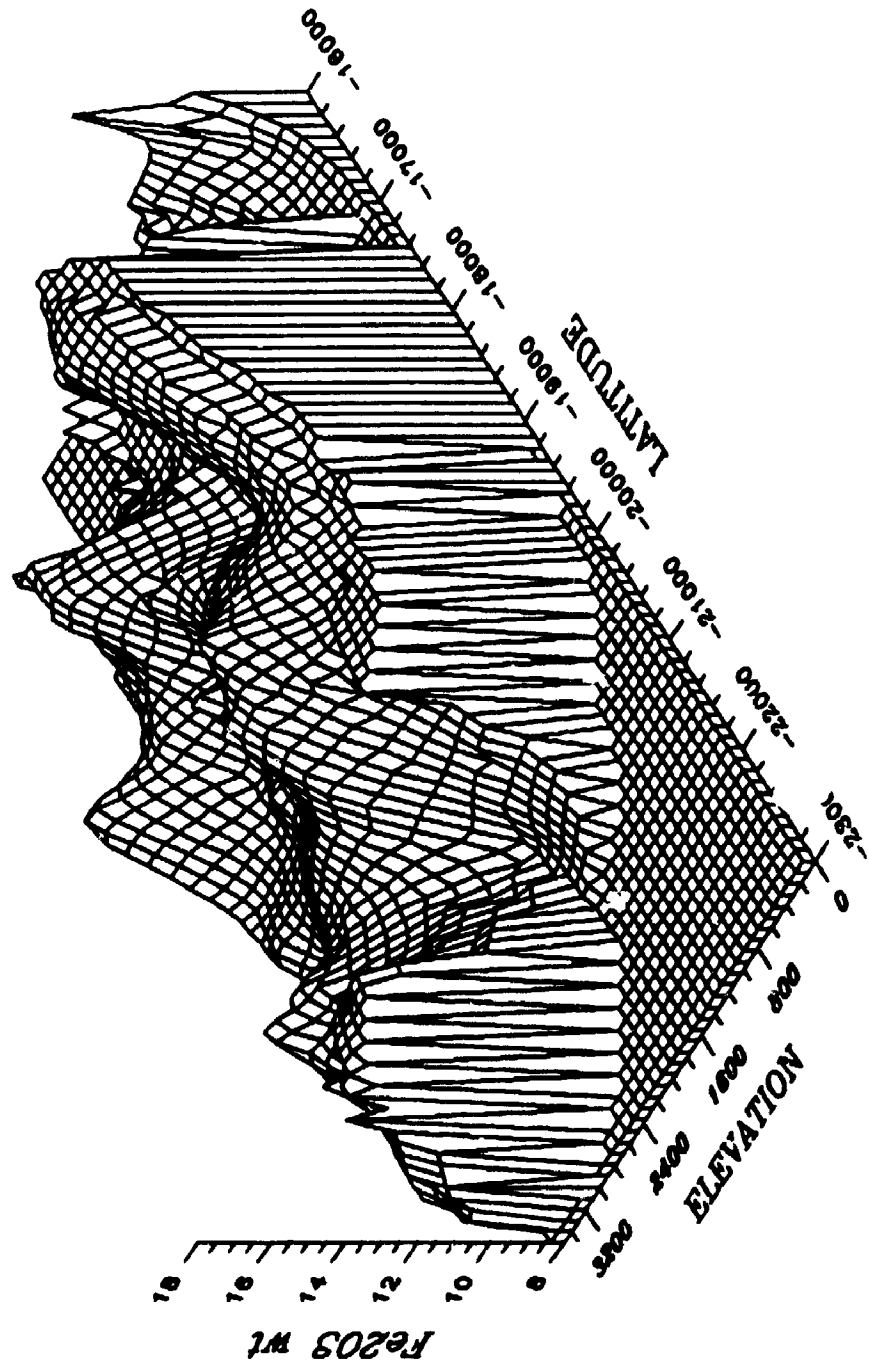
Sample Locations

SCALE 1 inch : 1000 FEET

CAMPBELL SHEAR ZONE

CAMPBELL SHEAR ZONE

CAMPBELL SHEAR ZONE

CAMPBELL SHEAR ZONE

CAMPBELL SHEAR ZONE

CAMPBELL SHEAR ZONE

Ga ppm

LATITUDE

ELEVATION

CAMPBELL SHEAR ZONE

CAMPBELL SHEAR ZONE

CAMPBELL SHEAR ZONE
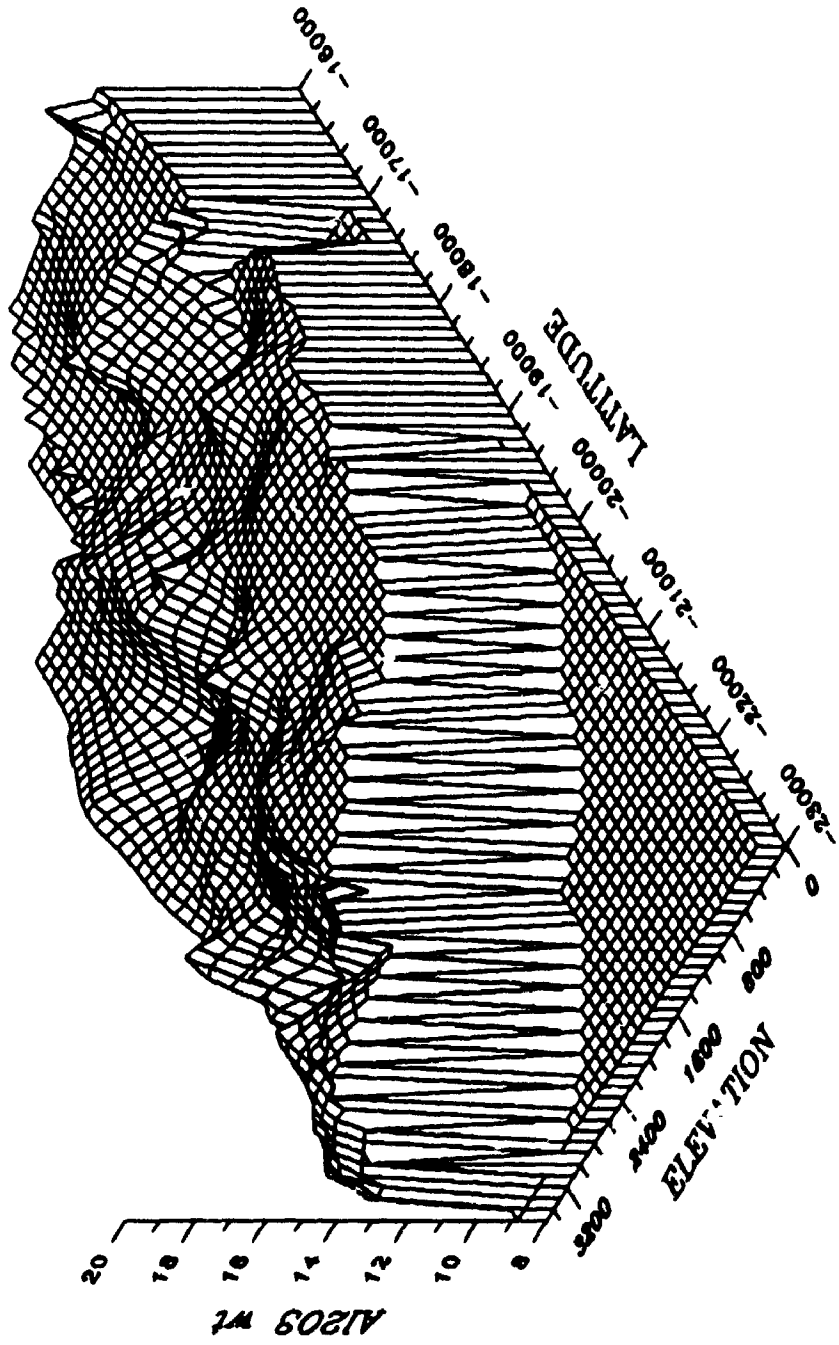
CAMPBELL SHEAR ZONE

CAMPBELL SHEAR ZONE

CAMPBELL SHEAR ZONE

CAMPBELL SHEAR ZONE

CAMPBELL SHEAR ZONE

CAMPBELL SHEAR ZONE

CAMPBELL SHEAR ZONE

LATITUDE

ELEVATION

LOI wt
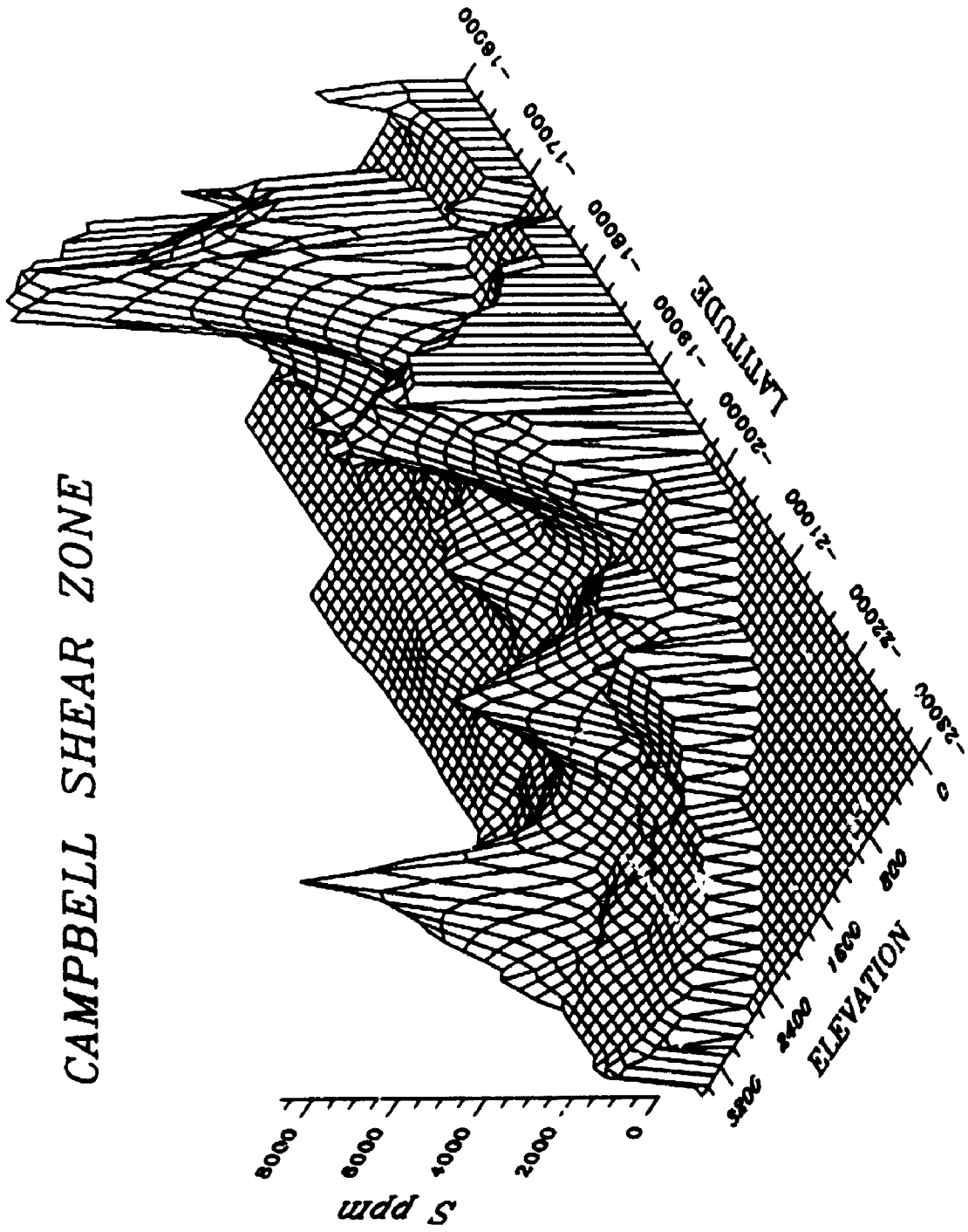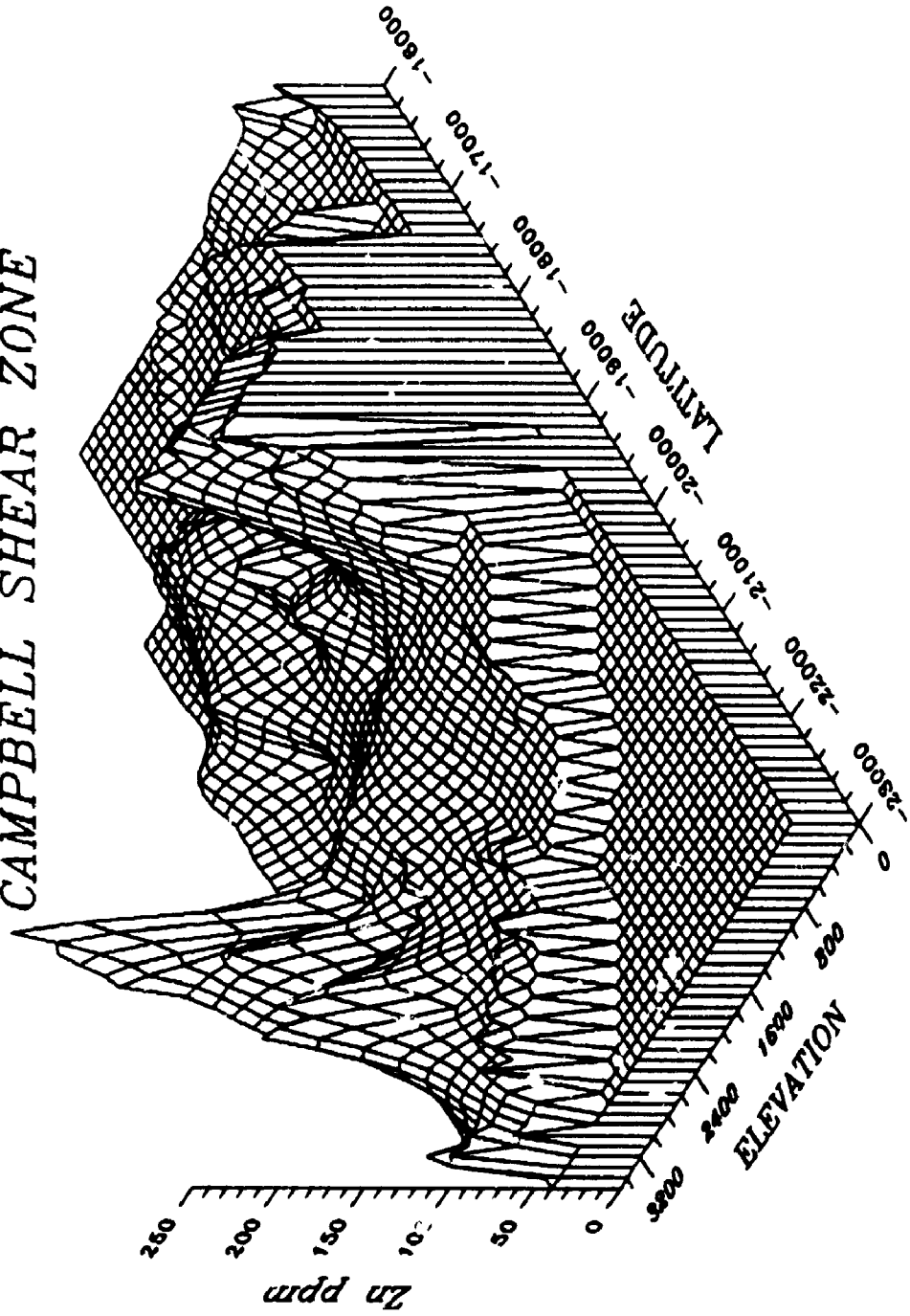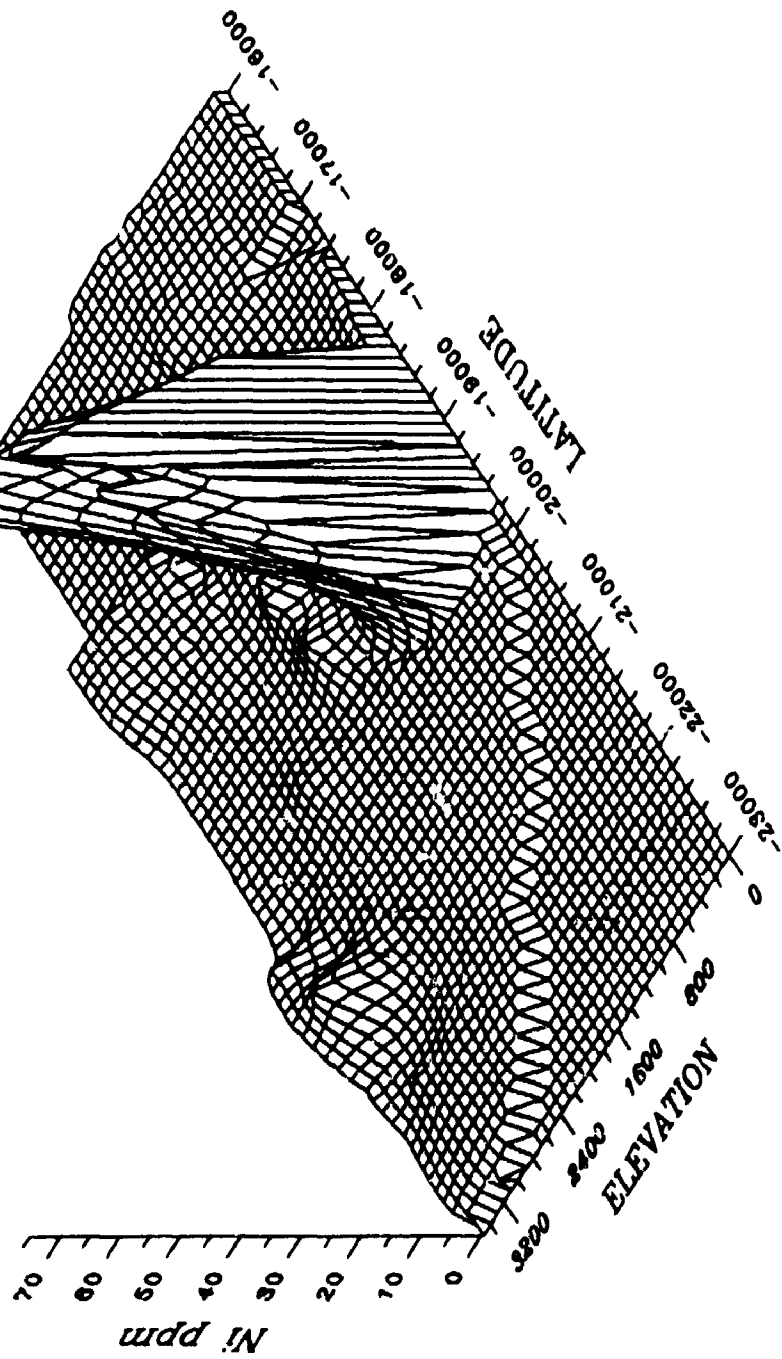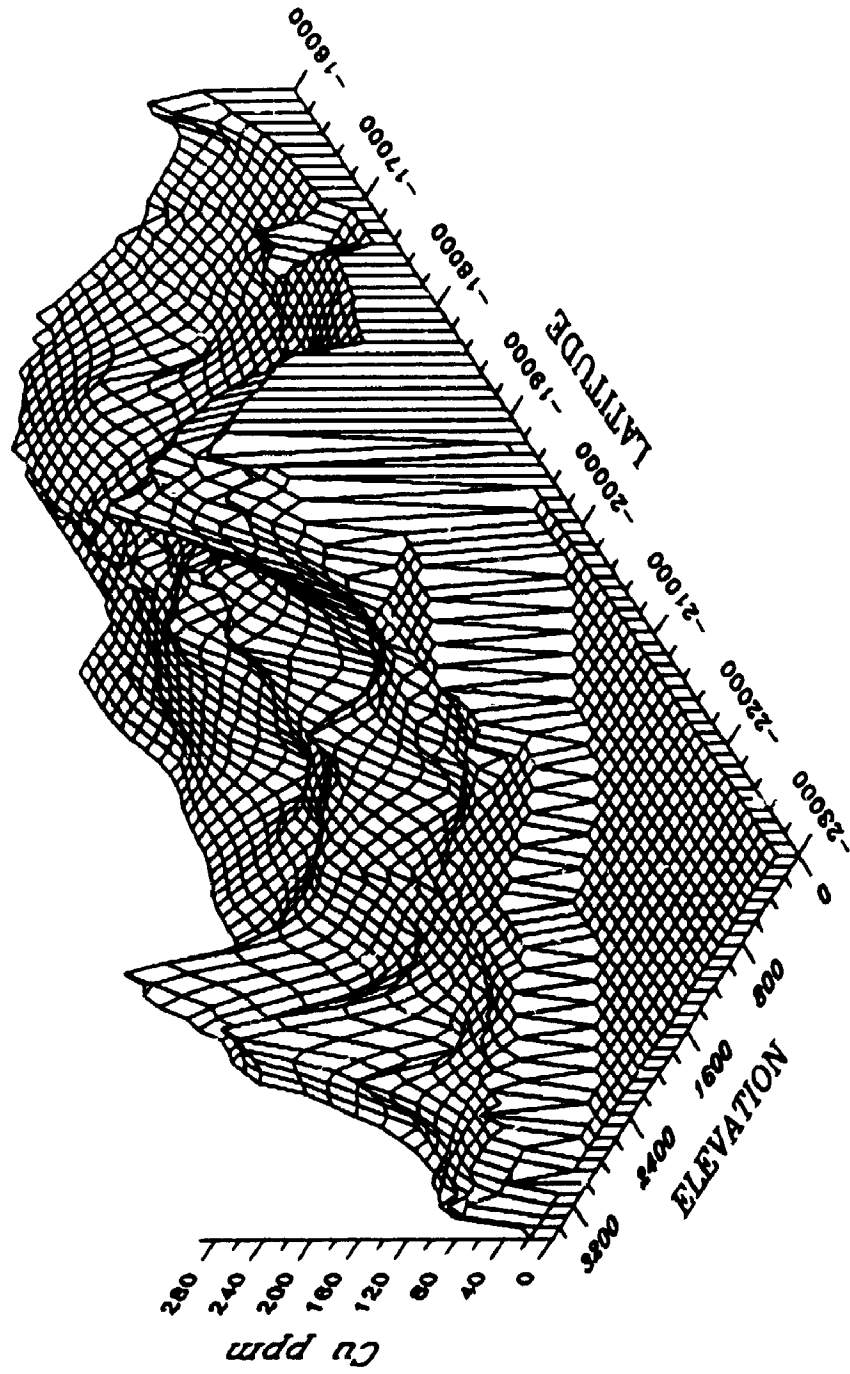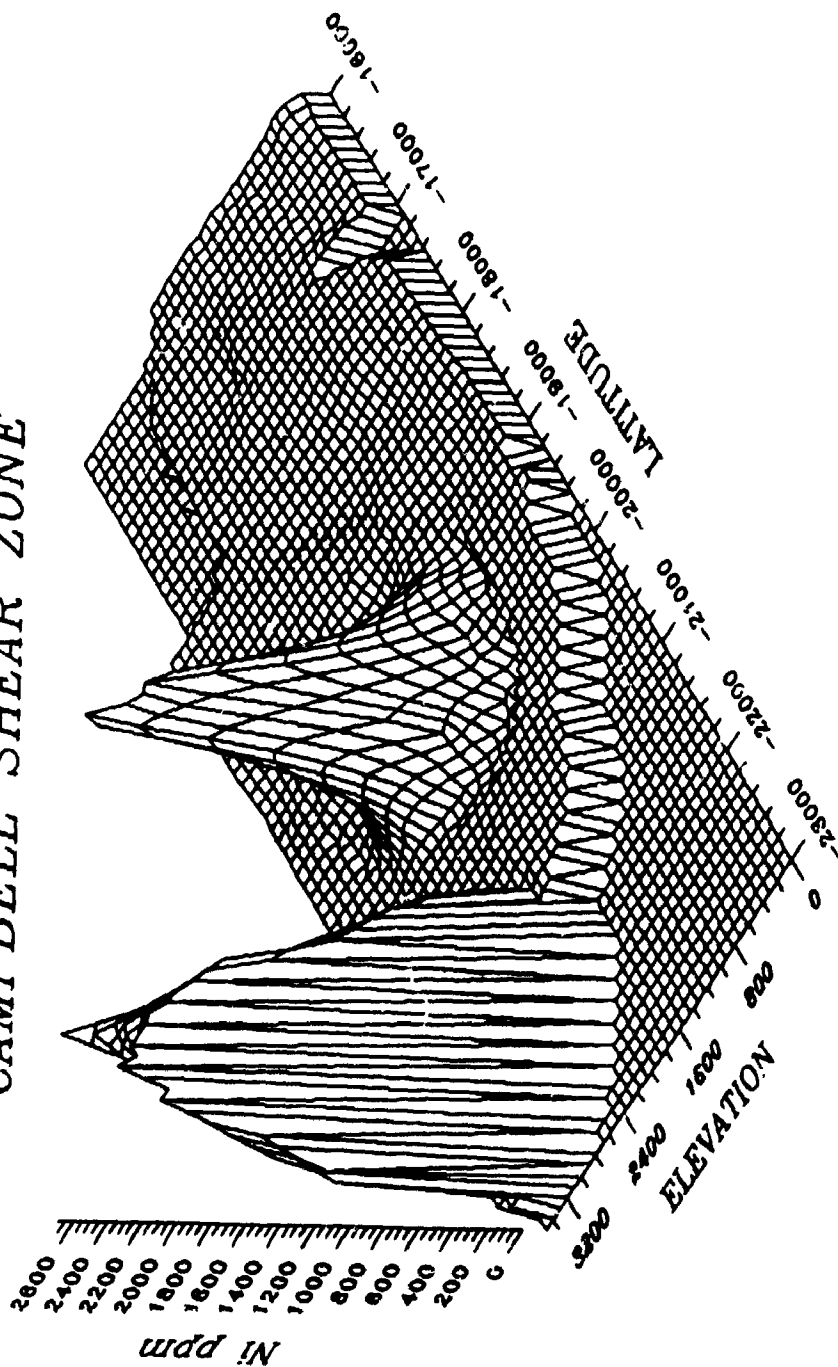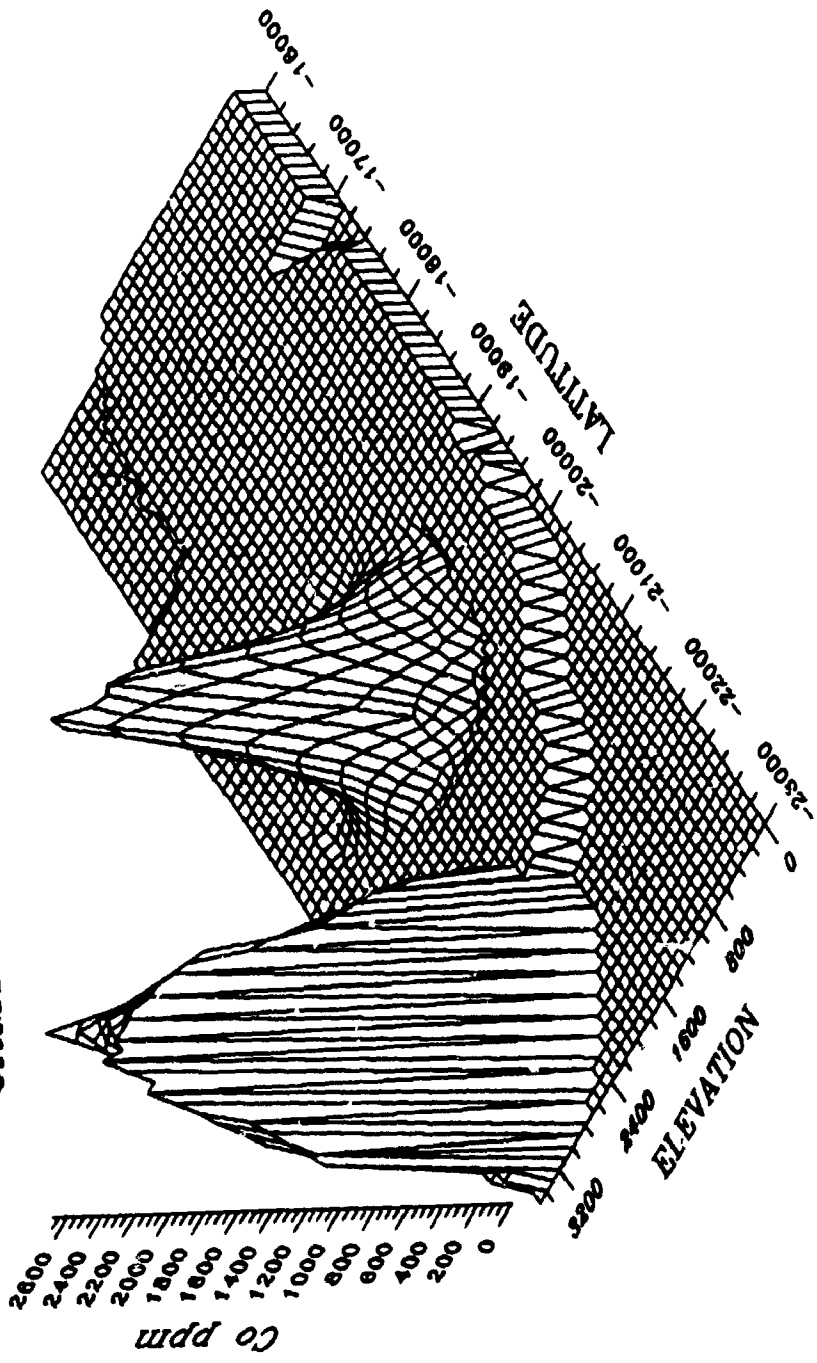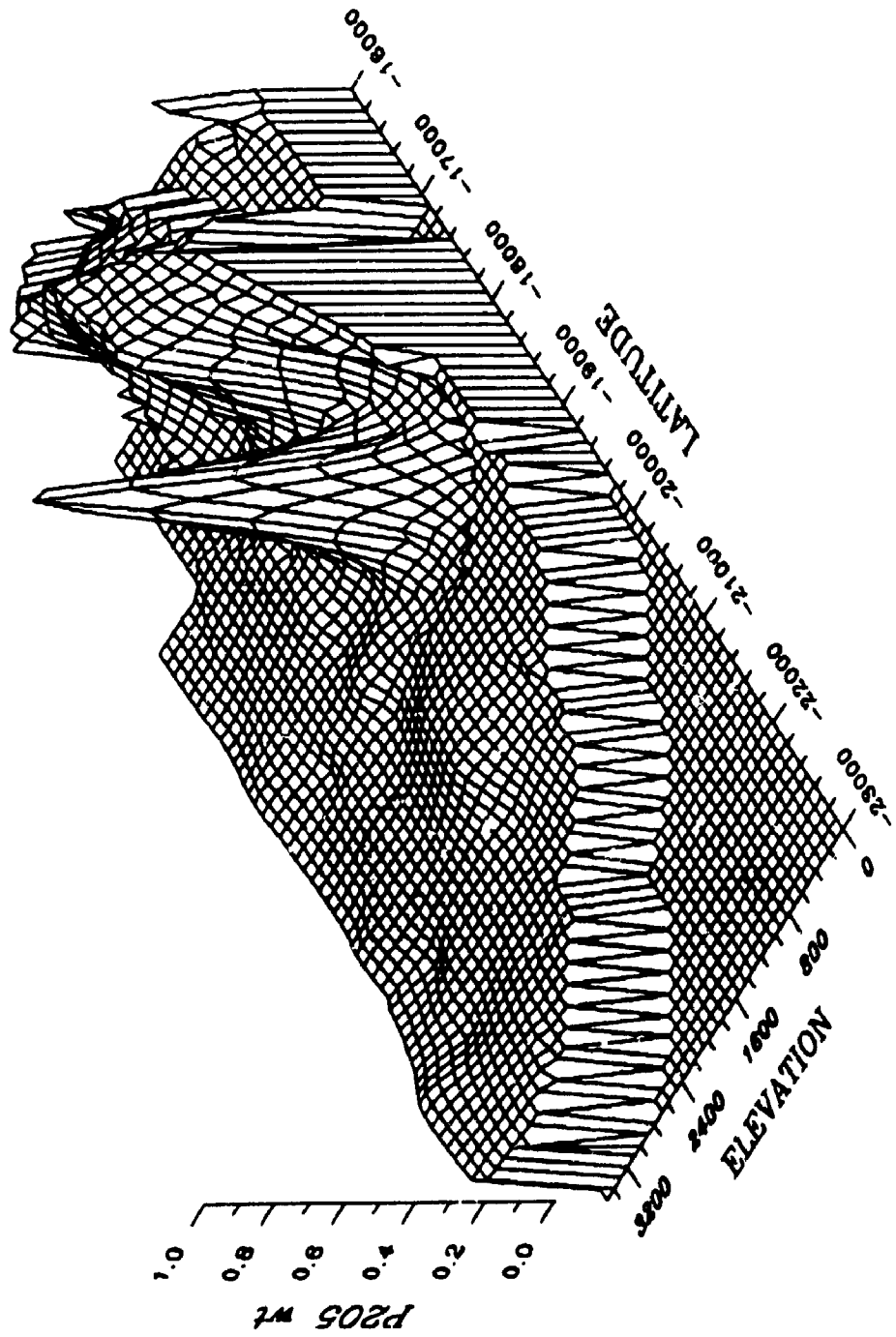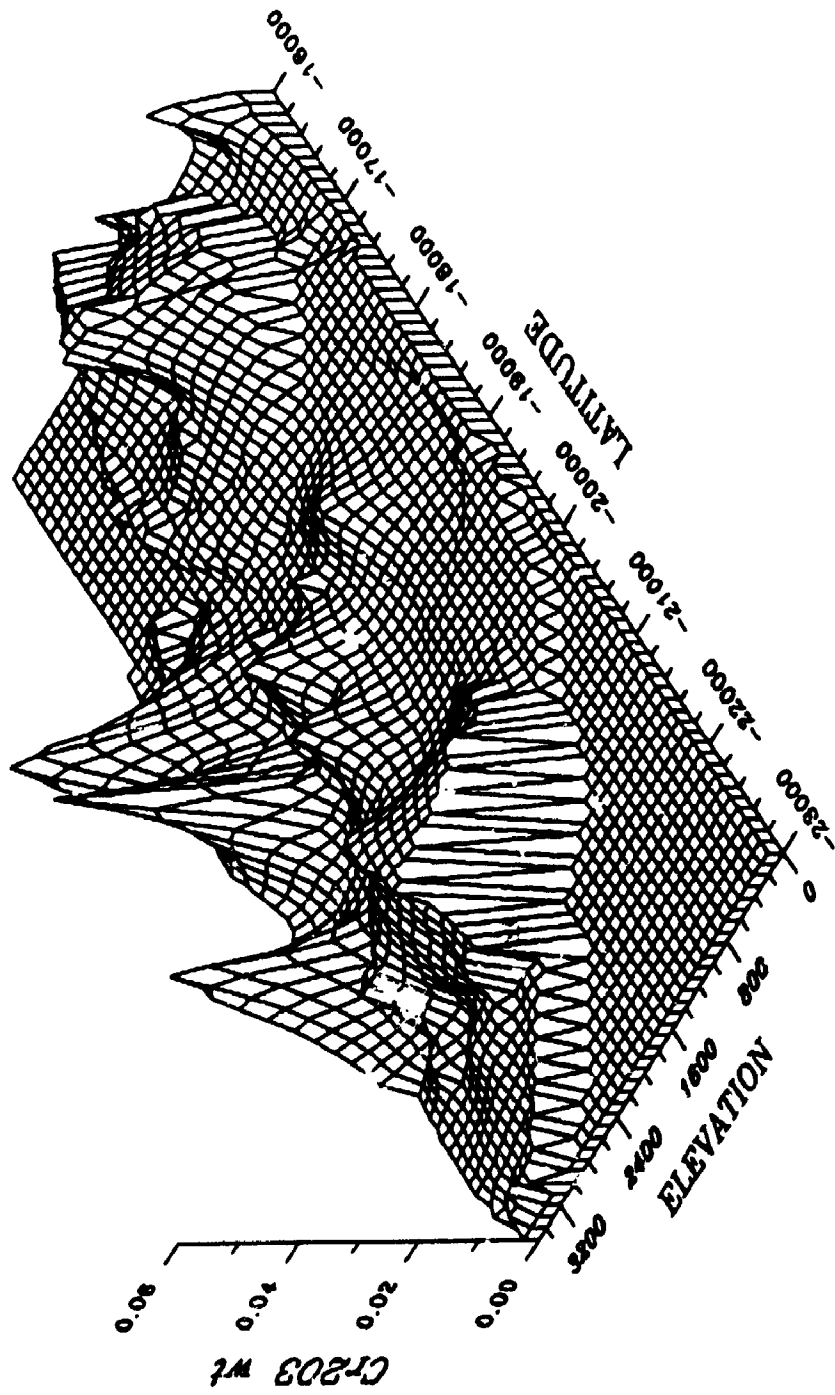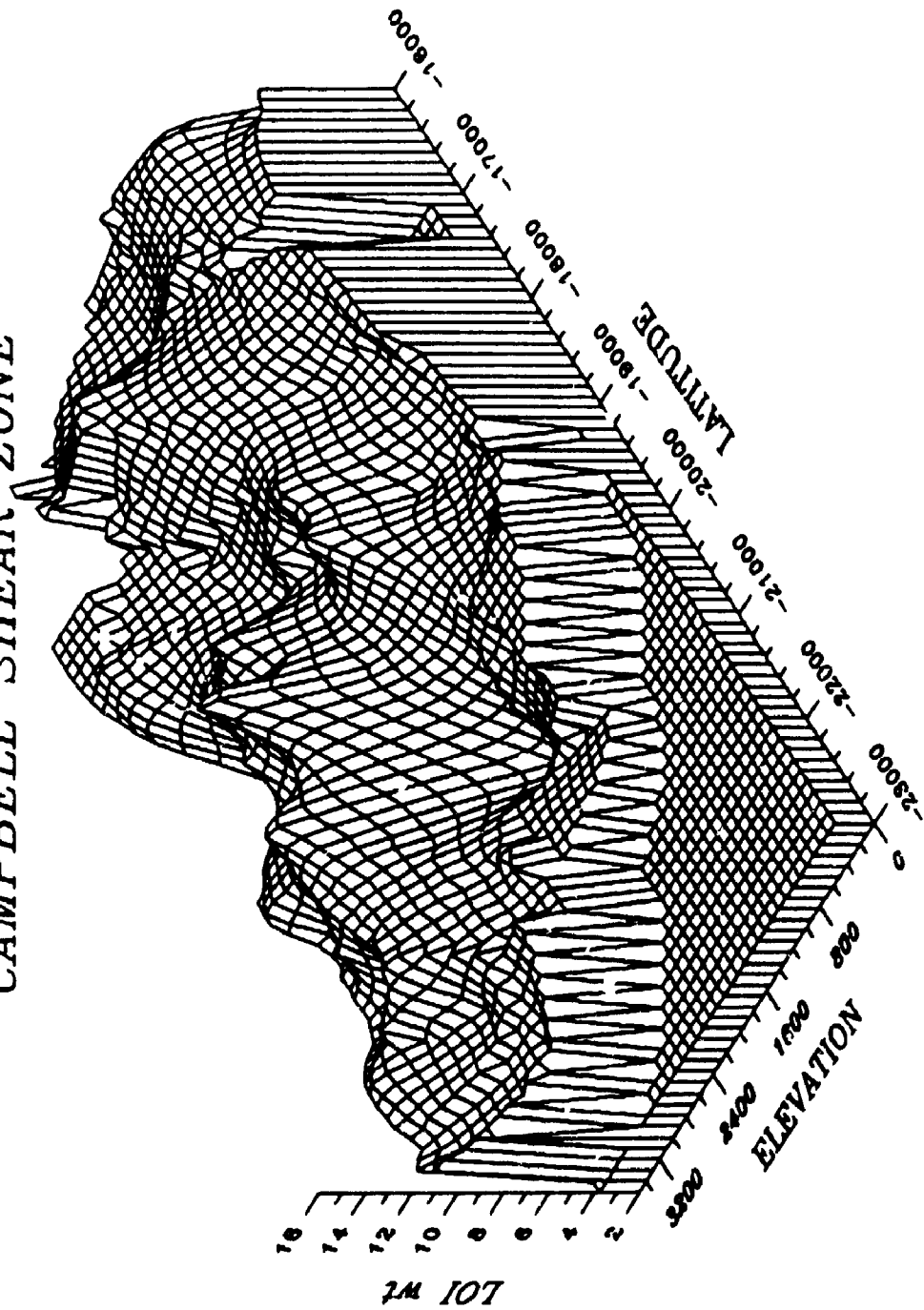
CAMPBELL SHEAR ZONE
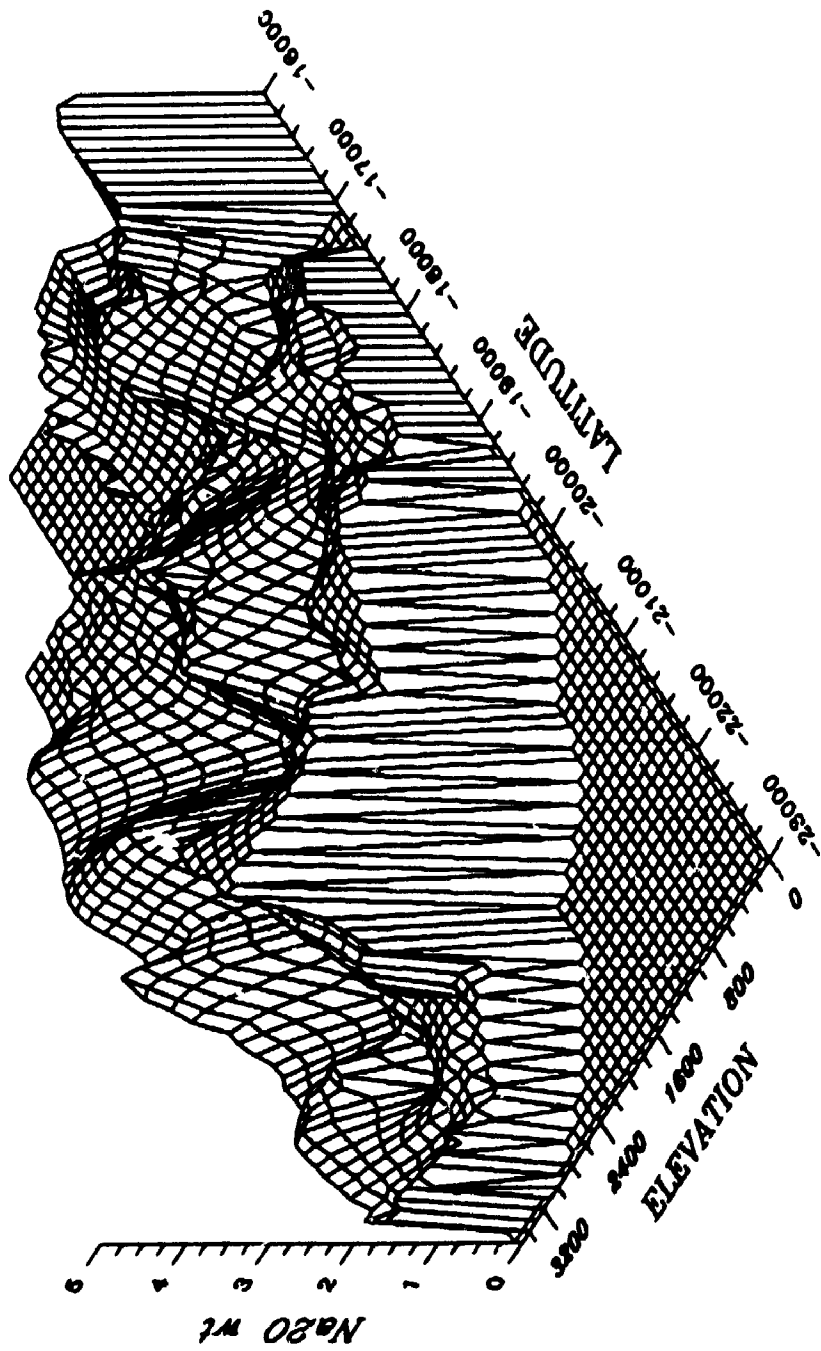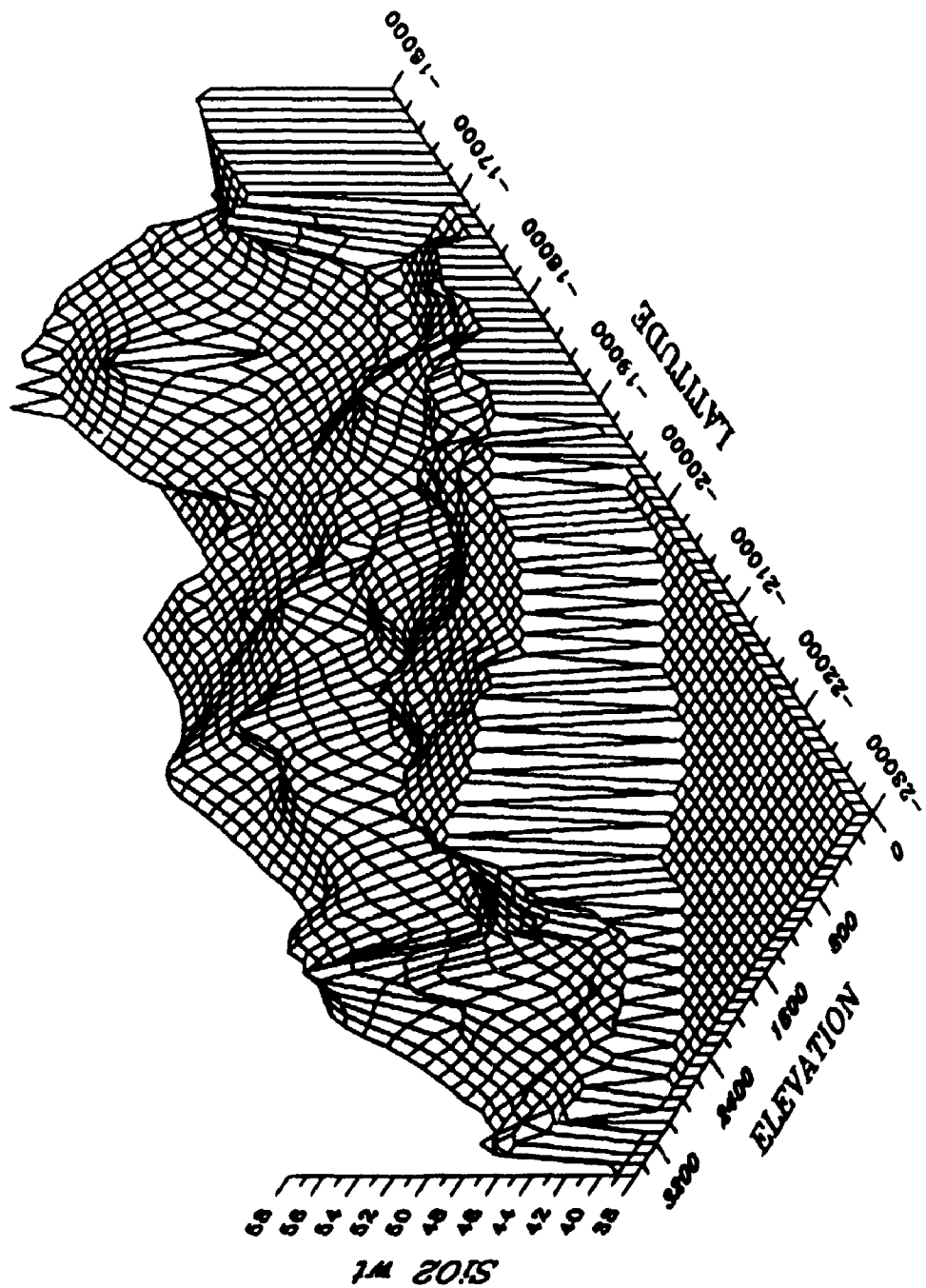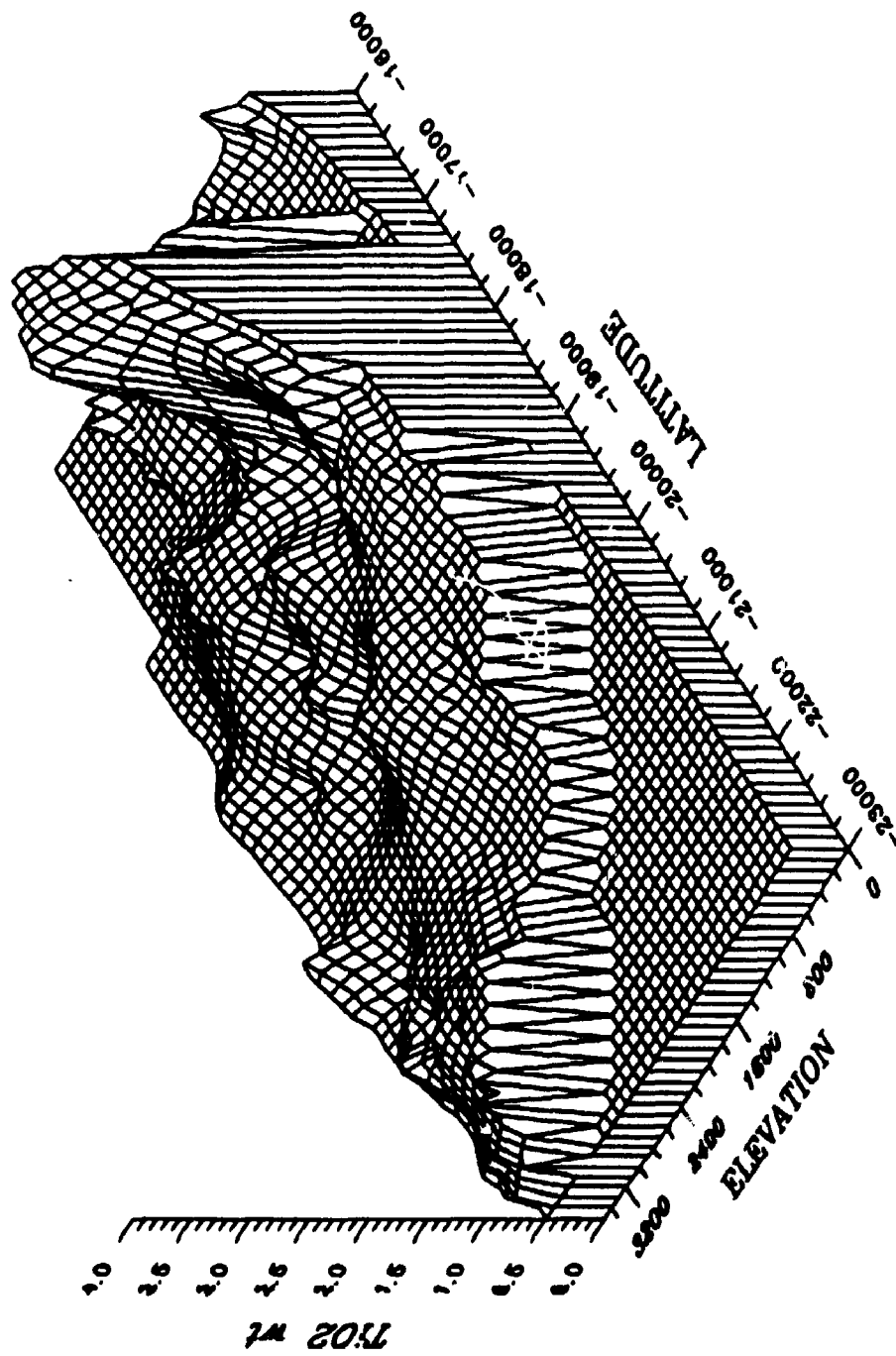
CAMPBELL SHEAR ZONE

CAMPBELL SHEAR ZONE

CAMPBELL SHEAR ZONE

CAMPBELL SHEAR ZONE

CAMPBELL SHEAR ZONE

CAMPBELL SHEAR ZONE

CAMPBELL SHEAR ZONE

REFERENCES

Allison, I., and Kerrich, R., 1980, History of deformation and fluid transport in shear zones in Yellowknife. in R.D. Morton, ed., Proceedings of the Gold Workshop, Yellowknife, Northwest Territories., p. 201-222.

Amor, S.D., and Nichol, I., 1983. Identification of diagnostic geochemical alteration in the wall rocks of Archean volcanic-exhalative massive sulphide deposits. J. Geochem. Explor., v. 19, p. 543-562.

Andrews, A.J., Hugon, H., Durocher, M., Corfu, F., and Lavigne, M.J., 1986, The anatomy of a gold-bearing greenstone belt: Red Lake, Northwestern Ontario, Canada. in A.J. Macdonald, ed., Gold '86, p 3-22.

Arch, J. and Maltman, A.J., 1988, Shear-zone geometries in experimentally deformed clays: The influence of water content, strain rate and primary fabric. Jour. Struct. Geol., v. 10, p. 91-99.

Armstrong, J.P., 1991, Metamorphic and alteration mineral assemblages, Con Shear Zone, NERCO-Con Mine, Yellowknife, NWT. in J.A. Brophy ed., Exploration Overview, 1991. NWT Geology Division, NAP, INAC, p. 14.

Armstrong, J.P., and Duke, N.A., 1990, An exploration update on the gold potential of the Con Shear System, NERCO-Con Mine, Yellowknife, NWT. in S.P. Goff ed., Exploration Overview 1990, NWT Geology Division, NAP, IANAC, p. 19.

Atkinson, D.J., 1989. Geology of the Western Plutonic Complex, Southwestern Slave Province. in Exploration Overview 1989. p. 25.

Atkinson, D.J., and van Breeman, O., 1990. Geology of the Western Plutonic Complex, Southwestern Slave Province: Late Archean crustal granites and gold mineralization in the Yellowknife District. in S.P. Goff ed., Exploration Overview 1990. INAC, p. 20.

Atkinson, D.J., and Fyfe, W.S., 1991. The Western Plutonic Complex, Southern Slave Province: Late cratonization and the granite gold connection at Yellowknife, Northwest Territories. Geological Association of Canada/Mineralogical Association of Canada Program with Abstracts, 1991. p. A5

Bachinski, S.W., and Scott, R.B., 1980, Authors' reply (to a critical comment by N.M.S. Rock). Geochim.

370

Cosmochim. Acta, v. 44, p 1389-1392.

Bailey, G., 1987, Stratigraphy of the Banting Group,
        Yellowknife greenstone belt, NWT.   MSc. thesis,
        Queen's University, Kingston, Ontario.

Baragar, W.R.A., 1966, Geochemistry of the Yellowknife
        volcanic rocks. Can. Jour. Earth Sci., v.3, p. 9-
        30.

Baragar, W.R.A., and Goodwin, A.M., 1966, Andesites and
        Archean volcanism in the Canadian Shield. in
        Proceedings of the Andesite Conference: edited byt
        A.R. McBirney; Oregon Department of Geology and
        Mineral Industries: Bulletin 65, p. 121-142.

Batchelor, E.W., 1990. Geology of the Ptarmigan and Tom
        Mines. in W.A. Padgham and D. Atkinson ed., Mineral
        deposits of the Slave Province, Northwest
        Territories. Geol. Surv. Can. Open File 2168. p.
        60-61.

Beach, A., 1975, The geometry of en échelon vein arrays.
        Tectonophysics, v. 28, p. 245-263.

Beach, A., 1976, The interrelation of fluid transport,
        deformation, geochemistry and heat flow in early
        Proterozoic shear zones in the Lewissian complex.
        Philisophical Transactions of the Royal Society of
        London, Series A280, p. 569-604.

Bibikova, E. Baadsgaard, H., and Folinsbee, R.E., 1986, U-
        Pb and Sm-Nd age dating of gneissic tonalite
        boulders from a diatreme in the Con Mine,
        Yellowknife, N.W.T., Canada, with South African
        comparisons. Prepublication abstract presented at
        the International Conference on Geochronology,
        Cambridge, England, 1986.

Boyle, R.W., 1961, The geology, geochemistry and origin of
        the gold deposits of the Yellowknife district:
        Geological Survey of Canada Memoir 310, 123 p.

Boyle, R.W., 1979. The Geochemistry of Gold and its
        Deposits. G.S.C. Bulletin 280. pp. 584.

Breakey, A.R., 1975. A mineralogical study of the gold quartz
        lenses in the Campbell Shear, Con Mine,
        Yellowknife, NWT.   unpub M.Sc. thesis, McGill
        University, Montreal, Quebec. pp. 116.

Brophy, J.A., 1987, Guide to the Crestaurum Formation in
        the area of Fred Henne Park.   in W.A. Padgham,
        ed., Yellowknife Guide Book. Geological Association

of Canada, p. 43-54

Brown, N., 1989, Structural evolution of the Giant shear zone complex. in Exploration Overview 1989, NWT Geology Division - NAP, p. 28.

Bullis, H.R., 1983, Unpublished technical report for Con Mine

Bullis, H.R., Pratico, V.P., and Webb, D.R., 1987, The Con Mine. in W.A. Padgham, ed., Yellowknife Guide Book. Geological Association of Canada, p. 175-182.

Burrows D.R., and Spooner, E.T.C., 1986, The McIntyre Cu-Au deposit, Timmins Ontario, Canada. in A.J. McDonald ed., Proceedings of Gold '86. Konsult International, Toronto. p. 23-39.

Burrows, D.R., Wood, P.C., and Spooner, E.T.C., 1986, Carbon isotope evidence for a magmatic origin for Archean gold-quartz vein ore deposits. NAture, v. 321, p. 851-854.

Bursnall, J.T., 1989, Review of mechanical principles, deformation mechanisms and shear zone rocks. in J.T. Bursnall, ed., Mineralization and Shear Zones. Geological Association of Canada, short course notes, v. 6, p. 1-28.

Campbell, N., 1947, The West Bay Fault, Yellowknife. Canadian Institute of Mining and Metallurgy, Transactions, v. 50 p. 509-526.

Chary, K.N., 1971, An isotopic and geochemical study of the gold-quartz veins in the Con-Rycon Mine Yellowknife. unpub. M.Sc. thesis, University of Alberta, 90 p.

Clayton, R.N., Jones, B.F., and Berner, R.A., 1968, Isotope studies of dolomite formation under sedimentary conditions. Geochim. Cosmochim. Acta, v. 32, p. 415-432.

Colvine, A.C., Fyon, J.A., Heather, K.B., Marmont, S., Smith, P.M., and Troop, D.G., 1988, Archean lode gold deposits in Ontario. Ontario Geological Survey, Misc Paper 139. pp.136.

Condie, K.C., and Baragar, W.R.A., 1974. Rare-earth element distributions in volcanic rocks from Archean greenstone belts. Contributions to Mineralogy and Petrology, v. 45, p. 237-246.

Cunningham, M.P., 1984, Petrochemistry of the Yellowknife

Greenstone Belt, Yellowknife, NWT. M.Sc. thesis, University of Alberta, Edmonton, Alberta.

Cunningham, M.P., and Lambert, R., 1989. Petrochemistry of the Yellowknife volcanic suite at Yellowknife, N.W.T., Can. J. Earth Sci. v 26, p. 1630-1646.

Davis, J.C., 1985, Statistics and data analysis in geology. 2nd edition. John Wiley and Sons, New York. pp. 550.

Deines, P. Langmuir, D., and Harmon, R.S., 1974, Stable carbon isotope ratios and the existence of a gas phase in the evolution of carbonate ground waters. Geochim. Cosmochim. Acta, v. 38, p. 1147-1164.

Donath, F.A., 1961, Experimental study of shear failure in isotropic rocks. Bulletin of the Geological Society of America. v. 72, p. 985-990.

Drury, S.A., 1977, Structures induced by granite diapirs in the Archean greenstone belt at Yellowknife, Canada: Implications for Archean geotectonics. Journal of Geology, v. 85, p. 345-358.

Drury, S.A., 1979, Rare-earth and other trace element data bearing on the origin of the Archean granitic rocks from Yellowknife, NWT. Can. Jour. Earth SCi., v. 16, p. 809-815.

Duke, N.A., Hauser, R.L., and Nauman, C.R., 1990. A guide to the geology of the NERCO-Con Mine, Yellowknife, NWT. in W.A. Padgham and D. Atkinson ed., Mineral deposits of the Slave Province, Northwest Territories. Geol. Surv. Can. Open File 2168. p. 41-52.

Duke, N.A., Barnett, R.L., and Kingston, D.M., 1991, The dynamic role played by amphibolatization of greenstone in gold concentration, NERCO-Con Mine, Yellowknife, N.W.T. in Program with Abstracts, Geological Association of Canada, Mineralogical Association of Canada Joint Annual Meeting with Society of Economic Geologists, v. 16, p. A32.

Duke, N.A., and McDonald, D., 1991, The evolution of auriferous metamorphic fluid: Yellowknife Greenstone Belt, NWT. in J.A. Brophy ed., Exploration Overview, 1991. NWT Geology Division, NAP, INAC, p. 19.

Easton, R.M., 1984, Compilation of geochronological data for the Yellowknife Greenstone Belt (85J/8 85J9) and vicinity, District of Mackenzie, NWT. in J.A. Brophy, ed., Contributions to the Geology of the

NWT, INAC, NAP, Geology Division, Yellowknife, NWT v. 1, p. 1-20.

Easton, R.M., Ellis, C.E., Helmstaedt, H., Jackson, V., O'Hearn, B., and Dean, M., 1982, Geology of the east side of Yellowknife Bay. DIAND, EGS 1982-5, Preliminary Map, 1:10,000.

Easton, R.M., and Jackson, V., 1981, Geology of the Walsh Lake map area. Department of Indian and Northern Affairs, Canada, Exploration and Geological Services Unit, EGS 1981-3.

Eisenlohr, B., 1987, Structural geology of the Kathleen Valley-Lawlers region, Western Australia, and some implications for Archean gold mineralization. in S.E. Ho, D.I. Groves, eds., Recent Advances in Understanding Precambrian Gold Deposits. Geology Department and University Extension, University of Western Australia, Western Australia, p. 85-96.

Eisenlohr, B.N., Groves, D., and Partington, G.A., 1989, Crustal-scale shear zones and their significance to Archean gold mineralization in Western Australia. Mineral. Deposita, v. 24, p. 1-8.

Falck, H., 1988. New ideas about the Yellowknife Volcanic Belt stratigraphy: Giant Section, Yellowknife. in Exploration Overview 1988, NWT Geology Division, DIAND, Yellowknife, p. 32.

Falck, H., and Atkinson, D.J., 1991, Regional distribution of gold and other elements in the Yellowknife Mining District, NWT (NTS 85 J/7,8,9 & 16). in J.A. Brophy ed., Exploration Overview, 1991. NWT Geology Division, NAP, INAC, p. 20.

Faure, G., 1986, Principles of Isotope Geology. 2nd edition. John Wiley and Sons, New York. pp. 589.

Franklin, J.M., Kasarda, J., and Poulsen, K.H., 1975. Petrology and chemistry of the alteration zone of the Mattabi massive sulphide deposit. Econ. Geol., v. 70, p. 63-79.

Friedman, I., and O'Neil, J.R., 1977, Compilation of stable isotope fractionation factors of geochemical interest. in I Freidman and J.R. O'Neil eds., Data of Geochemistry, 6th edition. U.S. Geol. Surv., Prof. Paper 440-KK.

Fritz, P., and Frape, S.K., 1982, Saline groundwaters in the Canadian Shield - a first overview. Chem. Geol., v. 36, p. 179-190.

Fyfe, W.S., 1978, Large scale crust - hydrosphere
interaction: large scale ore deposits. N.Z. Dep.
Sci. Ind. Res., Bull., 218, p. 71-75.

Fyfe, W.S., Price, N.J., and Thompson, A.B., 1978, Fluids in
the earth's crust. Elsevier, Amsterdam, 383 p.

Fyon, J.A., and Crocket, J.H., 1982, Gold exploration in the
Timmins District using field and lithogeochemical
characteristics of carbonate alteration zones. in
R.W. Hodder and W. Petruk eds., Geology of Canadian
Gold Deposits. Canadian Institute of Mining and
Metallurgy Special Volume 24, p. 113-129.

Fyson, W.K., 1982, Complex evolution of folds and cleavages
in Archean rocks, Yellowknife, NWT. Can. Jour.
Earth Sci., v. 19, p. 878-893.

Fyson, W.K., 1990, Structural development of angular volcanic
belts in the Archean Slave Province. Can. Jour.
Earth Sci., v. 27, p. 403-413.

Fyson, W.K., and Helmstaedt, H., 1.38, Structural patterns
and tectonic evolution of supracrustal domains in
the Archean Slave Province, Canada. Can. Jour.
Earth Sci., v. 25, p. 301-315.

Gates, B., 1979. Giant Yellowknife mines ltd., Giant rock
geochemistry project. Internal corporate report,
Giant Yellowknife Mines Ltd. pp. 13.

Gibb, R.A., and Thomas, M.D., 1980, Correlation of gravity
anomalies with Yellowknife Supergroup rocks, North
Arm, Great Slave Lake. Can. Jour. Earth Sci., v.
17, p. 1506-1516.

Gill, F.D., 1964. Diffusion of silica in the shear zone of
the Yellowknife Greenstone belt: Con office
report. Internal corporate report. pp. 16.

Gochnauer, E., 1988, Geological, geophysical, and diamond
drill report, Sito Lake Project (Bell 1-5, Sito 1-
6, Cowb, Jake, Percy, & Bruce Claims), District of
Mackenzie, Northwest Territories. Document 082620,
filed for assesment at the Mine Recorders Office,
Yellowknife, NWT., pp 81 plus maps.

Golding, S.D., Goves, S.I., McNaughton, N.J., Barley, M.E.,
and Rock, N.M.S., 1987, Carbon isotope composition
of carbonates from contrasting alteration styles in
supracrustal rocks of the Norseman-Wiluna Belt,
Yilgarn Block, Western Australia: their
significance to the source of Archean auriferous
fluids. in S.E. Ho and D.I. Groves eds., Recent

Advances in Understanding Precambrian Gold Deposits. Geology Department and University Extension, University of Western Australia, Western Australia, p. 287-306.

Goodwin, A.M., 1988, Geochemistry of the Slave Province volcanic rocks: Yellowknife belt. in Contributions to the Geology of the NWT, NWT Geology Division, Yellowknife, NWT, v. 3, p. 13-25.

Goucher, G., 1990. Giant Yellowknife Mine. in W.A. Padgham and D. Atkinson ed., Mineral deposits of the Slave Province, Northwest Territories. Geol. Surv. Can. Open File 2168. p. 64-66.

Green, D.C., and Baadsgaard, H., 1971, Temporal evolution and petrogenesis of an Archean crustal segment at Yellowknife, NWT. Jour. of Petr., v. 12, p. 177-217.

Harris, L.B., 1987, A tectonic framework for the Western Australian Shield and its significance to gold mineralization: a personal view. in S.E. Ho, D.I. Groves, eds., Recent Advances in Understanding Precambrian Gold Deposits. Geology Department and University Extension, University of Western Australia, Western Australia, p. 1-28.

Harrigan, D.B., and Maclean, W.H., 1976, Petrography and geochemistry of epidote alteration patches. Can. Jour. Earth Sci. V. 13, p. 500-511.

Hauer, l., 1979, Preliminary geological map of the northern end of the Yellowknife Greenstone Belt. Compilation of EGS 1979-10, sheets A and B, DIAND, Yellowknife, NWT.

Head, J., 1985, Report on the geochemistry of the Campbell Shear Zone, NERCO-Con Mine. Internal corporate report.

Helmstaedt, H., and Bailey, G., 1987. Problems of the structural geology in the Yellowknife Greenstone Belt. in W.A. Padgham, ed., Yellowknife Guide Book. Geological Association of Canada, p. 175-182.

Helmstaedt H., and Padgham, W.A., 1986a, A new look at the stratigraphy of the Yellowknife Supergroup at Yellowknife, NWT - implications for the age of the gold-bearing shear zones and Archean basin evolution. Can. Jour. Earth Sci., v. 23, p. 454-475.

Helmstaedt H., and Padgham, W.A., 1986b, Stratigraphic and

structural setting of the gold-bearing shear zones[7] in the Yellowknife greenstone belt. in L.A. Clark, ed., Gold in the Western Shield, CIM sp. v. 38, p. 322-345.

Helmstaedt H., Goodwin, J.A., Patterson, J.G., and King, J.E., 1979, Preliminary geological map, southern end of Yellowknife greenstone belt: INAC, NAP, Geology Division, Yellowknife, NWT., EGS 1979-9.

Helmstaedt H., King, J., and Boodle, R., 1980, Preliminary geology map of the Banting and Walsh Lakes area: INAC, NAP, Geology Division, Yellowknife, NWT., EGS 1980-5.

Helmstaedt H., King, J., Goodwin, J.A., and Patterson, J.G., 1981, Geology of the southwest end of the Yellowknife Greenstone Belt. in R.D. Morton, ed., Proceedings of the Gold Workshop, Yellowknife, NWT, p. 232-249.

Helmstaedt H., Padgham, W.A., and Brophy, J.A., 1986, Multiple dykes in the lower Kam Group, Yellowknife Greenstone Belt: Evidence for Archean sea floor spreading. Geology, v. 14, p. 562-566.

Henderson, J.F., and Brown, I.C., 1966, Geolo y and structure of the Yellowknife Greenstone Belt, District of Mackenzie. Geol. Surv. Can., bull., 141, 87 p.

Henderson, J.B., 1970, Stratigraphy of the Yellowknife Supergroup, Yellowknife Bay - Prosperous Lake area, District of Mackenzie. Geol. Surv. Can., Pap., 70-26, 12 p.

Henderson, J.B., 1975. Sedimentology of the Archean Yellowknife Supergroup at Yellowknife, District of Mackenzie. Geol Surv. Can., Bulletin 246, pp. 62.

Henderson, J.B., 1978. Age and origin of the gold-bearing shear zones at Yellowknife, Northwest Territories. Current Research, Part A, Geol. Surv. Can., Paper 78-1A, p. 259-262.

Henderson, J.B., 1985, Geology of the Yellowknife-Hearne Lake area, District of Mackenzie: A segment across an Archean basin. Geol Surv. Can., Mem. 414, 135 p.

Henderson, J.B., 1986, Stratigraphic and structural setting of the gold-bearing shear zones in the Yellowknife greenstone Belt. in L.A. Clark ed., Gold in the Western Shield. CIM Special Volume 38, p. 322-345.

Henderson, J.B., van Breeman, O., and Loveridge, W.D., 1987,[378] Some U-Pb zircon ages from Archean basement, supracrustal and intrusive rocks, Yellowknife-Hearne Lake area, District of Mackenzie. Geol. Surv. Canada, Paper 87-2, p. 111-121.

Hobbs, B.E. and Talbot, J.L., 1966, The analysis of strain in deformed rocks. Jour. Geol., v. 74, p. 500-513.

Hodgson, C.J., 1989, Patterns of mineralization. in J.T. Bursnall, ed., Mineralization and Shear Zones. Geological Association of Canada, short course notes, v. 6, p. 51-88.

Hodgson, C.J., and Troop, D.G., 1988, A new computer-aided methodology for area selection in gold exploration: a case study from the Abitibi Greenstone Belt. Econ. Geol., v. 83, p. 952-977.

Hubert, C., and Marquis, P., 1989, Structural framework of the Abitibi Greenstone Belt of Quebec and its implications for mineral exploration. in J.T. Bursnall, ed., Mineralization and Shear Zones. Geological Association of Canada, short course notes, v. 6, p. 219-238.

Hughes, C.J., 1973, Spilites, keratophyres and the igneous spectrum. Geological Magazine, v. 109, p. 513-527.

Hurdle, E., 1984, Geology of a volcanic pile at Clan Lake: in J.A. Brophy, ed., Contributions to the geology of the Northwest Territories. INAC, NAP, Geol. Div., Yellowknife, NWT., EGS 1984-5.

Isachsen, C.E., and Bowring, S.A., 1989. U-Pb zircon geochronology of the Yellowknife Volcanic Belt, NWT: Constraints on the timing and duration of the greenstone belt magmatism and deformation. in Exploration Overvie 1989. p. 25.

Isachsen, C.E., Bowring, S.A., and Padgham, W.A., 1990. Geochronology of the Yellowknife volcanic belt, NWT Canada. New constraints on the timing and duration of the greenstone belt magmatism. Journal of Geology, v.10 p.655-663.

Isachsen, C.E., Bowring, S.A., and Padgham, W.A., 1991a. U-Pb geochronology of the Yellowknife Supergroup at Yellowknife, NWT: Constraints on evolution. in Geological Association of Canada/ Mineralogical Associaction of Canada program with abstracts. v. 16, p A59.

Isachsen, C.E., Bowring, S.A., and Padgham, W.A., 1991b.

Geology and U-Pb geochronology of the Dwyer Formation and the underlying gneisses in the Southern Slave Province: A basement cover sequence beneath the Yellowknife Greenstone Belt? in Geological Association of Canada/ Mineralogical Associaction of Canada program with abstracts. v. 16, p A59.

Irvine T.N., and Baragar, W.R.A., 1971, A guide to the classification of the common volcanic rocks. Can. Jour. Earth Sci., v. 8, p. 523-549.

Jardine, D.E., 1974. A report on the geochemistry of the host rocks of gold in the Campbell Shear, Con Mine. Internal corporate report. Cominco Ltd, pp. 17.

Jardine, D.E., 1975. Con Mine Geochemistry: Contribution to Gold Workshop. Cominco Ltd., Exploration Research Laboratories, Vamcouver. Internal corporate report, Cominco Ltd.

Jenner, G.A., Fryer, B.J., and MacLennan, S.M., 1981, Geochemistry of the Archean Yellowknife Supergroup. Geochim. Cosmochim. Acta, v.45, p. 1111-1129.

Jolliffe, A.W., 1938, Preliminary report, Yellowknife Bay - Prosperous Lake area, Northwest Territories. Geol. Surv. Can., Pap. 38-21, 41 p.

Jolliffe, A.W., 1942, Prosperous Lake area, Northwest Territories. Geol. Surv. Can., Map 868A

Jolliffe, A.W., 1946, Yellowknife Bay, District of Mackenzie, Northwest Territories. Geol. Surv. Can., Map 709A.

Kermeen, J.S., 1990. Nicholas Lake gold deposit. in W.A. Padgham and D. Atkinson ed., Mineral deposits of the Slave Province, Northwest Territories. Geol. Surv. Can. Open File 2168. p. 64-66.

Kerrich, R., 1981, Archean lode gold deposits: synthesis of data on metal distribution, fluid inclusions and stable isotopes, with special reference to Yellowknife. in R.D. Morton, ed., Proceedings of the Gold Workshop, Yellowknife, NWT, p. 95-173.

Kerrich, R., 1983. Geochemistry of gold deposits in the Abitibi Greenstone Belt. Canadian Institute of Mining and Metallurgy. Special Volume 27. pp. 75.

Kerrich, R., 1986, Fluid infiltration into fault zones: chemical, isotopic and mechanical effects. Journal of Pure and Applied Geophysics, v. 124, p. 225-268.

Kerrich, R., 1988, Source process for Archean Au-Ag vein deposits: evidence from lithophile-element systematics of the Hollinger-McIntyre and Buffalo Ankerite deposits, Timmins. Can. Jour. Earth Sci., v. 26, p. 755-781.

Kerrich, R, 1989a, Geodynamic setting and hydraulic regimes: Shear zone hosted mesothermal gold deposits. in J.T. Bursnall, ed., Mineralization and Shear Zones. Geological Association of Canada, short course notes, v. 6, p. 89-128.

Kerrich, R., 1989b, Geochemical evidence on the sources of fluids and solutes for shear zone hosted mesothermal Au deposits. in J.T. Bursnall, ed., Mineralization and Shear Zones. Geological Association of Canada, short course notes, v. 6, p. 129-197.

Kerrich, R., and Allison, I., 1978, Vein geometry and hydrostatics during Yellowknife mineralization. Can. Jour. Earth Sci., v.15, p. 1653-1660.

Kerrich, R., and Hodder, R.W., 1982. Archean Lode gold and base metal deposits: Evidence for metal separation into separate hydrothermal systems. in R.W. Hodder and W. Petruk ed., Geology of Canadian Gold Deposits. Canadian Institute of Mining and Metallurgy. Special volume 24. p. 144-160.

Kerrich, R., and Fyfe, W.S., 1981. The gold-carbonate associateion: Source of CO_2, and CO_2 fixation reactions in Archean lode gold deposits. Chemical Geology, v. 33, p. 265-294.

Kerrich, R., and Fyfe, W.S., 1988a. The formation of gold deposits with particular reference to Archean greenstone belts and Yellowknife. i. Geological boundary conditions and metal inventory. in Contributions to the Geology of the NWT, NWT Geology Division, Yellowknife, NWT, v. 3, p. 37-62.

Kerrich, R., and Fyfe, W.S., 1988b, The formation of gold deposits with particular reference to Archean greenstone belts and Yellowknife. ii. Source of hydrothermal fluids, alteration patterns and genetic models. in Contributions to the Geology of the NWT, NWT Geology Division, Yellowknife, NWT, v. 3, p. 63-96.

Kerrich, R., La Tour, T.E., and Willmore, L., 1984, Fluid participation in deep fault zones: Evidence from geological, geochemical, and $^{18}O/^{16}O$ relations. Journal of Geophysical Research, v. 89, p. 4331-

Kerrich, R., and Watson, G.P., 1984.   The Macassa Mine
          Archean lode gold deposit, Kirkland Lake, Ontario;
          Geology, patterns of alteration and hydrothermal
          regimes. Econ. Geol., v. 79, p. 1104-1130.

Kerrich, R., and Wyman, D., 1990,   late evolution of
          greenstone belts and gold deposits, in F. Robert,
          P.A. Sheahan, S.B. Green eds., Greenstone Gold and
          Crustal Evolution. NUNA Conference Volume., p. 91-
          94.

Kishida, A., and Kerrich, R., 1987. Hydrothermal alteration
          zoning and gold concentration at the Kerr-Addison
          Archean lode gold deposit, Kirkland Lake, Ontario.
          Econ Geol., v. 82, p.649-690.

Kyser, T.K., 1987,   Equilibrium frationation factors for
          stable isotopes. in T.K. Kyser, ed. Short course
          in stable isotope geochemistry of low temperature
          fluids. Mineral. Assoc. of Can. Short Course, v.13,
          p. 1-84.

LeCheminant, A.N., and Heaman, L.M., 1991.   U-Pb ages for
          the 1.27 Ga Mackenzie igneaous events, Canada:
          Support for a plume initiation model. in Geolor.cal
          Association of Canada/ Mineralogical Associaction
          of Canada program with abstracts. v. 16, p A73.

Leech, A., 1966,   Potassium-argon dates of basic intrusive
          rocks of the District of Mackenzie, NWT. Can. Jour.
          Earth Sci., v. 3, p. 389-412.

Leitch, C.H.B., 1990,   Geology, wallrock alteration and
          characteristics of the ore fluids at the Bralorne
          mesothermal gold deposit, SW British Columbia. in
          F. Robert, P.A. Sheahan, and S.B. G_een eds.,
          Greenstone Gold and Crustal Evolution, NUNA
          Conference volume, p.183-184.

Mandl, G., De Jong, N.J., and Maltha, A., 1977,   Shear zone
          in granular material: and experimental study of
          their structure and mechanical genesis.   Rock
          Mechanics, v. 9, p. 95-144.

Mason, R., and Melnik, N., 1986, The anatomy of an Archean
          gold system - The McIntyre - Hollinger complex at
          Timmins, Ontario, Canada. in A.J. MacDonald ed.,
          Gold '86. Konsult International, Toronto. p. 40-55.

Matsuhisa, Y., Goldsmith, J.R., and Clayton, R.N., 1979,
          Oxygen isotope fractionation in the system quartz-
          albite-anorthite-water. Geochim. Cosmochim. Acta,

Matthews, A., and Katz, A., 1977, Oxygen isotope fractionation during dolomitization of calcium carbonate. Geochim. Cosmochim. Acta, v. 47, p. 645-654.

McCartney, I.P., and Webb, D.R., 1986. Report on the geological and geochemical program, NERCO-Con Mine, Yellowknife, NWT. Internal corporate report.

McCrae, J.M., 1950, On the isotopic chemistry of carbonate and a paleotemperature scale. J. Chem. Phys., v. 18, p. 849-857.

McDougall, J.H., and Goad, R.E., 1990, A report on the geology, VLF-EM, and bulk sampling program on the Mon Gold Property (3004 to 3014), and the geology of the DIS1 (F14257) and 2 (F14260), Carjon 1 (F14252) and 2 (F14427), and LUC1 (F14251) claims, Yellowknife area, Mackenzie (South) District, Northwest Territories, Canada. internal corporate report. 54 p. plus appendexis.

McGlynn, J.C., and Irving, E., 1975, Paleomagnetism of early Aphebian diabase dykes for the Slave Structural Province, Canada. Tectonophysics, v. 26, p. 23-38.

McKinstry, H.E., 1953, Shears of the second order. Amer. J. Sci., v. 251, p. 401-414.

McNeil, A.M., and Kerrich, R., 1986, Archean lamprophyric dykes and gold mineralization, Matheson, Ontario: the conjunction of LIL-enriched mafic magmas, deep crustal structures and Au concentration. Can. Jour. Earth Sci., v. 23, p. 324-342.

Moore, J.C.G., 1953, Carp Lakes, District of Mckenzie, Northwest Territories. Geol. Surv. Canada, Preliminary Map, 51-8.

Morrison, G.W., 1980, Characteristics and tectonic setting of the shoshonitic rock association. Lithos, v. 13, p. 97-108.

Muller, A.G., and Harris, L.B., 1987, An application of wrench tectonic models to mineralized structures in the Golden Mile district, Kalgoorlie, Western Australia. in S.E. Ho and D.I. Groves ed., Recent Advances in Understanding Precambrian Gold Deposits. Publication No. 11, issued jointly by the Geology Depatment and University Extension, The University of Western Australia. p. 97-108.

Murphy, J.B., 1989, Tectonic environment and metamorphic [383] characteristics of shear zones. in J.T. Bursnall, ed., Mineralization and Shear Zones. Geological Association of Canada, short course notes, v. 6, p. 29-49.

Myers, D.E. Jr., 1976. Year-end report, 1976, Yellowknife gold research, Con Property, Cominco Ltd., Yellowknife, N.W.T. Internal corporate report, Cominco Ltd. pp. 111.

Myers, D.E. Jr., 1979. Geochemistry of the Con Mine, Yellowknife, N.W.T., in R.D. Morton, ed., Proceedings of the Gold Workshop, Yellowknife, N.W.T., p. 240-257.

Nikic, Z., Baadsgaard, H., Folinsbee, R.E., Krupicka, J., Leech, A.P., and Sasaki, A., 1980, Boulders from basement, the trace of ancient crust? in G.B. Morey and G.N. Hanson ed., Selected studies of Archean gneisses and lower Proterozoic rocks, Southern Canadian Shield, Geol. Soc. Am., Special Paper 182, p. 169-175.

Ohmoto, H., 1986, Stable isotope geochemistry of ore deposits. in J.W. Valley, H.P. Taylor, and J.R. O'Neil eds., Stable Isotopes in High Temperature Geological Processes, Mineral. Assoc. America, Reviews in Mineralogy, v. 16, p. 491-559.

Ohmoto, H., and Rye, R.O., 1979, Isotopes of sulfur and carbon. in H.L. Barnes ed., Geochemistry of Hydrothermal Ore Deposits. 2nd edition, John Wiley and Sons, New York, p. 509-567.

O'Neil, J.R., 1986, Theoretical and experimental aspects of isotope fractionations. in J.W. Valley, H.P. Taylor, and J.R. O'Neil eds., Stable Isotopes in High Temperature Geological Processes. Reviews in Mineral., v. 16, Mineral. Soc. Amer., p. 1-37.

O'Neil, J.R., Clayton, R.N., and Mayeda, T.K., 1969, Oxygen isotope fractionation in divalent metal carbonates. Jour. Chem. Phys. v. 51, p. 5547-5558.

Osatenko, M.J., 1971. A petrological and geochemical study of drillhole S1151, Con Mine. Internal corporate report. Cominco Ltd. pp. 31.

Osmani, I.A., Stott, G.M., Sanborn-Barrie, M., and Williams, H.R., 1989, Recognition of regional shear zones in south-central and northwestern Superior Province of Ontario and their economic significance. in J.T. Bursnall, ed., Mineralization and Shear Zones.

Geological Association of Canada, short course[384] notes, v. 6, p. 199-218.

Padgham, W.A., 1979, Geology of the Yellowknife volcanic belt. in R.D. Morton, ed., Proceedings of the Gold Workshop, Yellowknife, Northwest Territories., p. 288-322.

Padgham, W.A., 1980, An Archean ignimbrite at Yellowknife and its relationship to the Kam Formation basalts. Precambrian Res., v. 12, p. 99-113.

Padgham, W.A., 1981, Archean crustal evolution - A glimpse from the Slave Province. Geol. Society Australia, Spec. Pub. v. 7, p. 99-110.

Padgham, W.A., 1985, Observations and speculations on supracrustal successions in the Slave Structural Province. in L.D. Ayres, P.C. Thurston, K.D. Card, and W. Weber, eds., Evolution of Archean supracrustal sequences. Geological Association of Canada, Sp. Paper 28, p. 133-151.

Padgham, W.A., 1986, Turbidite-hosted gold-quartz veins in the Slave Structural Province, NWT. in J. Keppie, Duncan, R.W. Boyle, and S.J. Haynes eds., Turbidite-hosted gold deposits. Geological Association of Canada Sp. Paper 32, p. 119-134.

Padgham, W.A., 1987. The Yellowknife volcanic belt: Setting and stratigraphy. in W.A. Padgham, ed., Yellowknife Guide Book. Geological Association of Canada, p. 11-20.

Padgham, W.A., 1990. The Slave Province, and overview. in Mineral Deposits of the Slave Province, Northwest Territories. edited by W.A. Padgham and D. Atkinson. Geological Survey of Canada, open file 2168. p. 1-40.

Parslow, G.R., 1987. Lithogeochemical data from east Amisk area of the Flin Flon-Snow Lake volcanic belt: Implications for mineral exploration. J. Geochem. Explor., v. 28, p. 133-148.

Pelletier, K.S., 1987. Structural and stratigraphic implications of mapping in the northwest Mirage Islands, Yellowknife Bay, NWT. in C.E. Ellis ed., Exploration Overview 1987. INAC. p. 32.

Pelletier, K.S., and Wahlroth, J.M., 1985, Geology of the southwestern Yellowknife Bay area, parts of NTS 85 J/7, 8; 1:10,000 map. EGS 1986-12, Geology Division, NAP, INAC.

Perring, C.S., Groves, D.I., and Ho, S.E., 1987, Constraints on the source of auriferous fluids for Archaean gold deposits. in S.E. Ho and D.I. Groves eds., Recent Advances in Understanding Precambrian Gold Deposits. Geology Department and University Extension, University of Western Australia, Western Australia, p. 287-306.

Phillips, G.N., 1990, Nature of Archean gold-bearing fluids in Australian greenstone terranes. in F. Robert, P.A. Sheahan, and S.B. Green eds., Greenstone Gold and Crustal Evolution, NUNA Conference volume, p. 192.

Pleydell, S.M., Jones, B., Longstaffr, F.J., and Baadsgaard, H., 1990, Dolomitization of the Oligocene- Miocene Bluff Formation on Grand Cayman, British West Indies. Can. Jour. Earth Sci., v. 27, p. 1098-1110.

Poulsen, K.H., 1983, Structural setting of vein-type gold mineralization in the Mine Center-Fort Frances area: implications for the Wabigoon Subprovince. Ontario Geological Survey, Miscellaneous Paper 110, p. 174-180.

Poulsen, K.H., 1986, Auriferous shear zones with examples from the Western Shield. in L.A. Clark, ed., Gold in the Western Shield, CIM sp. v. 38, p. 86-103.

Poulsen, K.H., Robert, F., and Sibson, R.H., 1988, A fault-valve model for the origin of mesothermal lode gold deposits, Econ. Geol. v. 80

Poulsen, K.H., and Robert, F., 1989, Shear zones and gold: Practical examples from the southern Canadian Shield. in J.T. Bursnall, ed., Mineralization and Shear Zones. Geological Association of Canada, short course notes, v. 6, p. 239-266.

Ramsay, C.R., and Kamineni, D.A., 1977, Petrology and evolution of an Archean metamorphic aureole in the Slave craton, Canada. Jour. Petrol., v. 18, p. 460-486.

Ramsay, J.G., 1967, Folding and fracturing in rocks. McGraw-Hill Book Company, New York. p. 324.

Ramsay, J.G., 1980, Shear zone geometry: A review. Jour. Structural Geol., v. 2, p. 83-99.

Ramsay, J.G., and Graham, R.H., 1970, Strain variation in shear belts. Can. Jour. Earth Sci., v. 7, p. 786-813.

Ramsay, J.G., and Huber, M.I., 1987, The techniques of modern structural geology, Volume II: Folds and fractures. Academic Press, Orlando, 700 p.

Ransom, D.M., 1974, The structural geology and controls of gold mineralization in the Con Mine and environs, Yellowknife NWT., Canada. unpublished technical report, Cominco Ltd.

Relf, C., 1986, A study of shear zone alteration in the "Mirage Island Formation", Yellowknife Bay. in Exploration Overview 1986, NWT Geology Division - NAP, p. 30-31.

Relf, C., and Nicholson, D.C., 1985, Geology of the West Mirage Islands, NWT. Preliminary Map, EGS 1986-5, Geology Division, INAC.

Richards, J.P., McCulloch, M.T., Chappell, B.W., and Kerrich, R., 1991, Sources of metals in the Porgera gold deposit, Papua New Guinea: Evidence from alteration, isotope, and noble metal geochemistry. Geochim. et Cosmochim. Acta, v. 55, 565-580.

Ridley, J., 1990, Can alteration assemblages give information about the source of the ore-bearing fluids? in F. Robert, P.A. Sheahan, and S.B. Green eds., Greenstone Gold and Crustal Evolution, NUNA Conference volume, p.199.

Riverin, G., and Hodgson, C.J., 1980. Wall rock alteration at the Millenbach Cu-Zn mine, Noranda, Quebec. Econ. Geol., v. 75, p. 424-444.

Robert, F., and Brown, A.C., 1986a, Archean gold-bearing quartz veins at the Sigma mine, Abitibi greenstone belt, Quebec: Part I. Geological relations and formation of the vein system. Economic Geology, v. 81, p. 578-592.

Robert, F., and Brown, A.C., 1986a, Archean gold-bearing quartz veins at the Sigma mine, Abitibi greenstone belt, Quebec: Part II. Vein paragenesis and hydrothermal alteration. Economic Geology, v. 81, p. 593-616.

Roberts, R.G., 1987, Ore Deposits Models #11. Archean Lode Gold Deposits. Geoscience Canada, v. 76, p. 37-52.

Rock, N.M.S., 1983. Nature and origin of calc-alkaline lamprophyres: minettes, vogesites, kerantites, and spessartites. Trans. R. Soc. Edinburgh: Earth Science, v. 74, p. 193-227.

Rock, N.M.S., 1986, The nature and origin of ultramafic lamprophyres. J. Petrol., v. 27, p. 155-196.

Rock, N.M.S., and Groves, D.I., 1988, Can lamprophyres resolve the genetic controversy over mesothermal gold deposits? Geology, v. 16 p. 538-541.

Rosenbaum, J., and Sheppard, S.M.F., 1986, An isotopic study of siderites, dolomites and ankerites at high temperatures, Geochim. Cosmochim. Acta, v. 50, p. 1147-1150.

Rubinson, M., and Clayton, R.N., 1969, Carbon-13 fractionation between aragonites and calcite. Geochim. Cosmochim. Acta, v. 33, p. 997-1002.

Rye, K., 1987, The geology and geochemistry of the Hoyle Pond gold deposit, Timmins, Ontario. unpub. M.Sc. thesis, University of Western Ontario, London, Ontario, Canada. pp. 220.

Sharma, T., and Clayton, R.N., 1965, Measurement of O^{18}/ O^{16} ratios of total oxygen of carbonates. Geochim. Cosmochim. Acta, v. 29, p. 1347-1353.

Sheppard, S.M.F., and Schwartz, H.P., 1970, Fractionation of carbon and oxygen isotopes and magnesium between coexisting metamorphic calcite and dolomite. Contrib. Miner. Petrol. v. 26, p. 161-198.

Sibson, R.H., 1987, Earthquake rupturing as a mineralizing agent in hydrothermal systems. Geology, v. 15, p. 701-704.

Sibson, R.H., 1989, Earthquake faulting as a structural process. Jour. Struct. Geol., v. 11, p. 1-14.

Sibson, R.H., Robert, F., and Poulsen, K.H., 1989, High angle faults, fluid pressure cycling and mesothermal gold-quartz deposits. Geology, v. 16, p. 551-555.

Skwarnecki, M.S., 1987, Controls on Archaean gold mineralization in the Lenora district, Western Australia. in S.E. Ho, D.I. Groves, eds., Recent Advances in Understanding Precambrian Gold Deposits. Geology Department and University Extension, University of Western Australia, Western Australia, p. 109-136.

Sproule, W.R., 1952, Control of ore deposition, Con, Rycon, and Negus Mines, Yellowknife, NWT. unpub. M.Sc. thesis, Queen's University, Canada, pp.77.

Streckeisen, A., 1979. Classification and nomenclature of
volcanic rocks, lamprophyres, carbonatites, and
melitic rocks. Geology, v. 7, p. 331-335.

Stockwell, C.H., 1964. Fourth report on structural provinces,
orogenies and time classification of rocks of the
Canadian Precambrian Shield. Part II Geological
studies. Geol Surv. Can., Paper 64-17 pp. 1-7.

Taylor, B.E., 1987, Stable isotope geochemistry of ore-
forming fluids. in T.K. Kyser ed., Short Course in
Stable Isotope Geochemistry of Low Temperature
Fluids, Mineral. Assoc. of Canada, v. 13, p. 337-
445.

Taylor, H.P. Jr., 1974, The application of oxygen and
hydrogen isotope studies to problems of
hydrothermal alteration and ore deposition. Econ.
Geol., v. 69, p. 843-883.

Tchalenko, J.S., 1968, The evolution of kink bands and the
development of compression textures in sheared
clays. Tectonophysics, v. 6, p. 159-174.

Thompson, R.N., Morrison, M.A., Hendrey, G.L., and Parry,
S.J., 1984. An assesment of the relative roles of
crust and mantle in magma genesis: an elemental
approach. Phil. Trans. R. Soc. London. A310, p.
549-590.

Tremblay, L.B., 1952, Giauque Lake, District of Mackenzie,
NWT. Geol. Surv. Can., Map 1017A.

Tuborg, J.F., 1975. Con gold project, July 1973 - December
1974. Internal corporate report, Cominco Ltd. pp.
47.

Turner, F.J., 1981, Metamorphic petrology, 2nd edition.
McGraw-Hill Book Company, New York. pp. 524.

Venturelli, G., Thorpe, R.S., Dal Piaz, G.V., Del Moro, A.,
and Potts, P.J., 1984, Petrogenesis of calc-
alkaline, shoshonitic and associated ultrapotassic
Oligocene volcanic rocks from the northwestern
Alps, Italy. Contr. Mineralogy Petrology. v. 86,
p. 209-220.

Watson, G.P., and Kerrich, R., 1983, Macassa Mine, Kirkland
Lake - production history, geology, gold ore types
and hydrothermal regimes. Ontario Geological
Survey Misc. Paper 110, p. 56-74.

Webb, D.R., 1983. The relationship of ore to structural
features of the Campbell Shear Zone and hanging

wall stratigraphy in the Con Mine, Yellowknife,[389] Northwest Territories. unpub. M.Sc. thesis, Queen's University, Kingston, Ontario. pp. 181.

Webb, D.R., 1988, Geochemistry of the ore-related metasomatic alteration peripheral to mineralization at the Nerco Con mine, Yellowknife, NWT. in Exploration Overview 1988, NWT Geology Division - NAP, p. 61.

Webb D.R., and Kerrich, R., 1988, Constraints on the nature of the fluids implicated in the formation of the shear zone-hosted gold deposits at Yellowknife, NWT. in Exploration Overview 1988, NWT Geology Division - NAP, p. 60.

Webb, D.R., 1986, A large Archean Lamprophyre dyke at the Con gold mine, Yellowknife, NWT. in Exploration Overview 1986, NWT Geology Division - NAP, p. 33.

Webb, D.R., 1983, The relationship of ore to structural features of the Campbell shear zone and hanging wall stratigraphy in the Con Mine, Yellowknife, NWT. unpub. M.Sc. thesis, Queen's University, Canada. pp. 180.

Webb, D.R., 1986, A large Archean lamprophyre dyke at Yellowknife, NWT. GAC program with abstracts.

Webb, D.R., 1987, Evidence of large-scale deformation of ore zones at the Con Mine. in W.A. Padgham, ed., Yellowknife Guide Book. Geological Association of Canada, p. 183-190.

Webb D.R., and Kerrich, R., 1986, Recent age-dating on the gold-bearing quartz veins at the Con Mine, Yellowknife, NWT. in Exploration Overview 1986, NWT Geology Division - NAP, p. 33.

Webb D.R., and Kerrich, R., 1987, An Archean ultramafic lamprophyre, Yellowknife: Implications for tectonics and source regions. in W.A. Padgham ed., Contributions to the Geology of the Northwest Territories. v. 3, p. 115-122.

Wesolowski, D., and Ohmoto, H., 1986, Calculated oxygen isotope fractionation factors between water and the minerals sheelite and powellite, Econ. Geol., v. 81, p. 471-477.

Wise, D.U., Dunn, D.E., Enbelder, J.T., Geiser, P.A., Hatcher, R.D., Kish, S.A., Odum, A.L., and Shamel, S., 1984, Fault-related rocks: suggestions for terminology. Geology, v. 12, p. 391-394.

Wyman, D.A., and Kerrich, R., 1988. Archean lamprophyres, gold deposits and transcrustal structures: implications for greenstone belt gold metallogeny. Econ Geol., v. 83., p. 454-459.

Wyman, D.A., and Kerrich, R., 1989. Archean shoshonitic lamprophyres associated with Superior Province gold deposits: Distribution, tectonic setting, nobel metal abundances, and significance for gold mineralization. Journal of Geophysical Research.

Yardley, D.H., 1949, Wecho River, East Half, District of Mckenzie, Northwest Territories. Geol. Surv. Canada, Preliminary Map 49-14.